MONOMETALLIC AND BIMETALLIC CHALCOGEN-RICH, EXTENSIVELY CONJUGATED AND PLANAR COMPLEXES FOR ELECTRICALLY CONDUCTING MATERIALS

By

ANTHONY E. PULLEN

A DISSERTATION PRESENTED TO THE GRADUATE SCHOOL
OF THE UNIVERSITY OF FLORIDA IN PARTIAL FULFILLMENT
OF THE REQUIREMENTS FOR THE DEGREE OF
DOCTOR OF PHILOSOPHY

UNIVERSITY OF FLORIDA

1996

To my parents

ACKNOWLEDGMENTS

First and foremost, I would like to thank my advisor, Professor John R. Reynolds, for giving me the opportunity to work in his research group on an interesting project. He has shown a tremendous amount of patience, guidance and direction to assist in my development as a scientist.

I would like to thank Associate Professor James Boncella, Associate Professor Daniel R. Talham, Professor David B. Tanner and Professor Kenneth B. Wagener for reading this dissertation and serving on my supervisory committee.

I would like to thank all former and present fellow research group members for their friendship and interesting conversation: Peter Balanda, Mark Bratt, Don Cameron, Dr. Michael DiVerdi, David Irvin, Jennifer Irvin, Dr. Seungho Kim, Fernando Larmat, Dr. Myoungho Pyo, Jerry Reddinger, Dr. Bala Sankaran, Shawn Sapp, Greg Sotzing, Chris Thomas and Dean Welsh. I would also like to thank fellow friends and colleagues of the polymer floor. I am indebted to Dr. Michael DiVerdi for his invaluable teaching and insight of synthetic laboratory techniques during my early "influential" years as a graduate student.

I would like to express my gratitude to Hsiang-Lin Liu for doing optical and electrical measurements of some of my compounds and his help in aiding my understanding of solid state physics. I would also like to thank his advisor, Professor David B. Tanner, for providing the collaboration and giving us the opportunity to have our materials studied in his laboratory. I would like to extend my thanks to Leipzig, Germany, for the collaboration with the research group of Professor Hoyer at the Institute for Inorganic Chemistry at the University of Leipzig. Specifically I would like to thank both Dr. Jens Piotraschke for his stay in our lab, and Dr. Ruth-Maria Olk during my stay at the

University of Leipzig, for teaching me how to think like a coordination chemist. I would also like to thank Leipzigers Dr. Reinhard Kirmse, Hannelore Morgner, Dr. Peter Strauch, Dr. Michael Wagner, Grit Zdobinsky and Dr. Stephan Zeltner for helping me to have a wonderful experience in Europe and for the many jokes about hamburgers and Coca-Cola. I would like to thank Dr. Khalil A. Abboud for solving the X-ray crystal structures of our materials and taking his time to provide numerous drawings for publications and presentations.

Finally, but most importantly, a very special and sincere thanks to my wife and friend, Sande, whose constant love, support, encouragement and guidance led me to the path and helped me to stay there.

TABLE OF CONTENTS

ACKNOWLEDGMENTS iii

ABSTRACT vii

CHAPTERS

1 BACKGROUND AND INTRODUCTION 1

1–1 Organic Superconductors 3
1–1–1 BEDT-TTF-Based Conductors 3
1–1–2 Fullerenes 4
1–2 Metal Oxide Superconductors 6
1–3 Coordination Complex Conductors and Superconductors 7
1–3–1 MBDT-Based Conductors 7
1–3–2 M(dmit)$_2$-Based Conductors 9
1–4 Electrocrystallization 16
1–4–1 Mechanism of Electrocrystallization 17
1–5 Bimetallic and Monometallic Complexes 20
1–6 Applications of Organic-Based Conducting Materials 25
1–7 Synopsis of Work 25

2 NEW MOLECULAR CONDUCTORS BASED ON Ni(dmit)$_2$ 27

2–1 Experimental 27
2–2 Results 35
2–2–1 X-ray Structures 35
2–2–2 Conductivity Properties 46
2–2–3 Optical Spectroscopy 49
2–3 Conclusions 54

3 EXTENSIVELY CONJUGATED, CHALOGEN-RICH, DIANIONIC TETRATHIOOXALATO-BRIDGED COPPER(II) COMPLEXES 56

3–1 Experimental 57
3–2 Results 64
3–2–1 Synthesis of $(Bu_4N)_2\{tto[Cu(dmit)]_2\}$ (**105**), $(Bu_4N)_2\{tto[Cu(mnt)]_2\}$ (**106**), $(Bu_4N)_2\{tto[Cu(dsit)]_2\}$ (**107**) and $(Bu_4N)_2\{tto[Cu(dmid)]_2\}$ (**108**) 64
3–2–2 X-ray Structures of **105-108** 67
3–2–3 Redox Properties of **105-108** 75
3–2–4 Conductivity Properties of $(Bu_4N)_2\{tto[Cu(dmit)]_2\}$ (**105**) 81
3–3 Conclusions 81

4 PREPARATION, STRUCTURE AND PROPERTIES OF AN ANIONIC TETRAMERIC COPPER COMPLEX CONTAINING A PLANAR, EIGHT-MEMBERED RING CORE 85

4–1 Experimental 87
4–2 Results 90
4–2–1 Synthesis of $(Bu_4N)_2[Cu(dmt)]_4$ (**126**) 90
4–2–2 X-ray Structure of $(Bu_4N)_2[Cu(dmt)]_4$ (**126**) 90
4–2–3 Redox Properties of $(Bu_4N)_2[Cu(dmt)]_4$ (**126**) 93
4–2–4 UV-Vis Absorption Properties of $(Bu_4N)_2[Cu(dmt)]_4$ (**126**) 93
4–3 Conclusions 93

5 EXTENSIVELY CONJUGATED, CHALCOGEN-RICH, DIANIONIC TETRATHIOOXALATO-BRIDGED NICKEL(II) COMPLEXES 97

5–1 Experimental 98
5–2 Results 106
5–2–1 Synthesis of Complexes $(Bu_4N)_2\{tto[Ni(dmit)]_2\}$ (**131**), $(Et_4N)_2\{tto[Ni(dmit)]_2\}$ (**132**), $(Me_4N)_2\{tto[Ni(dmit)]_2\}$ (**133**), $(Bu_4N)_2\{tto[Ni(dsit)]_2\}$ (**134**) and $(Bu_4N)_2\{tto[Ni(dmise)]_2\}$ (**135**) 106
5–2–2 X-ray Structures of **131-135** 108
5–2–3 Redox Properties of $(Bu_4N)_2\{tto[Ni(dmit)]_2\}$ (**131**), $(Bu_4N)_2\{tto[Ni(dsit)]_2\}$ (**134**) and $(Bu_4N)_2\{tto[Ni(dmise)]_2\}$ (**135**) 123
5–2–4 Electrocrystallization, Slow Interdiffusion, Chemical Oxidation and Conductivity Experiments of $(Bu_4N)_2\{tto[Ni(dmit)]_2\}$ (**131**) 127
5–3 Conclusions 128

APPENDIX 129

TABLES OF CRYSTALLOGRAPHIC DATA 130

LIST OF REFERENCES 189

BIOGRAPHICAL SKETCH 199

Abstract of Dissertation Presented to the Graduate School
of the University of Florida in Partial Fulfillment of the
Requirements for the Degree of Doctor of Philosophy

MONOMETALLIC AND BIMETALLIC CHALCOGEN-RICH, EXTENSIVELY CONJUGATED AND PLANAR COMPLEXES FOR ELECTRICALLY CONDUCTING MATERIALS

By

Anthony E. Pullen

December, 1996

Chairperson: John R. Reynolds
Major Department: Chemistry

The design, synthesis and characterization of new monometallic and bimetallic chalcogen-rich, extensively conjugated and planar complexes has been investigated. The monometallic complexes studied are of the general formula $(C)_x[Ni(dmit)_2]$ (where C = monocation; $0.29 \leq x \leq 0.5$; dmit = 2-thione-1,3-dithiole-4,5-dithiolato). In particular, the complexes $(Bu_4N)_2[Ni(dmit)_2]_7 \cdot 2CH_3CN$, $(Ph_4P)[Ni(dmit)_2]_3$, $(Me_3S)[Ni(dmit)_2]_2$ and $(MePh_3P)[Ni(dmit)_2]_3$ have been synthesized via electrocrystallization and investigated by X-ray crystallography, elemental analyses, temperature-dependent conductivity and reflectance spectroscopy. The complex $(Ph_4P)[Ni(dmit)_2]_3$, exhibits a unique packing structure characterized by stacks of $Ni(dmit)_2$ units separated by orthogonal $Ni(dmit)_2$ spacer units. All of the complexes display semiconducting electrical behavior.

To improve the electrical properties of the bis-dmit ligand complexes, a new family of bimetallic Cu(II) and Ni(II) compounds has been designed and synthesized. The Cu(II) compounds have the general formula $(Bu_4N)_2\{tto[Cu(L)]_2\}$ (where tto = tetrathiooxalato;

L = dmit, mnt = 1,2-dicyanoethene-1,2-dithiolato, dsit = 2-thione-1,3-dithiole-4,5-diselenolato and dmid = 2-oxo-1,3-dithiole-4,5-dithiolato). They have been characterized by X-ray crystallography, elemental analyses, cyclic voltammetry and conductivity measurements. $(Bu_4N)_2\{tto[Cu(mnt)]_2\}$ is the first completely planar, tto-bridged, bimetallic complex synthesized. $(Bu_4N)_2\{tto[Cu(dmit)]_2\}$ was chemically oxidized and the resulting materials showed at least an eight order of magnitude increase in the conductivity over the single-crystal dianionic complex.

A series of bimetallic tto-bridged Ni(II) complexes have also been synthesized. They have the general formula $(C)_2\{tto[Ni(L)]_2\}$ (where L = dmit, C = Bu_4N, Et_4N, Me_4N and L = dsit, dmise = 2-selenoxo-1,3-dithiole-4,5-dithiolato, C = Bu_4N) and have been characterized by X-ray crystallography, elemental analyses and cyclic voltammetry. $(Bu_4N)_2\{tto[Ni(dmit)]_2\}$ has been used in electrocrystallization, slow interdiffusion and chemical oxidation experiments to synthesizes materials with high pressed-powder conductivities.

CHAPTER 1
BACKGROUND AND INTRODUCTION

In 1911, superconductivity, defined as the state where a material exhibits zero electrical resistance, was first discovered in metallic mercury by Kamerlingh Onnes who reported a T_c (superconducting transition temperature) of 4.15 K.[1] During that same year in an article by McCoy and Moore, it was proposed that composite substances could be assembled from nonmetallic elements that might exhibit metallic-like properties.[2,3] It was not until in the mid-1960s that William Little proposed that organic materials could be assembled to not only exhibit metallic-like properties, but even superconducting properties.[4,5] Thereafter in 1973, the first organic-based molecular metal was synthesized. The charge-transfer complex composed of the electron donor molecule tetrathiafulvalene (TTF, **1**) and the electron acceptor molecule 7,7,8,8-tetracyano-*p*-quinodimethane (TCNQ, **2**) was found to display metallic electronic properties down to 54 K at ambient pressure where the material undergoes a metal-to-insulator transition.[6] X-ray structure analysis showed that the material consists of segregated stacks of TTF (**1**) and TCNQ (**2**) molecules. The planarity of the molecules allow them to stack into a "poker-chip-like" manner. The p orbitals of the conjugated molecules, along with the orbitals of the large sulfur atoms, allow for a large amount of intermolecular overlap which stabilizes the stacks. This effective intermolecular orbital overlap is needed to establish a delocalized band structure. It was also found in the TTF-TCNQ (**3**) material that there is charge-transfer of 0.59 e^- from **1** to **2**. This is also a needed prerequisite to the establishment of a metallic state in a molecular system, the partial occupation by electrons of the delocalized band structure. These results began a plethora of research in the early 1970's into the

design and synthesis of various organic electron donor and acceptor molecules aimed at structures that are fully conjugated, planar and chalcogen-rich to be used in the construction of molecular metals and potentially superconductors.

In keeping with the structural requirements of the components that proved necessary for the formation of the molecular metal TTF-TCNQ (**3**), Klaus Bechgaard synthesized the electron donor molecule tetramethyltetraselenafulvalene (TMTSF, **4**).[7]

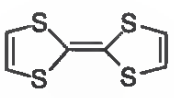

TTF (**1**)

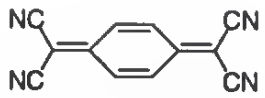

TCNQ (2)

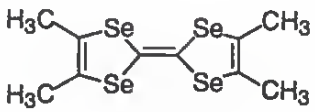

TMTSF (**4**)

Figure 1–1. Structures of the electron donors TTF (**1**) and TMTSF (**4**) and electron acceptor molecule TCNQ (2).

TMTSF (**4**) is similar to TTF (**1**) with four selenium atoms replacing the four sulfur atoms along with four methyl groups substituted in the periphery of the molecule. This molecule soon played a very important role in the development of the molecular conductor field. In 1979 using the monovalent inorganic anion PF_6^-, the material $(TMTSF)_2PF_6$ (**5**) was synthesized by the technique of electrocrystallization by Bechgaard and coworkers. This material turned out to be the first organic superconductor ever synthesized with a T_c of 0.9 K under 12 kbar pressure.[8] The goal of superconductivity that Little proposed 15 years earlier was realized. Bechgaard followed up by reporting in 1980 the electrocrystallization of a series of the selenium-based TMTSF (**4**) superconducting materials known as the Bechgaard salts[9] which have the general formula $(TMTSF)_2X$ (where $X = PF_6^-$ (**5**), AsF_6^- (**6**), SbF_6^- (**7**), TaF_6^- (**8**), ReO_4^- (**9**), FSO_3^- (**10**)). They all display

superconducting behavior with T_c values of approximately 1 K under pressures ranging from 5 to 12 kbar. The next year Bechgaard and coworkers reported another first. They reported the synthesis via electrocrystallization of the first organic crystal $(TMTSF)_2ClO_4$ (**11**) which exhibited superconductivity under ambient pressure.[10] The success of Bechgaard using **4** to synthesize highly conducting materials led to the beginning of a significant effort into the design and synthesis of new chalcogen-rich donor molecules which subsequently led to the synthesis and characterization of new families of highly conducting partial oxidation state salts.

1–1 Organic Superconductors

1–1–1 BEDT-TTF-Based Conductors

Another system that has shown considerable interest since the discovery of the Bechgaard salts are materials based on the bis(ethylenedithio)tetrathiafulvalene (BEDT-TTF, **12**) donor molecule. The synthesis of **12** was first reported in 1978 by Mizuno et al.[11] The compound consists of the TTF (**1**) core with terminally bis-substituted ethylenedithio groups. This donor was used in the formation of $(BEDT\text{-}TTF)_2ReO_4$ (**13**),

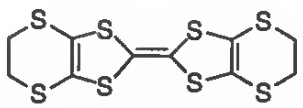

BEDT-TTF (**12**)

Figure 1–2. Structure of electron donor BEDT-TTF (**12**).

the first superconductor based on **12** and also the first sulfur-based superconductor. It was reported in 1983 to have a T_c of 2.0 K (4.5 kbar).[12] This discovery was soon followed up by the first ambient pressure superconductor (T_c = 1.4 K) based on the BEDT-TTF (**12**), β-$(BEDT\text{-}TTF)I_3$ (**14**).[13] To date, the BEDT-TTF-based materials comprise

the largest number of organic superconductors. Also the material k-(BEDT-TTF)$_2$Cu[N(CN)$_2$]Cl (**15**), holds the highest superconducting critical temperature to date for a molecular superconductor of 12.8 K[14] at ambient pressure with the bromide analog κ-(BEDT-TTF)$_2$Cu[N(CN)$_2$]Br (**16**), holding the second highest T_c of 11.6 K.[15,16] Most recently a significant finding in the world of organic superconductors was reported that contained BEDT-TTF (**12**). Peter Day and coworkers reported the synthesis of β-(BEDT-TTF)$_4$[(H$_2$O)Fe(C$_2$O$_4$)$_3$]·C$_6$H$_5$CN (**17**).[17] This complex is the first of its kind to exhibit superconductivity (T_c = 7.0 K) containing a magnetic counterion that contains the paramagnetic Fe(III) metal ion. It has long been thought that the properties of superconductivity and magnetism are inimical.

The success of the BEDT-TTF (**12**) donor in the synthesis of highly conducting superconducting materials has led researchers to study a large array of chalcogen-based symmetrical and unsymmetrical analogs of **12**. Some examples of similar symmetrical BEDT-TTF (**12**) analogs are bis(methylenedithio)tetrathiafulvalene (BMDT-TTF, **18**), hexamethylenetetraselenafulvalene (HMTSF, **19**) and bis(ethylenedioxo)tetrathiafulvalene (BEDO-TTF, **20**). A couple of examples of unsymmetrical analogs of **12** that have been studied are dimethyl(ethylenedithio)diselenadithiafulvalene (DMET, **21**) and ethylenedithiotetrathiafulvalene (EDT-TTF, **22**). These analogs have also led to non-integer oxidation state complexes that have exhibited metallic and even superconducting properties.[16,18]

1–1–2 Fullerenes

The class of molecular conductors based on fullerenes is a new but exciting area of research. Buckminsterfullerene (C$_{60}$, **23**) was first reported only recently in 1990 by Krätschmer and coworkers.[19] The structure of **23** is that of sixty carbon atoms in a spherical soccer ball-like array. C$_{60}$ (**23**) is synthesized by the resistive heating of graphite

at high temperatures under an inert atmosphere. The resulting soot is extracted a number of times with hexane or toluene to isolate **23** from a number of other C_n derivatives.[20] This

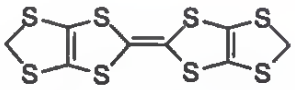

BMDT-TTF (**18**)

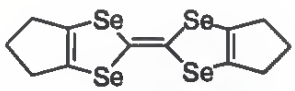

HMTSF (**19**)

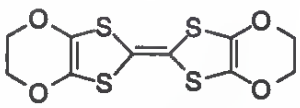

BEDO-TTF (**20**)

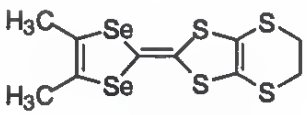

DMET (**21**)

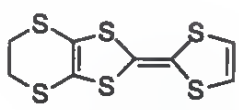

EDT-TTF (**22**)

Figure 1–3. Structures of selected BEDT-TTF (**4**) electron donor analogs BMDT-TTF (**18**), HMTSF (**19**), BEDO-TTF (**20**), DMET (**21**) and EDT-TTF (**22**).

compound has been used to synthesize new superconducting materials with the first being reported only a year after the report of the first synthesis and identification of C_{60} (**23**). The alkali metal fulleride complex, K_3C_{60} (**24**), reported by Hebard et al. displayed superconducting behavior with a T_c of 18 K.[21] Shortly thereafter, the synthesis and conductivity properties of the salt $RbTl_2C_{60}$ (**25**) was published and showed to have superconducting electrical behavior with a T_c of 45 K.[22] This T_c value is the highest for an alkali metal fulleride and is almost four times greater than that of the highest BEDT-TTF salt T_c of 12.8 K (κ-(BEDT-TTF)$_2$Cu[N(CN)$_2$]Cl, **15**).[14]

1–2 Metal Oxide Superconductors

An area of synthetic conductors based solely on inorganic materials are the "high T_c" copper oxide superconductors. Research efforts in this area exploded in 1986 when a group of scientists at IBM Zurich synthesized a lanthanum-barium-copper oxide ceramic ($La_{2-x}Ba_xCuO_4$, **26**) which reaches a superconducting transition state at 30 K.[23] At that time this material set the record for the highest T_c value. This value was quickly surpassed a few months later when a collaboration of research groups at the Universities of Houston and Alabama reported the synthesis of $YBa_2Cu_3O_7$ (**27**) which has a T_c of 93 K.[24] The significance of this discovery was that the material not only reached a new record for T_c, but the superconducting state was reached at a higher temperature than that of liquid nitrogen of 77 K. About a year after the discovery of **27**, a group at IBM San Jose increased the T_c value by more than 30 K with the discovery of $Tl_2Ba_2Ca_2Cu_3O_{10}$ (**28**) which has a T_c of 125 K.[25] Much effort has subsequently gone into the high T_c materials after the initial discovery in 1986 with the material $HgBa_2Ca_2Cu_3O_{8+\delta}$ (**29**) reported by Schilling et al. holding the current highest T_c of ~150 K under high pressure.[26] This, like many of the other high T_c materials, is synthesized by mixing powdered samples of the component atoms in their elemental forms or as salts. This is followed by placing the finely ground and mixed samples in containers made of steel or quartz. The contained samples are then placed in annealing ovens and are heated to high temperatures followed by controlled and gradual decreases in temperature typically over a period of several hours to several days.

Lastly, later in the same year as the discovery of **29**, a French group reported that a sequentially deposited cuprate film was suggested to have evidence of superconductivity at 250 K.[27] While the stoichiometry of the film was not exactly determined, they report the material belongs to the BiSrCaCuO family of compounds. This film, with a thickness of approximately 30 nm, showed a five orders of magnitude drop in resistivity at 250 K and

showed a resistivity low of <1 Ω/cm at 208 K but did not eventually reach zero resistance.[27] These results clearly show a sample of the incredible electrical properties of the high T_c materials which continues to be a well researched area of science.

1–3 Coordination Complex Conductors and Superconductors

1–3–1 MBDT-Based Conductors

Another class of materials that have played an important role in the development of solid state chemistry of molecular conductors are the metal bis-dithiolene (MBDT) complexes of general formula $[M(S_2C_2R_2)_2]^{n-}$ (**30**) (where M = Ni(II), Pd(II), Pt(II), Cu(II); R = H, CH_3, CN, CF_3; $0 \leq n \leq 2$). The MBDT complexes being more inorganic in nature, are similar to TCNQ (**2**) because they both are capable of forming stable anion

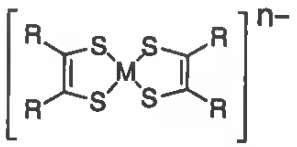

MBDT (**30**)

Figure 1–4. Structure of metal bis-dithiolene anion radical complexes.

radical species from reversible electron transfer reactions.[28,29] By using square planar coordinating metal centers along with the extensive conjugation and chalcogen atoms in the backbone of the planar bis-dithiolene ligands, the complexes become structurally similar to TTF (**1**) and TCNQ (**2**). This type of structure allows for the MBDT complexes to stack in close packed arrangements in the crystal lattice with a large amount of intermolecular overlap which results in the establishment of a delocalized band structure. The MBDT complexes are advantageous over **2** in the respect that they can be systematically varied and tuned via changing the metal atom and the substituents on the dithiolene ligands without

changing the overall charge on the MBDT species.[30] When M = Ni(II) and R = H, the neutral $Ni(S_2C_2H_2)_2$ (**31**) was reacted with TTF (**1**) and a similar charge transfer reaction similar to the TTF-TCNQ (**3**) system resulted. Two different materials of compositions $(TTF)_2[Ni(S_2C_2H_2)_2]$ (**32**) and $(TTF)_2[Ni(S_2C_2H_2)_2]_3$ (**33**) were isolated. The complexes showed similar electrical properties with each exhibiting semiconductivity with room-temperature conductivities of 10^{-7}-10^{-2} S/cm.[31-33] By changing the substituent from H to CF_3 and keeping M = Ni(II), the 1:1 complex $(TTF)[Ni(S_2C_2(CF_3))_2]$ (**34**) is formed. This is also seen when M = Pt. Unfortunately, the complexes are insulators as the TTF (**1**) and $M(S_2C_2(CF_3))_2$ units form stacks of alternating donor and acceptor units.[34-36] Because of this manner of alternated stacking, these donor-acceptor complexes along with when M = Cu and Au (which are synthesized differently), have exhibited interesting ferro- and antiferromagnetic properties but poor electrical conductivity properties.[37-41] A significance of the MBDT work is that it shows that organic-based systems with metal ions can behave similar to purely organic donor and acceptor molecules such as TTF (**1**) and TCNQ (**2**). These results opened up a new area of molecules made up of coordination complexes to be used in the construction of new electrically conducting materials.

Another variation to the MBDT complexes is when the dithiolene substituents are cyano groups. Amongst the MBDT complexes these have been the most widely studied. The ligand termed mnt (mnt = $C_4N_2S_2^{2-}$ = maleonitriledithiolate = *cis*-1,2-dicyanoethylene-1,2-dithiolate, **35**), was first synthesized by Bähr and Schleitzer in 1955.[42] In 1981, the first one-dimensional metal complex based on the mnt ligand was reported. This complex $Li_{0.82}(H_3O^+)_{0.33}[Pt(mnt)_2]\cdot 1.67H_2O$ (**36**),[43-45] which was reported by Underhill and coworkers, contains the $[Pt(mnt)_2]$ unit which exhibits room-temperature single-crystal conductivities ranging from 20 to 300 S/cm, and retains metallic behavior down to 200 K where there is a metal-to-semiconducting transition. In this material, X-ray structure analysis has shown that the planar $[Pt(mnt)_2]^{1.18-}$ units are

arranged and packed in eclipsed equidistant stacks within the crystal lattice with short Pt-Pt distances of only 3.639 Å along the long axis of the needle crystals.[43,44] This type of stacking where infinite chains of Pt atoms are formed from the overlap of $5dz^2$ orbitals is seen in the thoroughly studied tetracyanoplatinate (TCP)[46] and bis(oxalato)platinate salts.[47] Most notably amongst the TCP salts is the complex $K_2[Pt(CN)_4Br_{0.3}]\cdot 3H_2O$ (KCP, **37**).[48,49] This complex was synthesized from bromine oxidation of $K_2[Pt(CN)_4]\cdot 3H_2O$ (**38**). Electrical conductivity measurements of **37** revealed a range of room-temperature single-crystal measurements of 4 to 1050 S/cm and exhibits metallic-like electrical behavior down to 100 K where it undergoes a metal to semiconducting transition. The KCP (**37**) material is interesting because of its band structure where the main interaction pathway is through the metal-based dz^2 orbitals and upon oxidation by bromine, charge is removed from the HOMO dz^2 orbitals. This results in a highly conducting non-integer oxidation state material and shortening of the Pt-Pt distance.

Another mnt-based complex is (BEDT-TTF)$[Ni(mnt)_2]$ (**39**).[50,51] This complex first reported in 1985 by Underhill and coworkers, was electrocrystallized from a solution of BEDT-TTF (**12**) and $[Ni(mnt)_2]^-$ (**40**). Although composed of materials that have been used in the assembly of metallic and superconducting materials, in this instance only an integer oxidation state material was obtained. The room-temperature conductivity was low ($\sim 10^{-6}$ S/cm) and the material turned out to be only a semiconductor.

1–3–2 M(dmit)$_2$-Based Conductors

The coordination complexes that have shown the most interesting electronic properties has been that of the $[M(dmit)_2]^{n-}$ (**41**) (where M = Ni(II), Pt(II), Pd(II), Cu(II), etc.; dmit = $C_3S_5^{2-}$ = 2-thione-1,3-dithione-4,5-dithiolato, **42**; $0 \le n \le 2$) complexes and its analogs. Since its reported synthesis in 1977, a large amount of research has gone into the coordination, solid state characterization and organic chemistry of the dmit ligand which has resulted in the publishing of several review articles.[30,52-55]

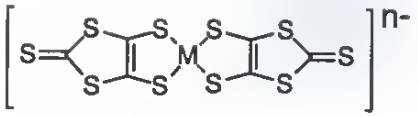

$[M(dmit)_2]^{n-}$ (**41**)

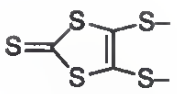

dmit (**42**)

Figure 1–5. Illustrations of the dmit ligand (**42**) and metal bis-dmit complexes (**41**).

The synthesis and characterization of dmit (**42**) was first reported in 1975,[56] but was probably first synthesized 48 years previous in 1927 by Fetkenheuer and coworkers.[57] They reported a procedure where carbon disulfide was reacted in the bulk with sodium metal followed by exhaustive methylation of the mixture. They believed they had synthesized the product which was assigned the structure dimethyl tetrathiooxalate (**43**), but had actually made the dimethylated version of **42**, 4,5-bis(methylthio)-1,3-dithiole-2-thione (**44**), as proven by the elemental analysis results.[55] Tetrathiooxalate (**45**) is an intermediate compound formed during the synthesis of the dmit ligand dianion (**42**). Nevertheless, **42** was first accurately reported in 1975 by Hoyer and coworkers at

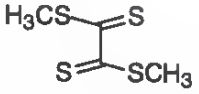

Dimethyl tetrathiooxalate (**43**)

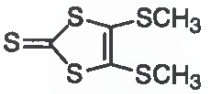

4,5-Bis(methylthio)-1,3-dithiole-2-thione (**44**)

Figure 1–6. Structures of dimethyl tetrathiooxalate (**43**) and 4,5-bis(methylthio)-1,3-dithiole-2-thione (**44**).

Leipzig.[56] They reacted potassium metal with an excess of carbon disulfide in DMF. A variety of products were made but the dmit ligand was isolated cleanly by its coordination to Zn^{2+} in a mixture of methanol and water followed by precipitation using a tetraalkylammonium cation to synthesize the salt $(R_4N)_2[Zn(dmit)_2]$ (**46**). The name of the

ligand, dmit (**42**), came about from the earlier days of nomenclature of heterocyclic sulfur chemistry. The 1,2-dithiole-3-thione portion of **42** was named isotrithione. The four and five positions of the molecule the dithiolato groups reside, or in earlier nomenclature, dimercapto groups. Thus the name dimercaptoisotrithione was used for the ligand and has been used ever since.[55,58,59]

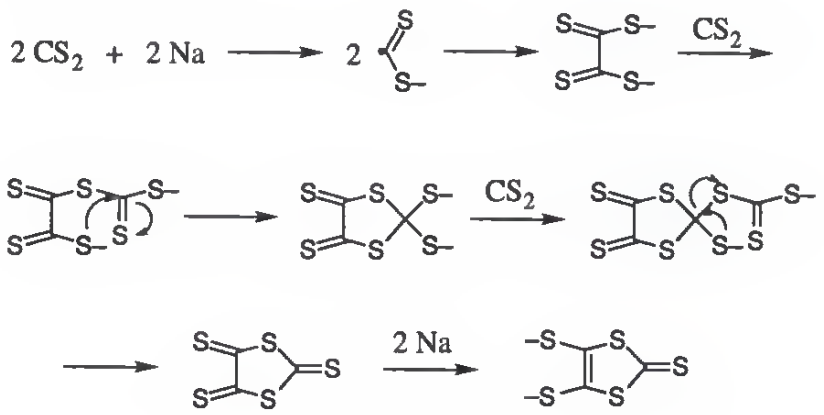

Figure 1–7. Reaction mechanism of the synthesis of dmit (**42**).

In a later full publication by the Hoyer group in 1979,[60] they reported the synthetic procedures to convert the Zn(II) metal center to Ni(II), via the dibenzoyl deriviative of **42**, and oxidation of the complex to the monoanionic form using NaI/I_2. Using the square planar coordinating metal center Ni(II), along with the planarity of the dmit ligand (**42**), the complex possessed interesting structural properties similar to the molecular donors TTF (**1**) and BEDT-TTF (**12**) along with the MBDT complexes of $[Ni(S_2C_2H_2)_2]$ (**31**) and $[Ni(mnt)_2]$ (**47**). The complex $[Ni(dmit)_2]^{n-}$ (**48**), which can be isolated as its dianionic, monoanionic or neutral form, displays full planarity and extensive π conjugation. Also there are ten sulfur atoms in the periphery of the molecule, two more than that of BEDT-TTF (**12**). These structural properties make it a viable compound to be used in the assembly of molecular electrically conducting materials. In 1983, the complex

$(Bu_4N)_2[Ni(dmit)_2]_7 \cdot 2CH_3CN$ (**49**) was reported by Cassoux and coworkers at Toulouse.[61,62] This complex, which was synthesized by the technique of electrocrystallization, showed semiconducting behavior with a room-temperature conductivity of approximately 10 S/cm. Although only semiconducting behavior was found, this discovery led many groups to begin studying $Ni(dmit)_2$ for use in the design and construction of molecular electrically conducting materials. Soon after in 1984, Cassoux and coworkers reported the non-integer oxidation state complex $(TTF)[Ni(dmit)_2]_2$ (**50**).[63-67] This was the first $Ni(dmit)_2$-based complex using an "open-shell" counterion. The complex was synthesized via slow inter-diffusion of saturated solutions of $(TTF)_3(BF_4)_2$ (**51**) and $(Bu_4N)[Ni(dmit)_2]$ (**52**) at 30-46 °C using a three-compartment H-shaped glass cell. This discovery was a breakthrough for $Ni(dmit)_2$ solid state chemistry because it was the first $Ni(dmit)_2$-based superconductor synthesized. The complex has a high single-crystal room-temperature conductivity of 300 S/cm and exhibits metallic-like behavior at ambient pressure down to 1.5 K where it had a peak conductivity at ambient pressure of 1.5×10^5 S/cm. Pressure-dependence studies of the material showed the material to behave as a superconductor with a T_c of 1.62 K under 7 kbar pressure.

The structure of $(TTF)[Ni(dmit)_2]_2$ (**50**) consists of segregated stacks of donor and acceptor molecules, but within the stacks of the $Ni(dmit)_2$ units, the units are separated by distances larger than the sum of the van der Waals radii of sulfur (3.70 Å)[68] which prevents intrastack interactions. There are though extensive interstack interactions from non-bonding S···S orbital overlap between the $Ni(dmit)_2$ stacks and also between the $Ni(dmit)_2$ and TTF stacks resulting in a three-dimensional network.

A second $Ni(dmit)_2$-based superconductor was synthesized by electrocrystallization in 1987. The salt, $(Me_4N)[Ni(dmit)_2]_2$ (**53**), was the first $Ni(dmit)_2$-based to behave as a metal with a spectator "closed-shell" counterion and did so down to 100 K.[69-71] Under a pressure of 7 kbar, the material has a T_c of 5.0 K. The room temperature conductivity is

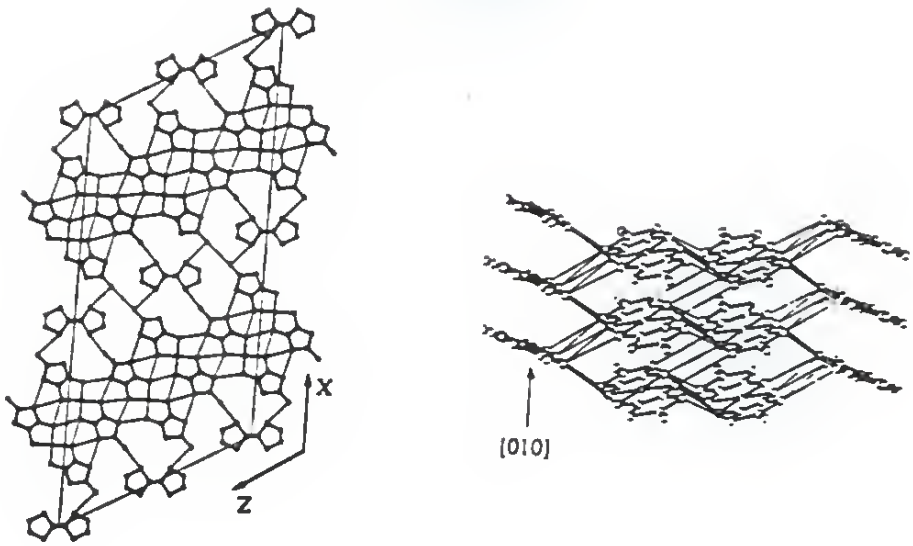

Figure 1–8. Two views of the three-dimensional crystal structure of (TTF)[Ni(dmit)$_2$]$_2$ (**50**).[64]

50 S/cm and the structure determined by X-ray was shown to have columns of stacked Ni(dmit)$_2$ units separated by columns of isolated Me_4N^+ counterions. There are extensive non-bonding S···S intermolecular and interstack interactions of the Ni(dmit)$_2$ units, but unlike in (TTF)[Ni(dmit)$_2$]$_2$ (**50**), there are no interactions between the columns of Ni(dmit)$_2$ and Me_4N^+ moieties. The structure has two-dimensional connectivity whereas in the TTF analog it is three-dimensional.[63-67]

A series of alkali metal Ni(dmit)$_2$-based complexes have been electrocrystallized in acetonirile solutions of general formula M[Ni(dmit)$_2$]$_2$ (M = Li, Na, K).[72,73] The material when M = Li (**54**), showed only semiconducting behavior with a 0.5 S/cm room temperature conductivity. When M = Na (**55**) or K (**56**), both materials behaved as metals with **56** having been reported a high conductivity of 230 S/cm. Pressure dependence studies of the conductivity although showed no evidence of supercondcutivity.

Soon after the initial successes of the $Ni(dmit)_2$-based complexes, the palladium analog of $M(dmit)_2$ was used to construct materials with interesting electrical properties. In 1986, the research group at Toulouse reported different phases of $(TTF)[Pd(dmit)_2]_2$.[74-82] The material was synthesized via slow interdiffusion of saturated solutions of $(TTF)_3(BF_4)_2$ (**51**) and $(Bu_4N)[Pd(dmit)_2]$ (**57**) in acetonitrile. The phases reported of $(TTF)[Pd(dmit)_2]_2$ are denoted α (58), α' (**59**) and δ (**60**). The α and α' phases are the same crystallographically and are the same as that of $(TTF)[Ni(dmit)_2]_2$ (**50**) (monoclinic, C-centered). In α-$(TTF)[Pd(dmit)_2]_2$ (**58**), the room-temperature conductivity is 750 S/cm, and upon cooling down to 220 K a phase change occurs to a triclinic β (**61**) phase where the conductivity becomes semiconducting from metal-like.[74-76] When the material is then warmed back to room temperature, another phase change occurs at 230-240 K after several temperature cycles. This new phase is a modification of the triclinic β phase and is denoted the γ phase (**62**). The α→β→γ transition is irreversible and is a unique characteristic of α-$(TTF)[Pd(dmit)_2]_2$ (**58**). When the material is subjected to high pressure, it displays superconducting electrical properties with a T_c of 1.7 K (22 kbar). Another phase of $(TTF)[Pd(dmit)_2]_2$ is the α' phase (**59**). It also has a room-temperature conductivity of 750 S/cm and undergoes a transition at approximately 200 K from a metal to a semiconductor. What is unique about the α' from the α phase is that the metal-to-semiconductor transition is reversible. The transition can also be suppressed under high pressures comparable to the α phase at pressures greater than 16 kbar. α'-$(TTF)[Pd(dmit)_2]_2$ (**59**) showed a maximum T_c value of 5.93 K under 24 kbar pressure.[77-79] The γ phase of $(TTF)[Pd(dmit)_2]_2$ (**62**) are plateletlike crystals obtained alongside needle crystals of the α and α' phases in the slow interdiffusion synthesis. In this phase, the $Pd(dmit)_2$ moieties form dimers with only 3.11 Å Pd···Pd intermolecular distances. The structure is also characterized by the dimers forming columns separated by sheets of TTF molecules and absent of intercolumn S···S interactions. The material also displays metallic character with a room-temperature conductivity of 100 S/cm but is not

able to achieve a superconducting state like the α and α' phases under applied pressures.[80-82]

The $M(dmit)_2$-based non-integer oxidation state compounds have shown superconducting behavior in three more instances. With "closed-shell" spectator ions, the complexes α-$(Et_2Me_2N)[Pd(dmit)_2]_2$ (**63**) and β-$(Me_4N)[Pd(dmit)_2]_2$ (**64**) exhibit T_c's of 4 (2.4 kbar)[83] and 6.2 K (6.5 kbar)[84] respectively. Most recently a Japanese group electrocrytsallized the material α-(EDT-TTF)$[Ni(dmit)_2]$ (**65**) which resulted in the seventh $M(dmit)_2$-based complex to exhibit superconductivity.[18] This complex is unique though from the rest of the $M(dmit)_2$ superconductors in that it is the only one to do so at ambient pressure with a T_c of 1.3 K. The β-phase, which is also obtained in the same electrocrystallization experiment, forms mixed stacks of EDT-TTF and $Ni(dmit)_2$ units which results in semiconducting electrical properties.

Several other chalcogen analogs of the dmit ligand (**42**) have also been used in highly electrically conducting semiconducting and metallic-like materials, but as yet only the all sulfur containing **42** has been used to make superconducting materials. The chalcogen analogs of dmit (**42**) include 2-oxo-1,3-dithiole-4,5-dithiolato (dmid, **66**),[85] 2-selenolato-1,3-dithiole-4,5-dithiolato (dmise, **67**),[86] 2-thioxo-1,3-dithiole-4,5-diselenolato (dsit, **68**),[87] 2-selenoxo-1,3-dithiole-4,5-diselenolato (dsise, **69**),[86] 2-selenoxo-1,3-diselenole-4,5-diselenolato (dsis, **70**)[88] and 3-thioxo-1,2-dithiole-4,5-dithiolato (dmt, **71**).[60,89,90]

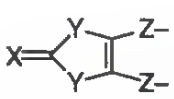

dmit (X=Y=Z=S) (**42**)
dmid (X=O, Y=Z=S) (**66**)
dmise (X=Se, Y=Z=S) (**67**)
dsit (X=Y=S, Z=Se) (**68**)
dsise (X=Z=Se, Y=S) (**69**)
dsis (X=Y=Z=Se) (**70**)

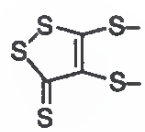

dmt (**71**)

Figure 1–9. Chalcogen analogs of the dmit ligand dianion (**42**).

Due to the extensive amount of research reported based on the dmit ligand (**42**), an exhaustive review of the work will not be covered. To name a few, other applications of **42** include using the ligand to form highly conducting thin films via the Langmuir-Blodgett technique,[91-93] the synthesis of magnetic materials,[94] other areas of coordination[95-97] and organic chemistry.[55]

1–4 Electrocrystallization

The electrocrystallization of non-integer oxidation salts at a platinum wire electrode is performed by applying minimal amounts of current to solutions containing the electroactive species and electrolyte of choice. A two-compartment glass H-cell with a fine

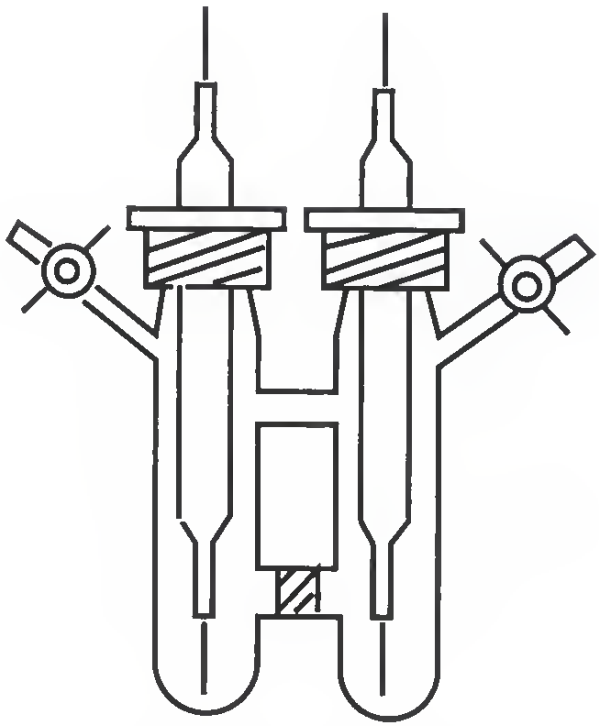

Figure 1–10. Drawing of the glass H-cell and electrodes used in electrocrystallization experiments.

porosity frit and an argon purge line separating the compartments is used. Each compartment contains a Pt wire electrode acting as either the anode or cathode with leads connected to a constant current source.

A minimal amount of current is applied such that the reaction and subsequent crystallization reaction takes place at a very slow rate. The current is then kept at this minimum value until the electrocrystallization is complete. Too high of current densities result in fast crystal growth which tends to lead to crystals of poor morphology. At the end of this period the crystals are harvested and studied. The technique of electrocrystallization is the most widely used general method today for the synthesis of molecular conductors and has been used in the synthesis of the majority of organic superconductors.[98]

1–4–1 Mechanism of Electrocrystallization

In the first paper published devoted to the study and understanding of the mechanism and kinetics of electrocrystallization, Michael Ward best states that electrocrystallization is, "...the electrochemical conversion of a reagent into an ionic species capable of forming a precipitate via condensation with a second reagent at the working electrode."[99] There have been few reported studies of the mechanism of electrocrystallization and those have only been published recently over the last few years.[99-102] Ward studied the electrocrystallization process of TTF (**1**) and TCNQ (**2**)-based partial oxidation state salts using an electrochemical quartz crystal microbalance (EQCM). The EQCM technique is able to determine mass changes such as deposition and crystallization of a non-integer oxidation state material at the surface of an electrode via changes in the frequency of the piezoelectric crystal.[99]

In 1993, Cassoux and coworkers published a paper on the electrochemical studies of the formation mechanism of $(cation)_x[Ni(dmit)_2]$ electrically conducting materials and their non-integer oxidation states.[102] They used the technique of cyclic voltammetry to study the formation mechanism of the salts. Fig. 1–11 shows the cyclic voltammogram of

$(NHMe_3)_2[Ni(dmit)_2]$ (**72**), the primary compound studied in their report. The first redox process denoted by peaks (a) and (b) ($E_{1/2}$ = –0.17 V) in the figure is reversible with a peak-to-peak separation of 58 mV. Scan rate dependence studies of this complex on the

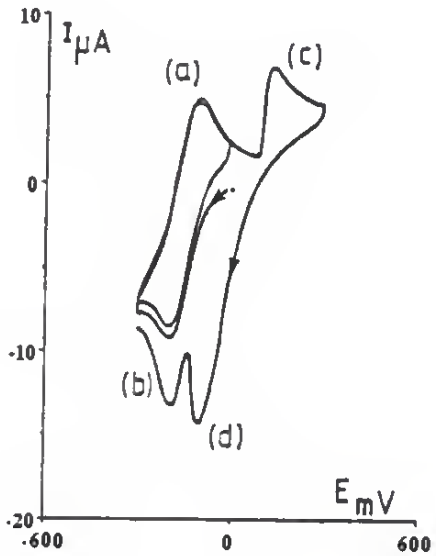

Figure 1–11. Cyclic voltammogram of $(NHMe_3)_2[Ni(dmit)_2]$ (**72**).[102]

first redox couple shows that the oxidation peak (I_p) is proportional to the square root of the potential-scan rate, $\upsilon^{1/2}$, and the process is diffusion controlled.[103] All of these results show that the first redox couple denoted by peaks (a) and (b) correponds to a simple monoelectronic process illustrated by:

$$[Ni(dmit)_2]^{2-} \rightleftharpoons [Ni(dmit)_2]^{-} + e^{-}$$

The peaks concerned with the second redox process are labeled (c) and (d) in Fig. 1–11. Scan rate dependence studies of the the oxidation peak of this second redox couple shows that it is not purely diffusion controlled. As they scanned to higher potentials the

current upon cycling increased and a black deposit was observed on the working electrode. Concerning the cathodic peak denoted (d), the intensity of the peak is proportional to the scan rate, υ. The redissolution peak intensity is also related to the amount of material deposited on the electrode, as their studies showed that an increase in current is observed when scanning to higher potentials which is indicative of the material being deposited is electrically conducting. All of these properties show that this is characteristic of a redissolution process. Elemental analysis results of the black deposited material showed that the stoichiometry is approximately $(NHMe_3)_{0.5}[Ni(dmit)_2]$ (**73**). This same material was obtained previously via electrocrystallization with the same stoichiometry proven by X-ray structure analysis and exhibited metallic-like behavior down to 120 K with room-temperature single-crystal conductivities ranging from 100 to 500 S/cm.[104-106] This second redox process can be attributed to non-integer oxidation state material formation illustrated by:

$$[Ni(dmit)_2]^- \longrightarrow [Ni(dmit)_2]^{x-} + (1 - x)e^-$$

The study by Cassoux and coworkers then went on to examine the redox processes at higher scan rates. At scan rates above approximately 800 V/s they observed the absence of the redissolution peak seen at lower scan rates, thus a material is not depositing. At increasing scan rates, the ratio $I_p(d)/I_p(c)$ tends to 1. This is indicative of the redox couple being reversible. Under these experimental conditions, the second redox couple can be attributed to the formation of a neutral species from a monoanionic one. Therefore the formation and deposition of a non-integer oxidation state material onto the electrode must be due to subsequent chemical reaction of the neutral species in the diffusion layer following its formation. This electrochemical-chemical process can be illustrated by the following schemes with firstly, the formation of the neutral species:

$$[Ni(dmit)_2]^- \longrightarrow [Ni(dmit)_2]^0 + e^-$$

This is followed by the formation of the partial oxidation state material from the chemical reaction in the diffusion layer between $[Ni(dmit)_2]^-$ and $[Ni(dmit)_2]^0$ shown as follows:

$$n[Ni(dmit)_2]^- + m[Ni(dmit)_2]^0 \longrightarrow \{[Ni(dmit)_2]^{x-}\}_{n+n}$$

(where $x = n/(n+m)$)

The last step is the deposition of the non-integer oxidation state material on to the electrode shown in the reaction scheme as follows:

$$\{[Ni(dmit)_2]^{x-}\}_{n+m}(solution) \longrightarrow \{[Ni(dmit)_2]^{x-}\}_{n+m}(electrode)$$

The study also proved using a variety of cations (i.e. Ph_4As^+, Bu_4N^+, H_3MeN^+ and $H_2Me_2N^+$), that the general electrochemical behavior of $[Ni(dmit)_2]^{2-}$ is not affected by the nature of the cation used. The final composition and structure of the deposited material and its ensuing conductivity behavior is dependent upon reaction conditions such as size and type of counterion of choice and the solvent used for the electrocrystallization experiment.

1–5 Bimetallic and Monometallic Complexes

In 1985, a paper by Roald Hoffman and associates was published that discussed the structural, chemical and electrical properties of transition-metal bisdithiolenes and tetrathiolenes via qualitative MO and band structure calculations.[107] In that article, Hoffman et al. propose that in the development of new materials, building blocks of appropriate materials must be used to construct materials of three-dimensional connectivity

to prevent Peierls distortions inherent in low-dimensional systems. A Peierls distortion is a transition from a state of higher energy to one of lower energy. With the lowering of temperature, one-dimensional metallic systems undergo periodic lattice distortions resulting in the opening up of a band gap at the Fermi level. This leads to a semiconducting or even insulating state of lower energy than the metallic state. Peierls distortions are commonly seen in one-dimensional chain systems such as in the tetracyanoplatinate (TCP) and bis(oxalato)platinate salts.[46,47] One way to suppress the Peierls distortion in low dimensional systems is to increase the dimensionality via building blocks that promote intra- and interstack interactions to stabilize a highly conducting metallic state. In (TTF)[Ni(dmit)$_2$]$_2$ (**50**), their are inter- and intrastack interactions that lead to a system with three-dimensional connectivity which results in the stabilization of a metallic state down to 4 K.[63-67] Hoffman and coworkers propose instead of using dithiolate ligands, to use bis-coordinating tetrathiolate ligands with square planar coordinating metals. Ligand systems they suggest to assemble highly dimensional architectures are ethylenetetrathiolate (ett, **74**), tetrathiosquarate (ttsq, **75**) and tetrathiafulvalenetetrathiolate (ttft, **76**).

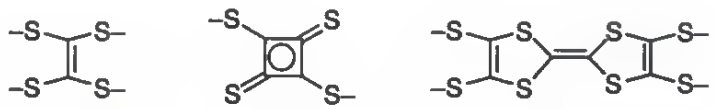

ett (**74**) ttsq (**75**) ttft (**76**)

Figure 1–12. Structures of bridging ligands ett (**74**), ttsq (**75**) and ttft (**76**).

They propose that a variety of stacking modes may result and will form two- and three-dimensional systems leading to suppression of Peierls distortions which in turn should lead to highly conducting systems. The stacking modes they propose are one-

dimensional ribbon-like, two-dimensional ribbon, two-dimensional slabs and a three-dimensional zig-zag network.[107]

There have been several systems constructed similar to the ribbon-like design proposed by Hoffmann et al. In 1979 a series of oligomeric $[M(ttsq)]_n$ (M = Ni(II) (**77**), Pd(II) (**78**) and Pt(II) (**79**)) materials were reported and had conductivities that ranged from ~10^{-7} to ~10^{-4} S/cm.[108] That same year ttft containing materials of composition $[M(ttft)]_n$ (M = Ni(II) (**80**), Pt(II) (**81**), Pd(II) (**82**), Cu(II) (**83**) and Fe(II) (**84**)) were reported with a low conductivity of ~10^{-5} for $[Fe(ttft)]_n$ (**84**) to a high of ~30 S/cm for **80**.[109] In 1983 Poleschner et al. report a high conductivity of ~10^{-1} S/cm for $[Ni(ett)]_n$

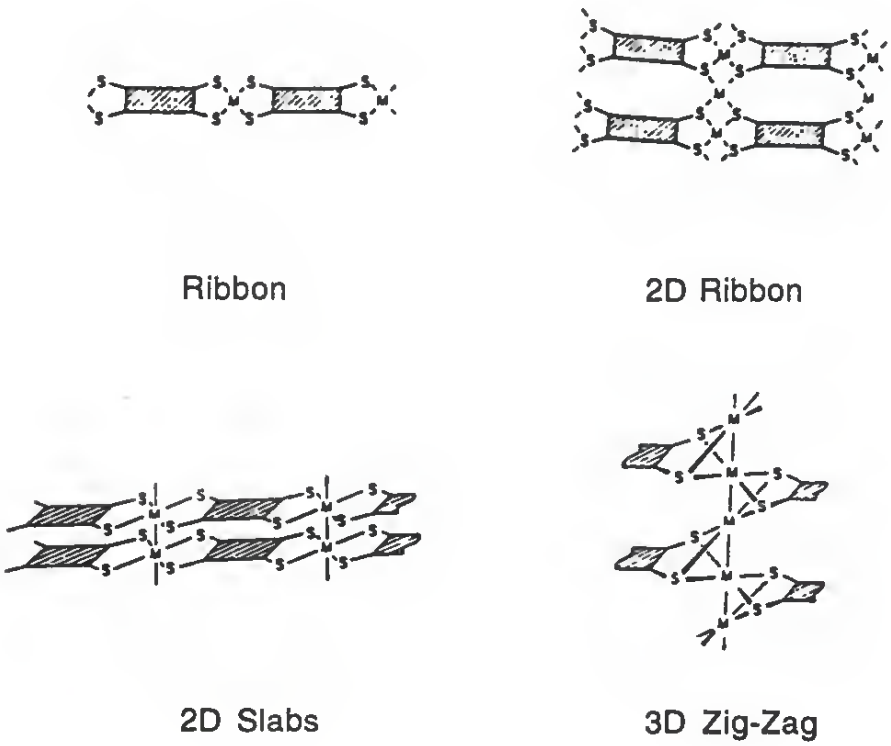

Figure 1-13. Proposed one-, two- and three-dimensional structures by Hoffmann et al.[107]

(**85**).[110] Cassoux and coworkers further studied metal-ett oligomeric materials and showed that the compound $[Na_{0.31}(Ni(ett))]_n$ (**86**) obtained from I_2 oxidation of **85** in solution, yielded a pressed pellet conductivity of 3.8 S/cm and exhibited temperature-dependent metallic behavior.[111]

In the mid-1980's a significant amount of work was completed by Reynolds and coworkers on the synthesis and characterization of metal containing oligomers using the bis-chelating dianionic tetrathiooxalate (tto) ligand (**45**). The general procedure for the formation of the metal-tto oligomers is reaction of $(Et_4N)_2$tto with the metal salt of choice in DMF/methanol mixtures and the resulting insoluble product is filtered and washed.[112] The material was pressed into pellet form and the conductivities range upwards to ~10^2 S/cm. They are intrinsically conducting due to the planar, ribbon-like and extensively delocalized structures resulting from the complexation of metal ions with unfilled d orbitals to planar sulfur-rich ligands with highly delocalized orbitals. A downside to the materials as a result of their structure is their lack of processibility and solublity in organic solvents.[112,113]

Another avenue to the formation of systems proposed by Hoffman et al. are planar, extensively conjugated and chalcogen-rich bimetallic systems using the tetrathiolate ligands as bridging ligands for the formation of molecular materials that are more soluble and easier to handle. Vicente et al. first reported the synthesis of $(Ph_4As)_2\{tto[Cu(dmid)]_2\}$ (**88**) in 1986.[111,114] This complex has Cu(II) metal centers bridged by the side-on coordination of tto and "capped" by dmid, a chalcogen analog of dmit. It was synthesized serendipitously through air oxidation of a solution of $(Ph_4As)_2[Cu(dmid)_2]$ (**89**) in a mixture of acetone and ethanol over a two week period. The synthesis is not reproducible. This complex is not completely planar though with a dihedral angle of 28° formed between the planes of the tto and dmid ligands. In 1994, Rauchfuss and coworkers reported a very interesting complex which was synthesized similar to **88** from air oxidation and degradation of $(As_4P)_2[Ni(S_2C_2S_2C_2(CO_2Me)_2)_2]$ (**90**) in acetonitrile over a period of 24 hours. The bimetallic complex $(Ph_4As)_2\{tto[Ni(S_2C_2S_2C_2(CO_2Me)_2)]_2\}$ (**91**) which has tto (**45**)

bridging Ni(II) metal centers, was synthesized that showed extensive conjugation but terminal out-of-plane methyl ester groups prevent the material from forming close packed structures.[115] Pressed-pellet conductivity measurements of the neutral species of this complex show a conductivity of 10^{-3} S/cm. This is high for an undoped or non-partial oxidation state molecular solid. Lastly, McCullough et al. recently reported a new bimetallic complex based on the ttft bridging ligand (**76**). The complex [Ti(η^5-i-$PrC_5H_4)_2]_2$ttft (**92**) was synthesized but delocalization in the complex is limited to ttft (**76**).[116-118] Synthetically, the complex is difficult to make due to a lengthy procedure, air

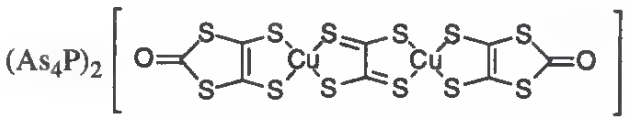

$(As_4P)_2\{tto[Cu(dmid)]_2\}$ (**88**)

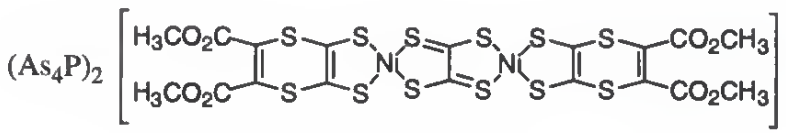

$(As_4P)_2\{tto[Ni(S_2C_2S_2C_2(CO_2Me)_2)]_2\}$ (**91**)

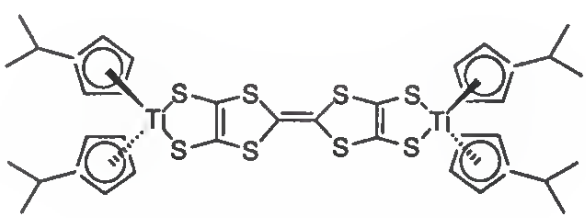

[Ti(h^5-i-$PrC_5H_4)_2]_2$ttft (**92**)

Figure 1–14. Structures of the recently reported extensively conjugated bimetallic complexes $(Ph_4As)_2\{tto[Cu(dmid)]_2\}$ (**88**), $(Ph_4As)_2\{tto[Ni(S_2C_2S_2C_2(CO_2Me)_2)]_2\}$ (**91**) and [Ti(η^5-i-$PrC_5H_4)_2]_2$ttft (**92**) as building blocks to new electronic materials.

and water instability of **76** during the synthesis, and the pyrophoric nature of the final product.

1–6 Applications of Organic-Based Conducting Materials

Charge-transfer and ion radical salt complexes are prevalent in many different areas of chemistry. They have been used in such diverse areas of chemistry such as in the synthesis of electron-donor acceptor copolymers,[119] and in photochemistry involving the design of photsynthesis mimicking energy storage devices.[120,121] Another potential application of these types of materials are in electrically conducting materials. With densities on the order of 1-2 g/cm^3, these lightweight materials have been proposed to be useful for electronics in computers, automobiles, and aircraft as opposed to highly dense copper metal which has a density of 8.96 g/cm^3.[16,122] Copper is the common material used in electrical wiring, with a room-temperature conductivity of approximately 10^6 S/cm. Although the room-temperature conductivity of most of the organic-based materials are much lower than copper, some of the materials reach a superconducting state at low temperatures, whereas copper cannot. This electrical property makes the materials an exciting and inviting area of research. The cuprate high T_c materials have also shown similar properties and the T_c values are usually an order of magnitude higher than their organic-based counterparts. An advantage of the organic materials are their ability to be systematically modified and tailored. As the requirements and mechanisms of superconductivity become better understood, these structurally modifiable organic materials will become increasingly more important.

1–7 Synopsis of Work

This dissertation will focus on the synthesis and characterization of new monometallic and bimetallic extensively conjugated, planar and chalcogen-rich complexes

based on the 2-thioxo-1,3-dithiole-4,5-dithiolato (dmit) ligand (**42**) and its derivatives. These complexes will then be used in the assembly of new electrically conducting non-integer oxidation state complexes.

The first phase of the work focuses on the $[Ni(dmit)_2]^{n-}$ anion. Four complexes have constructed using the Ph_4P^+, Bu_4N^+, Me_3S^+ and $MePh_3P^+$ cations utilizing the technique of electrocrystallization. The X-ray crystal structures of the Ph_4P^+, Me_3S^+ and $MePh_3P^+$ complexes have been characterized and the electronic properties have been examined closely using reflectance spectroscopy and temperature-dependent conductivity measurements.

The second phase of the work has been the design, synthesis and characterization of a series of new bimetallic anionic complexes to be used in the synthesis of a new family of transition metal-based anion radical salt complexes. These new complexes consist of the planar and sulfur-rich tetrathiooxalate (tto) ligand bridging square planar coordinating metal centers (Cu(II) and Ni(II)) and "capped" by the dmit and other analogous chalcogen atom containing dmit ligands. The complexes are designed to extend the delocalization and increase the amount of non-bonding interactions seen in the crystal lattice. This design has been used to increase the dimensionality of the systems to potentially improve the electrical properties and possibly even achieve superconductivity. The complexes of general formula $(C)_2\{tto[M(L)]_2\}$ (C = tetraalkylammonium cation; M = Ni(II) or Cu(II); L = dmit or a chalcogen analog of dmit) have been fully characterized including X-ray analysis and cyclic voltammetry, and also have been studied for their utilization in the formation of non-integer oxidation state complexes achieved chemically and by electrocrystallization.

CHAPTER 2
NEW MOLECULAR CONDUCTORS BASED ON $Ni(dmit)_2$

The $Ni(dmit)_2$ unit has been used in the construction of several metallic and superconducting systems.[53] Using electrocrystallization, non-integer oxidation state materials are assembled with the $Ni(dmit)_2$ units forming close packed arrays. The planarity, π-conjugation and sulfur-rich nature of the structure allows for extensive intermolecular non-bonding contacts which provides electrical conduction pathways within the material. To study and further provide information on the nature of the $Ni(dmit)_2$ complexes, we have synthesized four $Ni(dmit)_2$-based anion radical salt compounds with closed-shell cations, $(Bu_4N)_2[Ni(dmit)_2]_7 \cdot 2CH_3CN$ (**49**),[62,123] $(Me_3S)[Ni(dmit)_2]_2$ (**93**),[123-125] $(Ph_4P)[Ni(dmit)_2]_3$ (**94**),[123, 125-127] and $(MePh_3P)[Ni(dmit)_2]_3$ (**95**),[128,129] via electrocrystallization. These compounds have been characterized by X-ray structure analysis, temperature-dependent electrical conductivity and optical reflectance spectroscopy. Few optical studies have been reported on the $Ni(dmit)_2$-based complexes[126,127,130-135] despite the large number of the complexes that have been synthesized. The structural, transport and optical properties of **49**, **93–95** will be discussed and compared.

2–1 Experimental

General procedures. Elemental analysis was completed at Robertson Microlit Labs Inc. (Madison, NJ) for $(Bu_4N)_2[Ni(dmit)_2]_7 \cdot 2CH_3CN$ (**49**) and $(CH_3)_3SBF_4$ (**99**).

Materials. $(Bu_4N)[Ni(dmit)_2]$ (**52**) was prepared following the procedure described by Steimecke et al.[60] Tetrabutylammonium perchlorate (**96**), tetraphenylphosphonium bromide (**97**) and methyltriphenylphosphonium bromide (**98**) were obtained from Aldrich Chemical Co. and used as received. Trimethylsulfonium tetrafluoroborate (**99**) was obtained from the reaction of trimethylsulfonium chloride (**100**) and silver tetrafluoroborate (**101**, Eastman Chemical Co.) in water, followed by drying under high vacuum at 50 °C overnight. Acetone was used as received from Fisher Scientific and acetonitrile (Fisher Scientific) was dried and distilled over CaH_2 under a stream of nitrogen prior to use.

Prior to use, the glass electrocrystallization cells were soaked for 24 hours in a 10 M HNO_3 bath, followed by thorough washing with deionized water, methanol, and placed in a drying oven for a minimum of four hours or until needed. The platinum wire electrodes were cleaned by immersing them in 1 M H_2SO_4. The anode was connected to the negative end of a 3 V battery and the cathode was connected to the positive end for four minutes. Polarity was reversed for eight minutes, then reversed again for another four minutes. The electrodes were then soaked and rinsed with methanol followed by drying with a heat gun.[16] The electrodes consist of Pt wire (0.5 mm diameter) encased and sealed on one end of a glass tube and connected to copper wire using a small amount of mercury. The copper wire end is also sealed using epoxy resin. Electrocrystallization experiments were set up by placing the cells on racks mounted to a slab of marble which is placed on several layers of foam and carpet. The racks were enclosed in a box to keep out light.

$(Bu_4N)_2[Ni(dmit)_2]_7 \cdot 2CH_3CN$ (**49**).[62] The complex $(Bu_4N)_2[Ni(dmit)_2]_7 \cdot 2CH_3CN$ (**49**) was electrocrystallized in acetonitrile under an argon atmosphere in the presence of 0.1 M tetrabutylammonium perchlorate (**96**) electrolyte. A constant current density of 1.3 $\mu A/cm^2$ was used over a period of 24 days at which time the crystals were harvested and washed with methanol, followed by diethyl ether. Black shiny platelets and needles were obtained and the platelets were chosen for study. Anal. Calcd

for $C_{78}H_{78}N_4Ni_7S_{70}$: C, 25.14; H, 2.11; N, 1.50; Ni, 11.02; S, 60.22. Found: C, 25.10; H, 2.10; N, 1.41; Ni, 10.86; S, 59.97.

Trimethylsulfonium tetrafluoroborate (**99**). Trimethylsulfonium tetrafluoroborate (**99**) was synthesized by the reaction of 2.82 g (0.025 mol) of trimethylsulfonium chloride (**100**) and 4.87 g (0.025 mol) of silver tetrafluoroborate (**101**) dissolved in a minimal amount of water. The mixture was filtered and the solvent was removed from the filtrate to yield a white solid. The solid was washed with cold methanol followed by diethyl ether and was recrystallized from ethanol to yield white crystals of **99**. Yield 3.73 g (91%). Anal. Calcd for $C_3H_9BF_4S$: C, 21.97; H, 5.54. Found: C, 21.80; H, 5.50.

$(Me_3S)[Ni(dmit)_2]_2$ (**93**).[124] The complex $(Me_3S)[Ni(dmit)_2]_2$ (**93**) was electrocrystallized in 1:1 acetone/acetonitrile under an argon atmosphere in the presence of 0.1 M trimethylsulphonium tetrafluoroborate (**99**) electrolyte. A constant current density of 0.5 $\mu A/cm^2$ was used over a period of 26 days at which time the crystals were harvested and washed with methanol, followed by diethyl ether. Black, shiny platelets were obtained for study.

$(Ph_4P)[Ni(dmit)_2]_3$ (**94**). The complex $(Ph_4P)[Ni(dmit)_2]_3$ (**94**) was electrocrystallized in acetonitrile under an argon atmosphere in the presence of 0.075 M tetraphenylphosphonium bromide (**97**) electrolyte. A constant current density of 1.5 $\mu A/cm^2$ was used over a period of 15 days at which time the crystals were harvested and washed with methanol, followed by diethyl ether. Black, shiny, flat needles were obtained for study.

$(MePh_3P)[Ni(dmit)_2]_3$ (**95**). The complex $(MePh_3P)[Ni(dmit)_2]_3$ (**95**) was electrocrystallized in 3:1 acetonitrile/acetone under an argon atmosphere in the presence of 0.06 M methyltriphenylphosphonium bromide (**98**) electrolyte. A constant curent density of 0.9 $\mu A/cm^2$ was used over a period of 18 days at which time the crystals were harvested and washed with methanol, followed by diethyl ether. Black, shiny platelets and needles were obtained and platelets were chosen for study.

X-ray structure determinations. Crystallographic data for complexes **93–95** is compiled in Appendix Tables A-1 to A-9. Thermal ellipsoids drawings and molecular numbering schemes for the $Ni(dmit)_2$ units in complexes **93–95** are located in Figs. 2–1, 2–2 and 2–3 respectively. Data were collected at room temperature (298 K) on crystals of complexes $(Me_3S)[Ni(dmit)_2]_2$ (**93**) (crystal size: 0.41 x 0.34 x 0.05 mm^3) and $(Ph_4P)[Ni(dmit)_2]_3$ (**94**) (0.49 x 0.19 x 0.04 mm^3) and at 173 K for $(MePh_3P)[Ni(dmit)_2]_3$ (**95**) (0.23 x 0.1 x 0.08 mm^3). For complexes **93** and **94**, data were collected on a Siemens R3m/V diffractometer and for **95** on a Siemens SMART PLATFORM equipped with a graphite monochromator utilizing MoKα radiation (λ = 0.71073 Å). For $(Me_3S)[Ni(dmit)_2]_2$ (**93**), 6161, for $(Ph_4P)[Ni(dmit)_2]_3$ (**94**), 3837, and for $(MePh_3P)[Ni(dmit)_2]_3$ (**95**), 8192 reflections were collected using the ω-scan method. For **93** and **94**, four reflections were measured every 96 reflections, and for **95**, the first 50 frames were remeasured at the end of data collection to monitor instrument and crystal stability (maximum correction on I was < 1%). For $(Me_3S)[Ni(dmit)_2]_2$ (**93**) and $(Ph_4P)[Ni(dmit)_2]_3$ (**94**), psi scan absorption corrections were applied based on measured crystal faces using *SHELXTL plus*[136] and for $(MePh_3P)[Ni(dmit)_2]_3$ (**95**), on the entire data set.

For complexes **93–95**, structures were solved by direct methods in *SHELXTL*, and refined using full-matrix least squares. The non-H atoms were treated anisotropically, whereas the hydrogen atoms were refined with isotropic thermal parameters. For **93**, 343 parameters were refined in the final cycle of refinement using 3831 reflections. For $(Ph_4P)[Ni(dmit)_2]_3$ (**94**), 345 parameters were refined in the final cycle of refinement using 2203 reflections, and for $(MePh_3P)[Ni(dmit)_2]_3$ (**95**), 713 parameters were refined in the final cycle of refinement using 9941 reflections and $w = 1/[(\sigma|F_o|)^2 + 0.0004(F_o)^2]$. For **93–95**, $\Sigma w(|F_o| - |F_c|)^2$ was minimized; $\sigma(F_o) = 0.5kI^{-1/2}\{[\sigma(I)]^2 + (0.02I)^2\}^{1/2}$, I(intensity) = $(I_{peak} - I_{background})$(scan rate), $\sigma(I) = (I_{peak} + I_{bkgd})^{1/2}$(scan

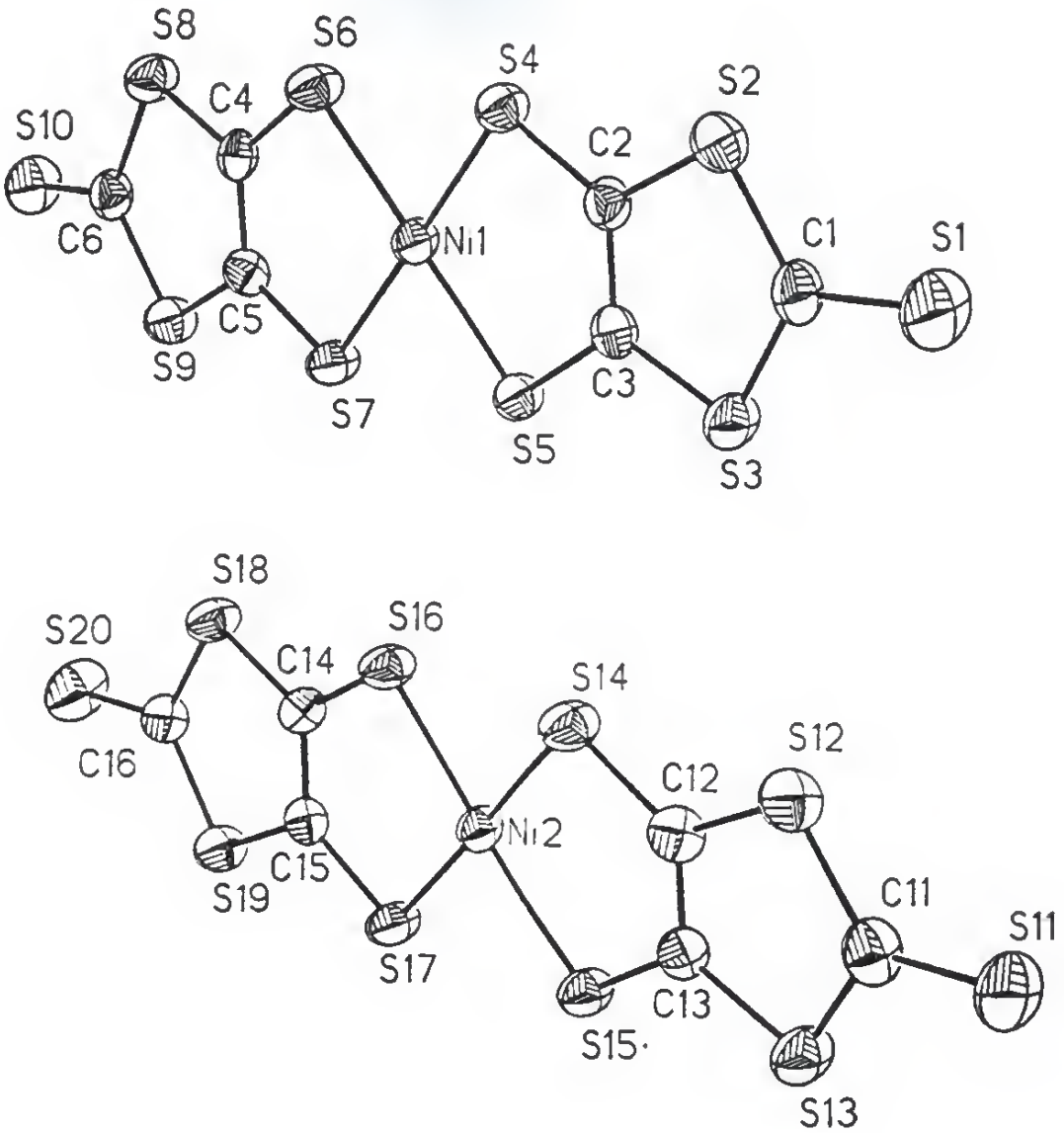

Figure 2–1. Thermal ellipsoids drawings (50% probability) and numbering schemes for the $Ni(dmit)_2$ units in $(Me_3S)[Ni(dmit)_2]_2$ (**93**).

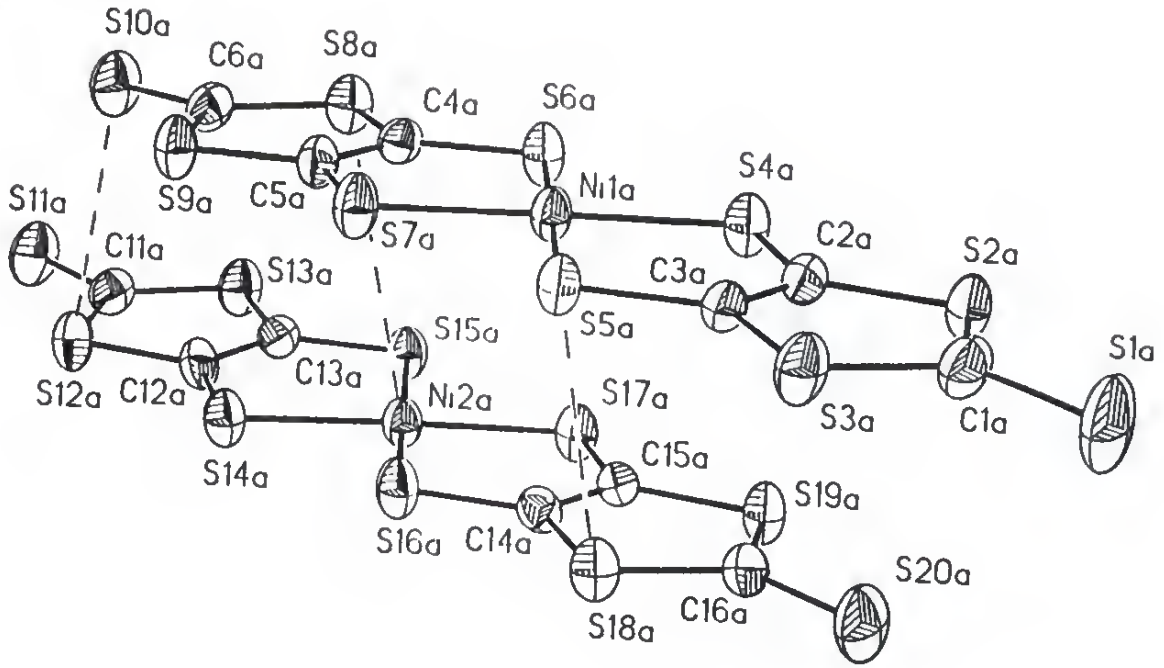

Figure 2–2. Thermal ellipsoids drawings (50% probability) and numbering schemes for the $Ni(dmit)_2$ moieties in $(Ph_4P)[Ni(dmit)_2]_3$ (**94**).

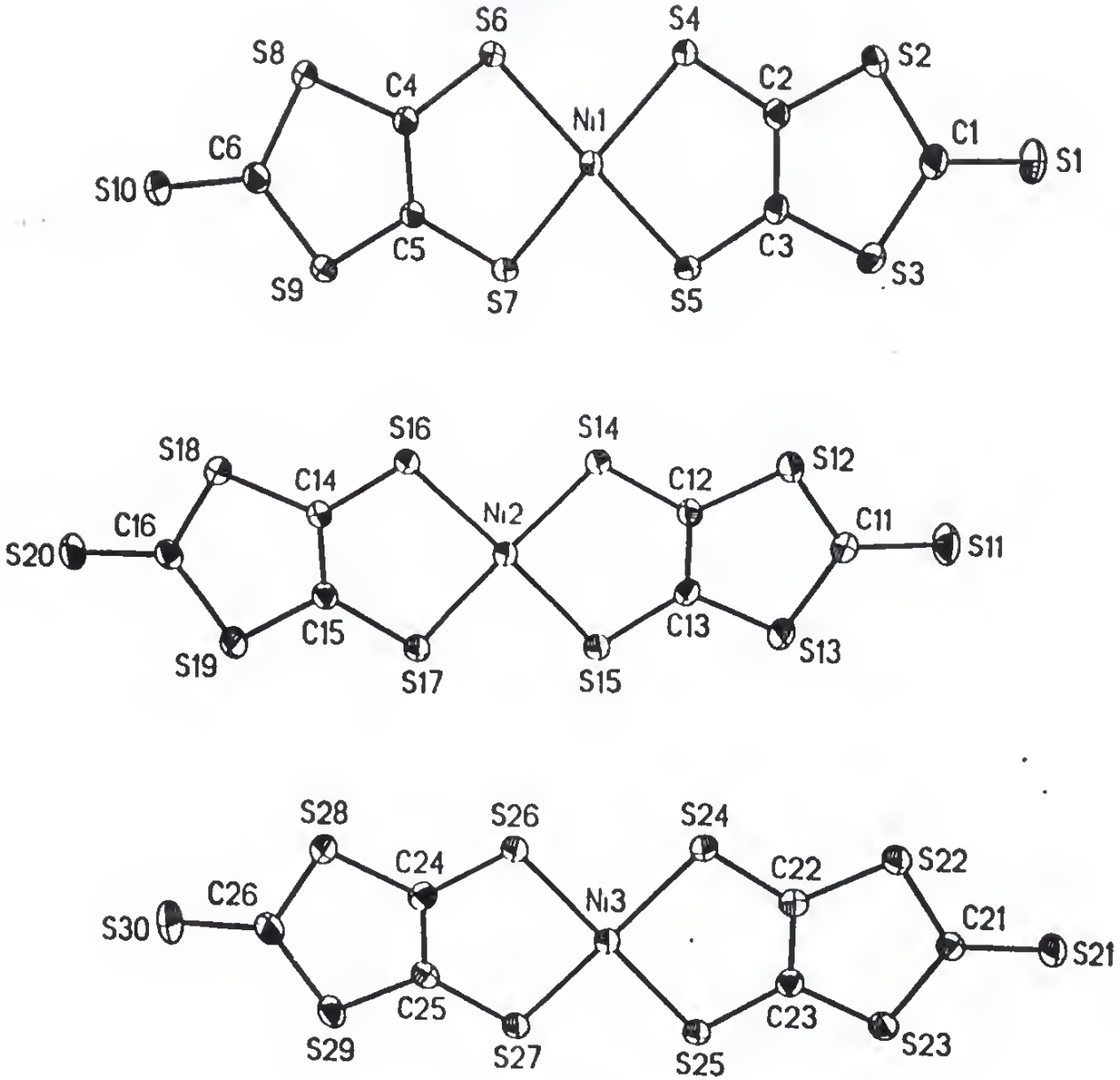

Figure 2–3. Thermal ellipsoid drawings (50% probability) and numbering schemes for the $Ni(dmit)_2$ units in $(MePh_3P)[Ni(dmit)_2]_3$ (**95**).

rate), *k* is the correction due to decay and Lp effects, and 0.02 is a factor used to downweight intense reflections and to account for instrument instability. The linear absorption coefficients and scattering factors for **93–95** were taken from the *International Tables for X-ray Crystallography.*[137] Scattering factors for non-hydrogen atoms were taken from Cromer and Mann[138] with anomalous-dispersion corrections from Cromer and Liberman,[139] while those of hydrogen atoms were taken from Stewart, Davidson and Simpson.[140]

Conductivity measurements. Temperature-dependent resistances for **49**, **93**, **94** (300 – 10 K) and for **95** (300 – 150 K) were measured by a four-probe method, using an ac technique. Two different platelet-shaped crystals of $(Bu_4N)_2[Ni(dmit)_2]_7 \cdot 2CH_3CN$ (**49**) (typically 3 x 0.1 x 0.05 mm^3), two platelet-shaped crystals of $(Me_3S)[Ni(dmit)_2]_2$ (**93**) (3 x 0.5 x 0.05 mm^3), five flat needle-shaped crystals of $(Ph_4P)[Ni(dmit)_2]_3$ (**94**) (3.5 x 0.2 x 0.04 mm^3) and two platelet-shaped crystals of $(MePh_3P)[Ni(dmit)_2]_3$ (**95**) (0.91 x 0.46 x 0.09 mm^3) were measured. Narrow gauge (0.02 mm diameter) gold wires were affixed to the crystal under a microscope using fast drying gold paint. The samples were thermally anchored to the cold head of a closed-cycle refrigerator (CTI Cryogenics). A typical run was done by first cooling the sample to the lowest temperature, and then taking the data while warming. Temperature reproducibility has been determined to be ±0.2 K or better over the temperature range measured.

Optical spectroscopy. Near-normal polarized reflectance measurements were made on single-crystal samples of $(Bu_4N)_2[Ni(dmit)_2]_7 \cdot 2CH_3CN$ (**49**), $(Me_3S)[Ni(dmit)_2]_2$ (**93**) and $(Ph_4P)[Ni(dmit)_2]_3$ (**94**). Far-infrared and mid-infrared measurements were carried out on a Bruker 113v Fourier-transform infrared spectrometer using a 4.2-K bolometer detector (30 – 600 cm^{-1}) and a B-doped Si photoconductor (450 – 4000 cm^{-1}). Wire grid polarizers on polyethylene and AgBr were used in the far and mid-infrared, respectively. A Perkin-Elmer 16U grating spectrometer in conjunction with thermocouple,

PbS, and Si detectors was used to measure the spectra in the infrared to the ultraviolet (1000 – 32000 cm^{-1}), using wire grid and dichroic polarizers.

Experiments were performed with light polarized parallel and perpendicular to the $Ni(dmit)_2$ stacking axis. The reflectance was calibrated with a reference aluminum mirror. In order to correct for size differences between sample and reference and to compensate for scattering losses, all samples were coated with a thin aluminum layer after the optical measurements were finished. The final corrected reflectance was obtained by ratioing the initial reflectance (no coating) to the reflectance of the coated sample, then multiplying the ratio by the aluminum reflectance. After the reflectance spectra were measured, the optical properties were determined by Kramers-Kronig analysis.[141] Because an extremely large frequency region was covered, Kramers-Kronig analysis should provide reasonably accurate values for the optical constants. To perform these transformations one needs to extrapolate the reflectance at both low and high frequencies. At very low frequencies the reflectance was assumed constant. Between the highest-frequency data point and 10^6 cm^{-1}, the reflectance was assumed to follow a power law of ω^{-1}, beyond this frequency range a free-electron-like behavior of ω^{-4} was used.

2–2 Results

2–2–1 X-ray Structures

Crystal structures of complexes **49, 93–95**. Several groups have reported different stoichiometries for $(Bu_4N)_2[Ni(dmit)_2]_7 \cdot CH_3CN$ (**102**).[53] According to Valade and et al.,[62] this complex has the stoichiometry $(Bu_4N)_2[Ni(dmit)_2]_7 \cdot 2CH_3CN$ (**49**) based on X-ray and elemental analysis. The structure can be described as consisting of thick layers of $Ni(dmit)_2$ entities oriented parallel to [001] and separated by sheets of Bu_4N^+ cations and CH_3CN molecules (Fig. 2–4). Within a layer the $Ni(dmit)_2$ species are arranged in stacks along the [110] direction. A stack consists of quasi-parallel quasi-planar $Ni(dmit)_2$ units arranged in alternating centrosymmetric triads and tetrads. The axes of the

triads and tetrads are parallel but make an angle of about 21° with the overall stacking direction [110]. Given the S···S interactions within the stacks on the one hand, and the interstack S···S nonbonding interactions on the other, it is clear that the structural arrangement of $(Bu_4N)_2[Ni(dmit)_2]_7 \cdot 2CH_3CN$ (**49**) cannot be viewed as a classical one-dimensional system, but is much more nearly two dimensional.

The structure of $(Me_3S)[Ni(dmit)_2]_2$ (**93**) is characterized by segregated stacks of $Ni(dmit)_2$ units and Me_3S^+ cationic units along [100] as shown in Fig. 2–5. Each $Ni(dmit)_2$ unit exhibits nonbonding interactions with seven other $Ni(dmit)_2$ units within the lattice. This results in not only intrastack interactions of $Ni(dmit)_2$ units, but also "side-by-side" and "end-to-end" interstack interactions (Fig. 2–6). An important feature of the lattice is the presence of two independent alternating interplanar distances, forming a quasidimer system within the stacks. Examining the intradimer $Ni(dmit)_2$ unit spacings within a stack, the shortest S···S value is 3.491 Å, this is less than the sum of the van der Waals radii of sulfur atoms of 3.70 Å.[68] Interdimer nonbonding interactions are also present as the S···S separation distance values range from the shortest, 3.58 Å, to the longest at 3.657 Å.

As mentioned already, "side-by-side" and "end-to-end" nonbonding interactions are prevalent in the lattice. Adjacent stacks of $Ni(dmit)_2$ units have separations in the range of 3.514 to 3.657 Å. The terminal thione groups also exhibit nonbonding interactions on the order of 3.571 Å. Therefore, $(Me_3S)[Ni(dmit)_2]_2$ (**93**) appears to have a quasi-three-dimensional network of S···S and Ni···S intermolecular interactions.

The crystal packing array of the $Ni(dmit)_2$ units in $(Ph_4P)[Ni(dmit)_2]_3$ (**94**) is unique among the $Ni(dmit)_2$ complexes. Shown in Figs. 2–7 and 2–8, the structure can be described as segregated, slightly staggered stacks of the planar $Ni(dmit)_2$ molecules along [010], separated "side-by-side" by planes of orthogonal spacers of the $Ni(dmit)_2$ units. The $Ni(dmit)_2$ units and spacers are separated "end-to-end" by closed-shell Ph_4P^+ spectator cations also in the [010] direction.

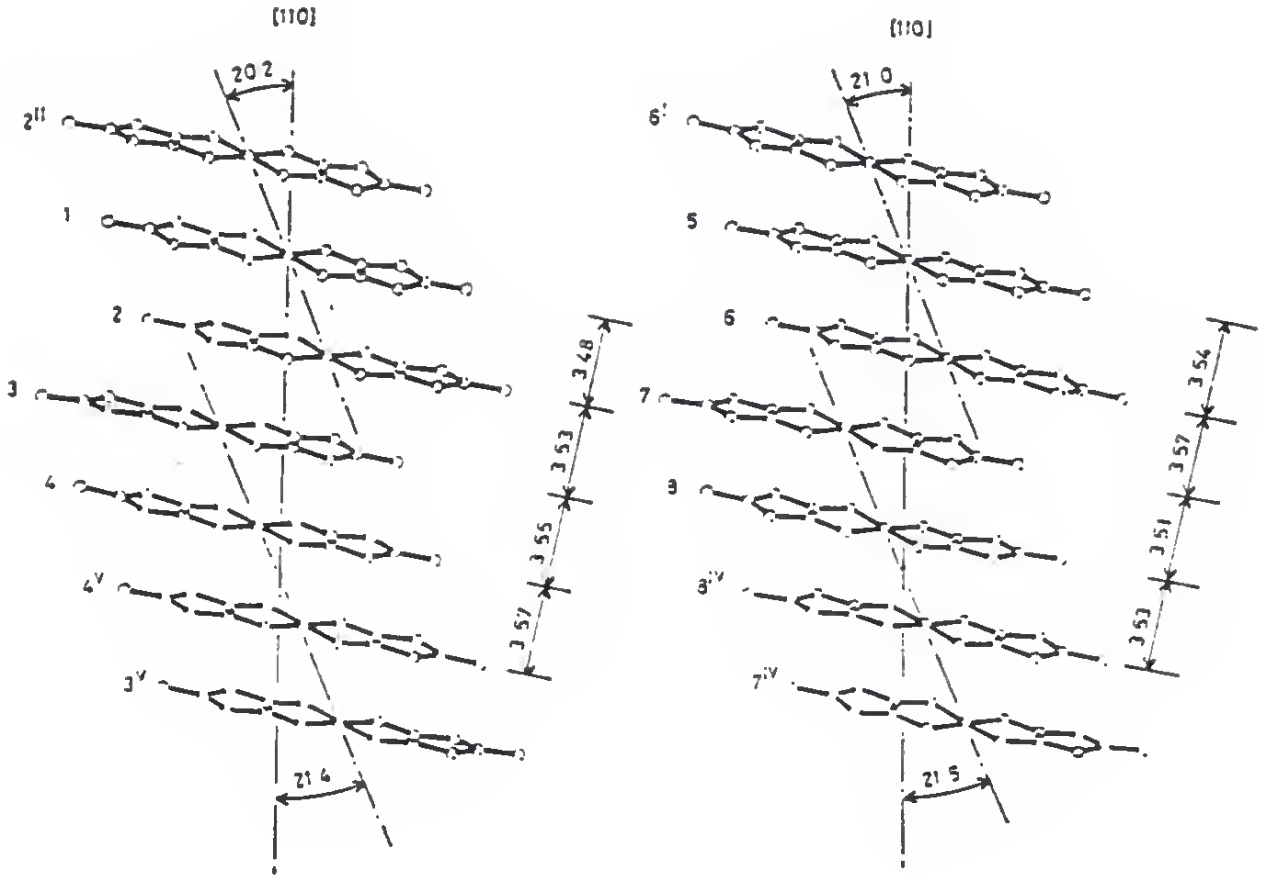

Figure 2–4. Stacking of the planar $Ni(dmit)_2$ units of $(Bu_4N)_2[Ni(dmit)_2]_7 \cdot 2CH_3CN$ (**49**) along the [110] direction. The view emphasizes the alternation of triads and tetrads tilted by almost 21° with respect to the overall stacking direction.[62]

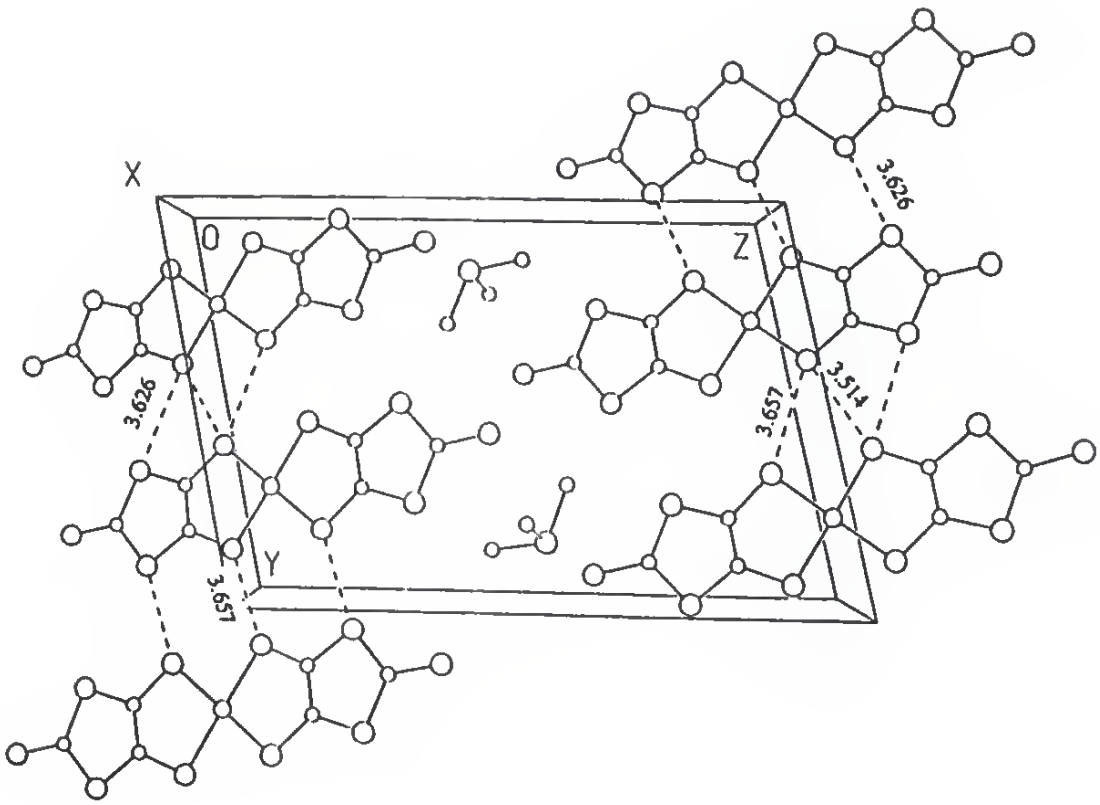

Figure 2–5. View down the a axis of $(Me_3S)[Ni(dmit)_2]_2$ (**93**) of the [100] plane of the crystal structure. Dotted lines represent distances less than the sum of the van der Waals radii.[68]

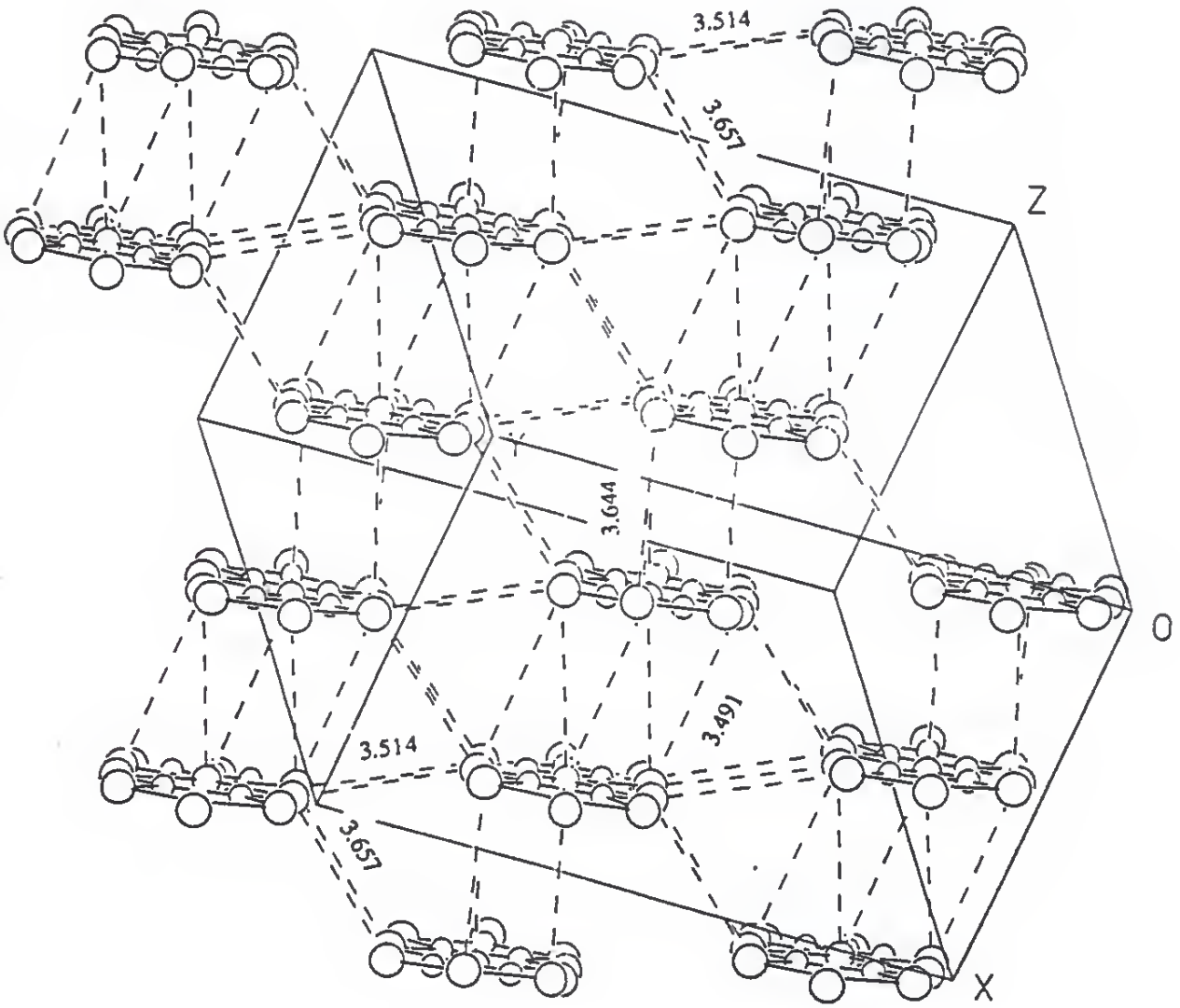

Figure 2–6. Viewing down the long axis of the Ni(dmit)$_2$ units, illustrating the stacking arrangement of (Me$_3$S)[Ni(dmit)$_2$]$_2$ (**93**).

There is an extensive number of nonbonding orbital interactions exhibited throughout the structure. Looking within the segregated stacks of $Ni(dmit)_2$ moieties, there is no S···S orbital overlap observed. However, there is Ni dz^2···S orbital overlap. As can be seen from Fig. 2–8, the interplanar $Ni(dmit)_2$ unit spacings are equidistant at ~3.76 Å. The orthogonal spacer $Ni(dmit)_2$ units have a separation of 4.058 Å, which results in intermolecular interspacer S···S distances well beyond the sum of the van der Waals radii of 3.70 Å. Despite the fact that there are no interspacer or interstack S···S interactions, there are a significant number of spacer-stack interactions. Each $Ni(dmit)_2$ spacer unit interacts with the six $Ni(dmit)_2$ units within adjacent stacks. The Ni dz^2 orbital in the spacers is directed toward a thiolate sulfur in $Ni(dmit)_2$ units of the two neighboring molecules. The spacing between stack and spacer is 3.426 Å. A number of spacer-stack interactions are also observed involving the peripheral thiolate and thiole groups of the $Ni(dmit)_2$ spacers. Each of these groups interact with two Ni(dmit)2 units within the adjacent stacks. The separations range from 3.609 to 3.628 Å; all are shorter than the van der Waals separation of 3.70 Å. Along the [001] direction, there are no nonbonding interactions observed between the terminal thione groups of the $Ni(dmit)_2$ unit and spectator Ph_4P^+ units. Therefore, $(Ph_4P)[Ni(dmit)_2]_3$ (**94**) has a quasi-two-dimensional network of S···S and Ni dz^2···S intermolecular interactions. The crystal structure of $(MePh_3P)[Ni(dmit)_2]_3$ (**95**) consists of one $MePh_3P^+$ cation and three crystallographically independent $Ni(dmit)_2$ units. The packing is characterized by columns of $Ni(dmit)_2$ dimers separated by columns of $MePh_3P^+$ counterions. The $Ni(dmit)_2$ units which are arranged in a dimeric fashion with the long axis of $Ni(dmit)_2$ molecules in the (100) direction as seen in Fig. 2–9. Each dimer is surrounded by six other dimers. Each of the dimers forms dihedral angles of 44.5(1)° and 51.2(1)° against four other dimers along the (001) direction and 6.7(1)° against two other dimers along the (010) direction. This packing motif is very similar to another phosphonium salt $(Me_4P)[Ni(dmit)_2]_2$ (**103**),[124] and to the κ-phase

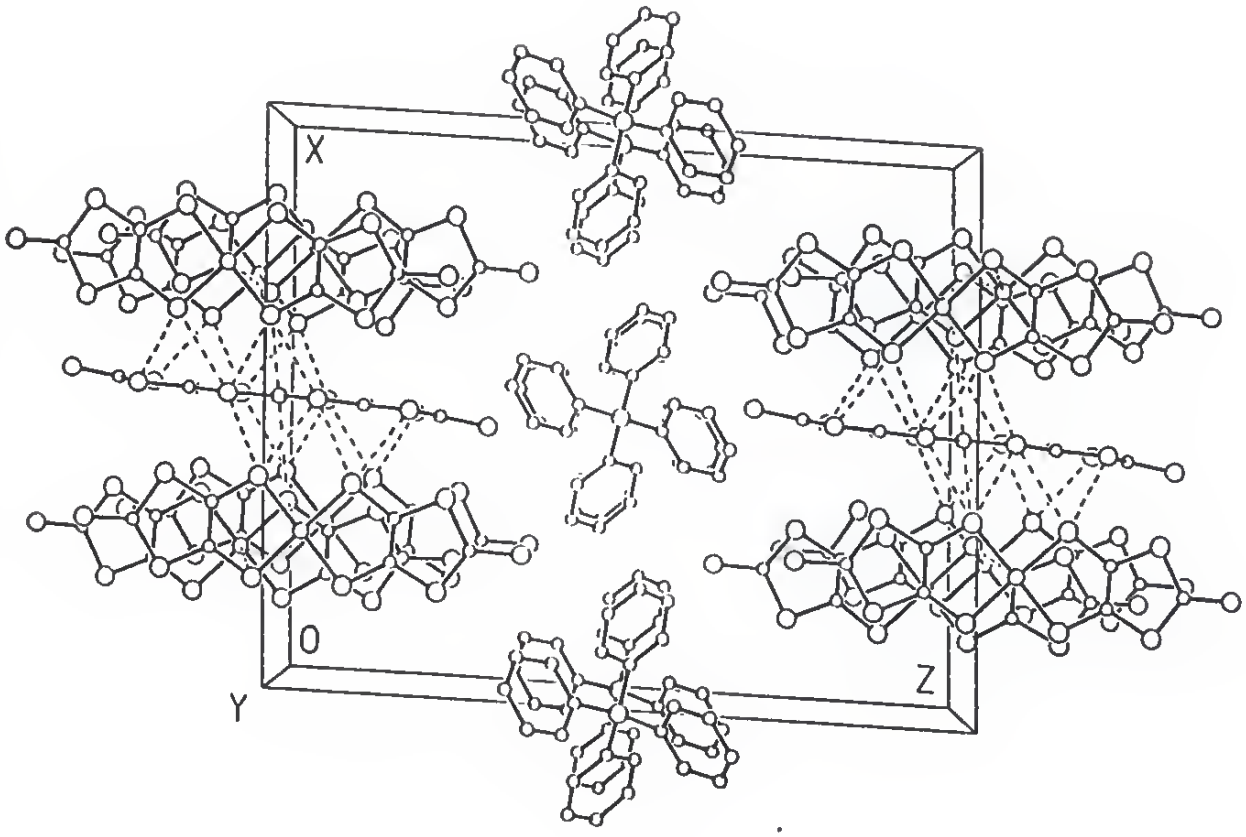

Figure 2–7. View down the b axis of $(Ph_4P)[Ni(dmit)_2]_3$ (**94**) showing non-bonding interactions between $Ni(dmit)_2$ orthogonal spacer and stacking units.

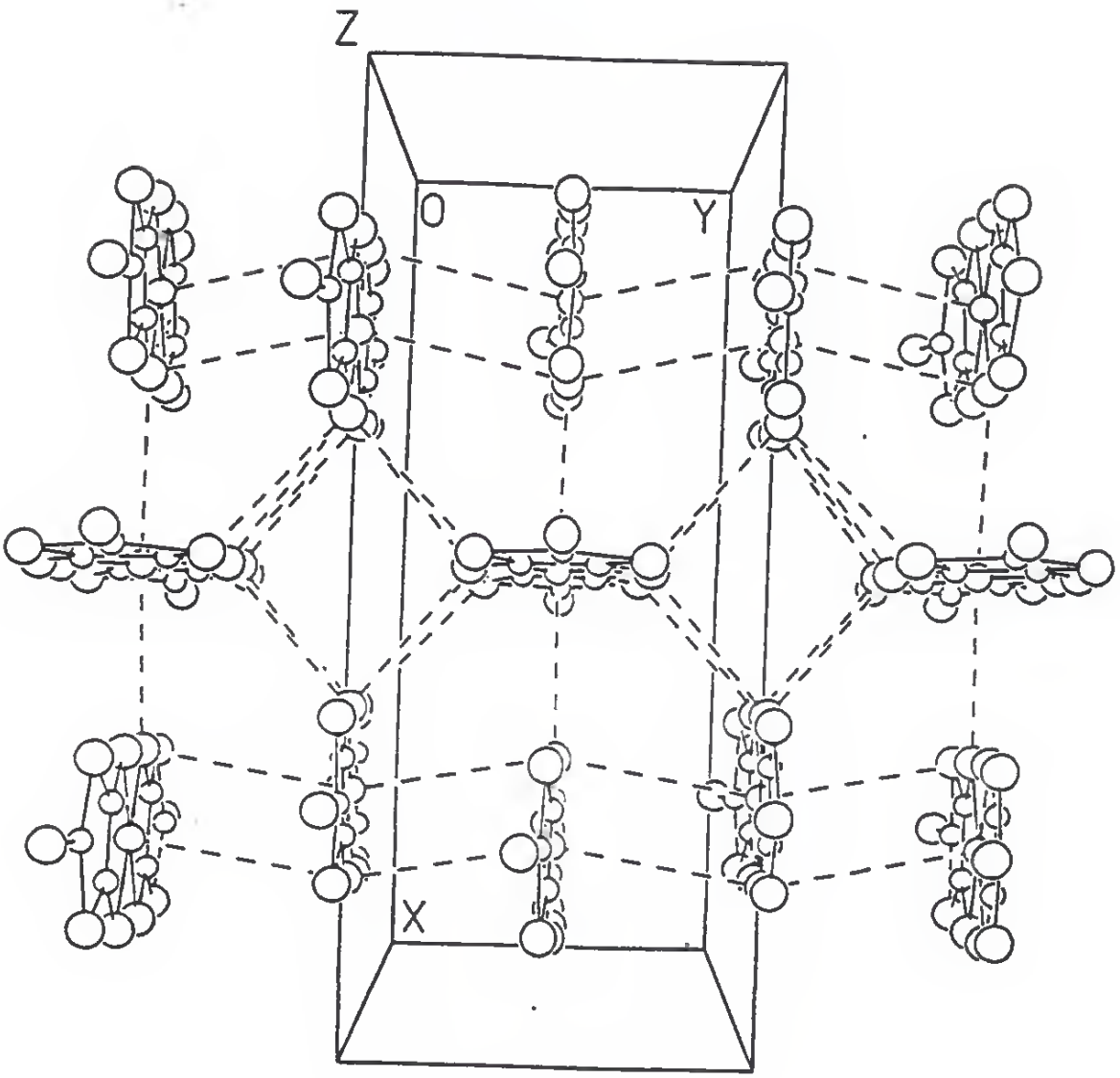

Figure 2–8. View down the c axis of $(Ph_4P)[Ni(dmit)_2]_3$ (**94**) showing array of stacks and orthogonal spacer $Ni(dmit)_2$ units (Ph_4P^+ cations have been omitted for clarity).

BEDT-TTF salts. Currently the complex κ-(BEDT-TTF)$_2$(Cu[N(CN)$_2$]Cl (**15**), with this packing array has the highest superconducting transition temperature measured to date of 12.8 K for a molecular material.[14] The $MePh_3P^+$ complex also forms dimers of Ni(dmit)$_2$ units with dihedral angles of 60° against four other adjacent dimers, and 0° against two other pairs of the six total surrounding dimers. There are extensive S···S non-bonding interdimer orbital interactions in a two-dimensional array resulting from close contacts with distances less than the sum of the van der Waals radii (3.70 Å). The S···S distances range from 3.440 Å resulting from thiolate-thiolate interactions, to 3.658 Å due to thiolate-thiole interactions. There are also several Ni dz^2···S non-bonding interdimer interactions observed in the crystal lattice. These range from 3.232 Å due to Ni dz^2···thiole sulfur orbital overlap to 3.856 Å due to Ni dz^2···thiolate sulfur orbital interactions.

Within the dimers, the Ni(dmit)$_2$ units stack in an eclipsed fashion. Two of the three crystallographically independent Ni(dmit)$_2$ units are in dimers with the units being slightly slipped (transverse offset) from perfectly eclipsed as seen in Fig. 2–10. These Ni(dmit)$_2$ units form dimers with intradimer spacings ranging from 3.443 to 3.652 Å. The third crystallographically independent Ni(dmit)$_2$ forms a dimer with a perfectly eclipsed stacking motif. This is mediated by a strong Ni dz^2···dz^2 orbital interaction. This interaction is shown by the solid line in the packing diagram in Figure 2–6. The distance is only 2.7837(7) Å between the Ni atoms. This results in a fold-like dmit-Ni-dmit dihedral angle of 13.0° of the dmit ligand planes from 0° for a perfectly square planar complex. This very short Ni···Ni interaction resulting from dimers arranged in an eclipsed fashion, is unique among Ni(dmit)$_2$-based complexes. This has been observed in several instances with Pd(dmit)$_2$ and Pt(dmit)$_2$-based materials.[53,142-146]

The packing of the anions and cations in $(MePh_3P)[Ni(dmit)_2]_3$ (**95**) is very different from other similar 3:1 phosphonium-based complexes $(Ph_4P)[Ni(dmit)_2]_3$ (**94**) and (BTP)[Ni(dmit)$_2$]$_3$ (BTP = benzyltriphenylphosphonium, **104**).[146] The Ph_4P^+ salt displays a unique packing scheme amongst the Ni(dmit)$_2$ complexes, with stacks of

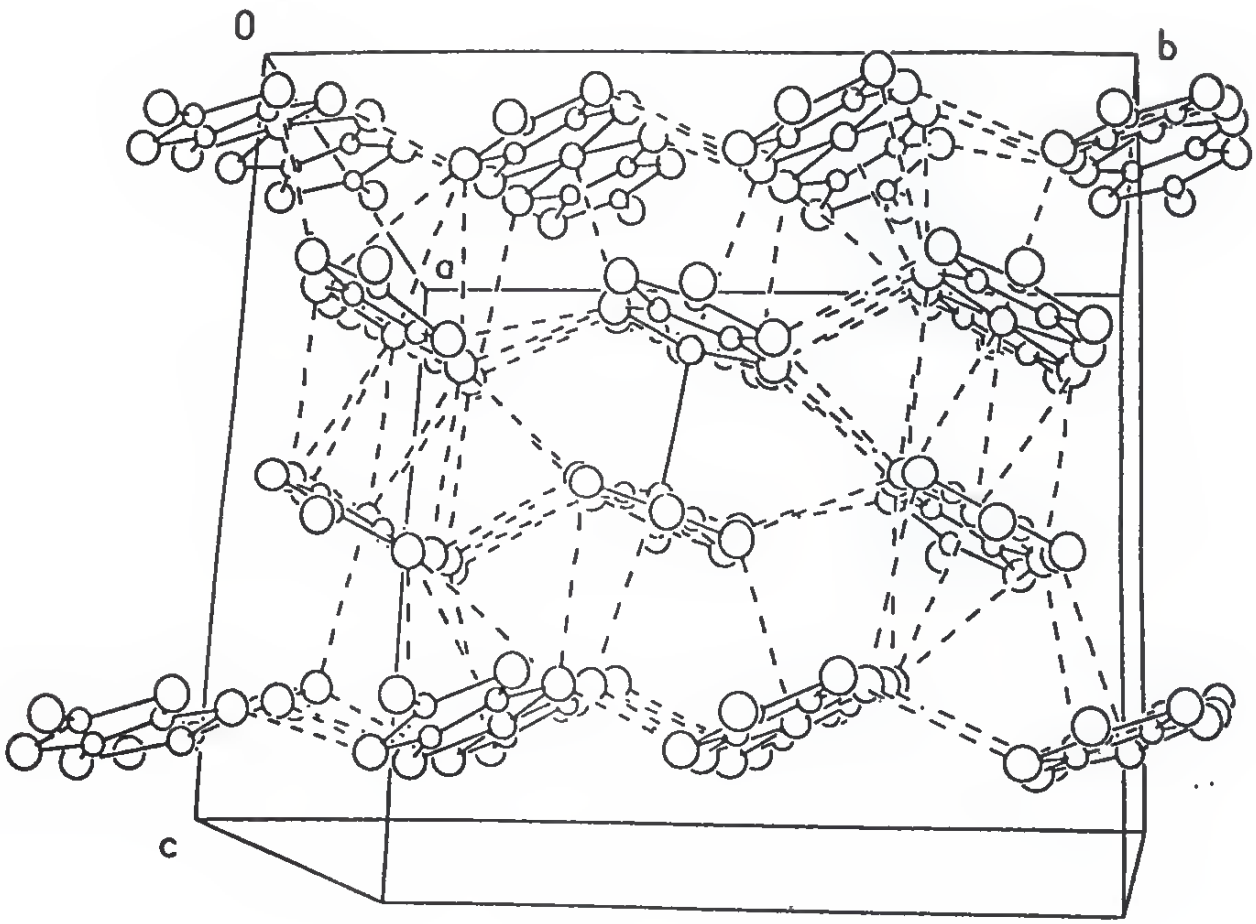

Figure 2–9. View along the long axis of the $Ni(dmit)_2$ moieties showing a dimeric packing arrangement in $(MePh_3P)[Ni(dmit)_2]_3$ (**95**) ($MePh_3P^+$ cations have been omitted for clarity). Also shown are extensive S···S, Ni···S and Ni···Ni (solid line) non-bonding orbital interactions.

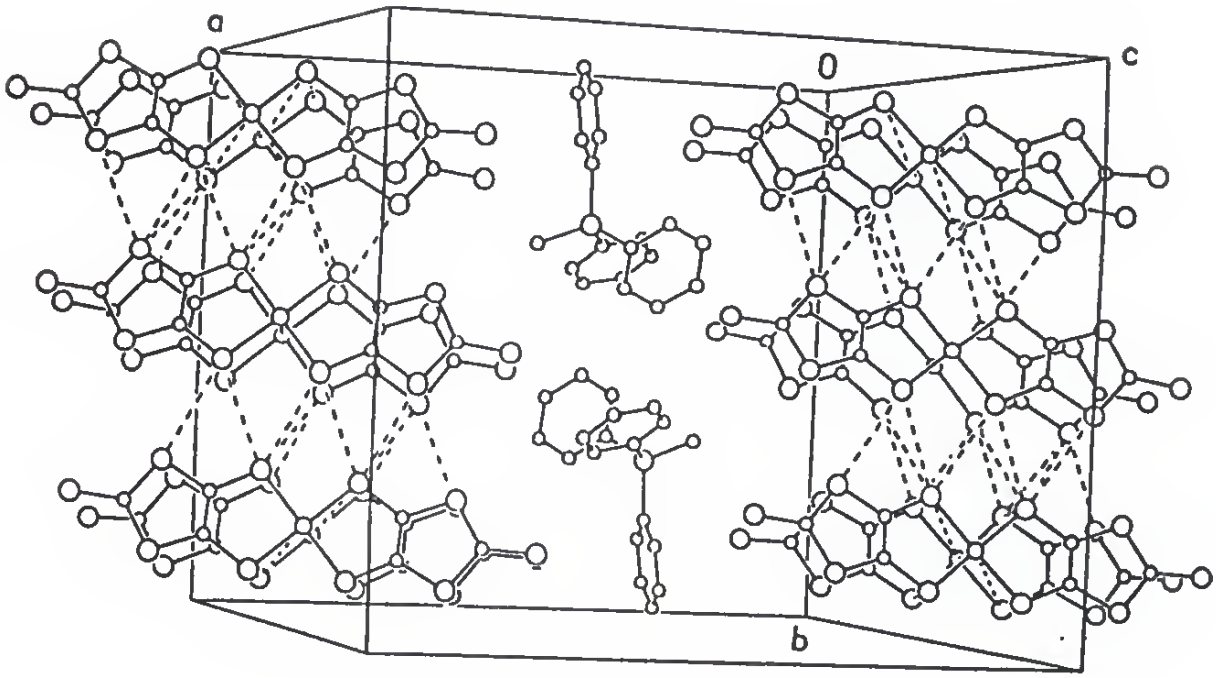

Figure 2–10. View perpendicular to the $Ni(dmit)_2$ moieties showing intradimer quasi-eclipsed stacking arrangements of the moieties in $(MePh_3P)[Ni(dmit)_2]_3$ (**95**). Also shown are the dimers packed in a columnar manner separated by $MePh_3P^+$ cations.

$Ni(dmit)_2$ units separated by orthogonal spacer $Ni(dmit)_2$ units. By simply adding a methylene spacer to one of the phenyl groups, all of the $Ni(dmit)_2$ molecules of $(BTP)[Ni(dmit)_2]_3$ (**104**) are in the same plane. By replacing a phenyl group with a methyl group, the material $(MePh_3P)[Ni(dmit)_2]_3$ (**95**) results with the same stoichiometry but with a very different packing as previously discussed than that seen in both the Ph_4P^+ and BTP^+-based salts.[146]

2-2-2 Conductivity Properties

Conductivity Properties of **49, 93–95**. Temperature-dependent four-probe electrical conductivity measurements are shown in Fig. 2–11. Semiconducting behavior is found for compounds **49, 93–95**. The conductivity decreases from its 300-K value when the temperature is decreased. The typical temperature dependence of the conductivity may

$$\sigma(T) = \sigma_0 e^{-E_g/2k_BT}$$

be expressed as where E_g is the semiconductor gap. The values of room-temperature conductivity and the thermal activation energy $E_a = E_g/2$, are listed in Table 2–1. The complex $(Ph_4P)[Ni(dmit)_2]_3$ (**94**) displays the highest room temperature conductivity of 7 S/cm and the lowest activation energy of 17 meV. Complexes $(Me_3S)[Ni(dmit)_2]_2$ (**93**) and $(MePh_3P)[Ni(dmit)_2]_3$ (**95**) display the lowest room temperature conductivities of around 0.1 S/cm, with $(MePh_3P)[Ni(dmit)_2]_3$ (**95**) having the highest activation energy of 220 meV.

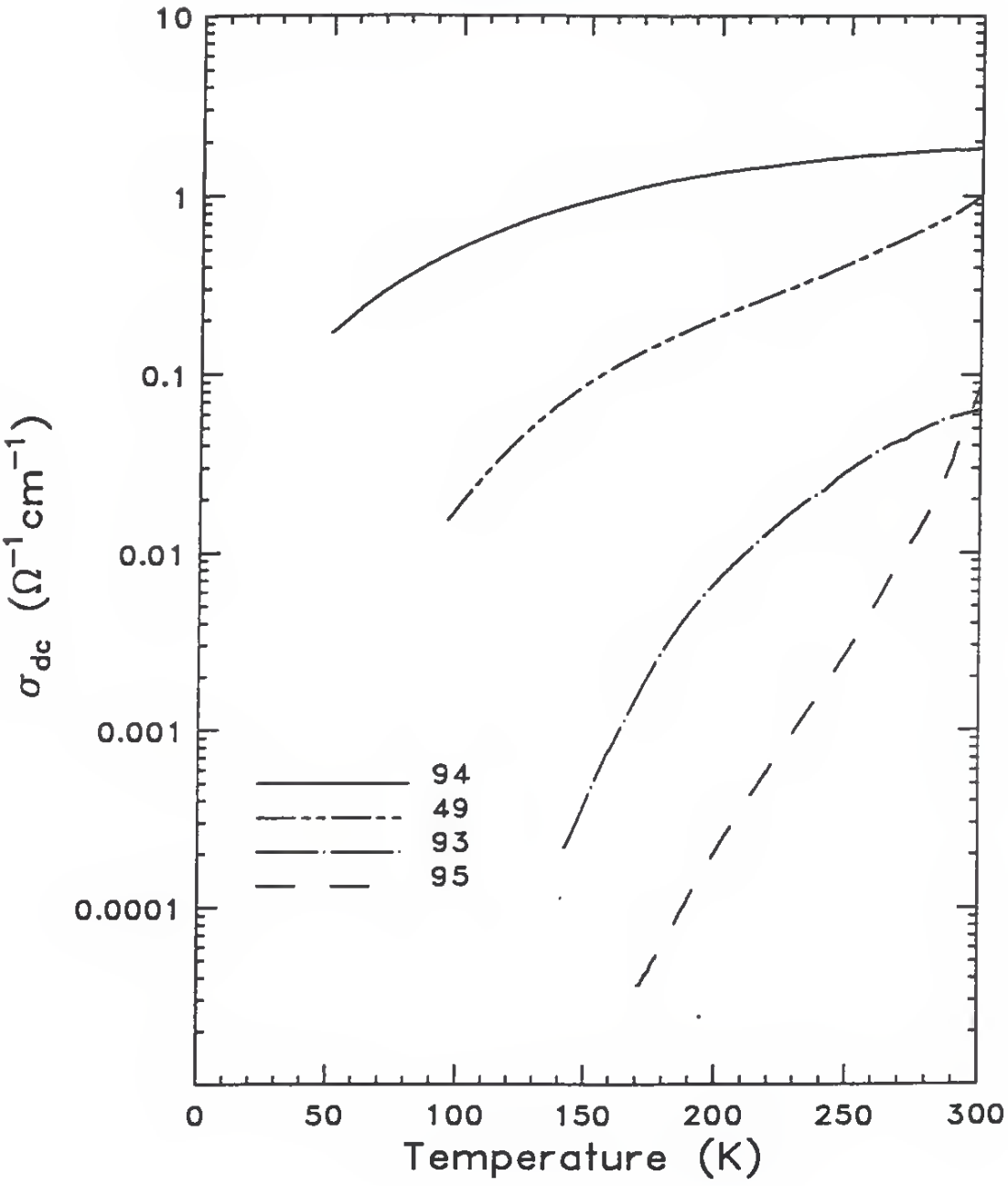

Figure 2–11. Logarithm of the temperature-dependent conductivity of $(Bu_4N)_2[Ni(dmit)_2]_7 \cdot 2CH_3CN$ (**49**), $(Me_3S)[Ni(dmit)_2]_2$ (**93**), $(Ph_4P)[Ni(dmit)_2]_3$ (**94**) and $(MePh_3P)[Ni(dmit)_2]_3$ (**95**).

Table 2–1. Room-temperature Conductivity and Activation Energy Values for Complexes **49**, **93–95**

Compound	σ_{RT} (S/cm)	E_a (meV)
$(Bu_4N)_2[Ni(dmit)_2]_7 \cdot 2CH_3CN$ (**49**)	1	42
$(Me_3S)[Ni(dmit)_2]_2$ (**93**)	0.065	130
$(Ph_4P)[Ni(dmit)_2]_3$ (**94**)	7	17
$(MePh_3P)[Ni(dmit)_2]_3$ (**95**)	0.07-0.1	220

2-2-3 Optical Spectroscopy

Polarized reflectance. Figure 2–12 shows the polarized room-temperature reflectance of $(Bu_4N)_2[Ni(dmit)_2]_7 \cdot 2CH_3CN$ (**49**), $(Me_3S)[Ni(dmit)_2]_2$ (**93**) and $(Ph_4P)[Ni(dmit)_2]_3$ (**94**) over the spectral range of 100 to 12000 cm^{-1}. The compound $(MePh_3P)[Ni(dmit)_2]_3$ (**95**), has not been studied by optical spectroscopy due to the inability to obtain crystals of adequate quality. Data are shown for polarizations parallel and perpendicular to the $Ni(dmit)_2$ stacking axis. For the electric field polarized parallel to the stacking direction, a common feature of the three compounds is a value of 40% to 60% reflectance in the far to midinfrared, with a drop to values of a few percent around 3000 to 4500 cm^{-1}. Also seen in this region are a series of narrow peaks typical of molecular vibrations. Higher frequencies for complexes **49**, **93** and **94** show only several weak electronic features. The reflectance when the polarization is perpendicular to the $Ni(dmit)_2$ stacking axis is also shown in Fig. 2–12. There is a marked contrast for polarization of the light parallel and perpendicular to the $Ni(dmit)_2$ stacking axis. The reflectivity is low (~15%), flat, and almost featureless for $(Bu_4N)_2[Ni(dmit)_2]_7 \cdot 2CH_3CN$ (**49**) and $(Me_3S)[Ni(dmit)_2]_2$ (**93**). In contrast, the $(Ph_4P)[Ni(dmit)_2]_3$ (**94**) perpendicular spectra are similar in shape to that with parallel polarization up to 1000 cm^{-1}, but differs in the deep minimum of the reflectance and in the higher-frequency region.

Optical conductivity. The Kramers-Kronig transformation of the stacking-axis reflectance data of Fig. 2–12 yield the real part of the conductivity $\sigma_1(\omega)$ shown in Fig. 2–13. The spectra display a broad low-energy band and several weak electronic structures at higher frequencies. In all cases, complexes **49**, **93** and **94** show a conductivity maximum at finite frequency and which shifts to higher frequencies as the dc conductivity decreases. The conductivity maximum for $(Ph_4P)[Ni(dmit)_2]_3$ (**94**) is observed at the lowest frequency of ~270 cm^{-1}, followed by $(Bu_4N)_2[Ni(dmit)_2]_7 \cdot 2CH_3CN$ (**49**) at ~650 cm^{-1} and the highest for $(Me_3S)[Ni(dmit)_2]_2$ (**93**) at ~1750 cm^{-1}. This behavior is in itself suggestive of an optical gap and possibly a transport gap of increasing magnitude.

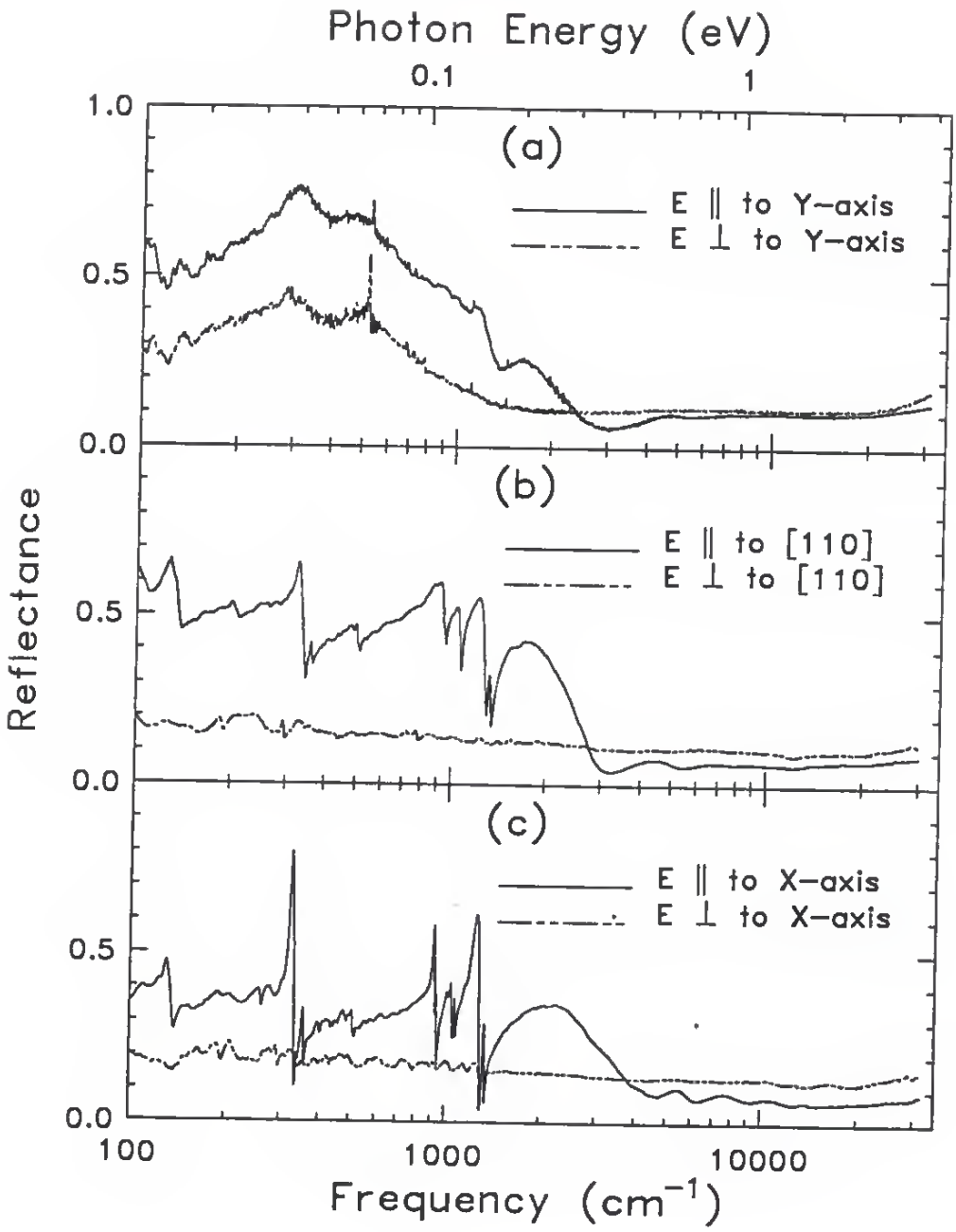

Figure 2–12. The polarized reflectance of (a) $(Ph_4P)[Ni(dmit)_2]_3$ (**94**), (b) $(Bu_4N)_2[Ni(dmit)_2]_7{\cdot}2CH_3CN$ (**49**), and (c) $(Me_3S)[Ni(dmit)_2]_2$ (**93**) at room temperature for polarization parallel (solid line) and perpendicular (dash-dotted line) to the stacking axis.

At low frequency, the spectra exhibit many sharp vibrational features. As the conductivity maximum shifts to higher frequencies, there is an increase in the amplitude of the mid-infrared vibrational structures. The appearance of these features also changes depending on their frequency location relative to the conductivity maximum. When their frequencies are well below that of the broad maximum they appear as ordinary (Lorentzian) resonances whereas when their frequencies overlap the electronic continuum, an antiresonance or dip preceded by a peak on the low-frequency side is observed.

Estimates of the dc conductivity and semiconducting energy gap can be obtained from the data in Fig. 2–13 by extrapolating the frequency-dependent conductivity to zero frequency. The estimates of the dc conductivity for $(Bu_4N)_2[Ni(dmit)_2]_7 \cdot 2CH_3CN$ (**49**) is 1–5 S/cm, for $(Me_3S)[Ni(dmit)_2]_2$ (**93**) is <1 S/cm and for $(Ph_4P)[Ni(dmit)_2]_3$ (**94**) is 5–15 S/cm at 300 K. These values are very similar to the four-probe dc measurements obtained and compiled in Table 2–1. The semiconducting energy gap values, E_g, can be obtained from the low-energy electronic band shown in Fig. 2–13. The frequency at which the conductivity has risen to half its maximum value yields an estimate of the gap values where $(Bu_4N)_2[Ni(dmit)_2]_7 \cdot 2CH_3CN$ (**49**) is ~81 meV (~650 cm^{-1}), $(Me_3S)[Ni(dmit)_2]_2$ (**93**) is ~220 meV (~1750 cm^{-1}) and $(Ph_4P)[Ni(dmit)_2]_3$ (**94**) is approximately 34 meV (~270 cm^{-1}). Converting these values to E_a using the equation $E_a = E_g/2$ as explained previously in Section 2–2–2, these values obtained from the Kramers-Kronig transformation of the reflectance data is in close agreement with the data obtained from transport measurements. Transport data gave E_g values for **49** of ~84 meV, **93** of ~260 meV and for **94** of ~34 meV as listed in Table 2–1.

As expected, the $\sigma_1(\omega)$ for polarization perpendicular to the stacking direction is rather flat. The extremely anisotropic behavior in the electronic properties of these $Ni(dmit)_2$ compounds have been observed for many other organic materials as well.[147]

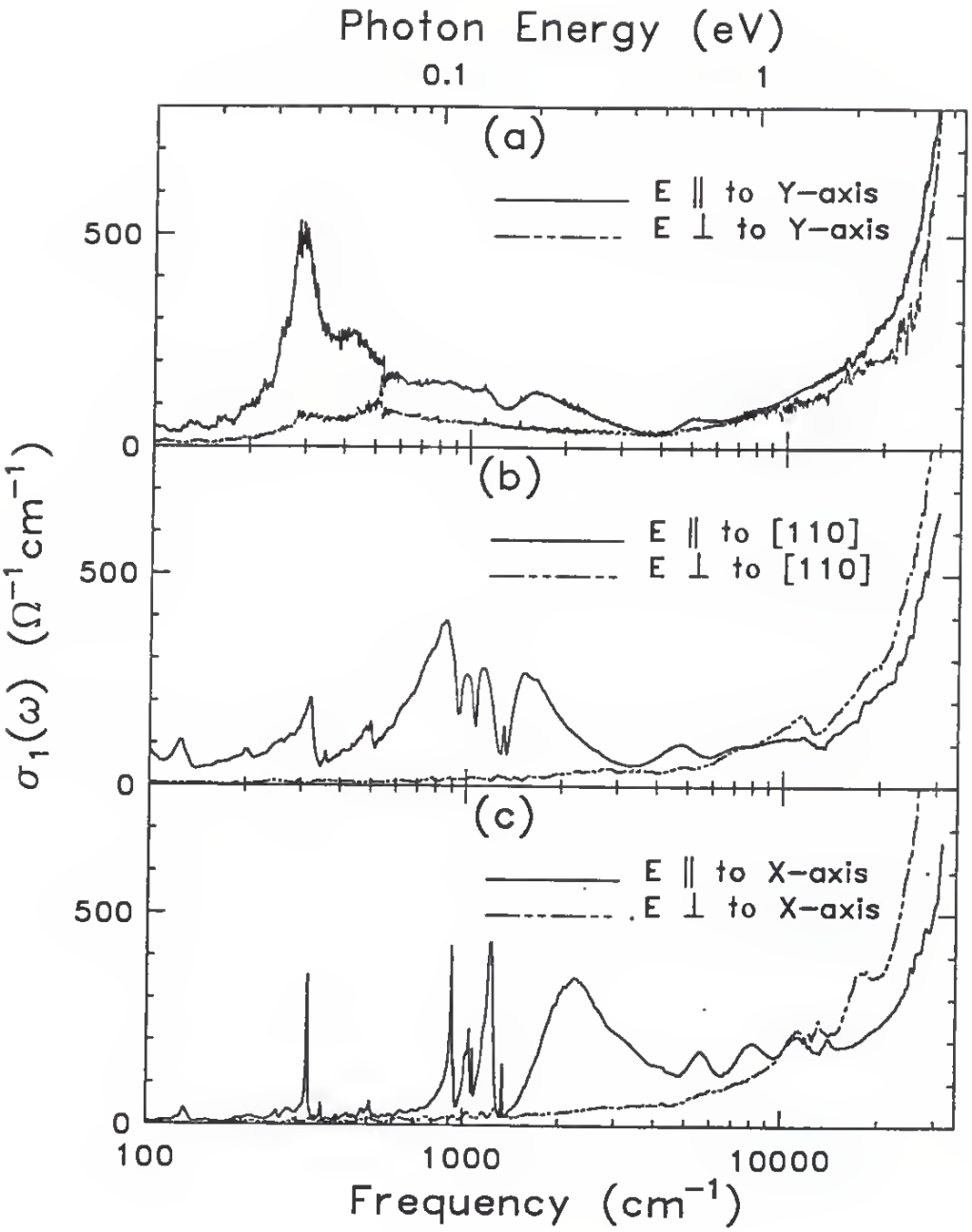

Figure 2-13. Frequency-dependent conductivity obtained by Kramers-Kronig analysis of the room-temperature reflectance of (a) $(Ph_4P)[Ni(dmit)_2]_3$ (**94**), (b) $(Bu_4N)_2[Ni(dmit)_2]_7{\cdot}2CH_3CN$ (**49**), and (c) $(Me_3S)[Ni(dmit)_2]_2$ (**93**). The conductivity is shown parallel and perpendicular to the stacking axis.

The vibrational lines appear as superimposed bands with no clear evidence for coupling effects. Thus, there is little evidence for low-energy electronic absorptions perpendicular to the $Ni(dmit)_2$ stacking axis. Only at high frequencies, above 10 000 cm^{-1}, is there electronic absorption observed.

Despite the significantly different stoichiometric ratios of $Ni(dmit)_2$ units and spectator ions, the $\sigma_1(\omega)$ spectra of $(Bu_4N)_2[Ni(dmit)_2]_7 \cdot 2CH_3CN$ (**49**), $(Me_3S)[Ni(dmit)_2]_2$ (**93**) and $(Ph_4P)[Ni(dmit)_2]_3$ (**94**) are similar in character and typical of semiconducting charge-transfer and anion radical salt complexes. In the case of $(Bu_4N)_2[Ni(dmit)_2]_7 \cdot 2CH_3CN$ (**49**), the stacking direction has a transition at ~1050 cm^{-1}, attributed as above to charge transfer from a $Ni(dmit)_2$ radical anion to a neutral molecule within a $Ni(dmit)_2$ triad or tetrad. The higher frequency peaks, at ~4000 and 7300 cm^{-1}, are attributed to charge transfer between two radical $Ni(dmit)_2$ anions. The spectrum perpendicular to the stacking axis shows transitions at ~10 000, 11 400, and 18 700 cm^{-1} which are due to the localized excitation of the isolated $Ni(dmit)_2$ anion. Again, some of these absorption bands are also observed along the stacking axis.

Additionally, in the case of $(Ph_4P)[Ni(dmit)_2]_3$ (**94**), there are two low-energy electronic excitations (at ~300–450 and 1000–1700 cm^{-1}) for the electric field polarized along the $Ni(dmit)_2$ stacking axis. The structure of this material is unique: two of the three $Ni(dmit)_2$ anions form stacking columns whereas the remaining $Ni(dmit)_2$ anion fills the spaces between the columns. The optical data can be correlated with this structural information. We attribute the 300–450 cm^{-1} peak to charge-transfer excitations within $Ni(dmit)_2$ stacking columns. The higher peak, at ~1000–1700 cm^{-1}, is attributed to a charge transfer to an adjacent neutral molecule. Interestingly, the spectrum perpendicular to the stacking axis displays peaks at similar energies, but has considerably smaller oscillator strength. The bands occurring at ~5000 and 7800 cm^{-1} are attributed to a charge-transfer excitation between $Ni(dmit)_2$ ions. The transitions of an electron excited to a higher orbital

or localized excitation are seen to be polarized along both parallel and perpendicular to stacking axis at frequencies of ~11 500 and 15 000 cm^{-1}.

Although these three $Ni(dmit)_2$ compounds have different chemical modifications of the spectator closed-shell cation, an interesting correlation can be made between spectral properties and available structural information. As previously mentioned, $(Bu_4N)_2[Ni(dmit)_2]_7 \cdot 2CH_3CN$ (**49**) and $(Ph_4P)[Ni(dmit)_2]_3$ (**94**) have a nearly two-dimensional structure as opposed to the rather quasi-three-dimensional network in $(Me_3S)[Ni(dmit)_2]_2$ (**93**). The obvious question now is, why does the increased dimensionality of $(Me_3S)[Ni(dmit)_2]_2$ (**93**) result in a lower electrical conductivity, a higher activation energy for conduction, and a larger value of optical gap than the other two $Ni(dmit)_2$ salts. In principle, the nature of the donor is primarily responsible for the different manner of stacking in these $Ni(dmit)_2$ materials. It particularly influences the mode of overlap between $Ni(dmit)_2$ molecules. Small cations such as Me_3S^+ promote close-packing arrangements, but also give room for dimerization. Larger cations encourage uniform spacing but also tend to give unusual stoichiometries or packing arrangements. There are always counter-examples; for instance, the $Ni(dmit)_2$ system with a small spectator cation, $(HMe_3N)[Ni(dmit)_2]_2$ (**72**),[104-106] $Na[Ni(dmit)_2]_2$ (**55**),[72,73] and $(Me_4N)[Ni(dmit)_2]_2$ (**53**),[69-71] all display metallic electronic properties with **53** even showing superconducting electronic properties under pressure. It is clear that the situation is complex, and to understand the electronic structures of the $Ni(dmit)_2$ compounds, one must not only understand the role of the $Ni(dmit)_2$ units, but also the role of the spectator cations in the electronic band structures.[82,148]

2–3 Conclusions

The series of $Ni(dmit)_2$ non-integer oxidation state complexes $(Bu_4N)_2[Ni(dmit)_2]_7 \cdot 2CH_3CN$ (**49**), $(Me_3S)[Ni(dmit)_2]_2$ (**93**), $(Ph_4P)[Ni(dmit)_2]_3$ (**94**) and $(MePh_3P)[Ni(dmit)_2]_3$ (**95**), have been synthesized by constant current

electrocrystallization. The complexes have been characterized by X-ray structure analysis, temperature-dependent conductivity and optical spectroscopy. X-ray analysis of **93** shows a network of three-dimensional intermolecular non-bonding S···S interactions. Complex **94** displays a unique packing array of the $Ni(dmit)_2$ units from stacks of $Ni(dmit)_2$ moieties separated by orthogonal spacers of $Ni(dmit)_2$ units. The packing structure of complex **95** is made up of dimers of $Ni(dmit)_2$ units, with one of every three dimers having an eclipsed intradimer stacking mode with a strong Ni···Ni interaction, not seen previously in other $Ni(dmit)_2$ complexes.

Four-probe temperature-dependent conductivity measurements of **49**, **93**–**95** show all of the complexes display semiconducting electronic properties. The complex $(Ph_4P)[Ni(dmit)_2]_3$ (**94**) has the highest of the room-temperature conductivities of all of the complexes of 7 S/cm.

The optical properties of $(Bu_4N)_2[Ni(dmit)_2]_7 \cdot 2CH_3CN$ (**49**), $(Me_3S)[Ni(dmit)_2]_2$ (**93**) and $(Ph_4P)[Ni(dmit)_2]_3$ (**94**) are dominated by vibrational features at low frequencies and by electronic excitations at higher frequencies. The observed vibrational features include ordinary intramolecular modes and seven "anomalous" infrared-active vibrational modes. A series of electronic excitations are observed for the electric field polarized along the $Ni(dmit)_2$ stacks. The low-lying peaks are attributed to a charge transfer from one $Ni(dmit)_2$ anion to an adjacent neutral molecule, whereas the excitations higher in frequency are attributed to a charge transfer between two $Ni(dmit)_2$ anions.

CHAPTER 3
EXTENSIVELY CONJUGATED, CHALCOGEN-RICH, DIANIONIC TETRATHIOOXALATE-BRIDGED COPPER(II) COMPLEXES

Within the search for new complexes exhibiting novel electronic properties, many metals (e.g. M = Ni(II), Pt(II), Pd(II), Cu(II)), with bischelating dmit-based ligands, and both closed-shell and open-shell counterions have been studied. They have shown semiconducting, metallic and even superconducting properties.[53] These classes of complexes have been well-studied and have still only yielded materials with superconducting properties at very low temperatures and under high pressures.[149] Efforts have therefore been directed towards the synthesis of new anionic systems similar to $[M(dmit)_2]^{n-}$ but with longer conjugation lengths. In keeping with structural requirements that have proved successful in forming electrically conducting systems with $[M(dmit)_2]^{n-}$ $(0 \leq n \leq 2)$ and other related systems, the following structural scheme is used as a template for tto (where tto = $C_2S_4^{2-}$ = tetrathiooxalato, **45**) bridged bimetallic complexes as precursors to new electronic materials:

X = S, Se

M = Ni(II), Pd(II), Pt(II), Cu(II)

It consists of square planar coordinating transition metals "bridged" and "capped" by chalcogen-rich, fully conjugated planar ligands. This type of complex has been designed in order to extend the delocalization and to increase interactions throughout the crystal lattice.

We have synthesized a series of extensively conjugated and planar, chalcogen-rich, dianionic tetrathiooxalato-bridged bimetallic Cu(II) complexes having the general formula $(Bu_4N)_2\{tto[Cu(L)]_2\}$ (L = dmit = $C_3S_5^{2-}$ = 2-thiooxo-1,3-dithiole-4,5-dithiolato for complex **105**, mnt = $C_4N_2S_2^{2-}$ = 1,2-dicyanoethene-1,2-dithiolato for complex **106**, dsit = $C_3Se_2S_3^{2-}$ = 2-thiooxo-1,3-dithiole-4,5-diselenelato for complex **107**, dmid = $C_3OS_4^{2-}$ = 2-oxo-1,3-dithiole-4,5-dithiolato for complex **108**). The complexes have been fully characterized including X-ray analysis, UV-vis, IR, elemental analysis and cyclic voltammetry.[150,151] The dianion of the complex $(Bu_4N)_2\{tto[Cu(dmid)]_2\}$ (**108**), has been previously reported in the complex $(Ph_4As)_2\{tto[Cu(dmid)]_2\}$ (**88**)[111,114] as mentioned in section 1–5. The complex could not be reproducibly synthesized using the synthetic procedures that were reported in Ref. 111 and 114. While we have developed a reproducible synthesis of this complex, its structure will be discussed using the X-ray data reported for $(Ph_4As)_2\{tto[Cu(dmid)]_2\}$ (**88**). The complex $(Bu_4N)_2\{tto[Cu(dmit)]_2\}$ (**105**), has been reacted with varied amounts of NaI/I_2 oxidant in order to obtain non-integer oxidation state materials, and the products have been investigated with elemental analysis and temperature-dependent conductivity measurements.[125,150]

3–1 Experimental

General procedures. Infrared spectra were recorded on a Perkin-Elmer 1725 FTIR spectrophotometer. Ultraviolet-visible spectra were obtained using a Shimadzu UV–160A UV–vis spectrophotometer. Melting points were measured using a Boetius melting point apparatus and are uncorrected. Elemental analysis for $(Bu_4N)_2\{tto[Cu(dmit)]_2\}$ (**105**), $(Bu_4N)_2\{tto[Cu(mnt)]_2\}$ (**106**) and $(Bu_4N)_{0.33}\{tto[Cu(dmit)]_2\}$ (**109**) was completed at Robertson Microlit Labs Inc., Madison, NJ, and for $(Bu_4N)_2\{tto[Cu(dsit)]_2\}$ (**107**) and

$(Bu_4N)_2\{tto[Cu(dmid)]_2\}$ (**108**) using a Heraeus CHN Rapid Analyzer at the University of Leipzig.

Materials. All solvents used in the synthetic procedures were used as received (Fisher Scientific). Water used in the synthetic procedures was purified using a Millipore Milli-Q water system.

Preparation of $(Bu_4N)_2\{tto[Cu(dmit)]_2\}$ (**105**). A 472 mg (0.500 mmol) sample of $(Bu_4N)_2[Zn(dmit)_2]$ (**110**), prepared according to Steimecke and coworkers,[56] was dissolved in 25 ml of CH_2Cl_2. To this solution was added a solution of 103 mg (0.250 mmol) of $(Et_4N)_2tto$ (**45**)[152] in 25 ml of water, after which the mixture was stirred for 5 minutes. With a pipet, a solution of 85 mg (0.500 mmol) of $CuCl_2{\cdot}2H_2O$ (**111**) dissolved in 15 ml of methanol was added slowly to the organic layer of the vigorously stirred solution. After the addition, the biphasic solution was stirred for 10 min. resulting in a deep-purple organic phase. The organic phase was removed, and the aqueous layer was washed twice with 20 ml portions of CH_2Cl_2, combined, and filtered. An equivalent amount of 2-propanol was added, and the mixture was allowed to evaporate to less than half its volume overnight and filtered again. To the resulting precipitate, CH_2Cl_2 was added dropwise until only slightly soluble product remained. The product was crystallized by slow evaporation from a 1:1 mixture of acetone/2-propanol. Crystals used for the structure determination were obtained via slow evaporation from previously crystallized material dissolved in acetone. Yield: 144 mg (25%). Mp: 147–148 °C. Anal. Calcd for $C_{40}H_{72}N_2S_{14}Cu_2$: C, 41.52; H, 6.28; N, 2.42; S, 38.79; Cu, 10.99. Found: C, 41.40; H, 6.11; N, 2.39; S, 39.30; Cu, 11.36. IR (KBr; cm^{-1}): υ(C-H) 2960, 2868; υ(C=C) 1484, 1372; υ(C=S) 1065. UV–vis [acetone; nm, (log ε)]: 465 (4.30), 513 (4.46), 557 (4.56), 700 (4.26), 1056 (3.99), 1365 (3.72).

$(Bu_4N)_2\{tto[Cu(mnt)]_2\}$ (**106**). 416 mg (0.500 mmol) of $(Bu_4N)_2[Zn(mnt)_2]$ (**112**) prepared following Gray and coworkers,[153] was dissolved in 25 ml of CH_2Cl_2. To this, a solution of 103 mg (0.250 mmol) of $(Et_4N)_2tto$ (**45**) in 25 ml of water was added

and stirred for 5 minutes. With a pipette, a solution of 85 mg (0.500 mmol) of $CuCl_2 \cdot 2H_2O$ (**111**) dissolved in 15 ml of methanol was added rapidly in small amounts to the vigorously stirred solution. After addition, the biphasic solution was stirred for 10 minutes resulting in a deep-purple colored organic phase. The organic phase was separated and the aqueous layer was washed twice with 20 ml portions of CH_2Cl_2, combined and filtered. An equivalent amount of 2-propanol was added and the mixture was allowed to evaporate to less than half and filtered again. To the resulting precipitate, CH_2Cl_2 is added dropwise until only slightly soluble product is remaining. The product was crystallized from slow evaporation of a 1:1 mixture of acetone/2-propanol. Crystals used for structure determination were obtained via slow evaporation from previously crystallized material dissolved in acetone. Yield: 100 mg (19%). Mp: 192–193°C dec. Anal. Calcd for $C_{42}H_{72}N_6Cu_2S_8$: C, 48.28; H, 6.96; N, 8.05; S, 24.55. Found: C, 48.12; H, 7.27; N, 8.08; S, 23.78. IR (KBr, cm^{-1}): υ(C-H) 2955, 2870; υ(C≡N) 2200; υ(C=C) 1448; υ(C=S) 1007. UV–vis [acetone, nm (log ε)]: 541 (4.44), 619 (4.38), 862 (3.97).

$(Bu_4N)_2\{tto[Cu(dsit)]_2\}$ (**107**). Complex **107** was prepared and isolated similar to $(Bu_4N)_2\{tto[Cu(dmit)]_2\}$ (**105**) and $(Bu_4N)_2\{tto[Cu(mnt)]_2\}$ (**106**) using minor modifications. A solution of 565 mg (0.500 mmol) of $(Bu_4N)_2[Zn(dsit)_2]$ (**113**)[87] in CH_2Cl_2 was added to a solution of 103 mg (0.250 mmol) of $(Et_4N)_2tto$ (**45**) in 25 ml of water and stirred for 5 minutes. With a pipette, 85 mg (0.500 mmol) of $CuCl_2 \cdot 2H_2O$ (**111**) dissolved in 15 ml of methanol was added slowly directly to the organic layer of the stirring biphasic solution. The precipitate was recrystallized by slow evaporative cooling under a stream of argon in a 1:1 mixture of acetone/2-propanol followed by refrigeration overnight. Yield: 170 mg (30%). Mp: 146–147°C. Anal. Calcd for $C_{40}H_{72}N_2Cu_2Se_4S_{10}$: C, 35.73; H, 5.40; N, 2.08. Found: C, 35.78; H, 5.18; N, 2.11. IR (KBr, cm^{-1}): υ(C-H) 2950, 2866; υ(C=C) 1461; υ(C=S) 1052. UV–vis [methylene chloride, nm (log ε)] 261 (4.58), 443 (4.24), 479 (4.20), 574 (4.48), 1013 (4.06).

$(Bu_4N)_2\{tto[Cu(dmid)]_2\}$ (**108**). Complex **108** was prepared and isolated similar to $(Bu_4N)_2\{tto[Cu(dmit)]_2\}$ (**105**), $(Bu_4N)_2\{tto[Cu(mnt)]_2\}$ (**106**) and $(Bu_4N)_2\{tto[Cu(dsit)]_2\}$ (**107**) with minor modifications. A solution of 455 mg (0.500 mmol) of $(Bu_4N)_2[Zn(dmid)_2]$ (**114**)[85] in a minimal amount of (~10 ml) CH_2Cl_2 was added to a solution of 103 mg (0.250 mmol) of $(Et_4N)_2tto$ (**45**) in 25 ml of water and stirred for 5 minutes. After slow addition of 85 mg (0.500 mmol) of $CuCl_2 \cdot 2H_2O$ (**111**) dissolved in 15 ml MeOH was added to the organic layer, the biphasic solution was stirred for 40 minutes. The organic layer was then separated, combined with two CH_2Cl_2 washings of the aqueous layer and filtered. The filtered blue-black micro-crystalline compound was recrystallized with 1:1 acetone/2-propanol. Yield: 80 mg (14%). Mp: 169–171°C dec. Anal. Calcd for $C_{40}H_{72}N_2Cu_2O_2S_{12}$: C, 42.70; H, 6.46; N, 2.69. Found: C, 42.92; H, 6.19; N, 3.08. IR (KBr, cm^{-1}): υ(C-H) 2959, 2870; υ(C=O) 1663, 1613; υ(C=C) 1456; υ(C=S) 897. (lit.,[114] υ(C=O) 1600 and υ(C=S) 910 cm^{-1}); UV–vis [acetone, nm (log ε)]: 460 (4.53), 555 (4.90), 700(sh) (3.58), 1070 (4.40). (lit.,[114] 460, 560, 720(sh) and 1100 nm).

Oxidation of $(Bu_4N)_2\{tto[Cu(dmit)]_2\}$ (**105**). Complex **105** was oxidized to various degrees using NaI/I_2 oxidant.[125] Equal amounts (230 mg, 0.200 mmol) of **105** dissolved in a minimal amount of acetone was used and reacted with 0.25 equivs. (12.7 mg, 0.050 mmol of I_2, **115** and 19 mg, 0.130 mmol of NaI, **116**), 0.50 equivs. (25.4 mg, 0.100 mmol of **115** and 39 mg, 0.260 mmol of **116**), 0.75 equivs. (38.1 mg, 0.150 mmol of I_2, **115** and 57 mg, 0.390 mmol of NaI, **116**), and 1.0 equivs. (50.8 mg, 0.200 mmol of **115** and 78 mg, 0.520 mmol of **116**), of NaI/I_2 in minimal amount of acetone. Approximately 2/3 amount of the acetone was removed under vacuum followed by addition of an equal amount of methanol. Half of the solvent was evaporated under a stream of argon and filtered. The remaining black ppt. was washed with methanol, then ethyl ether, and dried thoroughly under vacuum. Anal. Calcd for $C_{13.33}H_{12}N_{0.33}S_{14}Cu_2$: C, 21.27;

H, 1.61; N. 0.62; S, 59.63; Cu, 16.88. Found: C, 22.05; H, 1.83; N, 0.63; S, 57.50; Cu, 16.89.

X-ray structure determinations. Crystallographic data for complexes $(Bu_4N)_2\{tto[Cu(dmit)]_2\}$ (**105**), $(Bu_4N)_2\{tto[Cu(mnt)]_2\}$ (**106**) and $(Bu_4N)_2\{tto[Cu(dsit)]_2\}$ (**107**) are collected in Appendix Tables B–1 to B–9. Thermal ellipsoids drawings and molecular numbering schemes for the $Ni(dmit)_2$ units of complexes **105–107** are located in Fig. 3–1. Data was collected at room temperature on a Siemens R3m/V diffractometer. For **105**, purple-black needle-like crystals (0.55 x 0.13 x 0.13 mm^3) were chosen for study, for **106**, purple-black block-like crystals (0.39 x 0.28 x 0.15 mm^3) were chosen for study and for **107**, purple-black needles (0.46 x 0.09 x 0.08 mm^3) were chosen for study.

For **105** and **106**, the diffractometer was equipped with a graphite monochromator utilizing MoK_α radiation ($\lambda = 0.71073$ Å) and for **107** with a Ni filter using CuK_α radiation ($\lambda = 1.54178$ Å). For $(Bu_4N)_2\{tto[Cu(dmit)]_2\}$ (**105**), 32 reflections with $20.0^\circ \leq 2\theta \leq 22.0^\circ$, for $(Bu_4N)_2\{tto[Cu(mnt)]_2\}$ (**106**), 32 reflections with $20.0^\circ \leq 2\theta \leq 22.0^\circ$ and $(Bu_4N)_2\{tto[Cu(dsit)]_2\}$ (**107**), 32 reflections with $40.0^\circ \leq 2\theta \leq 44.0^\circ$ were used to refine the cell parameters. For **106**, 5042 reflections and for **107**, 3256 reflections were collected using the ω-scan method. For complexes **105-107**, four reflections were measured every 96 reflections to monitor instrument and crystal stability (maximum correction on I was < 2% for **106** and < 1% for **105** and **107**). Absorption corrections were applied based on measured crystal faces using *SHELXTL plus.*[136]

For $(Bu_4N)_2\{tto[Cu(mnt)]_2\}$ (**106**), the structure was solved by the heavy atom method and for $(Bu_4N)_2\{tto[Cu(dmit)]_2\}$ (**105**) and $(Bu_4N)_2\{tto[Cu(dsit)]_2\}$ (**107**) by direct methods in *SHELXTL plus*[136] from which the locations of the four Cu atoms was obtained. For complexes **105-107**, the structures were refined in *SHELXTL plus.*[136] The non-hydrogen atoms were treated anisotropically, whereas the positions of the

a)

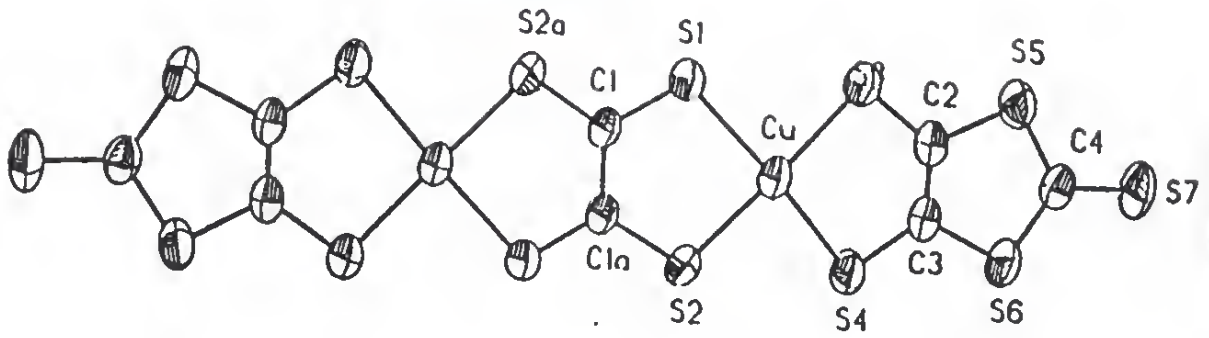

b)

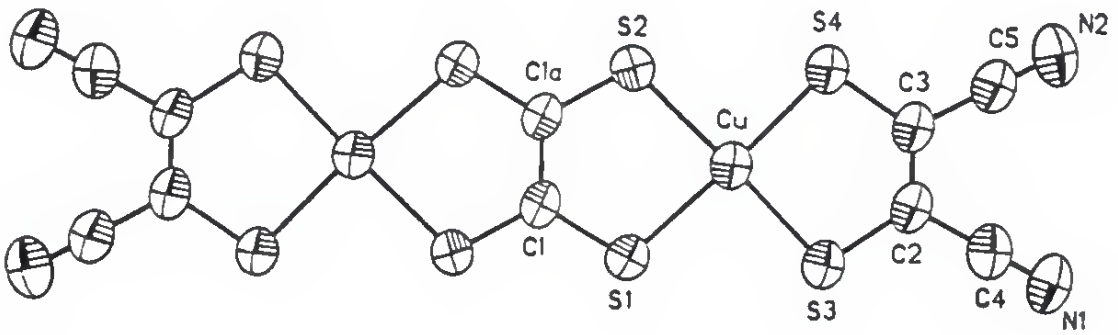

c)

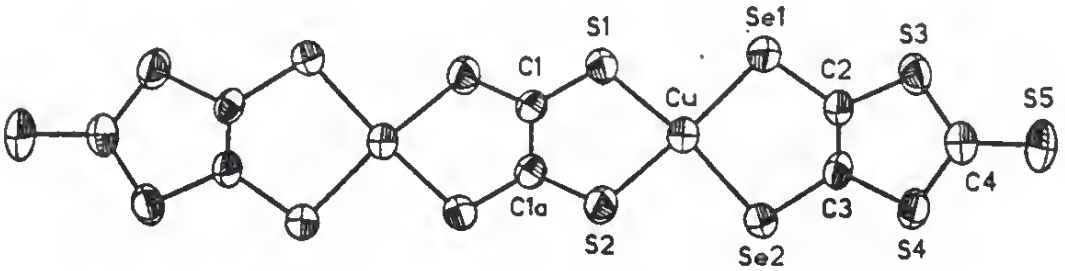

Figure 3–1. Thermal ellipsoids drawings (50% probability) and numbering schemes for the dianions of (a) $(Bu_4N)_2\{tto[Cu(dmit)]_2\}$ (**105**), (b) $(Bu_4N)_2\{tto[Cu(mnt)]_2\}$ (**106**) and (c) $(Bu_4N)_2\{tto[Cu(dsit)]_2\}$ (**107**).

hydrogen atoms were calculated in ideal positions and their isotropic thermal parameters were fixed.

For $(Bu_4N)_2\{tto[Cu(dmit)]_2\}$ (**105**), 262 parameters, for $(Bu_4N)_2\{tto[Cu(mnt)]_2\}$ (**106**), 150 parameters, and $(Bu_4N)_2\{tto[Cu(dsit)]_2\}$ (**107**), 262 parameters were refined and $w = 1/[(\sigma|F_o|^2 + 0.0004(F_o)^2]$. For **105-107**, $\sum w\ (|F_o| - |F_c|)^2$ was minimized, $\sigma(F_o) = 0.5\ kI^{-1/2}\{[\sigma(I)]^2 + (0.02I)^2\}^{1/2}$, I(intensity) = $(I_{peak} - I_{background})$(scan rate), and $\sigma(I) = (I_{peak} + I_{background})^{1/2}$(scan rate), k is the correction due to decay and Lp effects, 0.02 is a factor used to down weight intense reflections and to account for instrument instability. The linear absorption coefficients and scattering factors for **105-107** were taken from values from the *International Tables for X-ray Crystallography.*[137]

Electrochemical methods. Cyclic voltammetry was carried out on an EG&G Princeton Applied Research Scanning Potentiostat 362 with a Philips X-Y PM 8120 Recorder. Methylene chloride was used as is (Aldrich, 99.8%) and thoroughly degassed with argon prior to use. Ag/AgCl was used as reference electrode with platinum wire working electrode and platinum foil counter electrode. Electrochemistry was carried out under an argon atmosphere. Approximate concentrations of the complexes used in the CV experiments was 10^{-4} M.

Conductivity measurements. A single crystal of $(Bu_4N)_2\{tto[Cu(dmit)]_2\}$ (**105**) and the products obtained from the oxidation of **105** with varied amounts of NaI/I_2 oxidant were pressed into pellet form using an IR press. The pellets were cut into rectangular pieces with a razor blade of measured sizes for the products obtained using 0.25 equivs. (4.5 x 1.8 x 0.5 mm^3), 0.5 equivs. (3.0 x 2.5 x 0.5 mm^3), 0.75 equivs. (6.0 x 3.0 x 0.5 mm^3) and 1.0 equivs. (2.5 x 2.5 x 0.7 mm^3) of NaI/I_2 oxidant. Two narrow gauge (0.05 mm diameter) gold wires were affixed to the cut sample using fast drying gold paint (Ted Pella Corp.). The cut sample obtained from one equiv. reaction of Na/I_2 with $(Bu_4N)_2\{tto[Cu(dmit)]_2\}$ (**105**), four gold wires were affixed and the sample was

thermally anchored to the cold head of a close-cycle refrigerator (CTI Cryogenics). A typical run was done by first cooling the sample to the lowest temperature, and then taking the data while warming. Temperature reproducibility has been determined to be ±0.02 K or better over the temperature range covered. The conductivities (σ) were obtained using the values of the dimensions of the samples and the resistances in the equation, $\sigma = l/R \cdot t \cdot w$ (where R = resistance, l = length, t = thickness and w = width of the sample).

3–2 Results

3–2–1 Synthesis of Complexes $(Bu_4N)_2\{tto[Cu(dmit)]_2\}$ (105), $(Bu_4N)_2\{tto[Cu(mnt)]_2\}$ (106), $(Bu_4N)_2\{tto[Cu(dsit)]_2\}$ (107) and $(Bu_4N)_2\{tto[Cu(dmid)]_2\}$ (108)

The synthesis of the complexes **105–108** (Fig. 3–2) is based on the result of competing reactions in a stirring biphasic solution. Methanolic $CuCl_2 \cdot 2H_2O$ (**111**) solution is added to a biphasic solution of $(Et_4N)_2tto$ (**45**) dissolved in water and the corresponding ligand of choice as the bis-chelate of Zn^{2+} ($(Bu_4N)_2[Zn(L)_2]$), dissolved in methylene chloride. The competing reactions are metal exchange of thiophilic Cu^{2+} with the zinc containing bis-chelate in the organic layer, and with the tto^{2-} ligand at the interface of the aqueous and organic layers. The formation of the insoluble oligomeric $[Cu(tto)]_n$ (**117**)[112,113] highly soluble bis-chelate, $[Cu(L)_2]^{2-}$,[154] and lesser soluble $\{tto[Cu(L)]_2\}^{2-}$ allows the bimetallic complex of interest to be isolated based on solubility differences as explained in the experimental section. The synthetic procedures are readily reproducible for $(Bu_4N)_2\{tto[Cu(dmit)]_2\}$ (**105**) in 25 %, $(Bu_4N)_2\{tto[Cu(mnt)]_2\}$ (**106**) in 19%, $(Bu_4N)_2\{tto[Cu(dsit)]_2\}$ (**107**) in 30% and complex $(Bu_4N)_2\{tto[Cu(dmid)]_2\}$ (**108**) in 14% yield. All of the complexes exhibit a deep-blue color in acetone and CH_2Cl_2 solutions due to a characteristic strong absorption in the range of 541–574 nm (Fig. 3–3) assigned to $\sigma(S) \rightarrow Cu(II)$ ligand to metal transition.[155]

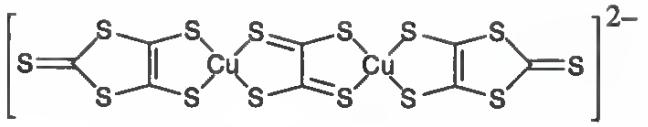

{tto[Cu(dmit)]$_2$}$^{2-}$ (**105**)

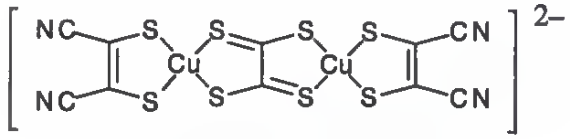

{tto[Cu(mnt)]$_2$}$^{2-}$ (**106**)

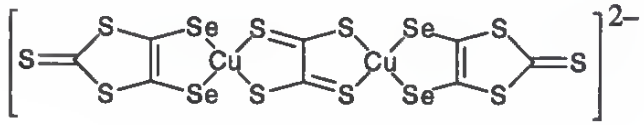

{tto[Cu(dsit)]$_2$}$^{2-}$ (**107**)

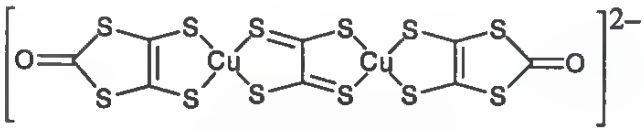

{tto[Cu(dmid)]$_2$}$^{2-}$ (**108**)

Figure 3–2. Bimetallic copper (II) complexes synthesized $(Bu_4N)_2$\{tto[Cu(dmit)]$_2$\} (**105**), $(Bu_4N)_2$\{tto[Cu(mnt)]$_2$\} (**106**), $(Bu_4N)_2$\{tto[Cu(dsit)]$_2$\} (**107**) and $(Bu_4N)_2$\{tto[Cu(dmid)]$_2$\} (**108**).

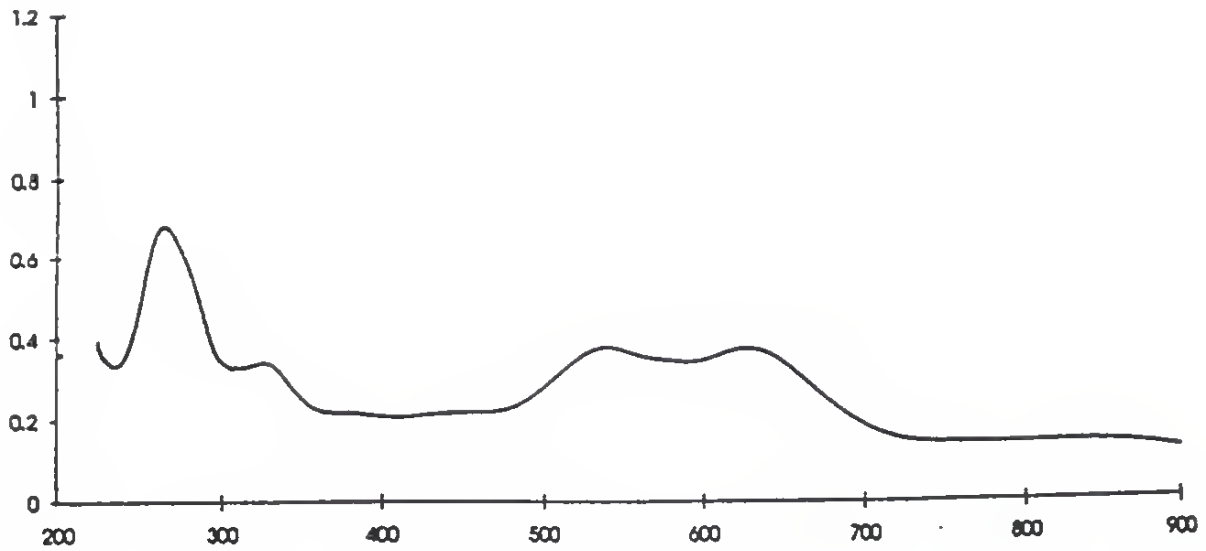

Figure 3–3. A representative UV-vis spectrum of $(Bu_4N)_2\{tto[Cu(mnt)]_2\}$ (**106**) in acetone of complexes **105–108**.

3–2–2 X-ray Structures of **105–108**.

Comparison of the structures of $(Bu_4N)_2\{tto[Cu(dmid)]_2\}$ (**108**) will be discussed using results reported for the dianion as its tetraphenylarsonium salt $(Ph_4As)_2\{tto[Cu(dmid)]_2\}$ (**88**),[114] along with $(Bu_4N)_2\{tto[Cu(dmit)]_2\}$ (**105**),[150] $(Bu_4N)_2\{tto[Cu(mnt)]_2\}$ (**106**) and $(Bu_4N)_2\{tto[Cu(dsit)]_2\}$ (**107**).[151] As seen in Fig. 3–1, two Cu(dmit) units in **105**, two Cu(mnt) units in **106** and two Cu(dsit) units in **107** are bridged by the side-on coordination of the tto ligand. This is also the case for the complexes $(Ph_4As)_2\{tto[Cu(dmid)]_2\}$ (**88**).[114] The C(1)–C(1a) bond of the tto in $(Bu_4N)_2\{tto[Cu(mnt)]_2\}$ (**106**) (1.483(9) Å), and in $(Bu_4N)_2\{tto[Cu(dsit)]_2\}$ (**107**) (1.483(8) Å), is essentially the same as $(Bu_4N)_2\{tto[Cu(dmit)]_2\}$ (**105**), and as was observed for $(Ph_4As)_2\{tto[Cu(dmid)]_2\}$ (**88**) (1.467(10) Å). These bond lengths are all comparable to the isolated tto^{2-} (1.461(11) Å) as its Ph_4P^+ salt,[156] and thus, the results indicate the C_2S_4 bridging unit of the Cu metal centers behaves as a dianion. This is supported by the fact that these central C–C tto bonds are similar in length to that observed in the neutral Cu(I) tto complex $tto[Cu(Ph_3P)_2]_2$ (**118**) (1.531(8) Å).[157] If the C_2S_4 unit behaved as a tetraanion in the form of ethylenetetrathiolate ($C_2S_4^{4-}$, **74**), the length of the C(1)–C(1a) bond would be considerably shorter (~1.332 Å).[114]

The $Cu(C_2S_4)Cu$ core of each complex is planar. $(Bu_4N)_2\{tto[Cu(mnt)]_2\}$ (**106**) is unique among the complexes discussed as it exhibits square planar Cu coordination resulting in a perfectly planar and highly conjugated molecule. This is the first fully planar, bimetallic complex with tetrathiooxalate as bridging ligand, which is an important structural feature for future studies in utilizing these complexes in electrically conducting materials. The coordination spheres of the Cu metal centers in $(Bu_4N)_2\{tto[Cu(dsit)]_2\}$ (**107**), $(Ph_4As)_2\{tto[Cu(dmid)]_2\}$ (**88**), and $(Bu_4N)_2\{tto[Cu(dmit)]_2\}$ (**105**) exhibit a slight tetrahedral distortion from square planar coordination at the Cu centers. This results in a twist formed between the bridging tto ligand and the capping ligands. A dihedral angle is thus formed from the planes of the tto and the capping ligands. The smallest dihedral angle

for the tetrahedrally distorted complexes is the dmit derivative **105** at 18.87(3)°. Complex **107** has a dihedral angle of 24.86(3)° with $\{tto[Cu(dmid)]_2\}^{2-}$ (**88**) being reported as the largest at 28.3°.[114]

For the dmit complex $(Bu_4N)_2\{tto[Cu(dmit)]_2\}$ (**105**), the equal lengths of the Cu–S bonds (2.269(1) Å) to the tto ligand indicate a fully conjugated Cu-tto-Cu system. This is also seen in the dsit-capped chelate $(Bu_4N)_2\{tto[Cu(dsit)]_2\}$ (**107**) (2.262(2) Å). In contrast to this, $(Bu_4N)_2\{tto[Cu(mnt)]_2\}$ (**106**) behaves similar to $(Ph_4As)_2\{tto[Cu(dmid)]_2\}$ (**88**) where two different types of Cu-tto bonds are observed. In **88**, the bond lengths are 2.258(2) and 2.245(2) Å for the chemically equivalent bonds and in complex **105** they are 2.256(2) and 2.273(2) Å.[114] This was also observed for the copper(I) complex $tto[Cu(Ph_3P)_2]_2$ (**118**).[157]

An interesting relationship between the ethylene bond lengths (C2–C3) of the capping ligands and the dihedral angles resulting from the slight tetrahedral distortion was found. As the length of the bond increases, the dihedral angle decreases. In $(Bu_4N)_2\{tto[Cu(mnt)]_2\}$ (**106**), the bond length of 1.355(10) Å corresponds to a planar structure with dihedral angle of 0° whereas in $(Ph_4As)_2\{tto[Cu(dmid)]_2\}$ (**88**), the bond distance of 1.326(8) Å leads to the largest dihedral angle value of 28.3°.[114]

Figs. 3–4 and 3–5 show views of the packing of the chelate anions for $(Bu_4N)_2\{tto[Cu(dmit)]_2\}$ (**105**), Figs. 3–6 and 3–7 for $(Bu_4N)_2\{tto[Cu(mnt)]_2\}$ (**106**), and Figs. 3–8 and 3–9 show packing views of $(Bu_4N)_2\{tto[Cu(dsit)]_2\}$ (**107**). Complex **106** exhibits packing of sheets of isolated planar dianions separated by sheets of isolated cations. In complex $(Ph_4As)_2\{tto[Cu(dmid)]_2\}$ (**88**), it was reported that the dianions were surrounded by six tetraphenylarsonium cations.[114] Complexes **105** and **107** exhibits a different packing scheme from $(Bu_4N)_2\{tto[Cu(mnt)]_2\}$ (**106**) and $(Ph_4As)_2\{tto[Cu(dmid)]_2\}$ (**88**). The packing is exhibited as sheets of one-dimensional chains of dianions separated by isolated tetrabutylammonium cations. The dianion chains

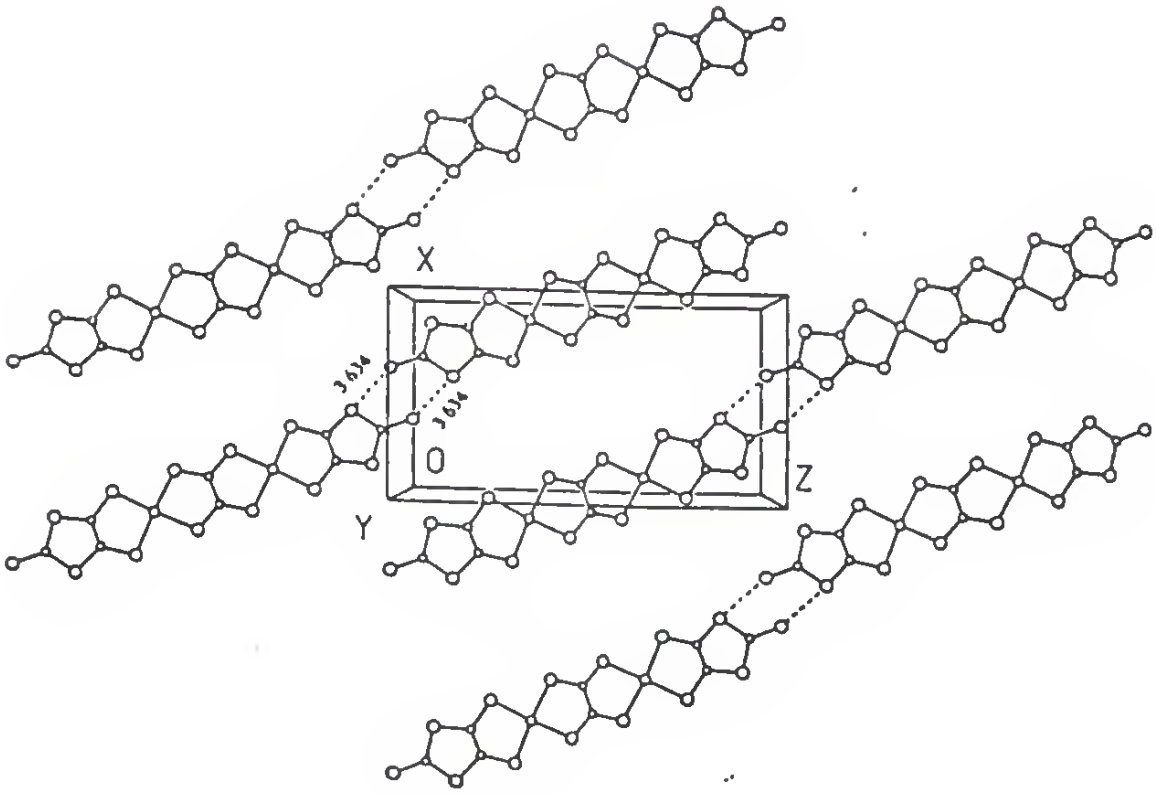

Figure 3–4. View down the y axis of $(Bu_4N)_2\{tto[Cu(dmit)]_2\}$ (**105**) showing one-dimensional chains formed from head-to-tail, thione-thiole groups of the dianions.

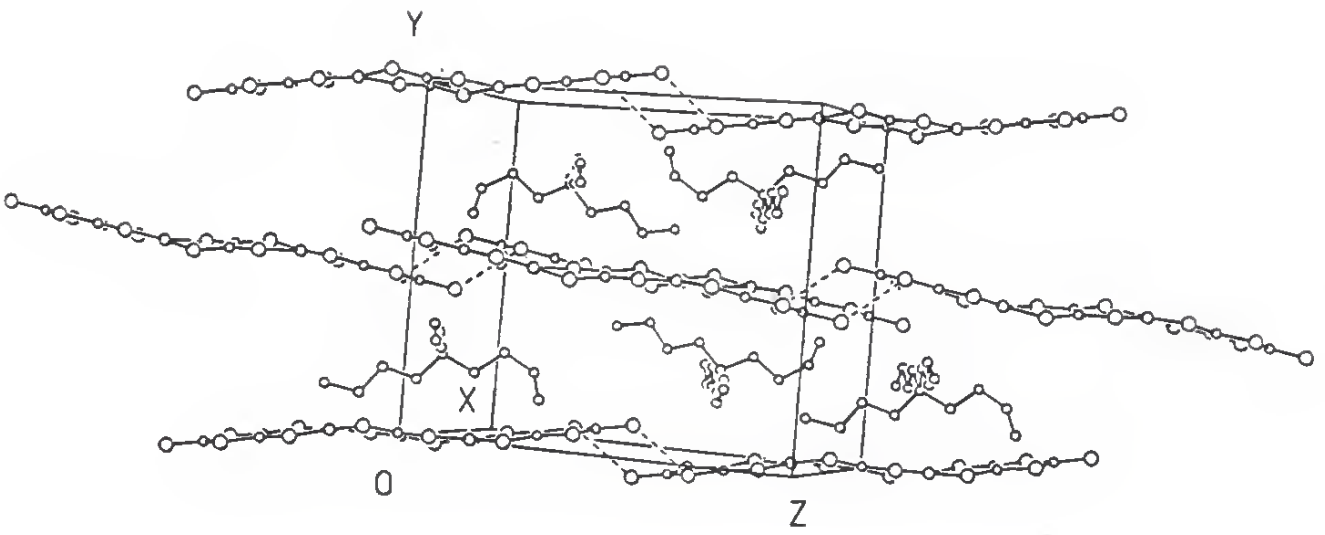

Figure 3–5. Packing diagram with unit cell labels of $(Bu_4N)_2\{tto[Cu(dmit)]_2\}$ (**105**) showing sheets of linear chains of complex dianions separated by tetrabutylammonium cations.

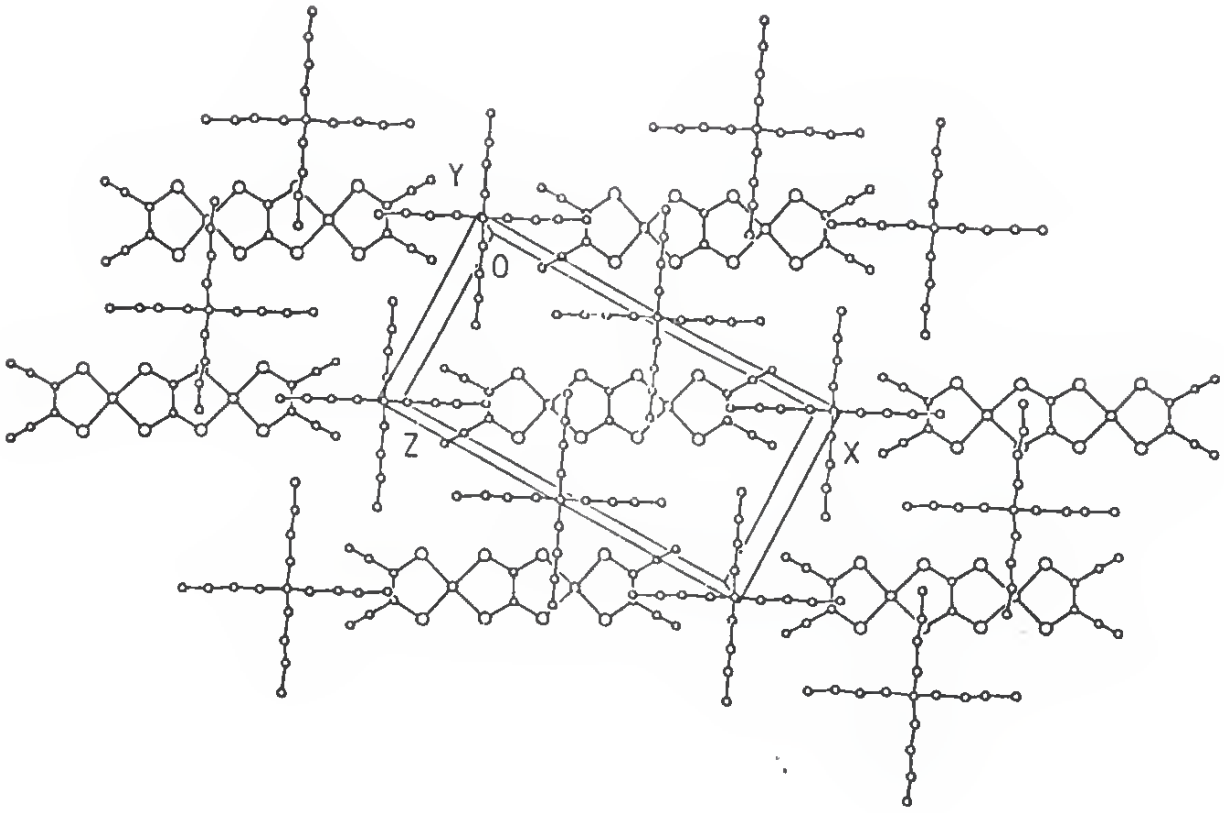

Figure 3–6. View down the y axis of $(Bu_4N)_2\{tto[Cu(mnt)]_2\}$ (**106**).

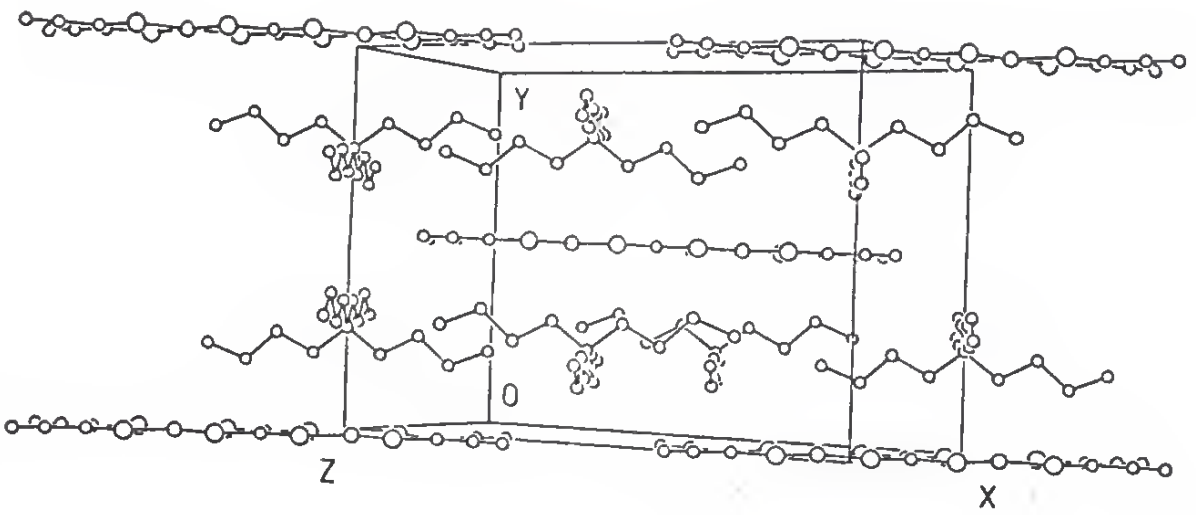

Figure 3–7. Packing diagram of $(Bu_4N)_2\{tto[Cu(mnt)]_2\}$ (**106**) illustrating the sheets of planar dianions separated by tetrabutylammonium cations.

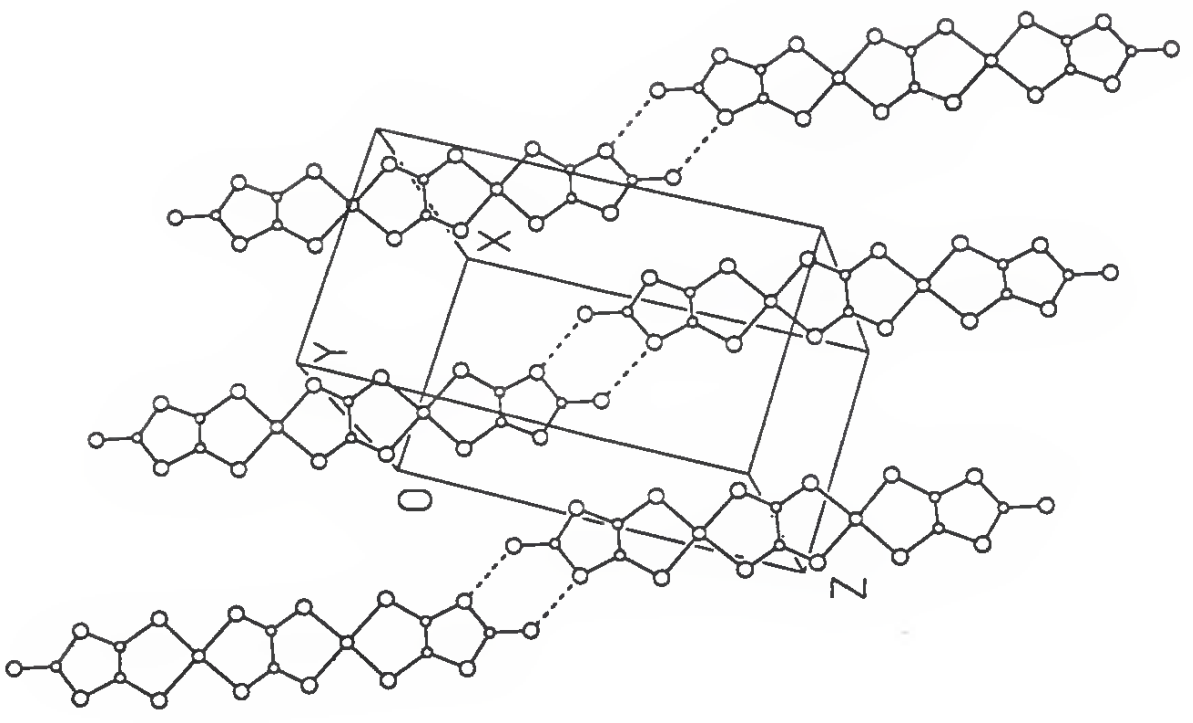

Figure 3–8. View down the y axis of $(Bu_4N)_2\{tto[Cu(dsit)]_2\}$ (**107**) showing one-dimensional chains formed from head-to-tail, thione-thiole non-bonding interactions.

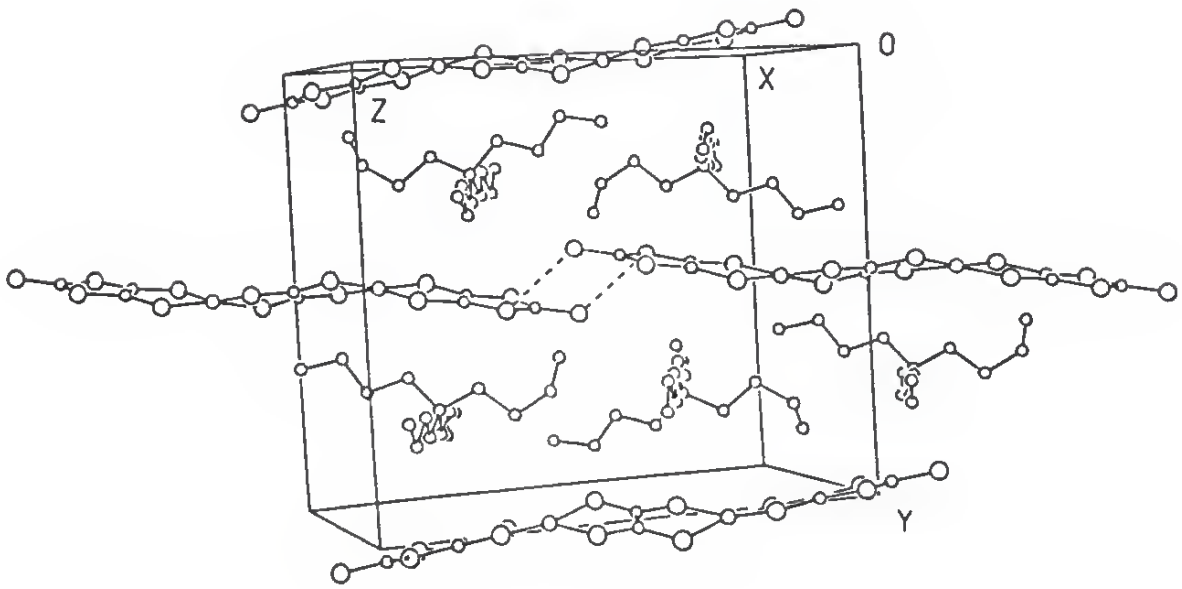

Figure 3–9. Packing diagram showing sheets of one-dimensional chains of the dianion of $(Bu_4N)_2\{tto[Cu(dsit)]_2\}$ (**107**) separated by tetrabutylammonium cations.

of $(Bu_4N)_2\{tto[Cu(dsit)]_2\}$ (**107**) are formed from interactions of thioxo(S5)–thiole(S4) groups on adjacent molecules (3.631(3) Å). In $(Bu_4N)_2\{tto[Cu(dmit)]_2\}$ (**105**), the distance is essentially identical at 3.634(3) Å.[150] The distances are shorter than the sum of the van der Waals radii of sulfur (3.70 Å).[68]

Based on the crystal structures discussed, $(Bu_4N)_2\{tto[Cu(dmit)]_2\}$ (**105**) and $(Bu_4N)_2\{tto[Cu(dsit)]_2\}$ (**107**) are isostructural. The intermolecular contacts lead to one-dimensional chains. These interactions may prove important for future electrical conductivity studies. Complex $(Bu_4N)_2\{tto[Cu(mnt)]_2\}$ (**106**) is unique due to its planarity, but displays no intermolecular interactions as seen in **105** and **107**. The dianion of $(Ph_4As)_2\{tto[Cu(dmid)]_2\}$ (**88**) exhibits neither intramolecular planarity as seen for the dianions of $(Bu_4N)_2\{tto[Cu(dmit)]_2\}$ (**105**) and $(Bu_4N)_2\{tto[Cu(dsit)]_2\}$ (**107**), nor intermolecular interactions as seen for the dianionic unit of $(Bu_4N)_2\{tto[Cu(mnt)]_2\}$ (**106**).[114]

3–2–3 Redox Properties of **105–108**

All of the complexes exhibit similar redox behavior with two separate reversible redox processes. Each complex is dianionic and stable in argon purged CH_3CN and CH_2Cl_2 based electrolytes. A representative cyclic voltammogram (CV) of $(Bu_4N)_2\{tto[Cu(dsit)]_2\}$ (**107**) for all complexes is shown in Figure 3–10. A compilation of the CV results is given in Table 3–1.

At potentials equal to –0.8 V, the complexes are stable and remain in their dianionic state. Scanning anodically, each complex exhibits a first low potential redox couple with $E_{1/2}$ values in the range of –0.79 to –0.63 V. Complex $(Bu_4N)_2\{tto[Cu(dmid)]_2\}$ (**108**) oxidizes at the lowest potential of –0.76 V with $(Bu_4N)_2\{tto[Cu(mnt)]_2\}$ (**106**) having a first oxidation at the highest potential of –0.59 V. This is expected for **106** due to the highly electronegative terminal cyano groups. All of the complexes first process is reversible with observed peak-to-peak separations of 70 mV for $(Bu_4N)_2\{tto[Cu(dmit)]_2\}$

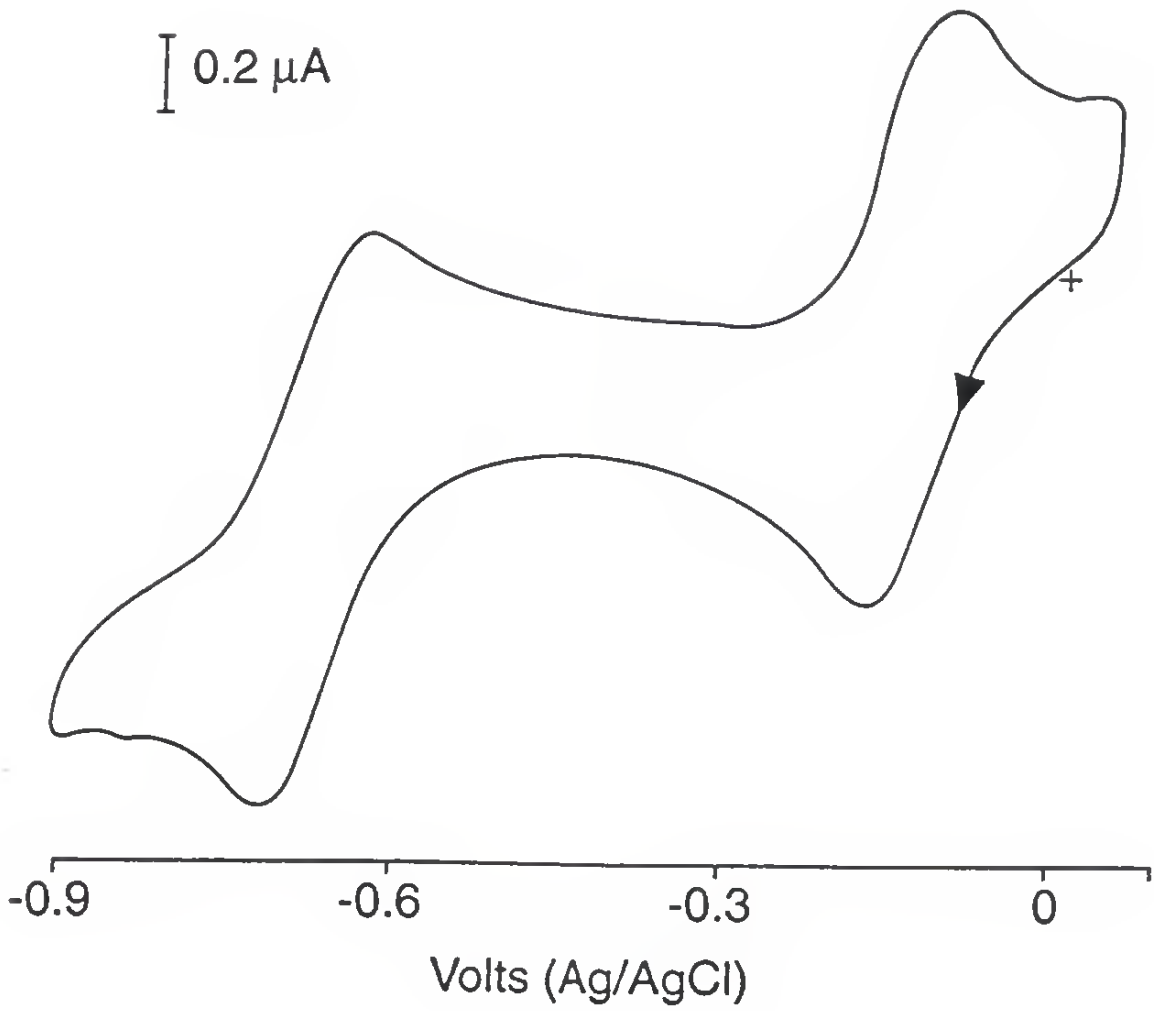

Figure 3–10. Cyclic voltammogram of $(Bu_4N)_2\{tto[Cu(dsit)]_2\}$ (**107**). Conditions: scan rate, 100 mV/s; reference electrode, Ag/AgCl; counter electrode, Pt foil; working electrode, Pt wire; 0.1 M Bu_4NClO_4 in CH_2Cl_2 under Ar at room temperature.

Table 3–1. Cyclic Voltammetric Peak Potentials of Complexes **105**, **106**, **107** and **108**[a]

Complex	potential (V)		
	$E_{p,a}$	$E_{p,c}$	$E_{1/2}$
$(Bu_4N)_2\{tto[Cu(dmit)]_2\}$ (**105**)	-0.08 -0.66	-0.15 -0.73	-0.12 -0.70
$(Bu_4N)_2\{tto[Cu(mnt)]_2\}$ (**106**)	+0.03 -0.59	-0.03 -0.67	0.00 -0.63
$(Bu_4N)_2\{tto[Cu(dsit)]_2\}$ (**107**)	-0.11 -0.63	-0.17 -0.71	-0.14 -0.67
$(Bu_4N)_2\{tto[Cu(dmid)]_2\}$ (**108**)	-0.13 -0.76	-0.18 -0.82	-0.15 -0.79

[a]Conditions: scan rate, 200 mV/s; reference electrode, Ag/AgCl; counter electrode, Pt foil; working electrode, Pt wire; 0.1 M Bu_4NClO_4 electrolyte in CH_2Cl_2 under Ar at room temperature.

(**105**), 80 mV for $(Bu_4N)_2\{tto[Cu(mnt)]_2\}$ (**106**), 80 mV for $(Bu_4N)_2\{tto[Cu(dsit)]_2\}$ (**107**), and 60 mV for $(Bu_4N)_2\{tto[Cu(dmid)]_2\}$ (**108**). This first redox process seen in all complexes may be assigned to the one-electron oxidation of the dianionic to the monoanionic species:

$$\{tto[Cu(L)]_2\}^{2-} \rightleftharpoons \{tto[Cu(L)]_2\}^{-} + e^{-}$$

Scanning to higher potentials, a second redox process is exhibited for each complex. $E_{1/2}$ values for this process range from –0.15 to 0.00 V. Complex **108** again oxidizes at the lowest potential of –0.18 V while **106** again oxidizes at the highest potential at +0.03 V. This second redox process for all complexes is also reversible with observed peak-to-peak separations of 70 mv for $(Bu_4N)_2\{tto[Cu(dmit)]_2\}$ (**105**), 60 mV for $(Bu_4N)_2\{tto[Cu(mnt)]_2\}$ (**106**), 60 mV for $(Bu_4N)_2\{tto[Cu(dsit)]_2\}$ (**107**), and 50 mV for $(Bu_4N)_2\{tto[Cu(dmid)]_2\}$ (**108**). This second redox process may be assigned to the one–electron oxidation of the monoanion to the neutral species:

$$\{tto[Cu(L)]_2\}^{-} \rightleftharpoons \{tto[Cu(L)]_2\}^{0} + e^{-}$$

Scan rate dependence studies (50 – 200 mV/s) show that all of the peak currents scale with the square root of the scan rate as expected for diffusion of the electroactive species to the electrode surface when the switching potential is maintained at < +0.20 V this indicates that, within this potential range and at these scan rates, the electroactive species remains in solution.

When scanning anodically to higher potentials, further oxidation processes are observed at approximately +0.20 V and +0.45 V for all the complexes **105–108** (Fig. 3–11), as shown in the representative cyclic voltammogram of $(Bu_4N)_2\{tto[Cu(dsit)]_2\}$

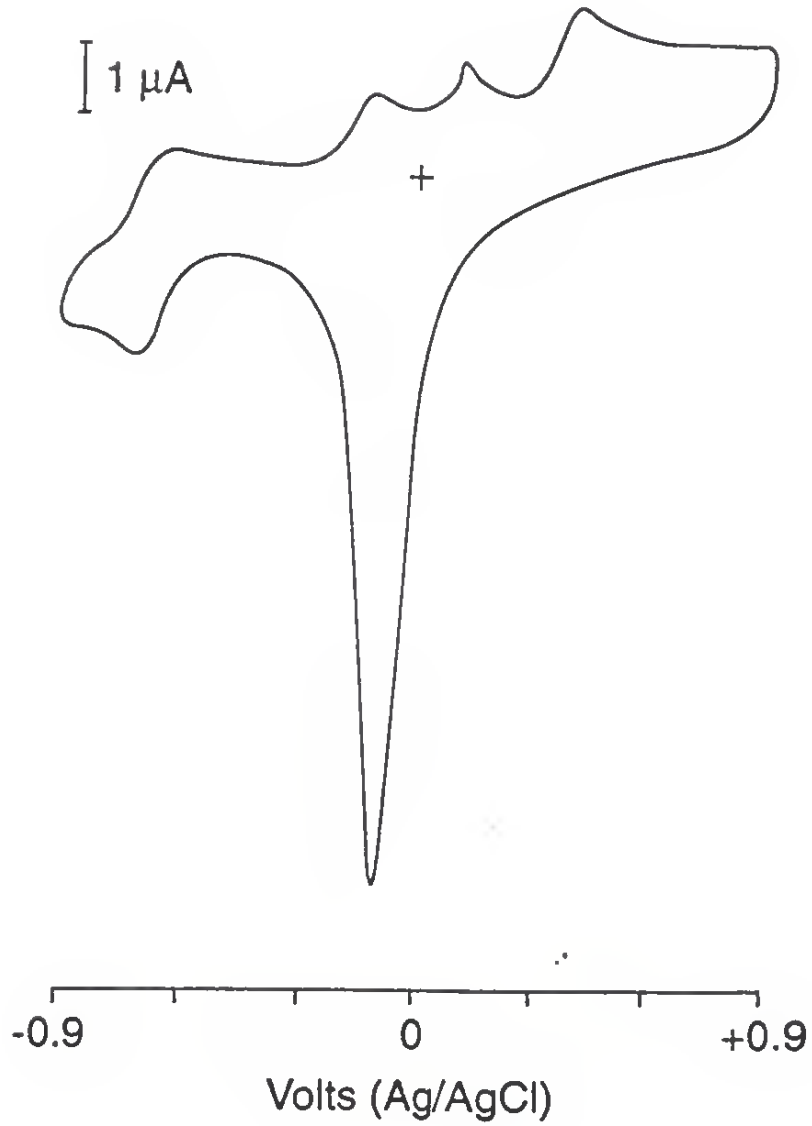

Figure 3–11. Cyclic voltammogram of $(Bu_4N)_2\{tto[Cu(dsit)]_2\}$ (**107**) showing a large cathodic wave upon anodically scanning to high potentials. Conditions: scan rate, 200 mV/s; reference electrode, Ag/AgCl; counter electrode, Pt foil; working electrode, Pt wire; 0.1 M Bu_4NClO_4 in CH_2Cl_2 under Ar at room temperature.

(**107**). These peaks may be due to oxidation of the tto ligand or further oxidation of the ligands to form a cationic species of the bimetallic complex. This is supported by the fact that recently, cationic bis-chelate Pd(II) and Pt(II) complexes of dithiolate ligands similar to dmit (i.e. dddt) have been synthesized and reported as counterions to anionic $[M(dmit)_2]^-$ (where M = Ni(II), Pd(II) and Pt(II)) complexes.[142,146] Switching at +0.90 V and scanning cathodically, a large peak at –.12 V dominates the cathodic process as shown for **107**. This behavior is observed for all the compounds studied.[151] When scanning to higher anodic potentials, an increase in the current for the cathodic wave was observed. This is characteristic of a redissolution process as the intensity is related to the amount of material deposited on the electrode. As one scans to higher and potentials, more material is allowed to deposit on the electrode thus increasing the redissolution peak intensity.[102] While a full study of the mechanism of the redox processes has not been carried out, it is possible that the species having higher oxidation states reacts chemically with the lesser or unoxidized species. This is followed by precipitation of some form of mixed-valence material on the electrode.[102] Electrocrystallization experiments with $(Bu_4N)_2\{tto[Cu(dmit)]_2\}$ (**105**) have as yet only yielded black insoluble precipitate on the electrode.

It has previously been reported[114,107] that the carbon–carbon π-bonding orbital of the C_2S_4 bridging ligand is the HOMO for this class of complexes. Oxidation of the complexes may result in the C_2S_4 unit becoming neutral resulting in cleavage of the carbon-carbon bond producing carbon disulfide, thereby ultimately resulting in the decomposition of the bimetallic bridged complex. This is not observed as the redox behavior presented indicates the stability of the complexes in solution in their dianionic, monoanionic, and neutral forms.

3–2–4 Conductivity Properties of $(Bu_4N)_2\{tto[Cu(dmit)]_2\}$ (**105**)

Reactions of $(Bu_4N)_2\{tto[Cu(dmit)]_2\}$ (**105**) with varied amounts of NaI/I_2 in acetone followed by precipitation with methanol were carried out to examine the feasibility of isolating higher oxidation states and to determine the conductivity of partially oxidized complexes. Two-probe conductivity measurements on the dianionic complex of **105** shows the complex is insulating as expected with single-crystal conductivities $<10^{-10}$ S/cm. The reactions have yielded black powders with pressed pellet conductivities up to 10^{-2} S/cm as shown in Table 3–2. Elemental analysis was completed on the product obtained from the oxidation of the dianionic complex with one equivalent of NaI/I_2 oxidizing agent. The analysis shows the formation of a non-integer oxidation state complex with the approximate stoichiometry $(Bu_4N)_{0.33}\{tto[Cu(dmit)]_2\}$ (**109**). Fig. 3–12 shows the temperature-dependence of the conductivity of **109**. It displays semiconducting electrical behavior with an activation energy (E_a) of 75 meV.

3–3 Conclusions

Using a unique, reproducible, three-solvent method, four new extensively conjugated, sulfur-rich bimetallic copper(II) complexes have been synthesized. The complexes $(Bu_4N)_2\{tto[Cu(dmit)]_2\}$ (**105**) and $(Bu_4N)_2\{tto[Cu(dsit)]_2\}$ (**107**) form one-dimensional chains from head-to-tail interactions, and as previously reported for $(Ph_4As)_2\{tto[Cu(dmid)]_2\}$ (**88**), the dianion exhibits a slight tetrahedral distortion at the metal centers. The complex $(Bu_4N)_2\{tto[Cu(mnt)]_2\}$ (**106**) is the first completely planar tetrathiooxalate bridged bimetallic complex synthesized with a dihedral angle of 0°. Unlike **105** and **107**, it does not form one-dimensional chains.

Cyclic voltammetry results for all complexes show two reversible redox couples are accessible and when scanning to higher potentials a large cathodic wave is observed. This is indicative of stripping of a deposit from the working electrode surface. The complex

Table 3–2. Electrical Conductivity of $(Bu_4N)_2\{tto[Cu(dmit)]_2\}$ (**105**) as a Function of NaI/I_2 Oxidant

NaI/I_2 (equivs)	σ (S/cm)	Sample Form
0	$<10^{-10}$	single crystal
0.25	5.1×10^{-5}	pressed pellet
0.5	4.3×10^{-3}	pressed pellet
0.75	1.9×10^{-3}	pressed pellet
1.0	1.5×10^{-2}	pressed pellet

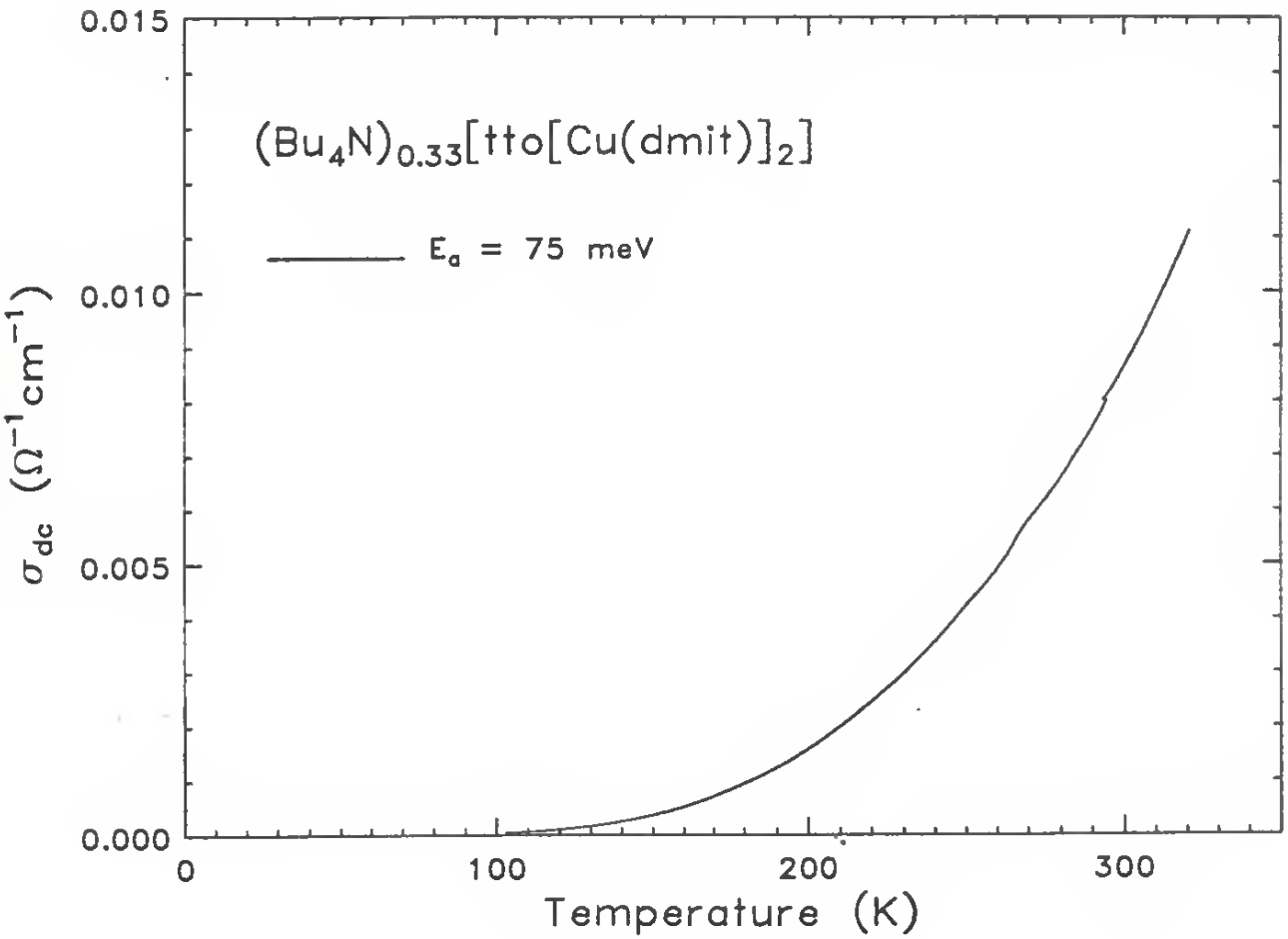

Figure 3–12. Pressed-pellet, temperature-dependent conductivity of $(Bu_4N)_{0.33}\{tto[Cu(dmit)]_2\}$ (**109**) showing semiconducting behavior.

$(Bu_4N)_2\{tto[Cu(dmit)]_2\}$ (**105**) can be chemically oxidized to give highly conducting powders. The elemental analysis data shows that the complex has the capability of forming complexes with partial oxidation states. As shown in the literature, this is a prerequisite for the formation of highly electrically conducting complexes.[30,53]

Electrocrystallization experiments have been carried out using $(Bu_4N)_2\{tto[Cu(dmit)]_2\}$ (**105**) with a variety of electrolytes and solvents. As yet the experiments have only yielded black insoluble films on the anode. As reported in the literature, copper bis-chelates of dmit-based ligands have not been successful in the formation of crystalline electrically conducting materials.[53] They have as yet only yielded materials with poor morphology.

CHAPTER 4
PREPARATION, STRUCTURE AND PROPERTIES OF AN ANIONIC TETRAMERIC COPPER COMPLEX CONTAINING A PLANAR, EIGHT-MEMBERED RING CORE

As mentioned in the introduction, square planar metal complexes (i.e. Ni(II), Pt(II), Pd(II)) with bis-coordination by the dmit (dmit = $C_3S_5^{2-}$ = 1,3-dithiole-2-thione-4,5-dithiolato, **42**) ligand have been actively researched as electronically conducting molecular materials over the past 10–15 years.[53] Chemists and physicists alike have studied their novel metallic and superconducting properties. Several other ligand systems similar to dmit have been studied, but have not afforded comparable electronic properties. One system in particular that has recieved less attention are dmt (dmt = $C_3S_5^{2-}$ = 1,2-dithiole-3-thione-4,5-dithiolato, **119**) ligand complexes. Dmt (**119**) can be synthesized directly from dmit via the "Steimecke rearrangement", where the dmit ligand (**42**) rearranges to the thermodynamically more stable product dmt (**119**) at increased temperature in dimethylformamide.[54]

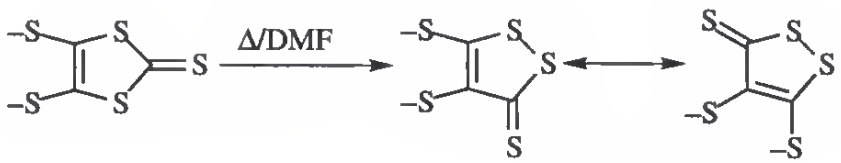

dmt (**119**)

Most of the work reported using dmt (**119**) has been the synthesis and characterization of bis-chelate complexes of **119** using a number of different metal centers.[54] In 1987, the first tris-chelate complexes were reported using the dmit (**42**) and dmt (**119**) ligands.[89] The metals In(II), Tl(III) and V(IV) were studied and had the general formulas $(Ph_4As)_3[M(L)_3]$ (M = In(II) and L = dmit, **120**; dmt, **121**; M = Tl(III) and L = dmit, **122**; dmt, **123**) and $(Bu_4N)_2[V(L)_3]$ (L = dmit, **124** and dmt, **125**) respectively. All of the complexes adopt an octahedral coordination environment. Lastly in 1993, Singh and Singh reported the synthesis of bis-chelate dmt complexes using Se(II) and Te(II) as the metal centers.[90] The study of dmt has received less attention in using the bis-chelate complexes in the formation of electrically conducting materials due to the fact they are remarkably less soluble than their dmit counterpart complexes. They have also been found to be much more difficult to crystallize.[54] These properties make them difficult to use in electrocrystallization experiments and hence their lack of study and absence in the formation of non-integer oxidation state materials.

In this dissertation, attempts were made to better understand the properties of the ligand in coordination complexes and to make a new bimetallic Cu(II) complex using dmt (**119**) as a capping ligand. Using a unique and facile three-solvent method, we have synthesized a series of bimetallic copper(II) complexes as presented in Chapter 3. This anionic complex has a tetrathiooxalate ligand bridging two copper(II) metal centers which are capped with the dmit ligand. Using the same synthetic methodology, attempts were made to synthesize a new complex with dmt replacing the dmit ligand. The synthesis of the anionic cluster complex $(Bu_4N)_2[Cu(dmt)]_4$ (**126**) instead has been obtained.[158] The tetrameric, dianionic complex is composed of four dmt ligands and four copper ion metal centers with two tetrabutylammonium cations.

4–1 Experimental

General procedures. All reactions were carried out in air and at 25°C. IR spectra were obtained using a KBr pellet on a Bio-Rad FTS-40A FTIR spectrometer. UV-VIS spectra were obtained using a Varian Instruments, Cary 5E spectrophotometer. Melting points were obtained under vacuum using a Thomas Hoover capillary melting point apparatus. Elemental analyses was completed at Robertson Microlit Labs Inc. (Madison, NJ).

All solvents, unless otherwise stated, were used as recieved from Aldrich. $(Bu_4N)_2[Zn(dmt)_2]$ (**127**) was prepared following Olk.[159] $(Et_4N)_2$tto (**45**) was prepared similar to the published procedure of Jeroschewski.[152]

$(Bu_4N)_2[Cu(dmt)]_4$ (**126**). A 472 mg (0.500 mmol) sample of $(Bu_4N)_2[Zn(dmt)_2]$ (**127**) was dissolved in ~30 ml CH_2Cl_2. In a separate vessel, 103 mg (0.250 mmol) of $(Et_4N)_2$tto (**45**) was dissolved in ~25 ml of H_2O purified by a Millipore Milli-Q water system. The two solutions were combined and stirred. To the stirring mixture, a solution of 85 mg (0.500 mmol) of $CuCl_2 \cdot 2H_2O$ (**111**) dissolved in a minimal amount of methanol was added. The organic layer was separated and filtered to remove insoluble oligomeric $[Cu(tto)]_n$ (**117**). The aqueous layer was washed with two portions of CH_2Cl_2, separated and filtered, and all solutions were combined. An equivalent amount of 2-propanol was added, evaporated to less than half, and filtered again this time to remove less soluble desired product from $[Cu(dmt)_2]^{2-}$. More product was obtained by evaporating the remaining solution to dryness and the residue was crystallized in 1:1 acetone/2-propanol three subsequent times. Yield 30 mg (8%). Anal. Calcd for $(Bu_4N)_2[Cu(dmt)]_4$ (**126**) are as follows: Mp: 261-262 °C (decomp). Calcd for $C_{44}H_{72}N_2S_{20}Cu_4$: C, 34.66; H, 4.77; N, 1.84. Found: C, 34.67; H, 4.64; N, 1.83. IR (KBr, cm^{-1}): ν(C-H) 2953, 2867, 733; ν(C-N) 1456; ν(C=C) 1338, 1283; ν(C=S) 1044; ν(C-C) 943; ν(C-S) 835. UV-vis [methylene chloride, nm (log ε)]: 269 (4.80), 344 (4.70), 374 (4.77), 508 (4.71).

X-ray structure determination. The crystallographic data for $(Bu_4N)_2[Cu(dmt)]_4$ (**126**) is located in Appendix Tables C–1 to C–3. Thermal ellipsoids drawing and molecular numbering schemes for $(Bu_4N)_2[Cu(dmt)]_4$ (**126**) is found in Fig. 4–1. The crystal chosen for data collection has dimensions 0.42 x 0.25 x 0.13 mm^3. X-ray intensity data were collected at room temperature on a Siemens R3m/V diffractometer equipped with a graphite monochromator utilizing MoK_α radiation ($\lambda = 0.71073$ Å). 32 reflections with $20.0^o \leq 2\theta \leq 22.0^o$ were used to refine cell parameters. Four reflections were measured every 96 reflections to monitor instrument and crystal stability (maximum correction on I was < 1%).

The structure of $(Bu_4N)_2[Cu(dmt)]_4$ (**126**) was solved by the heavy-atom method in *SHELXTL plus* (Sheldrick, G.M. (1990). *SHELXTL plus*. Nicolet XRD Corporation, Madison, Wisconsin, USA) from which the four Cu atoms were obtained. The rest of the non-hydrogen atoms were obtained from a subsequent difference Fourier map. The structure was refined in *SHELXTL plus* using full matrix least squares. The non-H atoms were treated anisotropically, whereas the positions of the hydrogen atoms were calculated in ideal positions and their isotropic thermal parameters were fixed.

Electrochemical methods. Cyclic voltammetry was carried out using an EG&G Princeton Applied Research Scanning Potentiostat 273 with a GRAPHTEC XY Chart Recorder. CH_2Cl_2 was used as the solvent and was dried and distilled over CaH_2 and was thoroughly degassed with argon prior to use. Ag/Ag^+ was used as the reference electrode with a platinum button working electrode and a platinum foil counter electrode. Electrochemistry was completed under an argon atmosphere. The concentration of tetrabutylammonium perchlorate electrolyte was 0.1 M and the approximate concentration of $(Bu_4N)_2[Cu(dmt)]_4$ (**126**) used in the CV experiments was 10^{-4} M.

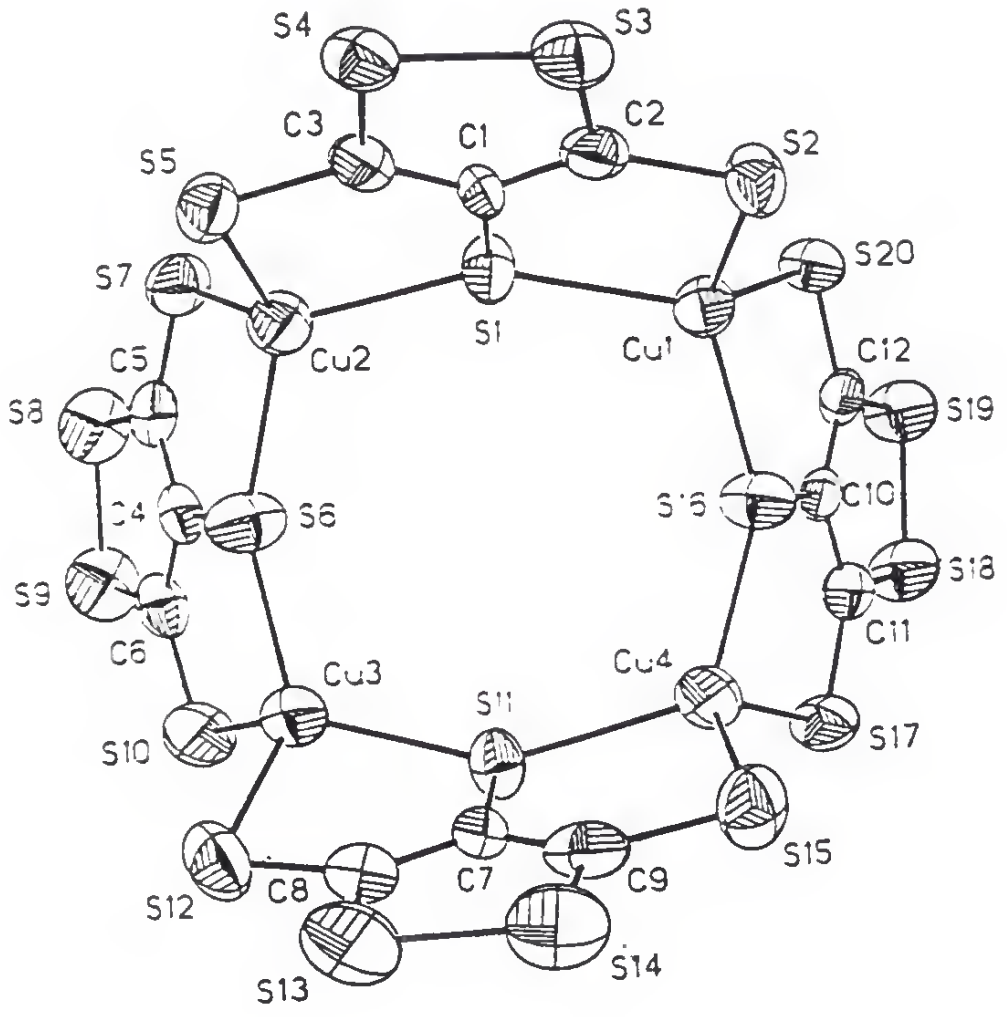

Figure 4–1. Thermal ellipsoids drawing and molecular numbering scheme of the dianion of $(Bu_4N)_2[Cu(dmt)]_4$ (**126**) with 40% probability ellipsoids.

4–2 Results

4–2–1 Synthesis of $(Bu_4N)_2[Cu(dmt)]_4$ (126)

The synthesis of $(Bu_4N)_2[Cu(dmt)]_4$ (**126**) was achieved using the same methodology used to make complexes **105–108** as discussed in Chapter 3. Two equivalents of $[Zn(dmt)_2]^{2-}$ (**127**) were dissolved in methylene chloride and mixed with an aqueous solution of one equiv of $(Et_4N)_2tto$ (**45**). A methanolic solution of two equivalents of $CuCl_2{\cdot}2H_2O$ (**111**) was then slowly added to the organic layer of the stirring biphasic solution. Unlike in the similar synthesis of complexes **105–108**, no bimetallic complexes were isolated using the dmt as a capping ligand. Instead, the tetrameric complex $(Bu_4N)_2[Cu(dmt)]_4$ (**126**) was isolated and found to be composed of four dmt and four copper ion metal centers in a ring. It is intriguing to note that the complex has an overall charge of –2, whereas one would expect a simple reaction between four Cu^{2+} and four dmt^{2-} ligands to yield a neutral complex. The tto^{2-} ligand thus plays an active role in the tetramerization as a reducing agent. The major products after the addition of methanolic $CuCl_2{\cdot}2H_2O$ (**111**) in the synthesis of **126** are $(Bu_4N)_2[Cu(dmt)_2]$ (**128**) and the insoluble oligomeric $[Cu(tto)]_n$ (**117**).[113] The synthesis of $(Bu_4N)_2[Cu(dmt)]_4$ (**126**) was then attempted without tto^{2-} being present in the solution. Only metal exchange occurs between $[Zn(dmt)_2]^{2-}$ (**127**) and Cu^{2+} as only $[Cu(dmt)_2]^{2-}$ (**128**) and $[Cu(tto)]_n$ (**117**) were isolated.

4–2–2 X-ray Structure of $(Bu_4N)_2[Cu(dmt)]_4$ (126)

In the complex $(Bu_4N)_2[Cu(dmt)]_4$ (**126**), each dmt ligand is coordinated to two copper ions as shown in Fig. 4–1. Of the over 30 dmt ligand complexes that have been reported, the ligand has never been seen to coordinate in this fashion.[53] As seen in the unit cell in Fig. 4–2, the crystal packing of $(Bu_4N)_2[Cu(dmt)]_4$ (**126**) is characterized by a columnar array of anions. The tetrabutylammonium counterions are intercalated throughout the lattice. There are S···S interactions between neighboring anions resulting from contacts

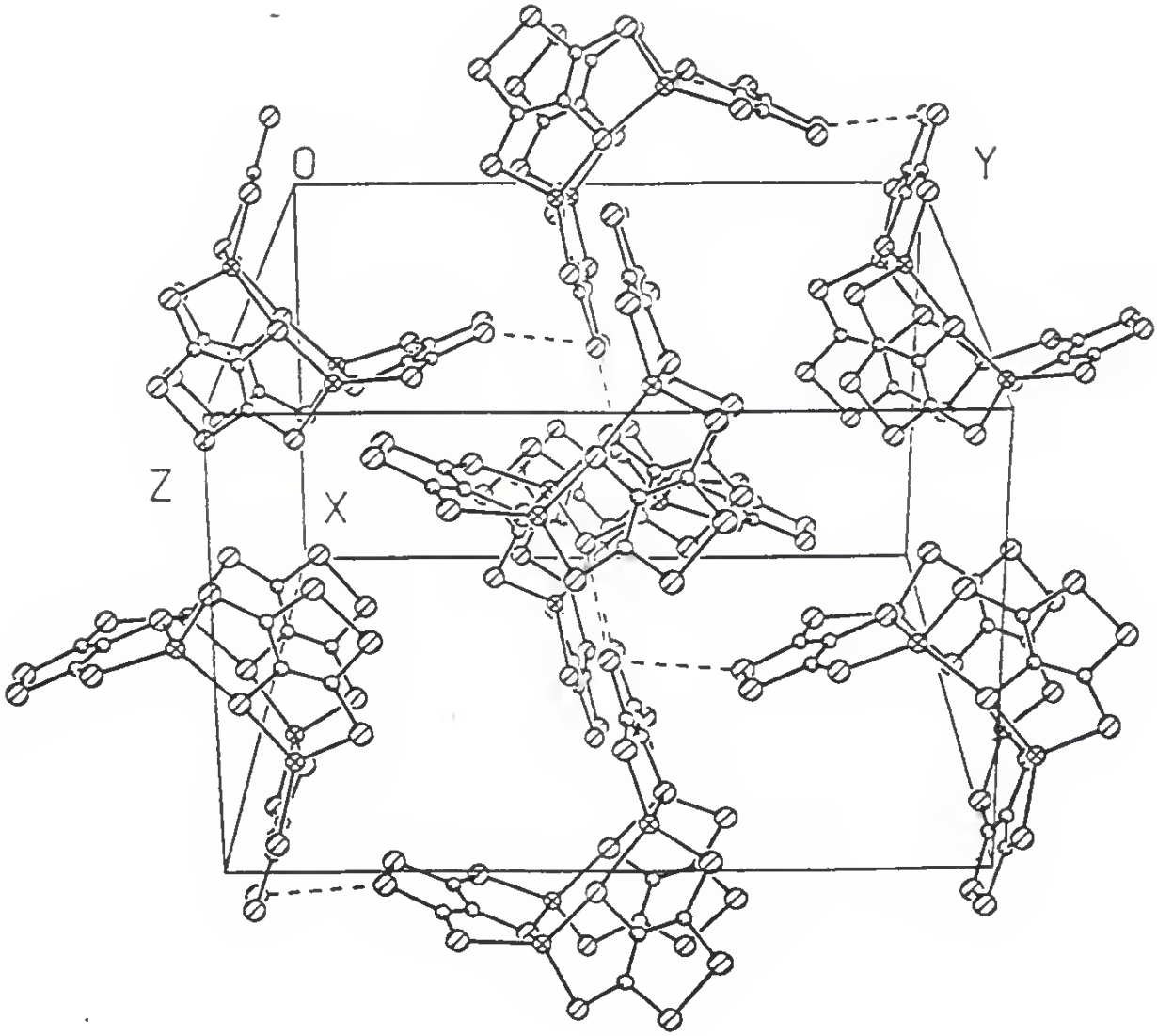

Figure 4–2. Packing diagram with unit cell labels of $(Bu_4N)_2[Cu(dmt)]_4$ (**126**) showing columnar arrays of dianions with nonbonding S···S interactions (dashed lines). Tetrabutylammonium cations have been omitted for clarity.

of the thiole groups of the dmt ligand. The distances are labeled in Fig. 4–2 and are less than the sum of the van der Waals radii 3.70 Å.[68] The structure of the anion consists of a central eight-membered ring core, with four Cu and four S atoms. Each of the four sulfurs are bonded to two Cu atoms and one carbon atom. The Cu-S distances in the core are on average 2.341(3) Å (see Appendix Table C–3) with S-Cu-S bond angles ranging from 114.52(12) to 121.69(13)°. The Cu-S-Cu angles range from 147.3(2) to 155.9(2)° making the core a distorted octagon from the perfect octagon of 135° bond angles. All other Cu-S distances are on average 2.327(3) Å. The Cu-S bond distances are all slightly longer than commonly seen in Cu(II) bisdithiolene complexes.[54] The coordination about the Cu metal centers is distorted tetrahedral.

Examining the four dmt ligands, the peripheral S-S bonds are all approximately 2.063(5) Å as expected. The distances of the eight-membered ring sulfur atoms and bonded carbon atoms have average lengths of 1.748(11) Å. This is similar to other dmt complexes. The C-S distances of the related groups such as C_3-S_5, C_5-S_7, and C_9-S_{15} are shorter than expected with average lengths of 1.696(12) Å. Lastly, the ethylene C-C bond lengths of $(Bu_4N)_2[Cu(dmt)]_4$ (**126**) are observed to be slightly longer than usually seen at 1.40(2) Å of bis- and tris-chelate dmt complexes.[54,89]

Based on the structural data, the dmt ligands of $(Bu_4N)_2[Cu(dmt)]_4$ (**126**) are likely completely delocalized. The copper metal centers have a formal charge of +1.5. Unlike $[Cu(dmt)_2]^{2-}$ (**128**), the dianionic cluster is absent of electron density localized to the central ethylene and peripheral thione groups. This greater electronic delocalization may be a driving force to the formation of the cluster complex. Considering the octagonal structure of the core of the molecule, interesting interactions with various cations may be possible as the result of crown ether-like coordination properties.

4–2–3 Redox Properties of $(Bu_4N)_2[Cu(dmt)]_4$ (**126**)

The redox behavior of the anionic tetrameric complex $(Bu_4N)_2[Cu(dmt)]_4$ (**126**) has been investigated by cyclic voltammetry (CV) in 0.1 M TBAP/CH_2Cl_2, at a Pt button working electrode. The CV data exhibits two anodic processes ($E_{p,a}$ = 0.15 V and 1.05 V vs. Ag/Ag^+), correlated with two cathodic processes ($E_{p,c}$ = –0.45 V and –0.75 V) as shown in Fig. 4–3. This data suggests that higher oxidation states of $(Bu_4N)_2[Cu(dmt)]_4$ (**126**) may be obtained. The cyclic voltammetry data for **126** is similar to that reported for $(PPN)_2[M(dmt)_2]$ (PPN = bis(triphenylphosphine)iminium; M = Se, **129**; Te, **130**) by Singh and Singh.[90]

4–2–4 UV-Vis Absorption Properties of $(Bu_4N)_2[Cu(dmt)]_4$ (**126**)

The absorption properties of $(Bu_4N)_2[Cu(dmt)]_4$ (**126**) were studied by UV-VIS spectroscopy as shown in Fig. 4–4. The complex is red-colored in methylene chloride solution as a result of an absorption band at 508 nm. This band, along with one found at 269 nm, may be attributed to excitations within the dmt ligand.[154] Absorptions at 344 and 374 nm can be assigned to Cu-L charge transfer bands as similarily seen in $Cu(mnt)_2^{2-}$ complexes.[160] All the absorption bands have molar absorptivities greater than 5.0×10^4 L mol^{-1} cm^{-1}.

4–3 Conclusions

Using a unique, three-solvent synthesis to assemble complexes **105–108** shown in Chapter 3, the tetrameric complex $(Bu_4N)_2[Cu(dmt)]_4$ (**126**), has been synthesized. Complex **126** is composed of four dmt ligands and four copper metal centers forming a central eight-membered ring, planar core. The dmt ligand (**119**) has never before been seen to coordinate in such a fashion. During the synthesis, the tto^{2-} ligand acts as a reducing agent in the formation of $(Bu_4N)_2[Cu(dmt)]_4$ (**126**). This behavior of the tto^{2-}

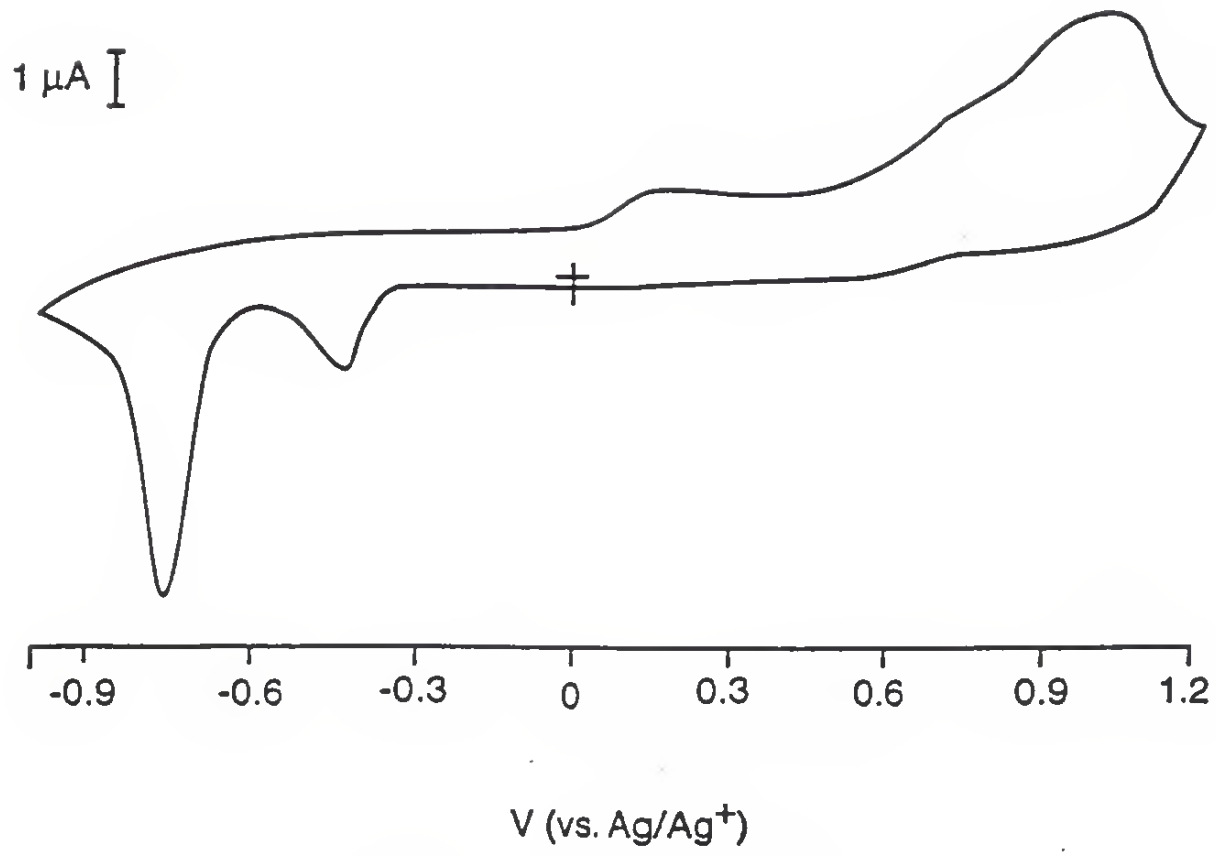

Figure 4–3. Cyclic voltammogram of $(Bu_4N)_2[Cu(dmt)]_4$ (**126**) showing two anodic processes are correlated with two cathodic processes. Conditions: scan rate, 100 mV/s; reference electrode Ag/Ag^+; counter electrode, Pt foil; working electrode, Pt button; 0.1 M Bu_4NClO_4 in CH_2Cl_2 under Ar at room temperature.

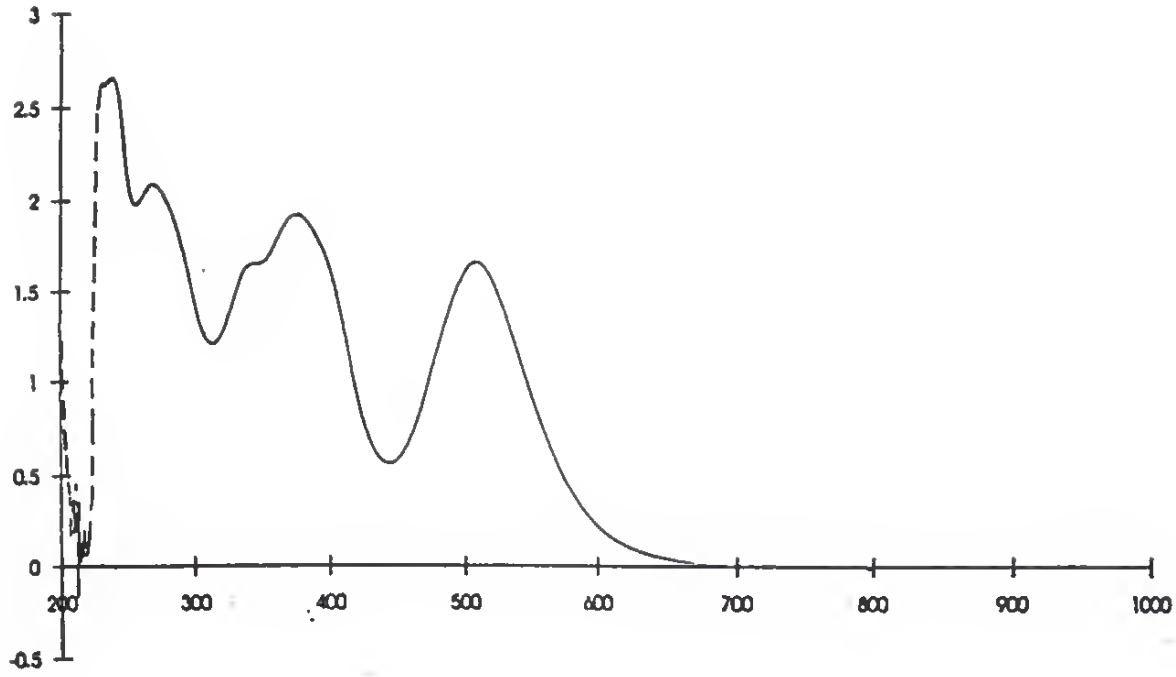

Figure 4–4. UV-vis spectrum of $(Bu_4N)_2[Cu(dmt)]_4$ (**126**) in methylene chloride.

ligand (**45**) has also never been reported previously. Upon further study of **126**, the complex may exhibit interesting chelating properties of small cations within the central core.

CHAPTER 5
EXTENSIVELY CONJUGATED, CHALCOGEN-RICH, DIANIONIC TETRATHIOOXALATO-BRIDGED NICKEL(II) COMPLEXES

As discussed in Chapter 1, all seven of the $M(dmit)_2$-based superconducting complexes reported contain either the square planar coordinating Ni(II) or Pd(II) metal centers. Therefore, a major goal of our work has been to synthesize new extensively conjugated and planar, chalcogen-rich, tetrathiooxalato-bridged bimetallic Ni(II) or Pd(II) complexes like the template presented in Chapter 3. The complexes have been designed in order to extend the delocalization and increase intermolecular interactions in the crystal lattice. We have assembled a new series of bimetallic Ni(II) complexes with the general formula $(C)_2\{tto[Ni(dmit)]_2\}$ (tto = $C_2S_4^{2-}$ = tetrathiooxalato **45**; where L = dmit, C = Bu_4N^+ = tetrabutylammonium **131**, C = Et_4N^+ = tetraethylammonium **132**, C = Me_4N^+ = tetramethylammonium **133**, where dsit = $C_3Se_2S_3^{2-}$ = 2-thione-1,3-dithiole-4,5-diselenolato, C = Bu_4N^+ = tetrabutylammonium **134**, and where dmise = $C_3SeS_4^{2-}$ = 2-selenone-1,3-dithiole-4,5-dithiolato, C = Bu_4N^+ = tetrabutylammonium **135**) using a new synthetic methodology. The complexes have been fully characterized including X-ray analysis, UV-vis, IR, elemental analysis and cyclic voltammetry.[128,161,162] Rauchfuss and coworkers have synthesized a similar bimetallic Ni(II) complex using the tetrathiooxalate (**45**) bridging ligand of formula $(As_4P)_2\{tto[Ni(S_2C_2S_2C_2(CO_2Me)_2)]_2\}$ (**91**).[115] This complex was synthesized from air oxidation followed by degradation of $(As_4P)_2[Ni(S_2C_2S_2C_2(CO_2Me)_2)_2]$ (**90**) in acetonitrile over a period of 24 hours. The complex contains terminal out-of-plane ester groups preventing close intermolecular contacts. In 1982, Dahl and coworkers reported the first crystallographically shown example of coordinated tetrathiooxalate in the compound $Ni_2(\eta^5\text{-}C_5Me_5)_2(C_2S_4)$ (**136**).[163]

In this complex, the tetrathiooxalate ligand bridges Ni(II) metal centers containing the bulky η^5-C_5Me_5 ligand. The complex was formed from a metal promoted reductive dimerization, followed by coordination of carbon disulfide. These compounds will be discussed along with **131-135**. The complex $(Bu_4N)_2\{tto[Ni(dmit)]_2\}$ (**131**) has been used to prepare electrically conducting powders using a variety of methods, including slow interdiffusion and electrocrystallization techniques, and have been characterized with elemental analysis and two-probe pressed-powder conductivity measurements.

5–1 Experimental

General procedures. Melting points were determined using a Fisher-Johns hot stage melting point apparatus, and are uncorrected. Infrared spectra were recorded on a Perkin Elmer 1310 IR spectrophotometer and a Perkin Elmer 1600 FTIR spectrophotometer. UV-vis spectra were recorded on a Shimadzu UV-160A spectrophotometer. Elemental analyses were completed at the University of Leipzig, FRG on a Hereaus CHN Rapid Analyzer and at Robertson Microlit Labs, Madison, NJ, USA.

Materials. All solvents were thoroughly degassed with argon prior to use and the acetonitrile was also dried and distilled over calcium hydride. All reactions were completed under argon atmosphere.

Preparation of $(Bu_4N)_2\{tto[Ni(dmit)]_2\}$ (**131**). In 75 ml of thoroughly degassed acetone, 0.231 g (0.500 mmol) of Cs_2dmit (**137**),[164] 0.193 g (0.600 mmol) of tetrabutylammonium bromide (**138**) and 0.103 g (0.250 mmol) of $(Et_4N)_2$tto (**45**) was added and stirred for 10 minutes. To the stirring solution, a solution of 0.119 g (0.500 mmol) of $NiCl_2 \cdot 6H_2O$ (**139**) in methanol was slowly dropped in with a pipette. The solution was then stirred for approximately 45 minutes and filtered to remove insoluble oligomeric $[Ni(tto)]_n$ (**140**) and unreacted $(Et_4N)_2$tto (**45**). Approximately 25 ml of 2-propanol was then added to the solution and allowed to evaporate to less than one-third of the initial volume overnight. The crystalline product was then filtered using gravity

filtration. The remaining product was recrystallized in 1:1 acetone/2-propanol. Yield: 117 mg (41%) of **131** was obtained. Mp: 270-5 °C (decomp). Anal. Calcd for $C_{40}H_{72}N_2S_{14}Ni_2$: C, 41.87; H, 6.34; N, 2.44; S, 39.12. Found: C, 41.89; H, 6.53; N, 2.49; S, 39.30. IR (KBr, cm^{-1}): υ(C=C) 1452; υ(C=S) 1080. UV-vis [acetone; nm, (log ε)]: 380 (4.89), 462 (4.27), 520 (4.17), 1062 (4.35).

$(Et_4N)_2\{tto[Ni(dmit)]_2\}$ (**132**). To 20 ml of a 0.05 M solution of Et_4NBr (**141**) in acetonitrile was added $(Bu_4N)_2\{tto[Ni(dmit)]_2\}$ (**131**) (0.030 g, 0.026 mmol) and stirred for approximately 15 min. to dissolve followed by filtration. The filtrate was allowed to sit under an argon atmosphere for 7 d. The lesser soluble $(Et_4N)_2\{tto[Ni(dmit)]_2\}$ (**132**) crystallizes out as black chunk-like crystals. Yield: 2 mg (8%). Mp: >300°C. Anal. Calcd for $C_{24}H_{40}N_2Ni_2S_{14}$: C, 31.23; H, 4.38; N, 3.04; S, 48.64. Found: C, 31.00; H, 4.31; N, 2.99; S, 48.19. IR (KBr; cm^{-1}); (C-H) 2951, 2864; (C=C) 1455, 1381; (C=S) 1080, 960.

$(Me_4N)_2\{tto[Ni(dmit)]_2\}$ (**133**). To 20 ml of a 0.100 M solution of Me_4NClO_4 (**142**) in acetonitrile was added $(Bu_4N)_2\{tto[Ni(dmit)]_2\}$ (**131**) (0.030 g, 0.026 mmol) and stirred for approximately 15 min. to dissolve followed by filtration. The filtrate was then allowed to sit under an argon atmosphere for 48 h. The lesser soluble $(Me_4N)_2\{tto[Ni(dmit)]_2\}$ (**133**) crystallizes out as black chunk-like crystals. Yield: 2 mg (10%). Mp: >300°C. Anal. Calcd for $C_{16}H_{24}N_2Ni_2S_{14}$: C, 23.70; H, 2.99; N, 3.46; S, 55.37. Found: C, 23.89; H, 2.98; N, 3.36; S, 54.68. IR (KBr; cm^{-1}); ν(C-H) 2950, 2866; ν(C=C) 1453, 1380; ν(C=S) 1077, 960.

Preparation of $(Bu_4N)_2\{tto[Ni(dsit)]_2\}$ (**134**). In 75 ml of acetone, Cs_2dsit (**143**)[165] (0.278 g, 0.500 mmol), Bu_4NBr (**138**) (0.193 g, 0.600 mmol) and $(Et_4N)_2tto$ (**45**) (0.103 g, 0.250 mmol) was added and stirred for 10 min. To the stirring solution, a solution of $NiCl_2{\cdot}6H_2O$ (**139**) (0.119 g, 0.500 mmol) in minimal amount of methanol was slowly added with a pipette. The solution was then stirred for approximately 45 min. and filtered to remove any undissolved $(Et_4N)_2tto$ (**45**) or insoluble oligomeric $[Ni(tto)]_n$ (**140**)

that may have formed. To the filtrate was added approximately 25 ml of 2-propanol and the solution was allowed to evaporate to less than one-fourth of the initial volume overnight. The remaining product was recrystallized in 1:1 acetone/2-propanol to yield $(Bu_4N)_2\{tto[Ni(dsit)]_2\}$ (**134**) as dark brown-black plateletlike crystals. Yield: 117 mg (41%). Mp: 247-249 °C dec. Anal. Calcd for $C_{40}H_{72}N_2Ni_2Se_4S_{10}$: C, 35.99; H, 5.44; N, 2.10; S, 24.02. Found: C, 36.19; H, 5.66; N, 2.44; S, 24.12. IR (KBr: cm^{-1}): ν(C-H) 2948, 2867; ν(C=C) 1476, 1376; ν(C=S) 1056, 986. UV-vis [acetone; λ, nm (log ε)]: 390 (4.80), 446 (4.26), 501 (4.09), 1053 (4.20).

$(Bu_4N)_2\{tto[Ni(dmise)]_2\}$ (**135**). In 75 ml of acetone, Cs_2dmise (**144**)[166] (0.254 g, 0.500 mmol), Bu_4NBr (**138**) (0.193 g, 0.600 mmol) and $(Et_4N)_2$tto (**45**) (0.103 g, 0.250 mmol) was added and stirred for 10 min. To the stirring solution, a solution of $NiCl_2 \cdot 6H_2O$ (**139**) (0.119 g, 0.500 mmol) in minimal amount of methanol was slowly added with a pipette. The solution was then stirred for approximately 45 min. and filtered to remove any undissolved $(Et_4N)_2$tto (**45**) or insoluble oligomeric $[Ni(tto)]_n$ (**140**) that may have formed. To the filtrate was added approximately 25 ml of 2-propanol and the solution was allowed to evaporate to less than one-fourth of the initial volume overnight. The remaining solid was then recrystallized in 1:1 acetone/2-propanol to yield $(Bu_4N)_2\{tto[Ni(dmise)]_2\}$ (**135**) as dark brown-black plateletlike crystals. Yield: 100 mg (32%). Mp: 298-300 °C dec. Anal. Calcd for $C_{40}H_{72}N_2Ni_2Se_2S_{12}$: C, 38.71; H, 5.86; N, 2.26; S, 31.00. Found: C, 38.25; H, 5.59; N, 2.21; S, 30.67. IR (KBr: cm^{-1}): ν(C-H) 2956, 2869; ν(C=C) 1467, 1412; ν(C=S) 959. UV-vis [acetone; λ, nm (log ε)]: 384 (4.64), 489 (4.18), 552 (4.19), 1061 (4.24).

Electrocrystallization of $(Bu_4N)_x\{tto[Ni(dmit)]_2\}$ (**145**). A black, microcrystalline and brittle material was obtained by constant current electrolysis of a CH_3CN/DMF (4:1) solution containing 0.01 M Bu_4NBr (**138**) and saturated with $(Bu_4N)_2\{tto[Ni(dmit)]_2\}$ (**131**). A glass, two-compartment H-cell separated by a medium porosity frit, and Pt wire (0.5 mm dia.) was used for the electrodes and the cell was flushed with argon as

previously explained in Section 2–1. A current density of 0.5 $\mu A/cm^2$ was applied over a period of 45 days at room temperature. The microcrystalline material was harvested and washed thoroughly with methanol followed by diethyl ether and dried under vacuum.

Synthesis of $(TTF)_x\{tto[Ni(dmit)]_2\}$ (**146**). A black precipitate of stoichiometry $(TTF)_x\{tto[Ni(dmit)]_2\}$ (**146**) was obtained from the rapid mixing of a slight excess of $(TTF)_3(BF_4)_2$ (**51**)[167] (1.1 equiv) and $(Bu_4N)_2\{tto[Ni(dmit)]_2\}$ (**131**) (1 equiv) in a minimal amount of a 1:1 mixture of CH_3CN/acetone. The precipitate was washed with acetone followed by methanol and diethyl ether and dried under vacuum.

Synthesis of $(TTF)_{0.57}\{tto[Ni(dmit)]_2\}$ (**147**). A black-brown precipitate of approximate stoichiometry $(TTF)_{0.57}\{tto[Ni(dmit)]_2\}$ (**147**) was obtained by slow interdiffusion of saturated solutions of $(TTF)_3(BF_4)_2$ (**51**) and $(Bu_4N)_2\{tto[Ni(dmit)]_2\}$ (**131**) in CH_3CN under an argon atmosphere at room temperature. A three-compartment glass cell separated by course porosity frits was used as seen in Figure 5–1. The precipitate was isolated after 60 days, washed with acetone, followed by methanol and diethyl ether and dried under vacuum. Anal. Calcd for $C_{74}H_{28}S_{84}Ni_8$: C, 21.79; H, 0.70; N, 0.00. Found: C, 21.92; H, 0.98; N, <0.02.

Chemical oxidation of $(Bu_4N)_2\{tto[Ni(dmit)]_2\}$ (**131**). A black precipitate of approximate stoichiometry $(Bu_4N)_{0.33}\{tto[Ni(dmit)]_2\}$ (**148**) was obtained from the rapid mixing of solutions of 3 mg (0.1 mmol) of I_2 (**115**) and 2 mg (0.1 mmol) of NaI (**116**) with 100 mg (0.090 mmol) of $(Bu_4N)_2\{tto[Ni(dmit)]_2\}$ (**131**) in acetone. A black precipitate was filtered, washed with acetone followed by methanol and diethyl ether and dried under vacuum. Anal. Calcd for $C_{40}H_{36}NS_{42}Ni_6$: C, 21.55; H, 1.63; N, 0.63; S, 60.40. Found: C, 21.23; H, 1.58; N, 0.60; S, 60.00.

X-ray structure determinations. Crystallographic data for $(Bu_4N)_2\{tto[Ni(dmit)]_2\}$ (**131**), $(Et_4N)_2\{tto[Ni(dmit)]_2\}$ (**132**), $(Me_4N)_2\{tto[Ni(dmit)]_2\}$ (**133**), $(Bu_4N)_2\{tto[Ni(dsit)]_2\}$ (**134**) and $(Bu_4N)_2\{tto[Ni(dmise)]_2\}$ (**135**) are listed in Appendix Tables D-1 through D-15. Data were collected at 173 K on a Siemens SMART

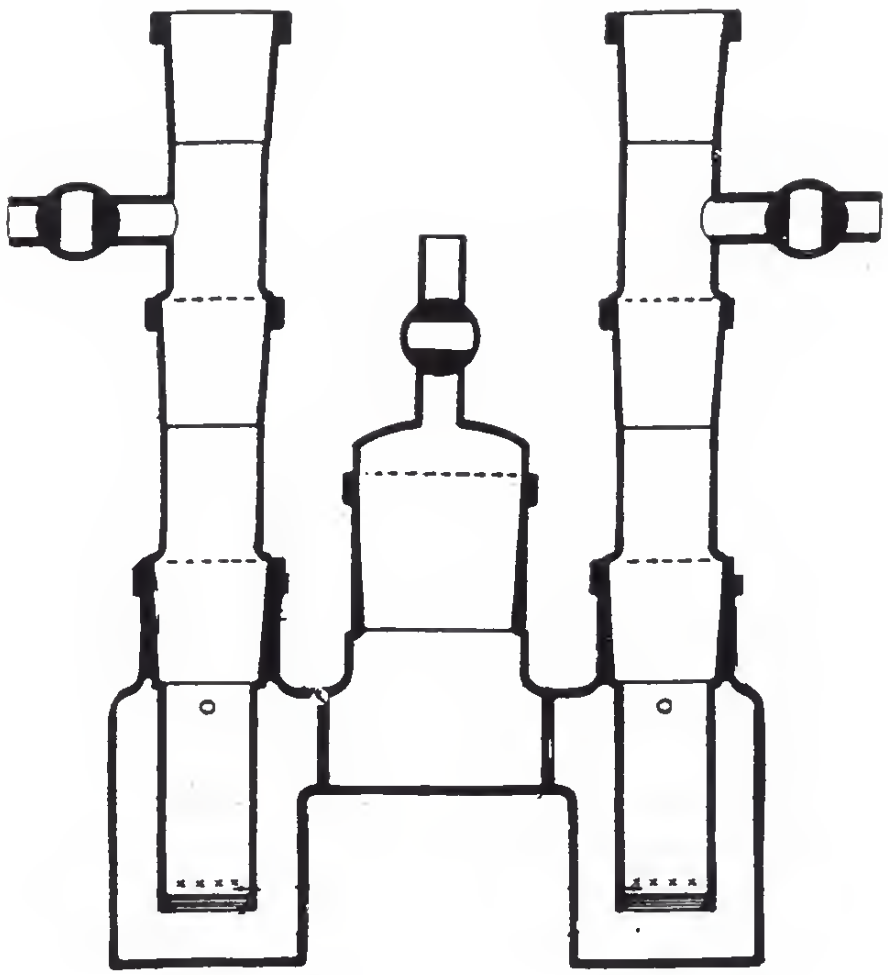

Figure 5–1. Drawing of the three-compartment glass cell used for slow interdiffusion experiments.

PLATFORM equipped with a CCD area detector. For complexes **131**, **134** and **135**, crystals suitable for X-ray were obtained by slow evaporation of a concentrated solution of the complexes in DMF. For **131**, dark brown-black platelets (0.38 x 0.27 x 0.03 mm^3) were chosen for study, for **132**, black chunk-like crystals (0.44 x 0.23 x 0.20 mm^3) were chosen, for **133**, black chunk-like crystals (0.32 x 0.21 x 0.07 mm^3) were chosen, for **134**, dark brown-black rectangular-shaped crystals (0.48 x 0.16 x 0.07 mm^3) were chosen and for **135**, dark brown-black block-like crystals (0.48 x 0.23 x 0.17 mm^3) were chosen for study.

The diffractometer was equipped with a graphite monochromator utilizing MoK_α radiation ($\lambda = 0.71073$ Å). Cell parameters were refined using up to 8192 reflections. A hemisphere of data (1381 frames) was collected using the ω-scan method (0.3° frame width). The first 50 frames were remeasured at the end of data collection to monitor instrument and crystal stability (maximum correction on I was <1%). Psi scan absorption corrections were applied based on the entire data set. The structures were solved by the direct methods in SHELXTL, and refined using full matrix least squares. The non-H atoms were treated anisotropically, whereas the hydrogen atoms were calculated in ideal positions and were riding on their respective carbon atoms except in $(Et_4N)_2\{tto[Ni(dmit)]_2\}$ (**132**) where all of the H atoms were refined without any constraints. All refinements were done using F^2.

Molecular numbering schemes for the dianion of $(Bu_4N)_2\{tto[Ni(dmit)]_2\}$ (**131**), $(Et_4N)_2\{tto[Ni(dmit)]_2\}$ (**132**) and $(Me_4N)_2\{tto[Ni(dmit)]_2\}$ (**133**) are shown in Figure 5–2 and for $(Bu_4N)_2\{tto[Ni(dsit)]_2\}$ (**134**) and $(Bu_4N)_2\{tto[Ni(dmise)]_2\}$ (**135**) in Figure 5–3.

Electrochemical methods. Cyclic voltammetry was performed on a EG&G Princeton Applied Research 362 scanning potentiostat and data was recorded with EG&G Princeton Applied Research Model 270/250 Electrochemistry Software 4.23 (Copyright 1995 EG&G Instruments Inc.). Acetonitrile was dried and distilled over CaH_2 and

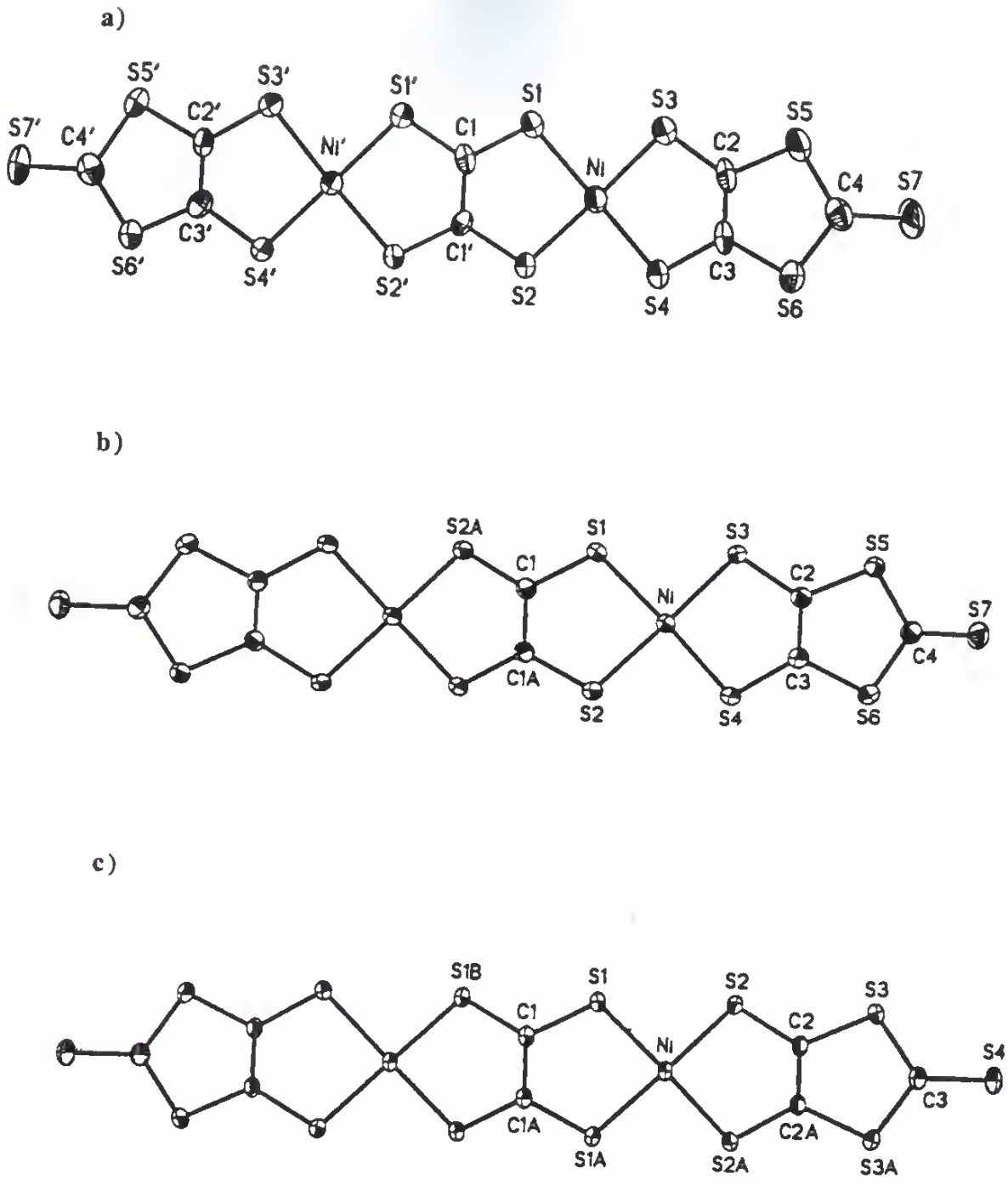

Figure 5–2. Thermal ellipsoids drawings (50% probability) and numbering schemes for the dianions of (a) $(Bu_4N)_2\{tto[Ni(dmit)]_2\}$ (**131**), (b) $(Et_4N)_2\{tto[Ni(dmit)]_2\}$ (**132**) and (c) $(Me_4N)_2\{tto[Ni(dmit)]_2\}$ (**133**).

a)

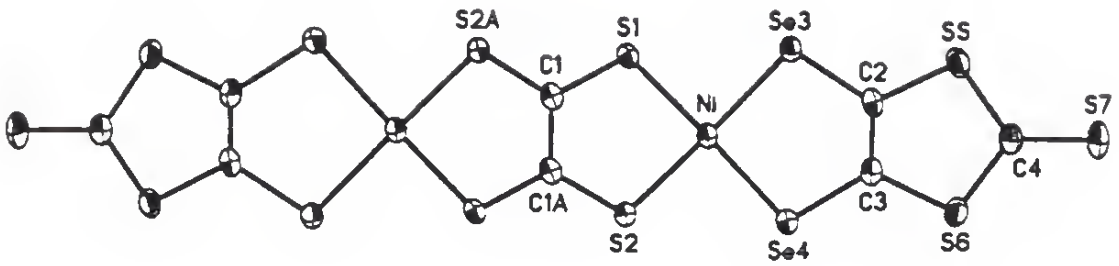

b)

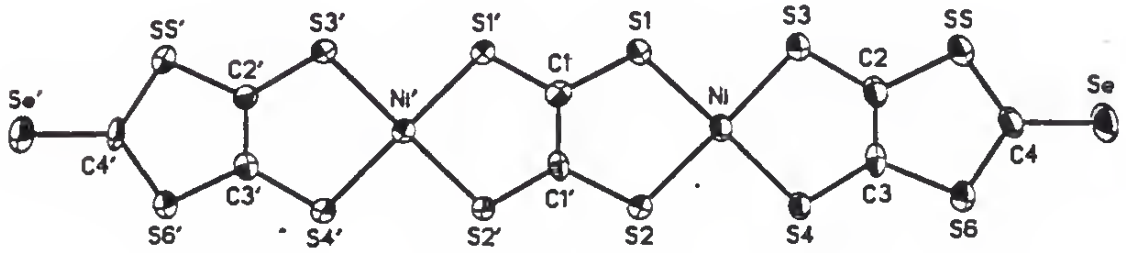

Figure 5–3. Thermal ellipsoids drawings (50% probability) and numbering schemes for the dianions of (a) $(Bu_4N)_2\{tto[Ni(dsit)]_2\}$ (**134**) and (b) $(Bu_4N)_2\{tto[Ni(dmise)]_2\}$ (**135**).

thoroughly degassed with argon prior to use. Me_4NClO_4 (**142**) was used as supporting electrolyte (0.05 M). Ag/Ag^+ was used as the reference electrode with a Pt button working electrode and Pt foil counter electrode. Electrochemistry was completed under an argon atmosphere. Saturated solutions of the complexes were used in the cyclic voltammetry experiments.

Conductivity measurements. Conductivity data was obtained at room temperature using a two-probe pressed-powder method in a glass capillary obtained from a 25 μl #702 Hamilton syringe. The glass capillary has an inner diameter of 0.029 in and a radius (r) of 0.37 mm. The samples were pressed by means of stainlees steel plungers and the distance (l) between the ends of the plungers was measured while taking the resistance (R) values. The equation $\sigma = l/R \cdot \pi \cdot r^2$ was used to determine sample conductivity (σ) values. A Keithley 169 multimeter was used to measure sample resistances. For $(Bu_4N)_x\{tto[Ni(dmit)]_2\}$ (**145**) (l = 0.08 cm, R = 40 Ω), a conductivity of 0.5 S/cm was obtained, for $(TTF)_x\{tto[Ni(dmit)]_2\}$ (**146**) (l = 0.07 cm, R = 41 Ω), a conductivity of 0.4 S/cm was found, for $(TTF)_{0.57}\{tto[Ni(dmit)]_2\}$ (**147**) (l = 0.06 cm, R = 255 Ω) a conductivity of 0.06 S/cm was obtained and for $(Bu_4N)_{0.33}\{tto[Ni(dmit)]_2\}$ (**148**) (l = 0.06 cm, R = 47 Ω) a conductivity of 0.3 S/cm was found. The resistance between the contacts of the steel plungers of 1.7 Ω was found and was subtracted from each resistance reading before calculating the conductivity values.

5–2 Results

5–2–1 Synthesis of Complexes $(Bu_4N)_2\{tto[Ni(dmit)]_2\}$ (131), $(Et_4N)_2\{tto[Ni(dmit)]_2\}$ (132), $(Me_4N)_2\{tto[Ni(dmit)]_2\}$ (133), $(Bu_4N)_2\{tto[Ni(dsit)]_2\}$ (134) and $(Bu_4N)_2\{tto[Ni(dmise)]_2\}$ (135)

In order to prepare the bimetallic, tetrathiooxalato-bridged Ni(II) complexes **131–135** (Fig. 5–4) similar to the Cu(II) bimetallic complexes presented in Chapter 3, a new synthetic methodology was developed. The synthetic method used to assemble Cu(II)

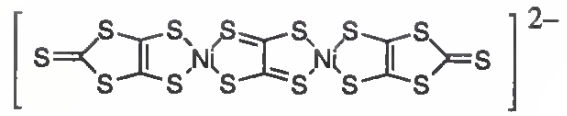

{tto[Ni(dmit)$_2$}$^{2-}$ (**131**, **132**, **133**)

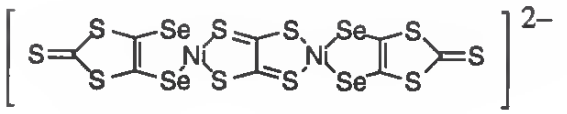

{tto[Ni(dsit)$_2$}$^{2-}$ (**134**)

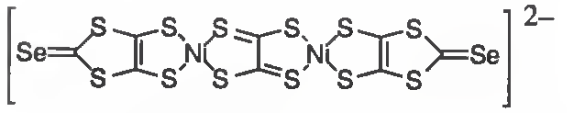

{tto[Ni(dmise)$_2$}$^{2-}$ (**135**)

Figure 5–4. Bimetallic nickel (II) complexes synthesized $(Bu_4N)_2$\{tto[Ni(dmit)$_2$\} (**131**), $(Et_4N)_2$\{tto[Ni(dmit)$_2$\} (**132**), $(Me_4N)_2$\{tto[Ni(dmit)$_2$\} (**133**), $(Bu_4N)_2$\{tto[Ni(dsit)$_2$\} (**134**) and $(Bu_4N)_2$\{tto[Ni(dmise)$_2$\} (**135**).

bimetallic complexes **105-108** could not be used to synthesize the Ni(II) analogs due to the fact that the rate of metal exchange with Zn(II) is much slower than the reaction with tto (**45**). This resulted in formation of primarily $[Ni(tto)]_n$ (**140**) oligomer. The new method is also based on competing reactions but with a slight variation. Methanolic $NiCl_2 \cdot 6H_2O$ (**139**) solution is added to a stirring acetone solution containing Bu_4NBr (**138**), $(Et_4N)_2tto$ (**45**) and the dicesium salt of the capping ligand of choice. The tto salt is only slightly soluble in acetone and gradually dissolves allowing it to slowly react with Ni(II) as the Ni(II) is also slowly reacting with the dithiolato capping ligands over a period of almost one hour. Once the reaction is complete the solution is filtered to remove undissolved $(Et_4N)_2tto$ (**45**) and any $[Ni(tto)]_n$ (**140**) oligomer that may have formed. An equivalent amount of 2-propanol is added to the solution and allowed to evaporate to less than half overnight. The lesser soluble bimetallic complexes crystallize out and are seperated. The synthetic procedures are readily reproducible for $(Bu_4N)_2\{tto[Ni(dmit)]_2\}$ (**131**) in 41%, $(Et_4N)_2\{tto[Ni(dmit)]_2\}$ (**132**) in 8%, $(Me_4N)_2\{tto[Ni(dmit)]_2\}$ (**133**) in 8%, $(Bu_4N)_2\{tto[Ni(dsit)]_2\}$ (**134**) in 41% and $(Bu_4N)_2\{tto[Ni(dmise)]_2\}$ (**135**) in 32% yield. All of the complexes exhibit a brown-red color in acetone and CH_2Cl_2 solutions due to a characteristic strong absorption in the range of 501–552 nm (Fig. 5–5).

5–2–2 X-ray Structures of **131–135**

As can be seen in Figure 5–4, all of the complexes are composed of Ni(II) metal centers bridged by the side-on coordination of the tto ligand and capped by the dithiolato ligand of dmit for $(Bu_4N)_2\{tto[Ni(dmit)]_2\}$ (**131**), $(Et_4N)_2\{tto[Ni(dmit)]_2\}$ (**132**) and $(Me_4N)_2\{tto[Ni(dmit)]_2\}$ (**133**), dsit for $(Bu_4N)_2\{tto[Ni(dsit)]_2\}$ (**134**) and the dmise ligand for $(Bu_4N)_2\{tto[Ni(dmise)]_2\}$ (**135**). From the crystal structure of $[(Ph_3P)_2Cu]_2(C_2S_4)$ (**149**) reported by Hansen et al., the tto ligand which is also side-on coordinated, has a carbon-carbon bond length of 1.53(8) Å[157] where the core is made up of a planar Cu-tto-Cu unit. This value should be better for comparison to our compounds

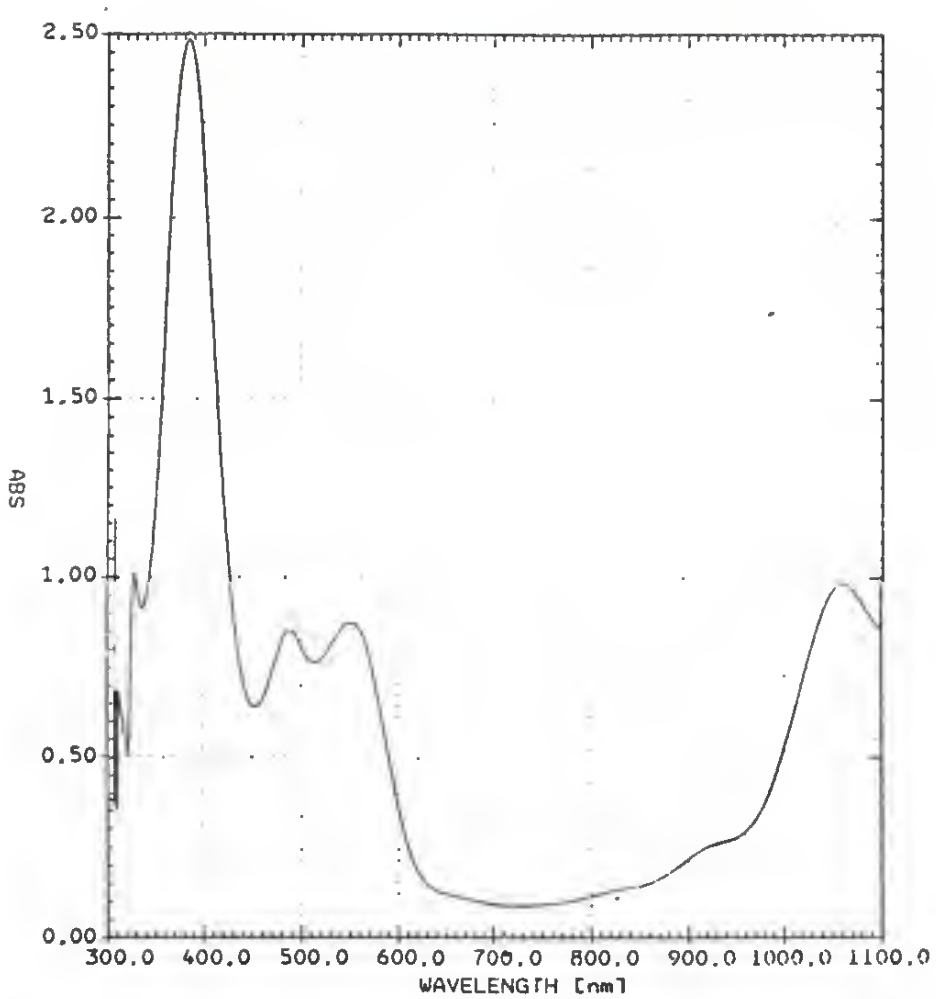

Figure 5–5. A representative UV-vis spectrum of $(Bu_4N)_2\{tto[Ni(dmit)]_2\}$ **(131)** in acetone of complexes **131-135**.

than the value reported from the crystal structure of $(Et_4N)_2$tto (**45**). This is because the S-C-S components of the uncoordinated tto ligand are in a staggered formation with respect to each other, but the values reported are still similar though with that of 1.516(6) Å[168] reported for **45**. The Ni(II) bimetallic complexes presented here have values in the narrow range of 1.416(7) Å for **131** to 1.444(5) Å for complex **134** which is closer to double bond character. It is interesting to note that there is a difference in this bond length between complex **131** (1.416(7) Å) and complexes **133** and **132** (1.430(6) and 1.434(4) Å respectively) simply due to a change of cation. In the Cu(II) bimetallic complexes previously reported, all of the lengths are longer with $(Bu_4N)_2\{tto[Cu(mnt)]_2\}$ (**106**) being the longest of 1.483(9) Å[151] to $(Ph_4As)_2\{tto[Cu(dmid)]_2\}$ (**88**) having the shortest bond length of 1.467(1) Å.[114] In the complex $Ni_2(\eta^5\text{-}C_5Me_5)_2(C_2S_4)$ (**136**) reported by Dahl and coworkers,[163] this complex also possesses a planar Ni-C_2S_4-Ni core where the C-C bond of the bridging tto ligand was reported to be 1.360(11) Å, which is similar in length to the ett (ett = ethylenetetrathiolate = $C_2S_4^{4-}$) ligand.[169] The complex $(As_4P)_2[Ni_2C_2S_4\{S_2C_2S_2C_2(CO_2Me)_2\}_2]$ (**91**) reported in 1994 by Rauchfuss and coworkers has a value of 1.43 Å of the C-C bond of the side-on coordinated tto ligand which is very similar to that of the central C-C bond of the C_2S_4 ligand of the complexes **131-135**. This approximate length was interpreted to be an intermediate between the central C_2S_4 ligand acting as tto (**45**) and ett (**74**).[115]

The Ni(C_2S_4)Ni core of each complex is planar and extensively delocalized. For complexes **131 - 135**, all Ni-S distances to the tto ligand are in the range of 2.1595(14) to 2.1677(14) Å. The bond lengths are essentially the same indicating as expected a highly conjugated Ni(C_2S_4)Ni core. This is seen in the previously reported similar Cu(II) bimetallic complexes.[150,151]

The coordination about the d^8 Ni(II) metal centers is square planar as expected. Examining the S-Ni-S bond angles with the tto bridging ligand, the values are very close to 90° and range from 91.05(3)° for $(Bu_4N)_2\{tto[Ni(dsit)]_2\}$ (**134**) to 91.35(7)° for

Table 5–1. Values of the Dihedral Angles (deg) Formed Between the Planes of the Bridging tto Ligand and the Capping Ligands where **X** Represents the Plane of a Capping Ligand while **Y** and **Z** Represents the Planes of the Capping Ligands (L(**X**) - Ni' - tto(**Y**) - Ni - L(**Z**))

complex	X - Y	Y - Z
$(Bu_4N)_2\{tto[Ni(dmit)]_2\}$ (**131**)	5.7	2.0[a]
$(Et_4N)_2\{tto[Ni(dmit)]_2\}$ (**132**)	24.5	24.5[b]
$(Me_4N)_2\{tto[Ni(dmit)]_2\}$ (**133**)	3.6	3.6[b]
$(Bu_4N)_2\{tto[Ni(dsit)]_2\}$ (**134**)	20.5	20.5[b]
$(Bu_4N)_2\{tto[Ni(dmise)]_2\}$ (**135**)	6.1	2.3[a]

[a]Crystallographically independent.

[b]Equal by symmetry.

$(Bu_4N)_2\{tto[Ni(dmit)]_2\}$ (**131**). The S-Ni-S bond angles with the capping ligands and the Se-Ni-Se bond angles for **134**, range from 93.28(3)° for $(Me_4N)_2\{tto[Ni(dmit)]_2\}$ (**133**) to 94.62(2)° for $(Bu_4N)_2\{tto[Ni(dsit)]_2\}$ (**134**). The complexes are not perfectly planar but have small dihedral angles formed between the planes of the bridging tto and capping ligands. The dihedral angles for **131-135** are listed in Table 5–1. In the Cu(II) bimetallic complexes, a dihedral angle was formed between the same ligand planes due to a twist at the metal center as a result of a tetrahedral distortion from square planarity.[150,151] The dianion $\{tto[Cu(dmid)]_2\}^{2-}$ (**88**) had the highest dihedral angle of 28.3° with $(Bu_4N)_2\{tto[Cu(mnt)]_2\}$ (**106**) being the only completely planar bimetallic Cu(II) complex with a dihedral angle of the dianion of 0°.[151,114] In the Ni(II) bimetallic complexes presented, dihedral angles are not a result of a tetrahedral distortion but rather a hingelike bend at the thiolate atoms of complexes **132, 133, 135** and selenolate atoms of **134**. The complex $(Bu_4N)_2\{tto[Ni(dmise)]_2\}$ (**135**) has the smallest dihedral angle of 2.3° with $(Et_4N)_2\{tto[Ni(dmit)]_2\}$ (**132**) having the largest dihedral angle of 24.5°. It is interesting to note that in complexes **131-133** where the dianion $\{tto[Ni(dmit)]_2\}^{2-}$ is the same, there are large differences in the dihedral angles found in the crystal structure as a result of changing the cation. In **131**, the large Bu_4N^+ cation induces the formation of dihedral angles of 2.0° and 5.7° for the crystallographically independent halves of the dianion. In **133** with the Me_4N^+ cation, the dihedral angle is only 3.6° while in complex **132** with the Et_4N^+ cation, the dihedral is very large at 24.5° between the planes of the tto bridging ligand and both capping ligands.

Figs. 5–6 and 5–7 shows views of the crystal packing of $(Bu_4N)_2\{tto[Ni(dmit)]_2\}$ (**131**), Figs. 5–8 and 5–9 for $(Et_4N)_2\{tto[Ni(dmit)]_2\}$ (**132**), Figs. 5–10 and 5–11 for $(Me_4N)_2\{tto[Ni(dmit)]_2\}$ (**133**), Figs. 5–12 and 5–13 for $(Bu_4N)_2\{tto[Ni(dsit)]_2\}$ (**134**) and Figs. 5–14 and 5–15 shows a packing diagrams of $(Bu_4N)_2\{tto[Ni(dmise)]_2\}$ (**135**). In complexes **131**, **134** and **135**, where the counterions are Bu_4N^+, the packing of the dianions is characterized by a sheet-like arrangement seperated by sheets of cations. In

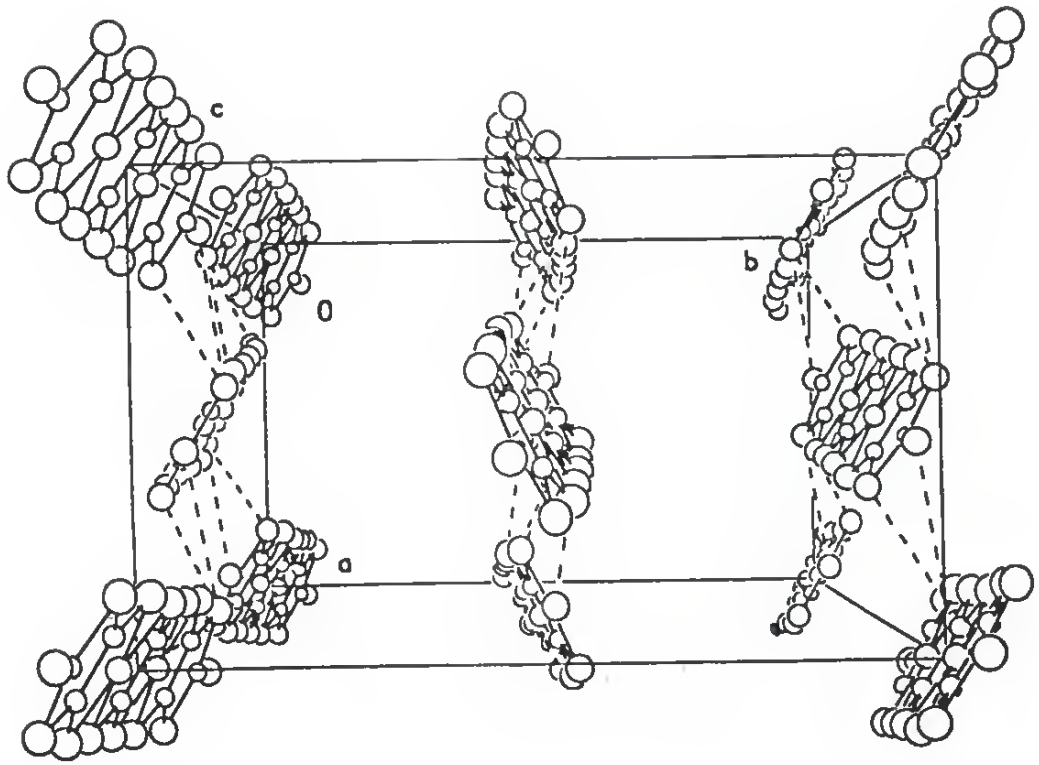

Figure 5–6. View of the packing diagram of $(Bu_4N)_2\{tto[Ni(dmit)]_2\}$ (**131**) along the c axis with unit cell labels showing sheets of canted dianions. Tetrabutylammonium cations have been omitted for clarity.

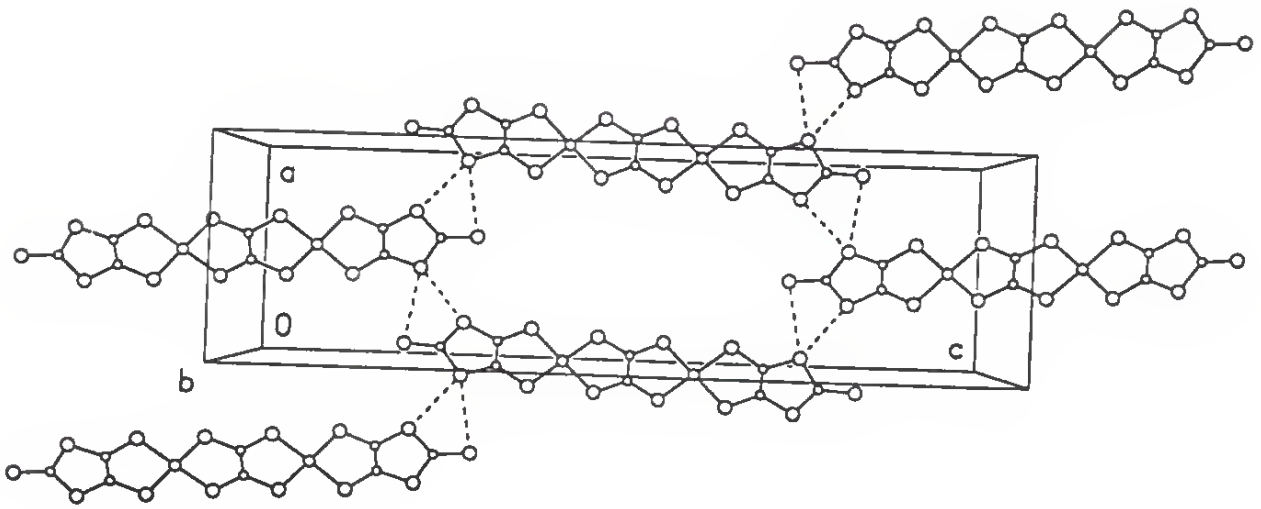

Figure 5–7. View down the b axis of $(Bu_4N)_2\{tto[Ni(dmit)]_2\}$ (**131**) showing side-by-side nonbonding interactions thioxo-thiole and thiole-thiole atoms.

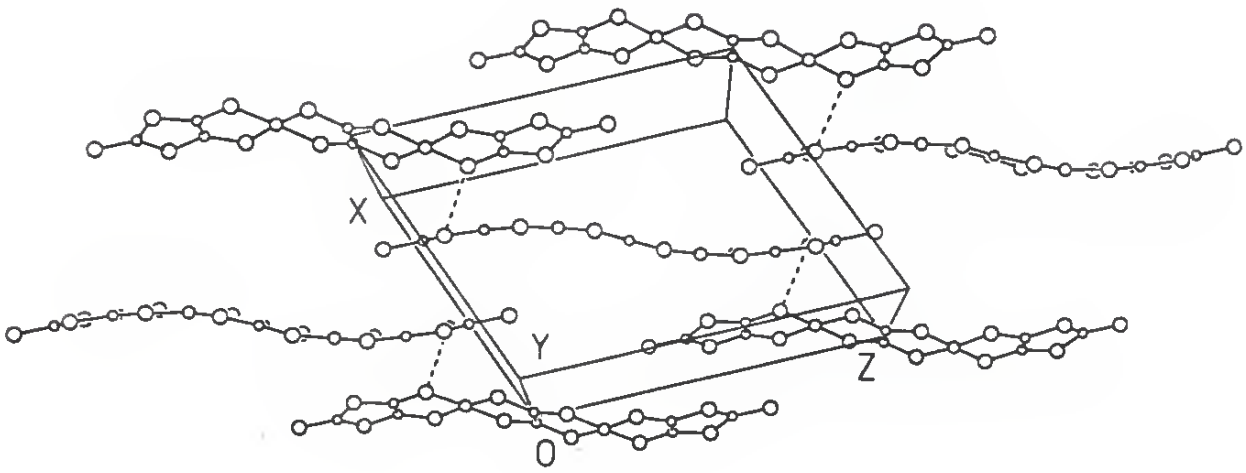

Figure 5–8. View of $(Et_4N)_2\{tto[Ni(dmit)]_2\}$ (**132**) showing the conformation of the dianionic units. Tetraethylammonium cations have been omitted for clarity.

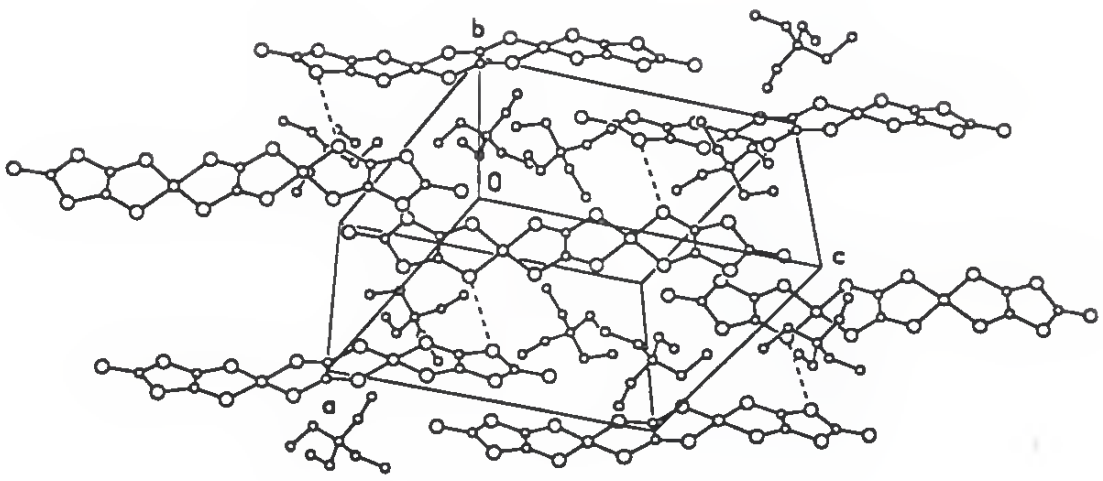

Figure 5–9. View of $(Et_4N)_2\{tto[Ni(dmit)]_2\}$ (**132**) perpendicular to the plane of the dianionic units showing side-by-side S···S interactions.

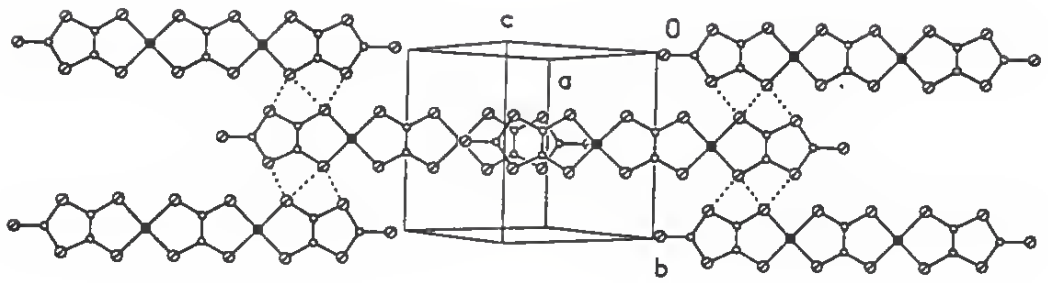

Figure 5–10. View of $(Me_4N)_2\{tto[Ni(dmit)]_2\}$ **(133)** showing side-by-side S···S contacts of the dianions.

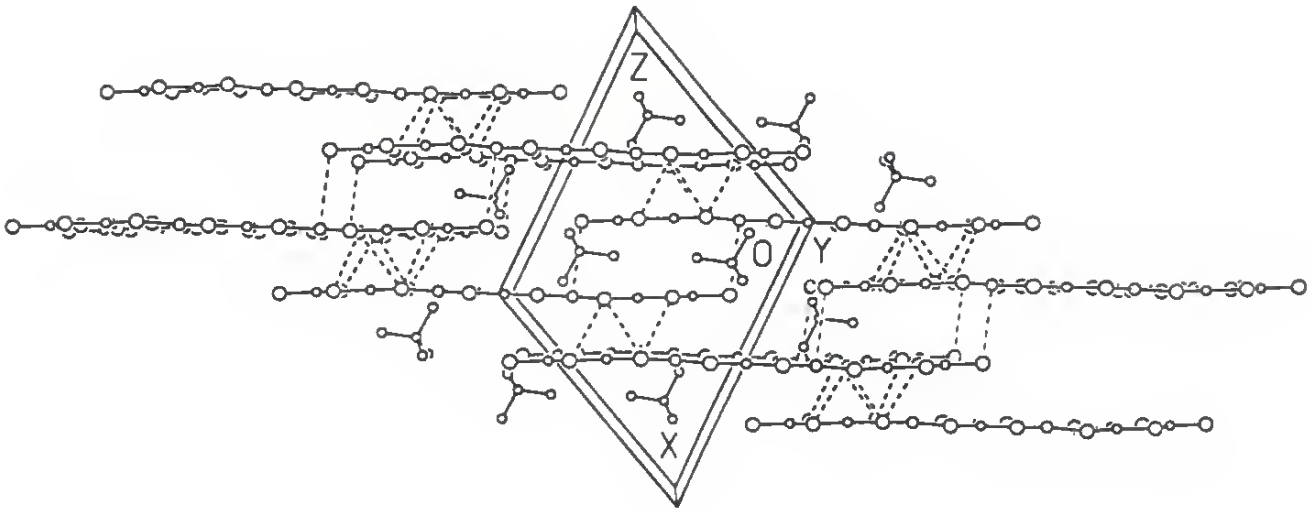

Figure 5–11. Packing diagram of $(Me_4N)_2\{tto[Ni(dmit)]_2\}$ (**133**) showing multiple Ni···S and S···S nonbonding interactions in a brick-like array.

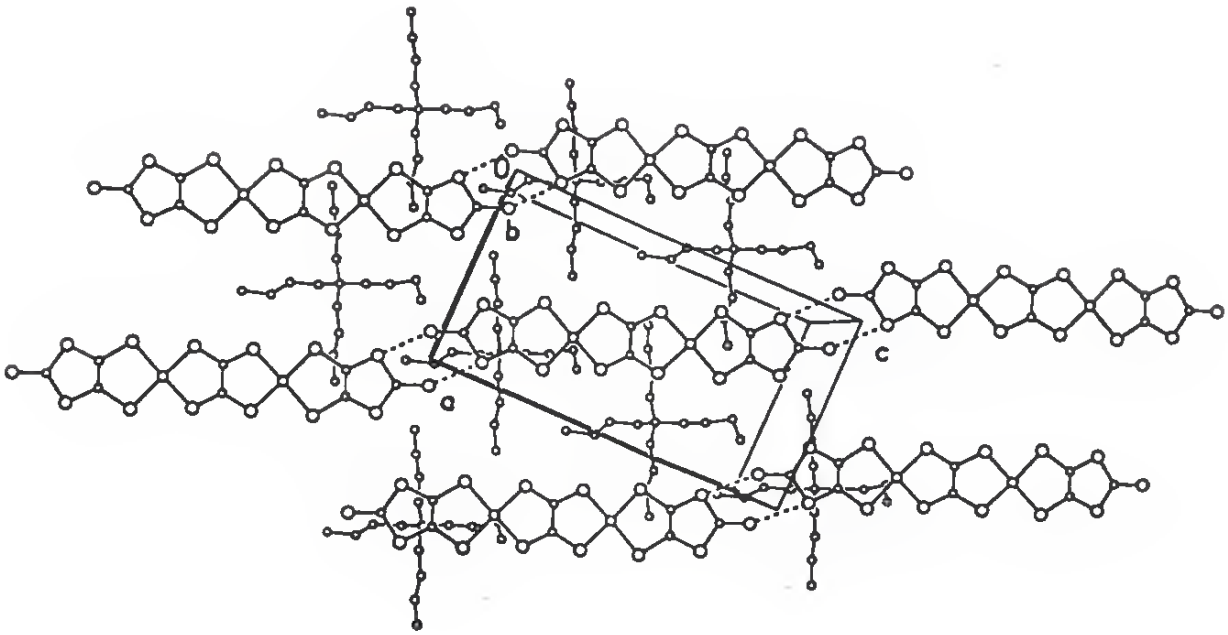

Figure 5-12. View down the b axis of $(Bu_4N)_2\{tto[Ni(dsit)]_2\}$ (**134**) showing one-dimensional chains of the dianionic units formed from head-to-tail thione-thiole nonbonding interactions.

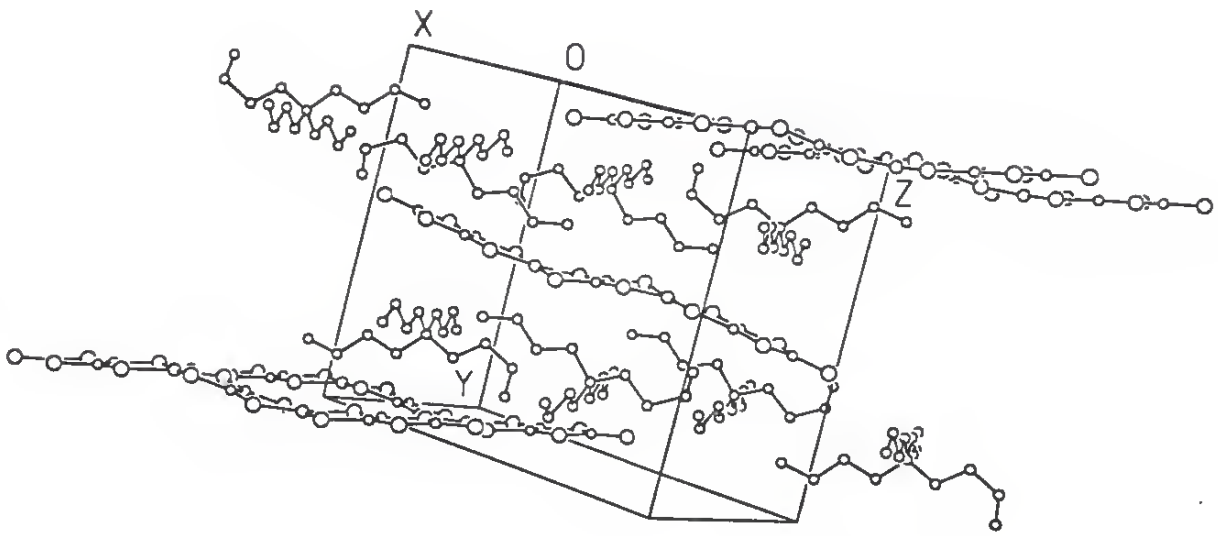

Figure 5–13. Edge on view of the dianions of $(Bu_4N)_2\{tto[Ni(dsit)]_2\}$ (**134**) showing sheets of the dianions seperated by sheets of tetrabutylammonium cations.

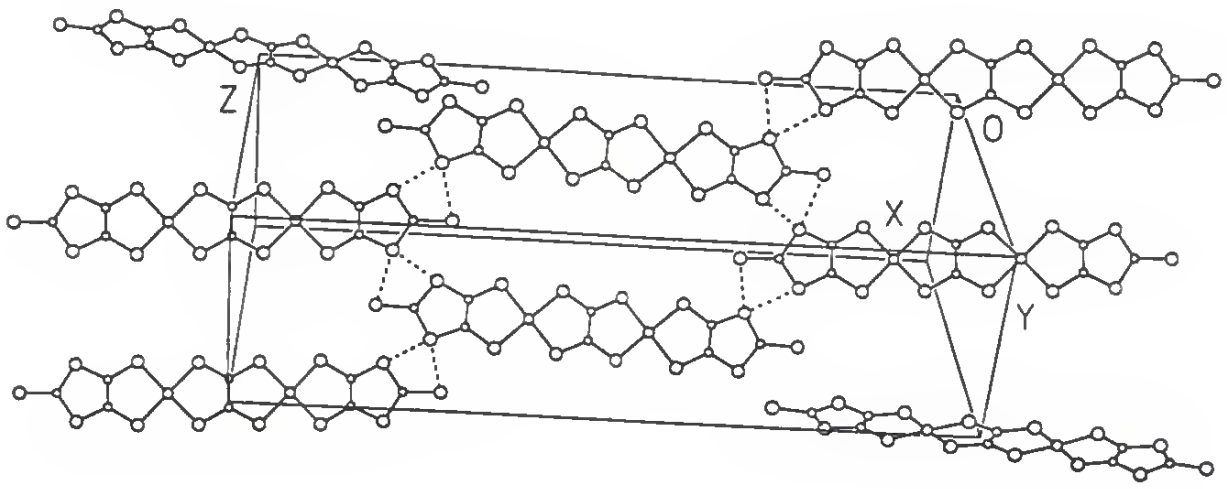

Figure 5–14. View of $(Bu_4N)_2\{tto[Ni(dmise)]_2\}$ (**135**) showing sheets of dianionic moieties in a two-dimensional array as a result of selenoxo-thiole and thiole-thiole orbital overlap. Tetrabutylammonium cations have been omitted for clarity.

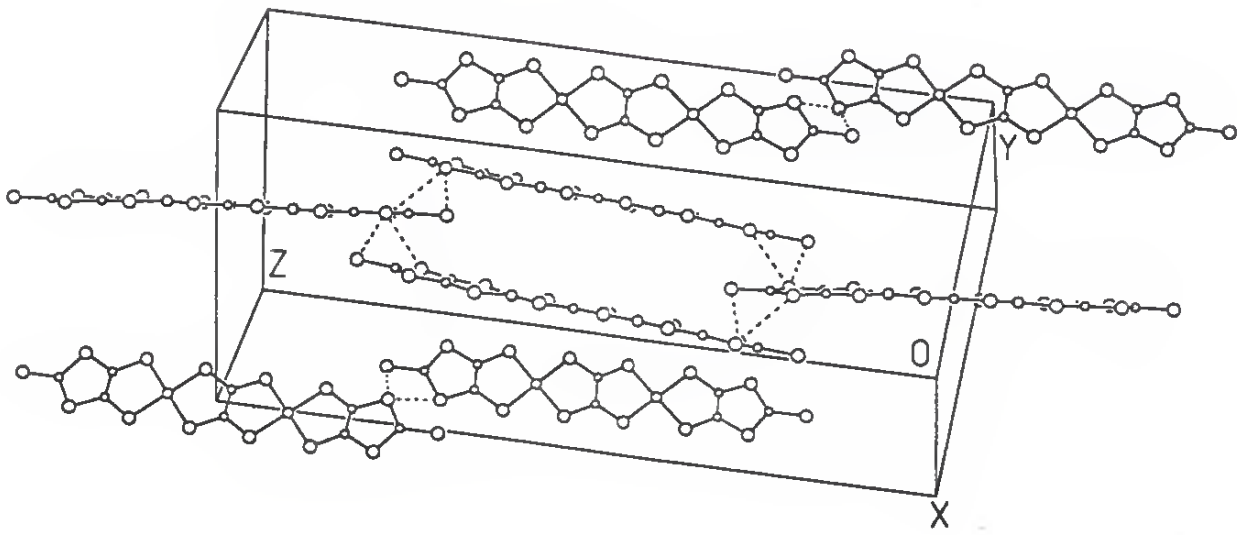

Figure 5–15. View of $(Bu_4N)_2\{tto[Ni(dmise)]_2\}$ (**135**) along the edge of the dianionic units illustrating the stacking interactions.

135, the sheets are formed from thiole-thiole (3.448-3.537 Å) and thiole-selenoxo (3.532-3.558 Å) nonbonding interactions in a two-dimensional array. In $(Et_4N)_2\{tto[Ni(dmit)]_2\}$ (**132**), only thiole-thiolato (3.623 Å) orbital interactions are observed in a one-dimensional array. Lastly in $(Me_4N)_2\{tto[Ni(dmit)]_2\}$ (**133**), the small cation tetramethylammonium leads to a three-dimensional packing array of the dianionic units. The units pack in a brick wall-like fashion with extensive intermolecular interactions including thiole-thiole (3.577 Å), thiole-thiolato (3.594 Å) and nickel-thioxo (3.454 Å) nonbonding interactions.

5–2–3 Redox Properties of $(Bu_4N)_2\{tto[Ni(dmit)]_2\}$ (**131**), $(Bu_4N)_2\{tto[Ni(dsit)]_2\}$ (**134**) and $(Bu_4N)_2\{tto[Ni(dmise)]_2\}$ (**135**)

The dianions of complexes **131**, **134** and **135** exhibit similar redox behavior. A representative cyclic voltammogram of $(Bu_4N)_2\{tto[Ni(dsit)]_2\}$ (**134**) for all complexes is shown in Fig. 5–16. Cyclic voltammetric data for **131**, **134** and **135** is compiled and located in Table 5–2.

At beginning potentials of –1.00 V, the compounds are stable in their dianionic form. As seen in the representative cyclic voltammogram when scanning anodically, each complex exhibits a first low-potential redox couple with essentially equal $E_{1/2}$ values ranging from –0.83 V for $(Bu_4N)_2\{tto[Ni(dmit)]_2\}$ (**131**) to –0.82 V for $(Bu_4N)_2\{tto[Ni(dsit)]_2\}$ (**134**) and $(Bu_4N)_2\{tto[Ni(dmise)]_2\}$ (**135**). This first redox couple is reversible as observed peak-to-peak separations for **131** is 60 mV, for **134** is 70 mV, and for complex **135** is 70 mV. Scan rate dependence studies (25 - 300 mV/s) for this first observed redox process also show that the peak currents scale with the square root of the scan rate as anticipated for diffusion of the electroactive species to the electrode surface. This first redox couple seen for all the complexes can be attributed to a reversible one-electron oxidation process between the dianionic and monoanionic states ($\{tto[Ni(L)]_2\}^{2-} \rightleftharpoons \{tto[Ni(L)]_2\}^{-}$).

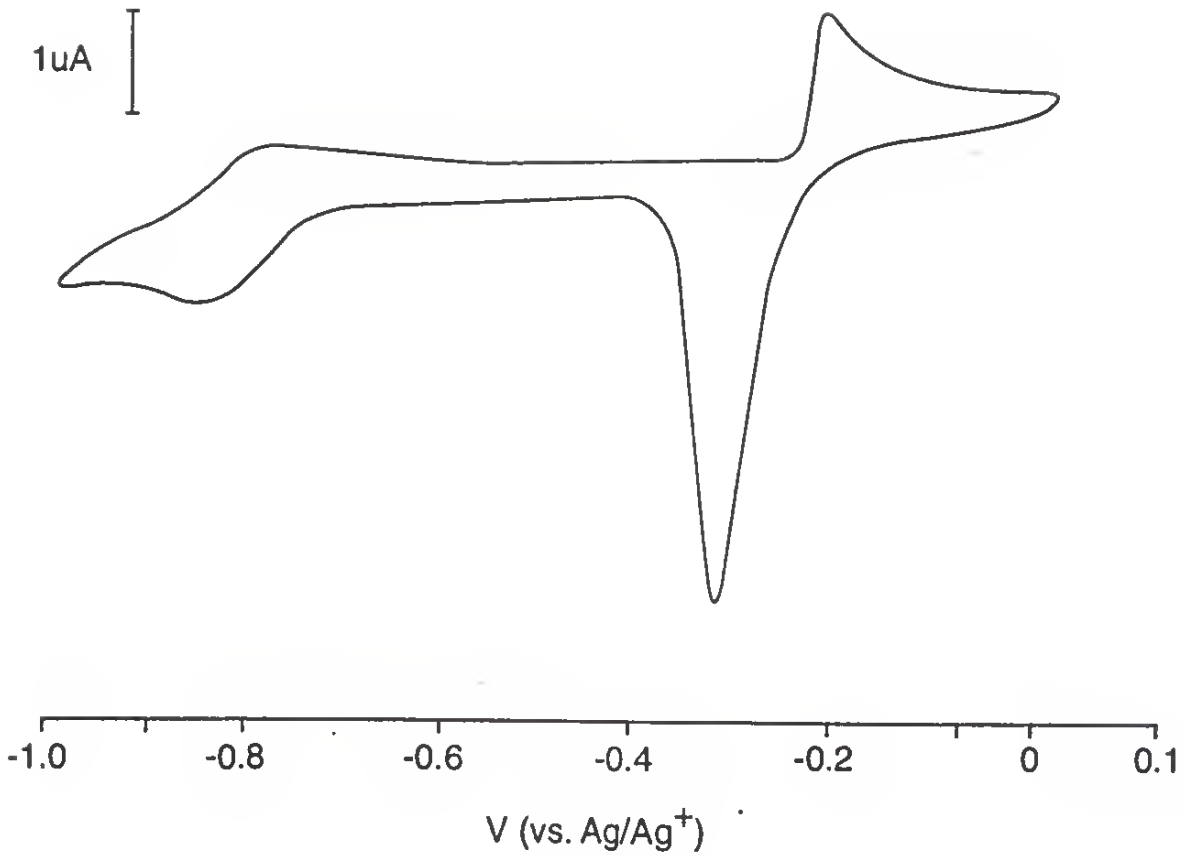

Figure 5–16. Cyclic voltammogram of $(Bu_4N)_2\{tto[Ni(dsit)]_2\}$ (**134**). Conditions: scan rate, 100 mV/s; reference electrode, Ag/Ag^+; counter electrode, Pt foil; working electrode, Pt button; 0.05 M Me_4NClO_4 in CH_3CN under Ar at room temperature.

Table 5–2. Cyclic Voltammetric Peak Potentials (V) for Complexes $(Bu_4N)_2\{tto[Ni(dmit)]_2\}$ (**131**), $(Bu_4N)_2\{tto[Ni(dsit)]_2\}$ (**134**) and $(Bu_4N)_2\{tto[Ni(dmise)]_2\}$ (**135**)[a]

complex	$E_{p,a}$	$E_{p,c}$	$E_{1/2}$
$(Bu_4N)_2\{tto[Ni(dmit)]_2\}$ (**131**)	-0.80	-0.86	-0.83
	-0.20	-0.25	
$(Bu_4N)_2\{tto[Ni(dsit)]_2\}$ (**134**)	-0.78	-0.85	-0.82
	-0.23	-0.34	
$(Bu_4N)_2\{tto[Ni(dmise)]_2\}$ (**135**)	-0.78	-0.85	-0.82
	-0.15	-0.29	

[a]Conditions: scan rate, 100 mV/s; reference electrode, Ag/Ag^+; counter electrode, Pt foil; working electrode, Pt button; 0.05 M Me_4NClO_4 electrolyte in CH_3CN under Ar at room temperature.

Upon scanning to higher potentials, a second irreversible redox process is observed for all the complexes. The complex $(Bu_4N)_2\{tto[Ni(dmise)]_2\}$ (**135**) oxidizes at the highest potential of –0.15 V to the lowest value observed of –0.23 V for $(Bu_4N)_2\{tto[Ni(dsit)]_2\}$ (**134**). Upon return scanning cathodically, a large reduction peak is observed for all the complexes with the highest reduction potential (–0.25 V) being seen for $(Bu_4N)_2\{tto[Ni(dmit)]_2\}$ (**131**) to the lowest potential of –0.34 V exhibited for $(Bu_4N)_2\{tto[Ni(dsit)]_2\}$ (**134**). The shape of the second redox couple is very similar to the previously reported cyclic voltammetric behavior for the similar $M(dmit)_2$-based bis-chelate complexes $[Ni(dmit)_2]^{2-}$ (**49**),[102] $[Pd(dmit)_2]^{2-}$ (**149**),[146] $[Ni(dsit)_2]^{2-}$ (**150**),[170,171] and $[Ni(dtdt)_2]^{2-}$ (**151**) (where dtdt = $C_4H_4S_5^{2-}$ = 5,7-dihydro-1,4,6-trithiin-2,3-dithiolato).[146] The large reduction peak is indicative of a redissolution process. Thorough studies of these types of materials in the mechanism of electrocrystallization have been reported by Cassoux and coworkers[102,146] that show that the large reduction peak observed is due to a redissolution process of deposited non-integer oxidation state material on the electrode surface formed in the diffusion layer. The formation of the deposited material of the bimetallic complexes can best be described by the following scheme:

$$\{tto[Ni(L)]_2\}^- \rightarrow \{tto[Ni(L)]_2\}^{n-} + (1-n)e^-$$

Upon scanning to higher potentials, an increase in current is observed which indicates that the non-integer oxidation state material deposited is electrically conductive. This type of behavior exhibited by the dianions of complexes **131**, **134** and **135**, plays an important role in the potential formation of highly electrically conducting non-integer oxidation state materials via electrocrystallization and slow-interdiffusion experiments.[102,146]

5–2–4 Electrocrystallization, Slow Interdiffusion, Chemical Oxidation and Conductivity Experiments of $(Bu_4N)_2\{tto[Ni(dmit)]_2\}$ (**131**)

Initial experiments have been carried out using $(Bu_4N)_2\{tto[Ni(dmit)]_2\}$ (**131**) in the construction of electrically conducting materials via electrocrystallization, slow interdiffusion and chemical oxidation techniques. A black precipitate of stoichiometry $(TTF)_x\{tto[Ni(dmit)]_2\}$ (**146**), was isolated from the rapid mixing of solutions of a slight excess of $(TTF)_3(BF_4)_2$ (**51**) and **131** in acetonitrile/acetone (1:1) which had a high pressed-pellet conductivity of 0.4 S/cm. Elemental analysis data was inconclusive for an exact stoichiometry. Slow interdiffusion experiments of saturated solutions of $(TTF)_3(BF_4)_2$ (**51**) and $(Bu_4N)_2\{tto[Ni(dmit)]_2\}$ (**131**) were carried out. A black precipitate of stoichiometry $(TTF)_{0.57}\{tto[Ni(dmit)]_2\}$ (**147**) was obtained as determined by elemental analysis. This is the same technique used for the synthesis of the superconductor $(TTF)[Ni(dmit)_2]_2$ (**50**).[64] The conductivity was determined to be 0.06 S/cm. This is approximately an order of magnitude less than that of the material obtained from the rapid mixing of solutions.

The synthesis of partial oxidation state materials using $\{tto[Ni(dmit)]_2\}^{2-}$ with Bu_4N^+ as the counterion was also investigated. The rapid mixing of solutions of NaI/I_2 and $(Bu_4N)_2\{tto[Ni(dmit)]_2\}$ (**131**) in acetone yielded a black precipitate of stoichiometry $(Bu_4N)_{0.33}\{tto[Ni(dmit)]_2\}$ (**148**) as determined by elemental analysis. A conductivity of 0.3 S/cm was found. Similar results were found for $(Bu_4N)_{0.33}\{tto[Cu(dmit)]_2\}$ (**109**) which was synthesized using the same technique. The conductivity was reported to be ~0.01 S/cm.[150] Electrocrystallization experiments of $(Bu_4N)_2\{tto[Ni(dmit)]_2\}$ (**131**) in a mixture of CH_3CN/DMF (4/1) in the presence of Bu_4NBr (**138**) were performed and a black, brittle, microcrystalline material was obtained. An approximate stoichiometry could not be determined as the elemental analysis results were ambiguous ($(Bu_4N)_x\{tto[Ni(dmit)]_2\}$ (**145**), $x \approx ?$). This may be due to solvent molecules being present in the unit cell. Two-probe pressed-powder conductivity measurements were

carried out and was found to have a conductivity of 0.6 S/cm, the highest observed for non-integer oxidation state materials based on the Ni(II) and Cu(II) bimetallic, tto-bridged complexes.[150,151,161]

5–3 Conclusions

Using a new synthetic methodology, five new dianionic extensively conjugated, chalcogen-rich, bimetallic Ni(II) complexes have been assembled. The complexes $(Bu_4N)_2\{tto[Ni(dmit)]_2\}$ (**131**), $(Et_4N)_2\{tto[Ni(dmit)]_2\}$ (**132**), $(Me_4N)_2\{tto[Ni(dmit)]_2\}$ (**133**), $(Bu_4N)_2\{tto[Ni(dsit)]_2\}$ (**134**) and $(Bu_4N)_2\{tto[Ni(dmise)]_2\}$ (**135**) form two-dimensional sheets from and side-by-side nonbonding interactions and three-dimensional arrays depending upon the cation used. The complexes are nearly perfectly planar with dihedral angles between the capping ligands and tto (**45**) ligands ranging from 2.0 to 24.5°.

Cyclic voltammetry results for all of the complexes show a first low potential reversible redox couple followed by a second non-reversible redox couple. The cathodic wave on the second redox couple is indicative of stripping of a deposit from the working electrode. The behavior is nearly identical to that of dianionic $M(dmit)_2$ bis-chelates and its analogs that have been used in the assembly of metallic and superconducting complexes. The formation of conducting materials has been investigated using the compound $(Bu_4N)_2\{tto[Ni(dmit)]_2\}$ (**131**). Electrocrystallization, slow interdiffusion and chemical oxidation experiments have been carried out on **131** to assemble partial oxidation state and potentially highly electrically conducting materials. Thus far, a microcrystalline material obtained from electrocrystallization experiments have yielded a pressed powder conductivity of 0.6 S/cm. An approximate stoichiometry could not be determined due to the possibility of solvent molecules incorporated in the crystalline material. This is the highest conductivity observed for materials based on bimetallic, tetrathiooxalate-bridged Cu(II) and Ni(II) complexes with capping ligands of dmit and its chalcogen analogs.

APPENDIX
TABLES OF CRYSTALLOGRAPHIC DATA

Appendix Table A-1: Crystallographic Data for $(Me_3S)[Ni(dmit)_2]_2$ (**93**).

A. Crystal data (298 K)	**93**
a, Å	7.923 (1)
b, Å	11.647 (1)
c, Å	17.812 (2)
α, deg.	77.46 (1)
β, deg.	85.93 (1)
γ, deg.	81.36 (1)
V, Å^3	1585.0 (3)
d_{calc}, g cm^{-3}(298 K)	
Empirical formula	$C_{15}H_9S_{21}Ni_2$
Formula wt, g	
Crystal system	Triclinic
Space group	P-1
Z	2
F(000), electrons	
Crystal size (mm^3)	0.41 x 0.34 x 0.05
B. Data collection (298 K)	
Radiation, λ (Å)	Mo-K_α, 0.71073
Mode	ω-scan
Scan range	Symmetrically over 1.2° about $K_{\alpha 1,2}$ maximum
Background	offset 1.0 and -1.0 in ω from $K_{\alpha 1,2}$ maximum
Scan rate, deg. min.$^{-1}$	4 – 8
2θ range, deg.	3 – 50
Range of *h k l*	$0 \leq h \leq 9$ $-13 \leq k \leq 13$ $-21 \leq l \leq 21$
Total reflections measured	6161
Unique reflections	5549
Absorption coeff. μ (Mo-K_α), cm^{-1}	
Min. & Max. Transmission	0.45, 0.86
C. Structure refinement	
S, Goodness-of-fit	1.24
Reflections used, I > 2σ(I)	3831
No. of variables	343
R, wR* (%)	0.0329, 0.0396
$R_{int.}$ (%)	0.0206
Max. shift/esd	0.0013

min. peak in diff. four. map (e $Å^{-3}$)	-0.43
max. peak in diff. four. map (e $Å^{-3}$)	0.30

* Relevant expressions are as follows, where in the footnote F_o and F_c represent, respectively, the observed and calculated structure-factor amplitudes.

Function minimized was $w(|F_o| - |F_c|)^2$, where $w = (\sigma(F))^{-2}$

$R = \sum(||F_o| - |F_c||) / \sum|F_o|$

$wR = [\sum w(|F_o| - |F_c|)^2 / \sum |F_o|^2]^{1/2}$

$S = [\sum w(|F_o| - |F_c|)^2 / (m-n)]^{1/2}$

Appendix Table A-2: Fractional Coordinates and Equivalent Isotropic[a] Thermal Parameters ($Å^2$) for the Non-H Atoms of $(Me_3S)[Ni(dmit)_2]_2$ (**93**).

Atom	x	y	z	U
Ni1	0.15473(7)	0.24064(4)	0.02306(3)	0.0285(2)
S1	0.4048(2)	0.07857(12)	0.41225(7)	0.0619(6)
S2	0.2940(2)	0.01603(9)	0.27153(6)	0.0381(4)
S3	0.3430(2)	0.25870(9)	0.26659(6)	0.0391(4)
S4	0.1803(2)	0.07493(9)	0.10701(6)	0.0350(4)
S5	0.2335(2)	0.33970(8)	0.10117(6)	0.0321(4)
S6	0.0683(2)	0.14345(9)	-0.05440(6)	0.0355(4)
S7	0.1246(2)	0.40664(9)	-0.06060(6)	0.0344(4)
S8	-0.0626(2)	0.22658(9)	-0.21561(6)	0.0372(4)
S9	-0.0095(2)	0.46948(9)	-0.22108(6)	0.0365(4)
S10	-0.1491(2)	0.41347(11)	-0.35665(7)	0.0475(5)
C1	0.3493(6)	0.1161(4)	0.3209(2)	0.038(2)
C2	0.2495(5)	0.1160(3)	0.1847(2)	0.0295(15)
C3	0.2732(5)	0.2309(3)	0.1823(2)	0.0288(14)
C4	0.0212(5)	0.2529(3)	-0.1340(2)	0.0282(14)
C5	0.0469(5)	0.3677(3)	-0.1364(2)	0.0297(15)
C6	-0.0752(5)	0.3707(3)	-0.2696(2)	0.033(2)
Ni2	0.43276(7)	0.72179(4)	0.07273(3)	0.0298(2)
S11	0.6910(2)	0.57709(12)	0.46111(7)	0.0573(5)
S12	0.5853(2)	0.50505(10)	0.32244(7)	0.0422(4)
S13	0.6182(2)	0.75166(10)	0.31459(7)	0.0440(5)
S14	0.4691(2)	0.55679(9)	0.15819(7)	0.0365(4)
S15	0.5085(2)	0.82534(9)	0.14913(6)	0.0336(4)
S16	0.3411(2)	0.62122(9)	-0.00062(6)	0.0349(4)
S17	0.4015(2)	0.88419(9)	-0.01455(6)	0.0357(4)
S18	0.2193(2)	0.69211(9)	-0.16325(6)	0.0365(4)
S19	0.2760(2)	0.93660(9)	-0.17653(7)	0.0368(4)
S20	0.1516(2)	0.86457(12)	-0.31033(8)	0.0557(5)
C11	0.6357(6)	0.6091(4)	0.3706(3)	0.039(2)
C12	0.5377(5)	0.6021(3)	0.2345(2)	0.033(2)
C13	0.5544(5)	0.7191(3)	0.2308(2)	0.0308(15)
C14	0.2968(5)	0.7248(3)	-0.0827(2)	0.0285(14)
C15	0.3241(5)	0.8409(3)	-0.0884(2)	0.0274(14)
C16	0.2131(5)	0.8326(3)	-0.2209(2)	0.033(2)
S21	-0.0585(2)	0.17427(10)	0.48089(8)	0.0611(6)
C21	0.0129(7)	0.3084(4)	0.4294(3)	0.058(2)
C22	-0.2741(8)	0.2235(5)	0.5057(3)	0.079(3)
C23	0.0473(8)	0.1496(5)	0.5695(3)	0.076(3)

[a]For anisotropic atoms, the U value is U_{eq}, calculated as $U_{eq} = 1/3\ \Sigma_i\Sigma_j\ U_{ij}\ a_i^*\ a_j^*\ A_{ij}$ where A_{ij} is the dot product of the i^{th} and j^{th} direct space unit cell vectors.

Appendix Table A-3: Bond Lengths (Å) and Angles (°) for the Non-H Atoms of $(Me_3S)[Ni(dmit)_2]_2$ (**93**).

1	2	3	1-2	1-2-3
S4	Ni1	S5	2.1620(11)	93.53(5)
S4	Ni1	S6		86.76(5)
S5	Ni1	S6	2.1663(13)	178.34(5)
S5	Ni1	S7		86.70(4)
S6	Ni1	S7	2.1678(14)	92.99(5)
S7	Ni1	S4	2.1625(11)	179.05(9)
C1	S1		1.664(4)	
C1	S2	C2	1.725(5)	97.3(2)
C2	S2		1.744(4)	
C1	S3	C3	1.727(4)	97.2(2)
C3	S3		1.745(5)	
C2	S4	Ni1	1.709(5)	101.97(13)
C3	S5	Ni1	1.716(4)	101.7(2)
C4	S6	Ni1	1.710(4)	102.0(2)
C5	S7	Ni1	1.696(5)	102.37(13)
C4	S8	C6	1.744(4)	97.1(2)
C6	S8		1.736(4)	
C5	S9	C6	1.744(4)	97.5(2)
C6	S9		1.736(5)	
C6	S10		1.644(4)	
S1	C1	S2		123.1(2)
S1	C1	S3		123.0(3)
S2	C1	S3		113.8(2)
C3	C2	S2	1.370(6)	115.8(3)
C3	C2	S4		121.5(3)
S2	C2	S4		122.7(2)
S3	C3	S5		122.8(2)
S3	C3	C2		115.9(3)
S5	C3	C2		121.3(3)
C5	C4	S6	1.373(6)	121.0(3)
C5	C4	S8		116.4(3)
S6	C4	S8		122.6(3)
S7	C5	S9		122.8(2)
S7	C5	C4		121.5(3)
S9	C5	C4		115.6(3)
S8	C6	S9		113.4(2)
S8	C6	S10		124.4(3)
S9	C6	S10		122.2(2)
S14	Ni2	S15	2.1723(11)	93.30(5)
S14	Ni2	S16		86.76(5)
S15	Ni2	S16	2.1708(14)	176.39(6)
S15	Ni2	S17		87.51(5)
S16	Ni2	S17	2.1591(14)	92.51(5)
S17	Ni2	S14	2.1663(11)	178.46(8)
C11	S11		1.650(5)	
C11	S12	C12	1.734(5)	97.4(2)
C12	S12		1.750(4)	

C11	S13	C13	1.732(4)	97.7(2)
C13	S13		1.743(5)	
C12	S14	Ni2	1.710(5)	101.96(13)
C13	S15	Ni2	1.713(4)	102.0(2)
C14	S16	Ni2	1.701(4)	102.9(2)
C15	S17	Ni2	1.690(5)	102.75(13)
C14	S18	C16	1.736(5)	96.8(2)
C16	S18		1.729(4)	
C15	S19	C16	1.747(4)	96.9(2)
C16	S19		1.730(5)	
C16	S20		1.647(4)	
S11	C11	S12		123.8(3)
S11	C11	S13		123.0(3)
S12	C11	S13		113.3(3)
C13	C12	S12	1.376(6)	115.8(3)
C13	C12	S14		121.5(3)
S12	C12	S14		122.7(2)
S13	C13	S15		122.9(3)
S13	C13	C12		115.8(3)
S15	C13	C12		121.3(3)
C15	C14	S16	1.382(6)	120.6(3)
C15	C14	S18		116.5(3)
S16	C14	S18		122.9(2)
S17	C15	S19		123.3(2)
S17	C15	C14		121.3(3)
S19	C15	C14		115.4(3)
S18	C16	S19		114.3(2)
S18	C16	S20		122.7(3)
S19	C16	S20		123.0(2)
C21	S21	C22	1.781(5)	102.1(2)
C22	S21	C23	1.775(6)	103.7(3)
C23	S21	C21	1.787(6)	101.8(3)

Appendix Table A-4: Crystallographic Data for $(Ph_4P)[Ni(dmit)_2]_3$ (**94**).

A. Crystal data (298 K)	**94**
a, Å	18.114(2)
b, Å	7.193(1)
c, Å	22.960(4)
α, deg.	90.00
β, deg.	92.60(1)
γ, deg.	90.00
V, Å^3	2988.5(7)
d_{calc}, g cm^{-3}(298 K)	1.882
Empirical formula	$C_{42}H_{20}PS_{30}NI_3$
Formula wt, g	1693.48
Crystal system	Monoclinic
Space group	C2
Z	2
F(000), electrons	1702
Crystal size (mm^3)	0.50 x 0.20 x 0.04
B. Data collection (298 K)	
Radiation, λ (Å)	Mo-K_α, 0.71069
Mode	ω-scan
Scan range	Symmetrically over 1.2° about $K_{\alpha 1,2}$ maximum
Background	offset 1.0 and -1.0 in ω from $K_{\alpha 1,2}$ maximum
Scan rate, deg. min.$^{-1}$	3 – 6
2θ range, deg.	3 – 55
Range of *h k l*	$0 \leq h \leq 23$ $0 \leq k \leq 9$ $-29 \leq l \leq 29$
Total reflections measured	3837
Unique reflections	3717
Min. & max. Transmission	0.677, 0.925
Absorption coeff. μ (Mo-K_α), mm^{-1}	2.05
C. Structure refinement	
S, Goodness-of-fit	3.85
Reflections used, $I > 2\sigma(I)$	2203
No. of variables	345
R, wR* (%)	4.55, 4.61
$R_{int.}$ (%)	2.01
Max. shift/esd	0.001

min. peak in diff. four. map (e $Å^{-3}$)	-0.66
max. peak in diff. four. map (e $Å^{-3}$)	0.80

* Relevant expressions are as follows, where in the footnote F_o and F_c represent, respectively, the observed and calculated structure-factor amplitudes.

Function minimized was $w(|F_o| - |F_c|)^2$, where $w= (\sigma(F))^{-2}$

$R = \sum(||F_o| - |F_c||) / \sum|F_o|$

$wR = [\sum w(|F_o| - |F_c|)^2 / \sum |F_o|^2]^{1/2}$

$S = [\sum w(|F_o| - |F_c|)^2 / (m-n)]^{1/2}$

Appendix Table A-5: Fractional Coordinates and Equivalent Isotropic[a] Thermal Parameters ($Å^2$) for the Non-H Atoms of $(Ph_4P)[Ni(dmit)_2]_3$ (**94**).

Atom	x	y	z	U
Ni1	0.5	-0.5	0.0	0.0302(5)
S1	0.4989(3)	-0.2804(10)	0.0645(2)	0.036(2)
S1a	0.5012(3)	-0.2804(10)	-0.0645(2)	0.036(2)
S2	0.4984(3)	-0.7163(10)	0.0645(2)	0.035(2)
S2a	0.5017(3)	-0.7163(10)	-0.0645(2)	0.035(2)
S3	0.4891(3)	-0.2941(9)	0.1955(2)	0.044(2)
S4	0.4852(3)	-0.6977(9)	0.1949(2)	0.040(2)
S5	0.4673(2)	-0.4923(13)	0.30569(12)	0.0724(13)
C1	0.4927(8)	-0.401(3)	0.1266(7)	0.040(6)
C2	0.4940(9)	-0.593(2)	0.1284(7)	0.028(5)
C3	0.4808(5)	-0.490(3)	0.2355(4)	0.047(4)
Ni2	0.72836(6)	0.0074(8)	-0.05364(5)	0.0305(3)
S6	0.81798(12)	0.0073(12)	-0.11175(11)	0.0423(8)
S7	0.64535(12)	0.0024(13)	-0.12415(10)	0.0420(8)
S8	0.8198(2)	-0.0128(13)	-0.24302(12)	0.0553(12)
S9	0.6607(2)	-0.019(2)	-0.25491(13)	0.079(2)
S10	0.7484(3)	-0.0659(10)	-0.3607(2)	0.086(2)
C4	0.7734(5)	0.006(4)	-0.1786(4)	0.041(3)
C5	0.6984(6)	-0.000(4)	-0.1840(4)	0.048(4)
C6	0.7462(7)	-0.022(5)	-0.2890(5)	0.086(9)
S11	0.81275(12)	0.0084(13)	0.01517(10)	0.0423(8)
S12	0.64120(12)	0.0084(13)	0.00692(10)	0.0413(8)
S13	0.80489(14)	0.0023(13)	0.14545(11)	0.0471(9)
S14	0.64483(14)	0.0025(12)	0.13879(11)	0.0471(9)
S15	0.7255(2)	-0.0100(13)	0.25467(13)	0.0684(14)
C7	0.7646(5)	0.013(3)	0.0748(4)	0.035(3)
C8	0.6877(5)	0.008(3)	0.0717(4)	0.034(3)
C9	0.7248(6)	0.015(4)	0.1834(5)	0.048(4)
P	0.5	0.6398(9)	0.5	0.0391(14)
C10	0.5182(7)	0.788(2)	0.4390(5)	0.041(4)
C10a	0.4818(7)	0.788(2)	0.5610(5)	0.041(4)
C11	0.5807(7)	0.755(2)	0.4074(5)	0.056(5)
C12	0.5918(9)	0.870(3)	0.3595(7)	0.074(7)
C13	0.5433(9)	1.021(4)	0.3465(5)	0.075(6)
C14	0.4807(9)	1.039(3)	0.3766(6)	0.068(7)
C15	0.4699(8)	0.929(2)	0.4232(6)	0.061(5)
C16	0.4205(6)	0.511(3)	0.4841(4)	0.049(4)
C16a	0.5795(6)	0.511(3)	0.5156(4)	0.049(4)
C17	0.3726(6)	0.512(4)	0.4372(5)	0.063(5)
C18	0.3109(9)	0.415(3)	0.4289(7)	0.095(9)
C19	0.2976(9)	0.275(3)	0.4692(8)	0.077(7)
C20	0.3450(9)	0.241(3)	0.5158(7)	0.072(6)
C21	0.4078(8)	0.350(2)	0.5243(6)	0.055(5)

[a]For anisotropic atoms, the U value is U_{eq}, calculated as $U_{eq} = 1/3 \sum_i \sum_j U_{ij} a_i^* a_j^* A_{ij}$ where A_{ij} is the dot product of the i^{th} and j^{th} direct space unit cell vectors.

Appendix Table A-6: Bond Lengths (Å) and Angles (°) for the Non-H Atoms of $(Ph_4P)[Ni(dmit)_2]_3$ (**94**).

1	2	3	1-2	1-2-3
S1	Ni1	S1a	2.166(6)	86.4(2)
S1	Ni1	S2		93.2(2)
S1a	Ni1	S2	2.166(6)	179.5(3)
S1a	Ni1	S2a		93.2(2)
S2	Ni1	S2a	2.149(6)	87.3(2)
S2a	Ni1	S1	2.149(6)	179.5(2)
C1	S1	Ni1	1.68(2)	102.0(7)
C2	S2	Ni1	1.72(2)	102.6(6)
C1	S3	C3	1.76(2)	97.5(9)
C3	S3		1.70(2)	
C2	S4	C3	1.72(2)	96.2(7)
C3	S4		1.76(2)	
C3	S5		1.640(10)	
C2	C1	S1	1.38(2)	122.7(13)
C2	C1	S3		114.3(12)
S1	C1	S3		122.9(12)
S2	C2	S4		122.9(8)
S2	C2	C1		119.5(12)
S4	C2	C1		117.5(12)
S3	C3	S4		114.3(6)
S3	C3	S5		124.0(13)
S4	C3	S5		121.7(13)
S6	Ni2	S7	2.148(3)	93.13(10)
S6	Ni2	S11		85.65(10)
S7	Ni2	S11	2.159(2)	178.6(3)
S7	Ni2	S12		88.75(9)
S11	Ni2	S12	2.148(2)	92.48(10)
S12	Ni2	S6	2.151(3)	178.12(13)
C4	S6	Ni2	1.701(9)	102.6(3)
C5	S7	Ni2	1.713(10)	101.9(3)
C4	S8	C6	1.740(10)	97.9(6)
C6	S8		1.664(13)	
C5	S9	C6	1.741(10)	95.8(5)
C6	S9		1.766(13)	
C6	S10		1.679(14)	
C5	C4	S6	1.360(14)	121.0(7)
C5	C4	S8		116.0(7)
S6	C4	S8		122.6(6)
S7	C5	S9		122.8(6)
S7	C5	C4		121.3(7)
S9	C5	C4		115.9(7)
S8	C6	S9		114.3(7)
S8	C6	S10		125.1(9)
S9	C6	S10		119.8(8)
C7	S11	Ni2	1.657(10)	103.0(3)
C8	S12	Ni2	1.675(9)	102.6(3)
C7	S13	C9	1.750(10)	98.1(5)

C9	S13		1.728(12)	
C8	S14	C9	1.758(9)	97.2(5)
C9	S14		1.738(11)	
C9	S15		1.646(12)	
C8	C7	S11	1.392(13)	121.3(7)
C8	C7	S13		114.9(7)
S11	C7	S13		123.5(6)
S12	C8	S14		123.6(5)
S12	C8	C7		120.6(7)
S14	C8	C7		115.8(7)
S13	C9	S14		113.4(6)
S13	C9	S15		121.8(7)
S14	C9	S15		123.3(7)
C10	P	C10a	1.800(13)	107.6(7)
C10	P	C16		109.3(6)
C10a	P	C16	1.800(13)	107.4(6)
C10a	P	C16a		109.5(6)
C16	P	C16a	1.74(2)	115.4(10)
C16a	P	C10	1.74(2)	107.2(6)
C11	C10	C15	1.39(2)	120.4(12)
C11	C10	P		119.3(10)
C15	C10	P	1.38(2)	120.3(10)
C12	C11	C10	1.40(2)	117.5(14)
C13	C12	C11	1.42(3)	120.6(15)
C14	C13	C12	1.36(2)	119.(2)
C15	C14	C13	1.35(2)	120.(2)
C10	C15	C14		121.7(14)
C17	C16	C21	1.353(15)	113.(2)
C17	C16	P		131.(2)
C21	C16	P	1.50(2)	115.5(8)
C18	C17	C16	1.33(3)	128.(2)
C19	C18	C17	1.39(3)	117.(2)
C20	C19	C18	1.36(2)	122.(2)
C21	C20	C19	1.39(2)	120.(2)
C16	C21	C20		119.6(12)

Appendix Table A-7: Crystallographic Data for $(MePh_3P)[Ni(dmit)_2]_3$ (**95**).

Empirical formula	C37 H18 P S30 Ni3
Formula weight	1631.41
Temperature	173(2) K
Wavelength	0.71073 Å
Crystal system	Monoclinic
Space group	P2(1)/c
Unit cell dimensions	a = 21.0872(1) Å, α = 90° b = 17.4930(2) Å, β = 107.072(1)° c = 15.7203(2) Å, γ = 90°
Volume, Z	5543.4(1) $Å^3$, 4
Density (calculated)	1.955 Mg/m^3
Absorption coefficient	2.202 mm^{-1}
F(000)	3276
Crystal size	0.23 x 0.1 x 0.08 mm^3
Theta range for data collection	1.54 to 27.50°
Limiting indices	–28<=h<=25, 0<=k<=22, 0<=l<=20
Reflections collected	34589
Independent reflections	12319 [R(int) = 0.0332]
Absorption correction	Semi-empirical from psi-scans
Max. and min. transmission	0.860 and 0.717
Refinement method	Full-matrix least-squares on F^2
Data / restraints / parameters	12219 / 0 / 713
Goodness-of-fit on F^2	1.131
Final R indices [I>2σ(I)]	R_1 = 0.0340, wR_2 = 0.0648
R indices (all data)	R_1 = 0.0511, wR_2 = 0.0781

Extinction coefficient	0.00019(2)
Largest diff. peak and hole	0.545 and –0.499 e.Å^{-3}

Appendix Table A-8: Atomic Coordinates (x 10^4) and Equivalent Isotropic[a] Thermal Parameters ($Å^2$ x 10^3) for the Non-H Atoms of $(MePh_3P)[Ni(dmit)_2]_3$ (**95**). U(eq) is defined as one third of trace of the orthogonalized Uij tensor.

atom	x	y	z	U(eq)
Ni(1)	-254(1)	-157(1)	9095(1)	16(1)
S(1)	-3560(1)	-591(1)	9308(1)	41(1)
S(2)	-2213(1)	-1222(1)	9533(1)	23(1)
S(3)	-2507(1)	342(1)	8901(1)	25(1)
S(4)	-801(1)	-1108(1)	9448(1)	18(1)
S(5)	-1116(1)	601(1)	8832(1)	20(1)
S(6)	565(1)	-955(1)	9126(1)	18(1)
S(7)	198(1)	759(1)	8526(1)	20(1)
S(8)	1868(1)	-683(1)	8730(1)	22(1)
S(9)	1496(1)	874(1)	8131(1)	21(1)
S(10)	2815(1)	309(1)	8137(1)	31(1)
C(1)	-2801(2)	-495(2)	9257(2)	24(1)
C(2)	-1555(1)	-716(2)	9339(2)	18(1)
C(3)	-1698(1)	32(2)	9048(2)	18(1)
C(4)	1092(1)	-383(2)	8786(2)	17(1)
C(5)	920(1)	363(2)	8497(2)	17(1)
C(6)	2099(2)	169(2)	8323(2)	21(1)
Ni(2)	114(1)	3253(1)	8816(1)	17(1)
S(11)	-3189(1)	2787(1)	9017(1)	37(1)
S(12)	-1789(1)	2258(1)	9456(1)	23(1)
S(13)	-2153(1)	3712(1)	8550(1)	24(1)
S(14)	-373(1)	2378(1)	9365(1)	19(1)
S(15)	-755(1)	3975(1)	8451(1)	20(1)
S(16)	988(1)	2531(1)	9132(1)	20(1)
S(17)	572(1)	4127(1)	8221(1)	21(1)
S(18)	2320(1)	2745(1)	8806(1)	22(1)
S(19)	1930(1)	4214(1)	7948(1)	23(1)
S(20)	3232(1)	3549(1)	7977(1)	31(1)
C(11)	-2415(2)	2910(2)	9010(2)	22(1)
C(12)	-1155(1)	2737(2)	9171(2)	19(1)
C(13)	-1328(1)	3432(2)	8749(2)	19(1)
C(14)	1524(1)	3057(2)	8747(2)	18(1)
C(15)	1338(1)	3759(2)	8339(2)	18(1)
C(16)	2533(2)	3507(2)	8236(2)	21(1)
Ni(3)	-849(1)	6468(1)	8885(1)	18(1)
S(21)	-4120(1)	6207(1)	9298(1)	28(1)
S(22)	-2777(1)	5541(1)	9521(1)	24(1)
S(23)	-3087(1)	7039(1)	8714(1)	23(1)
S(24)	-1375(1)	5582(1)	9375(1)	21(1)
S(25)	-1696(1)	7235(1)	8550(1)	20(1)
S(26)	10(1)	5728(1)	9230(1)	21(1)
S(27)	-351(1)	7325(1)	8318(1)	21(1)
S(28)	1354(1)	5872(1)	8924(1)	25(1)
S(29)	1016(1)	7349(1)	8055(1)	24(1)

S(30)	2324(1)	6641(1)	8175(1)	39(1)
C(21)	-3364(1)	6257(2)	9189(2)	20(1)
C(22)	-2135(2)	5998(2)	9223(2)	20(1)
C(23)	-2283(1)	6709(2)	8851(2)	19(1)
C(24)	567(2)	6219(2)	8853(2)	20(1)
C(25)	404(1)	6926(2)	8439(2)	19(1)
C(26)	1604(2)	6626(2)	8379(2)	24(1)
P(1)	4179(1)	-2028(1)	9046(1)	20(1)
C(31)	4718(2)	-1731(2)	10103(2)	21(1)
C(32)	4482(2)	-1319(2)	10701(2)	35(1)
C(33)	4922(2)	-1071(2)	11493(3)	41(1)
C(34)	5589(2)	-1224(2)	11686(2)	34(1)
C(35)	5826(2)	-1637(2)	11098(2)	32(1)
C(36)	5396(2)	-1889(2)	10310(2)	29(1)
C(41)	4141(1)	-3051(2)	8992(2)	20(1)
C(42)	4238(2)	-3461(2)	9773(2)	28(1)
C(43)	4142(2)	-4245(2)	9740(2)	33(1)
C(44)	3956(2)	-4616(2)	8934(2)	31(1)
C(45)	3867(2)	-4217(2)	8155(2)	29(1)
C(46)	3953(2)	-3430(2)	8174(2)	26(1)
C(51)	4496(2)	-1663(2)	8192(2)	22(1)
C(52)	4972(2)	-2076(2)	7927(2)	28(1)
C(53)	5247(2)	-1772(2)	7306(2)	33(1)
C(54)	5057(2)	-1050(2)	6952(2)	33(1)
C(55)	4585(2)	-644(2)	7208(2)	35(1)
C(56)	4301(2)	-943(2)	7825(2)	29(1)
C(60)	3362(2)	-1666(2)	8911(3)	29(1)

Appendix Table A-9: Bond Lengths (Å) and Angles (°) for the Non-H Atoms of $(MePh_3P)[Ni(dmit)_2]_3$ (**95**).

Ni(1)-S(7)	2.1856(8)	Ni(3)-S(26)	2.1615(8)
Ni(1)-S(4)	2.1871(8)	Ni(3)-S(27)	2.1670(8)
Ni(1)-S(5)	2.1890(8)	Ni(3)-S(25)	2.1712(8)
Ni(1)-S(6)	2.2106(8)	Ni(3)-S(24)	2.1749(8)
Ni(1)-Ni(1)#1	2.7837(7)	S(21)-C(21)	1.654(3)
S(1)-C(1)	1.634(3)	S(22)-C(21)	1.730(3)
S(2)-C(1)	1.740(3)	S(22)-C(22)	1.750(3)
S(2)-C(2)	1.745(3)	S(23)-C(21)	1.741(3)
S(3)-C(3)	1.739(3)	S(23)-C(23)	1.744(3)
S(3)-C(1)	1.746(3)	S(24)-C(22)	1.712(3)
S(4)-C(2)	1.693(3)	S(25)-C(23)	1.715(3)
S(5)-C(3)	1.690(3)	S(26)-C(24)	1.696(3)
S(6)-C(4)	1.695(3)	S(27)-C(25)	1.697(3)
S(7)-C(5)	1.686(3)	S(28)-C(26)	1.738(3)
S(8)-C(4)	1.744(3)	S(28)-C(24)	1.741(3)
S(8)-C(6)	1.746(3)	S(29)-C(26)	1.740(3)
S(9)-C(6)	1.732(3)	S(29)-C(25)	1.742(3)
S(9)-C(5)	1.737(3)	S(30)-C(26)	1.641(3)
S(10)-C(6)	1.640(3)	C(22)-C(23)	1.372(4)
C(2)-C(3)	1.390(4)	C(24)-C(25)	1.393(4)
C(4)-C(5)	1.394(4)	P(1)-C(51)	1.783(3)
Ni(2)-S(14)	2.1595(8)	P(1)-C(60)	1.790(3)
Ni(2)-S(15)	2.1600(8)	P(1)-C(41)	1.792(3)
Ni(2)-S(17)	2.1614(8)	P(1)-C(31)	1.794(3)
Ni(2)-S(16)	2.1674(8)	C(31)-C(32)	1.387(4)
S(11)-C(11)	1.650(3)	C(31)-C(36)	1.397(4)
S(12)-C(11)	1.729(3)	C(32)-C(33)	1.386(5)
S(12)-C(12)	1.745(3)	C(33)-C(34)	1.375(5)
S(13)-C(11)	1.741(3)	C(34)-C(35)	1.378(5)
S(13)-C(13)	1.745(3)	C(35)-C(36)	1.376(5)
S(14)-C(12)	1.705(3)	C(41)-C(42)	1.384(4)
S(15)-C(13)	1.707(3)	C(41)-C(46)	1.397(4)
S(16)-C(14)	1.700(3)	C(42)-C(43)	1.386(4)
S(17)-C(15)	1.697(3)	C(43)-C(44)	1.375(5)
S(18)-C(16)	1.737(3)	C(44)-C(45)	1.374(5)
S(18)-C(14)	1.743(3)	C(45)-C(46)	1.388(4)
S(19)-C(16)	1.735(3)	C(51)-C(56)	1.395(4)
S(19)-C(15)	1.739(3)	C(51)-C(52)	1.397(4)
S(20)-C(16)	1.641(3)	C(52)-C(53)	1.379(5)
C(12)-C(13)	1.382(4)	C(53)-C(54)	1.391(5)
C(14)-C(15)	1.388(4)	C(54)-C(55)	1.377(5)
C(55)-C(56)	1.384(5)		

S(7)-Ni(1)-S(4)	170.92(3)	C(14)-C(15)-S(17)	121.1(2)
S(7)-Ni(1)-S(5)	85.21(3)	C(14)-C(15)-S(19)	115.7(2)
S(4)-Ni(1)-S(5)	92.20(3)	S(17)-C(15)-S(19)	123.2(2)
S(7)-Ni(1)-S(6)	92.29(3)	S(20)-C(16)-S(19)	123.1(2)
S(4)-Ni(1)-S(6)	88.89(3)	S(20)-C(16)-S(18)	123.3(2)
S(5)-Ni(1)-S(6)	170.71(3)	S(19)-C(16)-S(18)	113.6(2)

S(7)-Ni(1)-Ni(1)#1	101.01(3)	S(26)-Ni(3)-S(27)	92.66(3)
S(4)-Ni(1)-Ni(1)#1	87.95(3)	S(26)-Ni(3)-S(25)	178.64(3)
S(5)-Ni(1)-Ni(1)#1	97.09(3)	S(27)-Ni(3)-S(25)	86.35(3)
S(6)-Ni(1)-Ni(1)#1	92.16(3)	S(26)-Ni(3)-S(24)	87.78(3)
C(1)-S(2)-C(2)	97.53(14)	S(27)-Ni(3)-S(24)	176.61(3)
C(3)-S(3)-C(1)	97.02(14)	S(25)-Ni(3)-S(24)	93.26(3)
C(2)-S(4)-Ni(1)	102.45(10)	C(21)-S(22)-C(22)	97.44(14)
C(3)-S(5)-Ni(1)	102.51(10)	C(21)-S(23)-C(23)	97.11(14)
C(4)-S(6)-Ni(1)	101.61(10)	C(22)-S(24)-Ni(3)	101.69(10)
C(5)-S(7)-Ni(1)	102.47(10)	C(23)-S(25)-Ni(3)	102.18(10)
C(4)-S(8)-C(6)	97.34(14)	C(24)-S(26)-Ni(3)	102.94(10)
C(6)-S(9)-C(5)	97.14(14)	C(25)-S(27)-Ni(3)	102.76(10)
S(1)-C(1)-S(2)	123.3(2)	C(26)-S(28)-C(24)	97.17(14)
S(1)-C(1)-S(3)	123.2(2)	C(26)-S(29)-C(25)	97.27(14)
S(2)-C(1)-S(3)	113.5(2)	S(21)-C(21)-S(22)	123.8(2)
C(3)-C(2)-S(4)	121.4(2)	S(21)-C(21)-S(23)	122.8(2)
C(3)-C(2)-S(2)	115.3(2)	S(22)-C(21)-S(23)	113.5(2)
S(4)-C(2)-S(2)	123.2(2)	C(23)-C(22)-S(24)	122.0(2)
C(2)-C(3)-S(5)	121.4(2)	C(23)-C(22)-S(22)	115.6(2)
C(2)-C(3)-S(3)	116.6(2)	S(24)-C(22)-S(22)	122.4(2)
S(5)-C(3)-S(3)	122.0(2)	C(22)-C(23)-S(25)	120.8(2)
C(5)-C(4)-S(6)	121.5(2)	C(22)-C(23)-S(23)	116.3(2)
C(5)-C(4)-S(8)	115.1(2)	S(25)-C(23)-S(23)	122.9(2)
S(6)-C(4)-S(8)	123.4(2)	C(25)-C(24)-S(26)	120.8(2)
C(4)-C(5)-S(7)	121.8(2)	C(25)-C(24)-S(28)	116.1(2)
C(4)-C(5)-S(9)	116.7(2)	S(26)-C(24)-S(28)	123.1(2)
S(7)-C(5)-S(9)	121.5(2)	C(24)-C(25)-S(27)	120.8(2)
S(10)-C(6)-S(9)	121.9(2)	C(24)-C(25)-S(29)	115.7(2)
S(10)-C(6)-S(8)	124.4(2)	S(27)-C(25)-S(29)	123.5(2)
S(9)-C(6)-S(8)	113.7(2)	S(30)-C(26)-S(28)	122.7(2)
S(14)-Ni(2)-S(15)	93.11(3)	S(30)-C(26)-S(29)	123.5(2)
S(14)-Ni(2)-S(17)	177.89(3)	S(28)-C(26)-S(29)	113.8(2)
S(15)-Ni(2)-S(17)	85.64(3)	C(51)-P(1)-C(60)	110.2(2)
S(14)-Ni(2)-S(16)	88.13(3)	C(51)-P(1)-C(41)	110.12(14)
S(15)-Ni(2)-S(16)	177.90(3)	C(60)-P(1)-C(41)	108.6(2)
S(17)-Ni(2)-S(16)	93.07(3)	C(51)-P(1)-C(31)	108.54(14)
C(11)-S(12)-C(12)	97.50(14)	C(60)-P(1)-C(31)	109.5(2)
C(11)-S(13)-C(13)	96.96(14)	C(41)-P(1)-C(31)	109.93(13)
C(12)-S(14)-Ni(2)	102.50(10)	C(32)-C(31)-C(36)	119.4(3)
C(13)-S(15)-Ni(2)	102.44(10)	C(32)-C(31)-P(1)	121.5(3)
C(14)-S(16)-Ni(2)	102.24(10)	C(36)-C(31)-P(1)	119.0(2)
C(15)-S(17)-Ni(2)	102.51(10)	C(33)-C(32)-C(31)	119.5(3)
C(16)-S(18)-C(14)	97.09(14)	C(34)-C(33)-C(32)	120.6(3)
C(16)-S(19)-C(15)	97.44(14)	C(33)-C(34)-C(35)	120.2(3)
S(11)-C(11)-S(12)	123.3(2)	C(36)-C(35)-C(34)	119.9(3)
S(11)-C(11)-S(13)	122.9(2)	C(35)-C(36)-C(31)	120.3(3)
S(12)-C(11)-S(13)	113.7(2)	C(42)-C(41)-C(46)	120.0(3)
C(13)-C(12)-S(14)	120.9(2)	C(42)-C(41)-P(1)	118.8(2)
C(13)-C(12)-S(12)	115.6(2)	C(46)-C(41)-P(1)	121.0(2)
S(14)-C(12)-S(12)	123.5(2)	C(41)-C(42)-C(43)	119.8(3)
C(12)-C(13)-S(15)	120.9(2)	C(44)-C(43)-C(42)	120.1(3)
C(12)-C(13)-S(13)	116.2(2)	C(45)-C(44)-C(43)	120.6(3)
S(15)-C(13)-S(13)	122.9(2)	C(44)-C(45)-C(46)	120.2(3)
C(15)-C(14)-S(16)	121.1(2)	C(45)-C(46)-C(41)	119.4(3)

C(15)-C(14)-S(18)	116.0(2)	C(56)-C(51)-C(52)	119.5(3)
S(16)-C(14)-S(18)	122.9(2)	C(56)-C(51)-P(1)	120.3(2)
C(52)-C(51)-P(1)	120.0(2)	C(55)-C(54)-C(53)	120.0(3)
C(53)-C(52)-C(51)	120.0(3)	C(54)-C(55)-C(56)	120.5(3)
C(52)-C(53)-C(54)	120.1(3)	C(55)-C(56)-C(51)	119.8(3)

Symmetry transformations used to generate equivalent atoms:
#1 -x,-y,-z+2

Appendix Table B-1: Crystallographic Data for $(Bu_4N)_2\{tto[Cu(dmit)]_2\}$(**105**).

A. Crystal data (298 K)	**105**
a, Å	9.941 (1)
b, Å	15.304 (2)
c, Å	18.084 (2)
α, deg.	90.00 (0)
β, deg.	90.92 (1)
γ, deg.	90.00 (0)
V, Å^3	2750.9 (5)
d_{calc}, g cm^{-3}(298 K)	1.397
Empirical formula	$(C_8S_{14}Cu_2)(NC_{16}H_{36})_2$
Formula wt, g	1156.92
Crystal system	Monoclinic
Space group	P 2_1/c
Z	2
F(000), electrons	1216.0
Crystal size (mm^3)	0.55 x 0.13 x 0.13
B. Data collection (298 K)	
Radiation, λ (Å)	Mo-K_α, 0.71073
Mode	ω-scan
Scan range	Symmetrically over 1.2° about $K_{\alpha 1,2}$ maximum
Background	offset 1.0 and -1.0 in ω from $K_{\alpha 1,2}$ maximum
Scan rate, deg. min.$^{-1}$	3 – 6
2θ range, deg.	3 – 50
Range of *h k l*	$0 \leq h \leq 11$ $-0 \leq k \leq 18$ $-21 \leq l \leq 21$
Total reflections measured	5042
Unique reflections	4859
Absorption coeff. μ (Mo-K_α), cm^{-1}	1.33
Min. & Max. Transmission	0.82, 0.889
C. Structure refinement	
S, Goodness-of-fit	1.10
Reflections used, I > 2σ(I)	2773
No. of variables	262
R, wR* (%)	0.0387 0.0396
$R_{int.}$ (%)	0.0156
Max. shift/esd	0.001

min. peak in diff. four. map (e $Å^{-3}$)	-0.23
max. peak in diff. four. map (e $Å^{-3}$)	0.35

* Relevant expressions are as follows, where in the footnote F_o and F_c represent, respectively, the observed and calculated structure-factor amplitudes.

Function minimized was $w(|F_o| - |F_c|)^2$, where $w = (\sigma(F))^{-2}$

$R = \sum(||F_o| - |F_c||) / \sum|F_o|$

$wR = [\sum w(|F_o| - |F_c|)^2 / \sum |F_o|^2]^{1/2}$

$S = [\sum w(|F_o| - |F_c|)^2 / (m-n)]^{1/2}$

Appendix Table B-2: Fractional Coordinates and Equivalent Isotropic[a] Thermal Parameters ($Å^2$) for the Non-H Atoms of $(Bu_4N)_2\{tto[Cu(dmit)]_2\}$(**105**).

Atom	x	y	z	U
Cu	0.10836(5)	0.00117(4)	0.15993(3)	0.0485(2)
S1	-0.09776(11)	0.00715(9)	0.10454(6)	0.0555(4)
S2	0.19570(12)	-0.02332(9)	0.04661(7)	0.0636(5)
S2a	-0.19570(12)	0.02332(9)	-0.04661(7)	0.0636(5)
S3	0.01026(12)	0.00953(9)	0.27054(6)	0.0636(5)
S4	0.31761(12)	0.02082(8)	0.20583(6)	0.0560(4)
S5	0.13861(14)	0.04552(9)	0.41998(6)	0.0641(5)
S6	0.40614(12)	0.05341(9)	0.36325(7)	0.0617(5)
S7	0.3665(2)	0.07940(10)	0.52460(7)	0.0796(6)
C1	-0.0689(4)	0.0075(3)	0.0137(2)	0.0431(14)
C1a	0.0689(4)	-0.0075(3)	-0.0137(2)	0.0431(14)
C2	0.1524(5)	0.0303(3)	0.3246(2)	0.049(2)
C3	0.2772(5)	0.0346(3)	0.2981(2)	0.048(2)
C4	0.3074(5)	0.0612(3)	0.4406(2)	0.054(2)
N	0.6607(4)	0.2456(2)	0.1852(2)	0.0461(13)
C11	0.7685(4)	0.2978(3)	0.1470(3)	0.054(2)
C12	0.8885(5)	0.2446(3)	0.1221(3)	0.065(2)
C13	0.9971(5)	0.2990(3)	0.0879(3)	0.071(2)
C14	1.1084(5)	0.2433(4)	0.0582(3)	0.094(3)
C21	0.6098(4)	0.1721(3)	0.1356(2)	0.050(2)
C22	0.5541(5)	0.1991(3)	0.0608(3)	0.067(2)
C23	0.4809(5)	0.1270(3)	0.0241(2)	0.070(2)
C24	0.4317(6)	0.1448(4)	-0.0530(3)	0.095(3)
C31	0.5464(5)	0.3084(3)	0.2030(2)	0.051(2)
C32	0.4265(5)	0.2683(3)	0.2396(3)	0.062(2)
C33	0.3123(5)	0.3316(3)	0.2487(3)	0.071(2)
C34	0.1919(5)	0.2904(4)	0.2849(3)	0.090(3)
C41	0.7147(5)	0.2014(3)	0.2550(2)	0.051(2)
C42	0.7684(5)	0.2625(3)	0.3138(3)	0.068(2)
C43	0.8401(6)	0.2134(4)	0.3760(3)	0.078(2)
C44	0.7597(6)	0.1434(4)	0.4117(3)	0.106(3)

[a]For anisotropic atoms, the U value is U_{eq}, calculated as $U_{eq} = 1/3\ \Sigma_i\Sigma_j\ U_{ij}\ a_i^*\ a_j^*\ A_{ij}$ where A_{ij} is the dot product of the i^{th} and j^{th} direct space unit cell vectors.

Appendix Table B-3: Bond Lengths (Å) and Angles (°) for the non-H atoms of $(Bu_4N)_2\{tto[Cu(dmit)]_2\}$(**105**).

1	2	3	1-2	1-2-3
S1	Cu	S2	2.268(1)	87.93(5)
S1	Cu	S3		89.36(5)
S2	Cu	S3	2.270(1)	173.09(6)
S2	Cu	S4		89.45(5)
S3	Cu	S4	2.243(1)	94.36(5)
S4	Cu	S1	2.247(1)	169.10(6)
C1	S1	Cu	1.672(4)	105.4(1)
C1a	S2	Cu	1.672(4)	105.6(1)
C1	S2a		1.672(4)	
C2	S3	Cu	1.734(5)	98.7(2)
C3	S4	Cu	1.735(4)	98.3(2)
C2	S5	C4	1.749(4)	98.1(2)
C4	S5		1.729(5)	
C3	S6	C4	1.750(5)	97.9(2)
C4	S6		1.726(4)	
C4	S7		1.644(4)	
C1a	C1	S1	1.481(6)	120.2(3)
C1a	C1	S2a		119.7(3)
S1	C1	S2a		120.1(2)
S2	C1a	C1		119.7(3)
C3	C2	S3	1.339(7)	124.0(3)
C3	C2	S5		115.7(3)
S3	C2	S5		120.3(3)
S4	C3	S6		119.3(3)
S4	C3	C2		124.6(3)
S6	C3	C2		116.1(3)
S5	C4	S6		112.2(2)
S5	C4	S7		123.7(3)
S6	C4	S7		124.1(3)
C11	N	C21	1.513(6)	110.7(3)
C11	N	C31		107.4(3)
C21	N	C31	1.519(5)	110.4(3)
C21	N	C41		105.7(3)
C31	N	C41	1.526(6)	111.0(3)
C41	N	C11	1.522(5)	111.7(3)
C12	C11	N	1.519(6)	114.7(4)
C13	C12	C11	1.505(7)	113.4(4)
C14	C13	C12	1.502(7)	111.7(4)
C22	C21	N	1.511(6)	116.1(3)
C23	C22	C21	1.474(7)	111.7(4)
C24	C23	C22	1.496(6)	115.8(4)
C32	C31	N	1.504(7)	115.7(4)
C33	C32	C31	1.505(7)	113.0(4)
C34	C33	C32	1.512(7)	112.5(4)
C42	C41	N	1.508(6)	115.2(3)
C43	C42	C41	1.520(7)	111.8(4)
C44	C43	C42	1.490(8)	115.3(4)

Appendix Table B-4: Crystallographic data for $(Bu_4N)_2\{tto[Cu(mnt)]_2\}$(**106**).

A. Crystal data (298 K)	**106**
a, Å	19.549(4)
b, Å	13.519(3)
c, Å	10.162(2)
β, deg.	90.33(1)
V, Å^3	2686(1)
d_{calc}, g cm^{-3}(298 K)	1.292
Empirical formula	$C_{42}H_{72}N_6S_8Cu_2$
Formula wt, g	1044.62
Crystal system	Monoclinic
Space group	C 2/m
Z	2
F(000), electrons	1104
Crystal size (mm^3)	0.39 x 0.28 x 0.15
B. Data collection (298 K)	
Radiation, λ (Å)	Mo-K_α, 0.71073
Mode	ω-scan
Scan range	Symmetrically over 1.2° about $K_{\alpha 1,2}$ maximum
Background	offset 1.0 and -1.0 in ω from $K_{\alpha 1,2}$ maximum
Scan rate, deg. min.$^{-1}$	4 – 8
2θ range, deg.	3 – 55
Range of *h k l (two equivalent sets)*	$0 \leq h \leq 25$ $-17 \leq k \leq 17$ $-13 \leq l \leq 13$
Total reflections measured	6378
Unique reflections	3241
Absorption coeff. μ (Mo-K_α), mm^{-1}	1.14
Min. & Max. Transmission	0.677, 0.859
C. Structure refinement	
S, Goodness-of-fit	1.44
Reflections used, $I > 2\sigma(I)$	1637
No. of variables	150
R, wR* (%)	4.90, 5.33
$R_{int.}$ (%)	2.43
Max. shift/esd	0.001

min. peak in diff. four. map (e $Å^{-3}$)	-0.39
max. peak in diff. four. map (e $Å^{-3}$)	0.66

* Relevant expressions are as follows, where in the footnote F_o and F_c represent, respectively, the observed and calculated structure-factor amplitudes.

Function minimized was $w(|F_o| - |F_c|)^2$, wherew= $1/[\sigma^2(F)+0.0004F^2]$

$R = \Sigma(||F_o| - |F_c||) / \Sigma|F_o|$

$wR = [\Sigma w(|F_o| - |F_c|)^2 / \Sigma |F_o|^2]^{1/2}$

$S = [\Sigma w(|F_o| - |F_c|)^2 / (m-n)]^{1/2}$

Appendix Table B-5: Fractional Coordinates and Equivalent Isotropic[a] Thermal Parameters ($Å^2$) for the Non-H Atoms of $(Bu_4N)_2\{tto[Cu(mnt)]_2\}$(**106**).

atom	x	y	z	U(eq)
Cu	0.13811(4)	0.0	0.35752(8)	0.0619(3)
S1	0.10329(10)	0.0	0.5688(2)	0.0827(8)
S2	0.02623(9)	0.0	0.2954(2)	0.0643(6)
S2a	-0.02623(9)	0.0	0.7046(2)	0.0643(6)
S3	0.24638(9)	0.0	0.4269(2)	0.0786(7)
S4	0.16583(9)	0.0	0.1458(2)	0.0732(7)
N1	0.4187(3)	0.0	0.2789(7)	0.087(3)
N2	0.3248(3)	0.0	-0.0531(7)	0.092(3)
C1	0.0185(3)	0.0	0.5639(6)	0.057(2)
C1a	-0.0185(3)	0.0	0.4361(6)	0.057(2)
C2	0.2877(3)	0.0	0.2770(7)	0.062(2)
C3	0.2542(3)	0.0	0.1599(7)	0.062(2)
C4	0.3609(4)	0.0	0.2804(7)	0.069(3)
C5	0.2930(3)	0.0	0.0392(8)	0.067(3)
N3	0.0	0.2656(3)	0.0	0.050(2)
C11	0.0273(2)	0.3321(3)	0.1090(4)	0.059(2)
C11a	-0.0273(2)	0.3321(3)	-0.1090(4)	0.059(2)
C12	0.0550(2)	0.2794(3)	0.2302(4)	0.066(2)
C13	0.0784(2)	0.3504(4)	0.3349(5)	0.077(2)
C14	0.1054(3)	0.2959(4)	0.4551(5)	0.097(2)
C21	0.0566(2)	0.1982(3)	-0.0508(4)	0.059(2)
C21a	-0.0566(2)	0.1982(3)	0.0508(4)	0.059(2)
C22	0.1176(2)	0.2487(4)	-0.1115(5)	0.069(2)
C23	0.1682(3)	0.1756(4)	-0.1595(5)	0.087(2)
C24	0.2299(3)	0.2160(4)	-0.2256(6)	0.105(3)

[a]For anisotropic atoms, the U value is U_{eq}, calculated as $U_{eq} = 1/3\ \Sigma_i\Sigma_j\ U_{ij}\ a_i^*\ a_j^*\ A_{ij}$ where A_{ij} is the dot product of the i^{th} and j^{th} direct space unit cell vectors.

Appendix Table B-6: Bond Lengths (Å) and Angles (°) for the non-H atoms of $(Bu_4N)_2\{tto[Cu(mnt)]_2\}$(**106**).

1	2	3	1-2	1-2-3
S1	Cu	S2	2.256(2)	88.24(7)
S1	Cu	S3		89.45(8)
S2	Cu	S3	2.273(2)	177.68(8)
S2	Cu	S4		88.32(7)
S3	Cu	S4	2.227(2)	94.00(7)
S4	Cu	S1	2.222(2)	176.56(9)
C1	S1	Cu	1.658(6)	106.2(2)
C1a	S2	Cu	1.680(6)	105.6(2)
C1	S2a		1.680(6)	
C2	S3	Cu	1.728(7)	99.7(2)
C3	S4	Cu	1.733(7)	99.7(2)
C4	N1		1.130(10)	
C5	N2		1.127(10)	
C1a	C1	S1	1.483(9)	120.6(5)
C1a	C1	S2a		119.4(5)
S1	C1	S2a		120.0(4)
S2	C1a	C1		119.4(5)
C3	C2	C4	1.355(10)	119.9(6)
C3	C2	S3		123.3(5)
C4	C2	S3	1.432(10)	116.8(5)
C5	C3	S4	1.445(10)	117.2(5)
C5	C3	C2		119.5(6)
S4	C3	C2		123.2(5)
N1	C4	C2		177.9(8)
N2	C5	C3		178.2(8)
C11	N3	C11a	1.521(5)	107.5(4)
C11	N3	C21		110.4(2)
C11a	N3	C21	1.521(5)	111.0(2)
C11a	N3	C21a		110.4(2)
C21	N3	C21a	1.525(5)	106.7(4)
C21a	N3	C11	1.525(5)	111.0(2)
C12	C11	N3	1.520(6)	115.8(3)
C13	C12	C11	1.502(7)	112.4(4)
C14	C13	C12	1.518(7)	111.3(4)
C22	C21	N3	1.509(6)	116.4(4)
C23	C22	C21	1.484(7)	111.3(4)
C24	C23	C22	1.487(8)	116.6(5)

Appendix Table B-7: Crystallographic data for $(Bu_4N)_2\{tto[Cu(dsit)]_2\}$(**107**).

A. Crystal data (298 K)	**107**
a, Å	9.903(1)
b, Å	15.589(1)
c, Å	18.218(1)
α, deg.	90
β, deg.	90.40(1)
γ, deg.	90
V, Å^3	2812.4(3)
d_{calc}, g cm^{-3}(298 K)	1.588
Empirical formula	$(C_8S_{10}Se_4Cu_2)(NC_{16}H_{36})_2$
Formula wt, g	1344.52
Crystal system	Monoclinic
Space group	P 2_1/c
Z	2
F(000), electrons	1360
Crystal size (mm^3)	0.46 x 0.09 x 0.08
B. Data collection (298 K)	
Radiation, λ (Å)	Cu-K$_\alpha$, 1.54178
Mode	ω-scan
Scan range	Symmetrically over 1.2° about $K_{\alpha 1,2}$ maximum
Background	offset 1.0 and -1.0 in ω from $K_{\alpha 1,2}$ maximum
Scan rate, deg. min.$^{-1}$	3 – 6
2θ range, deg.	3 – 110
Range of *h k l*	$0 \leq h \leq 9$ $0 \leq k \leq 15$ $-18 \leq l \leq 18$
Total reflections measured	3256
Unique reflections	2888
Absorption coeff. μ (Mo-K$_\alpha$), mm^{-1}	7.58
Min. & Max. Transmission	0.272, 0.591
C. Structure refinement	
S, Goodness-of-fit	1.51
Reflections used, I > 2σ(I)	2315
No. of variables	262
R, wR* (%)	3.59, 4.30
$R_{int.}$ (%)	1.29
Max. shift/esd	0.001

min. peak in diff. four. map (e $Å^{-3}$)	-0.53
max. peak in diff. four. map (e $Å^{-3}$)	0.42

* Relevant expressions are as follows, where in the footnote F_o and F_c represent, respectively, the observed and calculated structure-factor amplitudes.

Function minimized was $w(|F_o| - |F_c|)^2$, wherew= $1/[\sigma^2(F)+0.0004F^2]$

$R = \sum(||F_o| - |F_c||) / \sum|F_o|$

$wR = [\sum w(|F_o| - |F_c|)^2 / \sum |F_o|^2]^{1/2}$

$S = [\sum w(|F_o| - |F_c|)^2 / (m-n)]^{1/2}$

Appendix Table B-8: Fractional Coordinates and Equivalent Isotropic[a] Thermal Parameters ($Å^2$) for the Non-H Atoms of $(Bu_4N)_2\{tto[Cu(dsit)]_2\}$(**107**).

atom	x	y	z	U(eq)
Cu	0.89709(8)	-0.50268(5)	0.84132(4)	0.0505(3)
Se1	1.00266(7)	-0.50108(5)	0.72601(3)	0.0638(3)
Se2	0.67818(7)	-0.47784(4)	0.79585(3)	0.0577(3)
S1	1.1009(2)	-0.48867(10)	0.89663(8)	0.0587(6)
S2	0.8080(2)	-0.53131(12)	0.95284(8)	0.0648(6)
S3	0.8635(2)	-0.46028(11)	0.57449(8)	0.0652(6)
S4	0.5966(2)	-0.44394(11)	0.63227(9)	0.0657(6)
S5	0.6374(2)	-0.42252(12)	0.47103(9)	0.0819(8)
C1	1.0693(6)	-0.4908(3)	0.9871(3)	0.044(2)
C1a	0.9307(6)	-0.5092(3)	1.0129(3)	0.044(2)
C2	0.8486(6)	-0.4736(3)	0.6696(3)	0.047(2)
C3	0.7236(6)	-0.4649(3)	0.6960(3)	0.048(2)
C4	0.6951(6)	-0.4409(4)	0.5546(3)	0.058(2)
N	0.3368(5)	-0.2545(3)	0.8196(2)	0.047(2)
C11	0.2289(6)	-0.2033(3)	0.8583(3)	0.053(2)
C12	0.1073(6)	-0.2560(4)	0.8832(4)	0.072(3)
C13	-0.0002(7)	-0.2039(4)	0.9195(4)	0.075(3)
C14	-0.1123(7)	-0.2603(5)	0.9488(4)	0.098(4)
C21	0.3898(6)	-0.3262(3)	0.8682(3)	0.051(2)
C22	0.4434(7)	-0.2998(4)	0.9429(3)	0.065(3)
C23	0.5200(6)	-0.3726(4)	0.9769(3)	0.068(3)
C24	0.5672(7)	-0.3562(5)	1.0540(3)	0.094(3)
C31	0.2810(6)	-0.2975(3)	0.7505(3)	0.052(2)
C32	0.2276(7)	-0.2371(4)	0.6918(3)	0.067(3)
C33	0.1581(7)	-0.2863(5)	0.6302(3)	0.076(3)
C34	0.2433(8)	-0.3512(5)	0.5930(4)	0.102(4)
C41	0.4503(6)	-0.1918(3)	0.8009(3)	0.054(2)
C42	0.5699(6)	-0.2318(4)	0.7624(3)	0.063(2)
C43	0.6839(6)	-0.1692(4)	0.7522(4)	0.071(3)
C44	0.8035(7)	-0.2129(5)	0.7143(4)	0.095(4)

[a]For anisotropic atoms, the U value is U_{eq}, calculated as $U_{eq} = 1/3\ \Sigma_i\Sigma_j\ U_{ij}\ a_i^*\ a_j^*\ A_{ij}$ where A_{ij} is the dot product of the i^{th} and j^{th} direct space unit cell vectors.

Appendix Table B-9: Bond Lengths (Å) and Angles (°) for the non-H atoms of $(Bu_4N)_2\{tto[Cu(dsit)]_2\}$(**107**).

1	2	3	1-2	1-2-3
Se1	Cu	Se2	2.3531(10)	95.63(4)
Se1	Cu	S1		89.77(5)
Se2	Cu	S1	2.3475(10)	163.94(6)
Se2	Cu	S2		89.12(5)
S1	Cu	S2	2.260(2)	88.35(6)
S2	Cu	Se1	2.265(2)	168.84(6)
C2	Se1	Cu	1.884(6)	97.3(2)
C3	Se2	Cu	1.888(6)	97.6(2)
C1	S1	Cu	1.679(6)	105.3(2)
C1a	S2	Cu	1.666(6)	105.2(2)
C2	S3	C4	1.751(6)	98.0(3)
C4	S3		1.730(6)	
C3	S4	C4	1.736(6)	98.2(3)
C4	S4		1.725(6)	
C4	S5		1.648(6)	
C1a	C1	S1	1.483(8)	119.7(4)
S2	C1a	C1		120.2(4)
C3	C2	Se1	1.338(8)	125.1(4)
C3	C2	S3		115.4(4)
Se1	C2	S3		119.6(3)
Se2	C3	S4		119.2(3)
Se2	C3	C2		124.3(4)
S4	C3	C2		116.5(4)
S3	C4	S4		111.9(3)
S3	C4	S5		123.5(4)
S4	C4	S5		124.6(4)
C11	N	C21	1.512(7)	111.1(4)
C11	N	C31		111.3(4)
C21	N	C31	1.518(7)	106.2(4)
C21	N	C41		110.4(4)
C31	N	C41	1.526(7)	111.1(4)
C41	N	C11	1.529(7)	106.8(4)
C12	C11	N	1.529(8)	114.6(5)
C13	C12	C11	1.496(9)	113.8(5)
C14	C13	C12	1.516(10)	111.4(5)
C22	C21	N	1.514(8)	116.2(4)
C23	C22	C21	1.498(9)	109.8(5)
C24	C23	C22	1.499(9)	114.4(6)
C32	C31	N	1.517(8)	115.6(4)
C33	C32	C31	1.520(9)	111.2(5)
C34	C33	C32	1.484(10)	115.2(6)
C42	C41	N	1.514(9)	114.8(4)
C43	C42	C41	1.505(9)	112.4(5)
C44	C43	C42	1.535(10)	110.5(5)

Appendix Table C-1: Crystallographic data for $(Bu_4N)_2[Cu(dmt)]_4$ (**126**).

A. Crystal data (298 K)	**126**
a, Å	13.228(2)
b, Å	19.584(3)
c, Å	26.007(4)
β, deg.	95.06(1)
V, Å^3	6711(2)
d_{calc}, g cm^{-3}(298 K)	1.509
Empirical formula	$\{C_{12}S_{20}Cu_4\}^{2-}\{(C_{16}H_{36}N)^{1+}\}_2$
Formula wt, g	1524.40
Crystal system	Monoclinic
Space group	P $2_1/c$
Z	4
F(000), electrons	3144
Crystal size (mm^3)	0.42 x 0.25 x 0.13
B. Data collection (298 K)	
Radiation, λ (Å)	Mo-K_α, 0.71073
Mode	ω-scan
Scan range	Symmetrically over 1.2° about $K_{\alpha 1,2}$ maximum
Background	offset 1.0 and -1.0 in ω from $K_{\alpha 1,2}$ maximum
Scan rate, deg. min.$^{-1}$	4 – 8
2θ range, deg.	3 – 47
Range of *h k l*	$0 \leq h \leq 14$ $0 \leq k \leq 22$ $-29 \leq l \leq 29$
Total reflections measured	10781
Unique reflections	9930
Absorption coeff. μ (Mo-K_α), mm^{-1}	1.90
Min. & Max. Transmission	0.635, 0.786
C. Structure refinement	
S, Goodness-of-fit	1.27
Reflections used, I > 2σ(I)	4175
No. of variables	631
R, wR* (%)	5.58, 5.00
$R_{int.}$ (%)	6.61
Max. shift/esd	0.001

min. peak in diff. four. map (e $Å^{-3}$)	-0.42
max. peak in diff. four. map (e $Å^{-3}$)	0.53

* Relevant expressions are as follows, where in the footnote F_o and F_c represent, respectively, the observed and calculated structure-factor amplitudes.

Function minimized was $w(|F_o| - |F_c|)^2$, wherew= $1/[\sigma^2(F)+0.0004F^2]$

$R = \sum(||F_o| - |F_c||) / \sum|F_o|$

$wR = [\sum w(|F_o| - |F_c|)^2 / \sum |F_o|^2]^{1/2}$

$S = [\sum w(|F_o| - |F_c|)^2 / (m-n)]^{1/2}$

Appendix Table C-2: Fractional Coordinates and Equivalent Isotropic[a] Thermal Parameters ($Å^2$) for the Non-H Atoms of $(Bu_4N)_2[Cu(dmt)]_4$ (**126**).

Atom	x	y	z	U
Cu1	0.12181(10)	-0.07914(7)	0.15460(5)	0.0605(6)
Cu2	0.04880(10)	-0.05878(8)	0.32191(5)	0.0667(6)
Cu3	0.31438(11)	0.09133(8)	0.35298(5)	0.0732(7)
Cu4	0.36513(11)	0.08063(7)	0.18416(5)	0.0664(6)
S1	0.0491(2)	-0.0817(2)	0.23324(11)	0.0670(13)
S2	-0.0336(2)	-0.0558(2)	0.10900(11)	0.0744(14)
S3	-0.2267(2)	-0.0148(2)	0.14553(11)	0.0654(13)
S4	-0.2608(2)	-0.0080(2)	0.22149(11)	0.0589(12)
S5	-0.1208(2)	-0.0288(2)	0.31270(12)	0.0717(14)
S6	0.1827(2)	0.0114(2)	0.35597(12)	0.0807(15)
S7	0.0856(3)	-0.1407(2)	0.38596(12)	0.0746(14)
S8	0.2523(3)	-0.1504(2)	0.46585(13)	0.096(2)
S9	0.3728(3)	-0.0837(2)	0.47910(13)	0.104(2)
S10	0.4079(3)	0.0394(2)	0.42188(13)	0.095(2)
S11	0.3674(2)	0.1141(2)	0.27089(11)	0.0687(14)
S12	0.2934(3)	0.2086(2)	0.36679(14)	0.106(2)
S13	0.2278(3)	0.3109(2)	0.2887(2)	0.111(2)
S14	0.2416(3)	0.3044(2)	0.2106(2)	0.105(2)
S15	0.3243(3)	0.1904(2)	0.15631(13)	0.090(2)
S16	0.2609(2)	-0.0076(2)	0.15044(13)	0.0698(13)
S17	0.5083(2)	0.0265(2)	0.15729(12)	0.0714(14)
S18	0.5381(2)	-0.1152(2)	0.12803(14)	0.083(2)
S19	0.4274(3)	-0.1886(2)	0.11510(14)	0.084(2)
S20	0.2094(2)	-0.1722(2)	0.12409(12)	0.0667(13)
C1	-0.0717(8)	-0.0494(5)	0.2121(4)	0.046(4)
C2	-0.1032(8)	-0.0418(5)	0.1598(4)	0.054(5)
C3	-0.1404(8)	-0.0304(5)	0.2472(4)	0.051(4)
C4	0.2375(9)	-0.0434(6)	0.4042(4)	0.054(5)
C5	0.1906(9)	-0.1052(6)	0.4159(4)	0.060(5)
C6	0.3298(9)	-0.0268(6)	0.4314(4)	0.065(5)
C7	0.3146(8)	0.1951(6)	0.2626(5)	0.057(5)
C8	0.2838(9)	0.2332(6)	0.3037(5)	0.072(6)
C9	0.2973(8)	0.2241(6)	0.2138(5)	0.070(6)
C10	0.3514(8)	-0.0681(6)	0.1382(3)	0.047(4)
C11	0.4568(8)	-0.0507(5)	0.1409(4)	0.054(5)
C12	0.3267(8)	-0.1364(6)	0.1267(4)	0.054(5)
N1	0.1258(9)	0.2445(7)	0.0045(4)	0.085(5)
C13	0.0750(12)	0.2845(9)	-0.0402(6)	0.114(9)
C14	0.0172(14)	0.3448(12)	-0.0262(6)	0.167(12)
C15	-0.032(2)	0.3783(12)	-0.0749(12)	0.27(2)
C16	-0.071(2)	0.4433(13)	-0.0592(7)	0.32(2)
C17	0.0517(11)	0.2140(7)	0.0380(5)	0.091(7)
C18	-0.0240(12)	0.1646(8)	0.0116(6)	0.122(9)
C19	-0.0944(13)	0.1378(9)	0.0475(7)	0.149(11)
C20	-0.1724(14)	0.0872(10)	0.0195(7)	0.22(2)
C21	0.1856(11)	0.1903(8)	-0.0201(5)	0.097(7)
C22	0.2441(11)	0.1411(8)	0.0158(5)	0.106(8)

C23	0.3028(12)	0.0940(9)	-0.0153(6)	0.129(9)
C24	0.3617(12)	0.0430(8)	0.0140(6)	0.144(10)
C25	0.1944(11)	0.2901(7)	0.0399(5)	0.091(7)
C26	0.2793(12)	0.3250(9)	0.0154(6)	0.131(9)
C27	0.338(2)	0.3740(14)	0.0526(9)	0.22(2)
C28	0.301(2)	0.4190(14)	0.0736(10)	0.35(3)
N2	0.2944(9)	0.7287(6)	0.2855(4)	0.079(5)
C29	0.358(3)	0.7987(10)	0.2764(8)	0.23(2)
C30	0.338(2)	0.848(2)	0.2943(10)	0.30(3)
C31	0.407(2)	0.9164(9)	0.2877(7)	0.20(2)
C32	0.503(2)	0.9167(14)	0.2949(10)	0.37(3)
C33	0.3378(13)	0.6784(10)	0.2521(9)	0.172(13)
C34	0.334(2)	0.6687(14)	0.2042(7)	0.22(2)
C35	0.3570(14)	0.6170(9)	0.1701(8)	0.134(10)
C36	0.346(2)	0.6202(10)	0.1209(7)	0.218(15)
C37	0.182(2)	0.7294(10)	0.2750(8)	0.175(13)
C38	0.114(2)	0.6787(13)	0.2726(10)	0.28(2)
C39	0.005(2)	0.6852(15)	0.2740(15)	0.46(4)
C40	-0.044(2)	0.6306(13)	0.2594(13)	0.53(4)
C41	0.322(2)	0.7102(10)	0.3396(8)	0.26(2)
C42	0.379(2)	0.7160(10)	0.3762(8)	0.178(13)
C43	0.407(2)	0.6872(12)	0.4250(7)	0.213(14)
C44	0.450(2)	0.6985(13)	0.4654(7)	0.36(3)

[a]For anisotropic atoms, the U value is U_{eq}, calculated as $U_{eq} = 1/3 \sum_i \sum_j U_{ij} a_i^* a_j^* A_{ij}$ where A_{ij} is the dot product of the i^{th} and j^{th} direct space unit cell vectors.

Appendix Table C-3: Bond Lengths (Å) and Angles (°) for the non-H atoms of $(Bu_4N)_2[Cu(dmt)]_4$ (**126**).

1	2	3	1-2	1-2-3
S1	Cu1	S2	2.336(3)	92.10(11)
S1	Cu1	S16		116.28(12)
S2	Cu1	S16	2.327(3)	121.72(13)
S2	Cu1	S20		115.01(12)
S16	Cu1	S20	2.323(3)	92.08(12)
S20	Cu1	S1	2.336(3)	122.38(13)
S1	Cu2	S5	2.350(3)	91.85(11)
S1	Cu2	S6		114.52(12)
S5	Cu2	S6	2.311(3)	125.61(13)
S5	Cu2	S7		112.85(13)
S6	Cu2	S7	2.352(3)	91.73(12)
S7	Cu2	S1	2.333(3)	123.45(13)
S6	Cu3	S10	2.348(4)	91.65(13)
S6	Cu3	S11		116.02(12)
S10	Cu3	S11	2.321(4)	127.12(14)
S10	Cu3	S12		111.93(14)
S11	Cu3	S12	2.348(3)	90.14(13)
S12	Cu3	S6	2.345(4)	123.32(15)
S11	Cu4	S15	2.346(3)	91.41(12)
S11	Cu4	S16		121.69(13)
S15	Cu4	S16	2.316(4)	117.11(13)
S15	Cu4	S17		120.08(14)
S16	Cu4	S17	2.332(3)	91.12(12)
S17	Cu4	S11	2.330(3)	118.25(12)
C1	S1	Cu1	1.761(10)	98.7(4)
C1	S1	Cu2		99.1(4)
Cu1	S1	Cu2		153.05(14)
C2	S2	Cu1	1.697(11)	98.7(4)
S4	S3	C2	2.069(4)	95.6(4)
C2	S3		1.726(10)	
C3	S4	S3	1.728(11)	94.7(4)
C3	S5	Cu2	1.702(11)	99.2(4)
C4	S6	Cu2	1.758(11)	99.3(4)
C4	S6	Cu3		99.8(4)
Cu2	S6	Cu3		155.9(2)
C5	S7	Cu2	1.681(12)	99.1(4)
S9	S8	C5	2.066(5)	96.2(4)
C5	S8		1.718(11)	
C6	S9	S8	1.726(11)	95.0(4)
C6	S10	Cu3	1.689(12)	99.1(4)
C7	S11	Cu3	1.740(12)	97.9(4)
C7	S11	Cu4		99.5(4)
Cu3	S11	Cu4		147.3(2)
C8	S12	Cu3	1.703(13)	97.4(4)
S14	S13	C8	2.057(6)	95.5(5)
C8	S13		1.722(12)	
C9	S14	S13	1.735(12)	94.8(5)

C9	S15	Cu4	1.702(14)	98.4(4)
C10	S16	Cu1	1.734(11)	99.1(4)
C10	S16	Cu4		100.4(4)
Cu1	S16	Cu4		150.9(2)
C11	S17	Cu4	1.697(11)	99.3(4)
S19	S18	C11	2.058(5)	95.6(4)
C11	S18		1.711(11)	
C12	S19	S18	1.726(12)	96.1(4)
C12	S20	Cu1	1.699(11)	98.3(4)
C2	C1	C3	1.396(15)	117.0(9)
C2	C1	S1		121.8(8)
C3	C1	S1	1.39(2)	121.2(8)
S2	C2	S3		116.8(6)
S2	C2	C1		127.3(8)
S3	C2	C1		115.9(8)
S4	C3	S5		115.8(6)
S4	C3	C1		116.5(8)
S5	C3	C1		127.6(8)
C5	C4	C6	1.41(2)	118.3(10)
C5	C4	S6		121.2(8)
C6	C4	S6	1.39(2)	120.5(9)
S7	C5	S8		117.1(7)
S7	C5	C4		128.2(8)
S8	C5	C4		114.7(8)
S9	C6	S10		115.7(6)
S9	C6	C4		115.6(9)
S10	C6	C4		128.6(9)
C8	C7	C9	1.39(2)	116.5(11)
C8	C7	S11		122.3(9)
C9	C7	S11	1.39(2)	121.2(10)
S12	C8	S13		117.5(7)
S12	C8	C7		125.9(9)
S13	C8	C7		116.5(9)
S14	C9	S15		115.5(8)
S14	C9	C7		116.7(10)
S15	C9	C7		127.8(9)
C11	C10	C12	1.432(15)	116.4(10)
C11	C10	S16		120.9(8)
C12	C10	S16	1.40(2)	122.7(8)
S17	C11	S18		117.6(6)
S17	C11	C10		126.3(8)
S18	C11	C10		116.1(8)
S19	C12	S20		117.7(7)
S19	C12	C10		115.7(8)
S20	C12	C10		126.6(9)
C13	N1	C17	1.51(2)	112.8(11)
C13	N1	C21		104.7(11)
C17	N1	C21	1.49(2)	111.3(11)
C17	N1	C25		105.7(10)
C21	N1	C25	1.50(2)	111.3(11)
C25	N1	C13	1.52(2)	111.3(11)
C14	C13	N1	1.47(3)	115.5(13)
C15	C14	C13	1.52(3)	109.(2)
C16	C15	C14	1.45(4)	106.(2)

C18	C17	N1	1.51(2)	115.7(11)
C19	C18	C17	1.47(2)	111.7(13)
C20	C19	C18	1.56(3)	110.9(14)
C22	C21	N1	1.51(2)	116.7(11)
C23	C22	C21	1.49(2)	108.9(12)
C24	C23	C22	1.44(2)	115.1(13)
C26	C25	N1	1.50(2)	116.0(11)
C27	C26	C25	1.52(3)	112.0(15)
C28	C27	C26	1.17(4)	124.(3)
C29	N2	C33	1.64(3)	104.1(14)
C29	N2	C37		119.(2)
C33	N2	C37	1.46(2)	109.6(13)
C33	N2	C41		108.8(14)
C37	N2	C41	1.49(2)	109.9(15)
C41	N2	C29	1.47(2)	104.8(13)
C30	C29	N2	1.12(4)	122.(3)
C31	C30	C29	1.63(4)	120.(3)
C32	C31	C30	1.26(3)	123.(2)
C34	C33	N2	1.26(3)	135.(2)
C35	C34	C33	1.40(3)	138.(2)
C36	C35	C34	1.28(3)	126.(2)
C38	C37	N2	1.34(3)	131.(2)
C39	C38	C37	1.45(4)	127.(2)
C40	C39	C38	1.29(4)	113.(3)
C42	C41	N2	1.16(3)	148.(2)
C43	C42	C41	1.41(3)	143.(2)
C44	C43	C42	1.17(3)	143.(2)

Appendix Table D-1: Crystallographic data for $(Bu_4N)_2\{tto[Ni(dmit)]_2\}$ (**131**).

Empirical formula	C40 H72 N2 Ni2 S14
Formula weight	1147.26
Temperature	173(2) K
Wavelength	0.71073 Å
Crystal system	Orthorhombic
Space group	P2(1)2(1)2(1)
Unit cell dimensions	a = 9.8188(3)Å, $\alpha = 90°$
	b = 16.1038(4)Å, $\beta = 90°$
	c = 34.1910(9)Å, $\gamma = 90°$
Volume, Z	5406.3(3) $Å^3$, 4
Density (calculated)	1.410 Mg/m^3
Absorption coefficient	1.268 mm^{-1}
F(000)	2424
Crystal size	0.38 x 0.27 x 0.03 mm^3
Theta range for data collection	1.40 to 22.50°
Limiting indices	-8<=h<=13, -22<=k<=17, -47<=l<=29
Reflections collected	17498
Independent reflections	7067 [R(int) = 0.0483]
Refinement method	Full-matrix least-squares on F^2
Data / restraints / parameters	7015 / 119 / 714
Goodness-of-fit on F^2	1.471
Final R indices [I>2sigma(I)]	R1 = 0.0496, wR2 = 0.0891
R indices (all data)	R1 = 0.0645, wR2 = 0.0963
Absolute structure parameter	0.45(2)
Largest diff. peak and hole	0.483 and -0.271 e.$Å^{-3}$

Appendix Table D-2: Fractional Coordinates and Equivalent Isotropic[a] Thermal Parameters ($Å^2$) for the Non-H Atoms of $(Bu_4N)_2\{tto[Ni(dmit)]_2\}$ (**131**).

atom	x	y	z	U(eq)
Ni	4796(1)	5045(1)	-734(1)	36(1)
Ni'	5194(1)	4999(1)	1013(1)	29(1)
S(1)	3607(2)	4503(1)	-274(1)	44(1)
S(1')	3750(2)	4518(1)	594(1)	35(1)
S(2)	6224(2)	5556(1)	-317(1)	34(1)
S(2')	6454(2)	5497(1)	551(1)	32(1)
S(3)	3329(2)	4541(1)	-1142(1)	53(1)
S(3')	3873(2)	4519(1)	1467(1)	32(1)
S(4)	6047(2)	5576(1)	-1190(1)	35(1)
S(4')	6693(2)	5449(1)	1426(1)	37(1)
S(5)	3168(2)	4671(1)	-2032(1)	57(1)
S(5')	4266(2)	5617(1)	-2075(1)	45(1)
S(6')	6887(2)	5246(1)	2309(1)	41(1)
S(7)	4232(2)	5190(2)	-2812(1)	69(1)
S(7')	5797(2)	4758(1)	3091(1)	57(1)
C(1)	4402(7)	4786(4)	148(2)	30(2)
C(2')	4814(7)	4732(3)	1885(2)	29(2)
C(3)	5132(7)	5325(4)	-1607(2)	33(2)
C(3')	6033(6)	5111(4)	1869(2)	35(2)
C(4)	4337(7)	5167(5)	-2333(2)	45(2)
C(4')	5686(7)	4815(4)	2616(2)	40(2)
N(1)	1144(5)	6745(3)	1195(2)	31(1)
C(11)	-71(8)	7226(4)	1027(2)	37(2)
C(12)	-1214(8)	7459(5)	1299(2)	45(2)
C(13)	-2392(9)	7837(6)	1076(3)	50(2)
C(14)	-3515(10)	8142(7)	1340(3)	67(3)
C(21)	698(8)	5883(4)	1314(2)	34(2)
C(22)	195(8)	5307(4)	1002(2)	38(2)
C(23)	-29(8)	4448(4)	1159(2)	41(2)
C(24)	-573(10)	3862(5)	856(3)	62(2)
C(31)	2246(8)	6699(5)	888(2)	38(2)
C(32)	2998(8)	7497(4)	792(2)	44(2)
C(33)	4012(9)	7382(5)	472(3)	56(2)
C(34)	3440(14)	7225(8)	74(3)	76(3)
C(41)	1653(8)	7191(4)	1558(2)	37(2)
C(42)	2908(8)	6847(5)	1751(2)	40(2)
C(43)	3394(10)	7072(6)	2289(3)	59(2)
N(2)	3617(6)	1749(3)	1060(2)	43(2)
C(51)	2634(7)	1663(4)	1399(2)	51(2)
C(52)	2077(13)	2511(6)	1520(4)	53(4)
C(53)	938(14)	2412(9)	1821(3)	62(4)
C(54)	1506(20)	2042(12)	2199(4)	99(7)
C(52')	2223(26)	2314(13)	1702(6)	65(6)
C(53')	1258(32)	1969(16)	2013(7)	71(6)
C(54')	1009(32)	2618(18)	2332(7)	104(9)
C(61)	4885(8)	2238(4)	1170(2)	59(2)

C(62)	5599(8)	2015(7)	1536(3)	101(4)
C(63)	6732(16)	2651(11)	1514(5)	84(6)
C(64)	7377(19)	2912(12)	1897(5)	81(6)
C(63')	7051(14)	2207(9)	1655(8)	76(6)
C(64')	6991(22)	3145(10)	1684(8)	73(7)
C(71)	2984(9)	2217(4)	722(3)	60(2)
C(72)	1651(8)	1869(5)	568(2)	57(2)
C(73)	1247(10)	2291(6)	181(3)	71(3)
C(74)	2067(9)	2016(5)	-165(2)	68(3)
C(81)	4002(7)	868(4)	944(2)	38(2)
C(82)	4657(7)	744(4)	547(2)	40(2)
C(83)	5020(7)	-186(4)	498(2)	41(2)
C(84)	5232(8)	-402(4)	75(2)	57(2)

Appendix Table D-3: Bond Lengths (Å) and Angles (°) for the non-H atoms of $(Bu_4N)_2\{tto[Ni(dmit)]_2\}$ (**131**).

Ni-S(1)	2.145(2)	N(1)-C(11)	1.533(8)
Ni-S(4)	2.161(2)	C(11)-C(12)	1.505(10)
Ni-S(3)	2.162(2)	C(12)-C(13)	1.514(11)
Ni-S(2)	2.163(2)	C(13)-C(14)	1.508(12)
Ni'-S(1')	2.159(2)	C(21)-C(22)	1.497(9)
Ni'-S(2')	2.163(2)	C(22)-C(23)	1.499(9)
Ni'-S(3')	2.164(2)	C(23)-C(24)	1.498(10)
Ni'-S(4')	2.165(2)	C(31)-C(32)	1.518(10)
S(1)-C(1)	1.704(6)	C(32)-C(33)	1.493(11)
S(1')-C(1)	1.710(6)	C(33)-C(34)	1.492(14)
S(2)-C(1')	1.711(6)	C(41)-C(42)	1.503(9)
S(2')-C(1')	1.699(6)	C(42)-C(43)	1.497(11)
S(3)-C(2)	1.722(7)	C(43)-C(44)	1.501(11)
S(3')-C(2')	1.735(6)	N(2)-C(71)	1.513(10)
S(4)-C(3)	1.733(6)	N(2)-C(51)	1.514(9)
S(4')-C(3')	1.735(6)	N(2)-C(61)	1.519(9)
S(5)-C(4)	1.735(7)	N(2)-C(81)	1.521(8)
S(5)-C(2)	1.746(6)	C(51)-C(52')	1.529(7)
S(5')-C(2')	1.756(6)	C(51)-C(52)	1.529(7)
S(5')-C(4')	1.765(7)	C(52)-C(53)	1.529(7)
S(6)-C(4)	1.733(7)	C(53)-C(54)	1.529(7)
S(6)-C(3)	1.746(6)	C(52')-C(53')	1.529(7)
S(6')-C(4')	1.724(7)	C(53')-C(54')	1.529(7)
S(6')-C(3')	1.736(6)	C(61)-C(62)	1.480(12)
S(7)-C(4)	1.641(7)	C(62)-C(63')	1.515(10)
S(7')-C(4')	1.631(7)	C(62)-C(63)	1.515(10)
C(1)-C(1')	1.416(7)	C(63)-C(64)	1.515(10)
C(2)-C(3)	1.365(9)	C(63')-C(64')	1.515(10)
C(2')-C(3')	1.344(8)	C(71)-C(72)	1.517(11)
N(1)-C(31)	1.509(9)	C(72)-C(73)	1.541(11)
N(1)-C(21)	1.510(8)	C(73)-C(74)	1.497(11)
N(1)-C(41)	1.521(8)	C(81)-C(82)	1.513(9)
C(82)-C(83)	1.548(8)	C(83)-C(84)	1.502(8)
S(1)-Ni-S(4)	178.35(8)	S(6)-C(4)-S(5)	112.8(4)
S(1)-Ni-S(3)	87.55(8)	S(7')-C(4')-S(6')	125.6(4)
S(4)-Ni-S(3)	93.58(7)	S(7')-C(4')-S(5')	122.7(4)
S(1)-Ni-S(2)	91.35(7)	S(6')-C(4')-S(5')	111.7(4)
S(4)-Ni-S(2)	87.54(7)	C(31)-N(1)-C(21)	110.4(5)
S(3)-Ni-S(2)	178.58(8)	C(31)-N(1)-C(41)	110.8(5)
S(1')-Ni'-S(2')	91.35(7)	C(21)-N(1)-C(41)	108.1(5)
S(1')-Ni'-S(3')	87.37(7)	C(31)-N(1)-C(11)	108.8(5)
S(2')-Ni'-S(3')	178.08(7)	C(21)-N(1)-C(11)	109.8(5)
S(1')-Ni'-S(4')	177.96(8)	C(41)-N(1)-C(11)	108.8(5)
S(2')-Ni'-S(4')	87.90(7)	C(12)-C(11)-N(1)	118.4(6)
S(3')-Ni'-S(4')	93.43(7)	C(11)-C(12)-C(13)	111.0(7)
C(1)-S(1)-Ni	105.3(2)	C(14)-C(13)-C(12)	112.7(8)
C(1)-S(1')-Ni'	104.8(2)	C(22)-C(21)-N(1)	118.4(6)
C(1')-S(2)-Ni	104.9(2)	C(21)-C(22)-C(23)	111.5(6)

C(1')-S(2')-Ni'	104.9(2)	C(24)-C(23)-C(22)	112.7(7)
C(2)-S(3)-Ni	102.2(2)	N(1)-C(31)-C(32)	117.2(6)
C(2')-S(3')-Ni'	101.5(2)	C(33)-C(32)-C(31)	112.2(7)
C(3)-S(4)-Ni	101.9(2)	C(34)-C(33)-C(32)	116.1(9)
C(3')-S(4')-Ni'	102.1(2)	C(42)-C(41)-N(1)	117.0(6)
C(4)-S(5)-C(2)	98.0(3)	C(42)-C(43)-C(44)	114.1(7)
C(2')-S(5')-C(4')	97.5(3)	C(71)-N(2)-C(51)	111.6(6)
C(4)-S(6)-C(3)	97.4(3)	C(71)-N(2)-C(61)	105.5(5)
C(4')-S(6')-C(3')	98.4(3)	C(51)-N(2)-C(61)	112.4(6)
C(1')-C(1)-S(1)	119.6(4)	C(71)-N(2)-C(81)	111.5(6)
C(1')-C(1)-S(1')	119.3(4)	C(51)-N(2)-C(81)	105.8(5)
S(1)-C(1)-S(1')	121.2(4)	C(61)-N(2)-C(81)	110.1(5)
C(1)-C(1')-S(2')	119.6(4)	N(2)-C(51)-C(52')	128.6(11)
C(1)-C(1')-S(2)	118.8(4)	N(2)-C(51)-C(52)	110.6(7)
S(2')-C(1')-S(2)	121.6(4)	C(53)-C(52)-C(51)	110.5(9)
C(3)-C(2)-S(3)	121.2(5)	C(52)-C(53)-C(54)	110.1(12)
C(3)-C(2)-S(5)	115.2(5)	C(53')-C(52')-C(51)	113(2)
S(3)-C(2)-S(5)	123.6(4)	C(52')-C(53')-C(54')	110(2)
C(3')-C(2')-S(3')	122.1(5)	C(62)-C(61)-N(2)	118.1(7)
C(3')-C(2')-S(5')	115.5(5)	C(61)-C(62)-C(63')	128.6(12)
S(3')-C(2')-S(5')	122.4(4)	C(61)-C(62)-C(63)	98.1(10)
C(2)-C(3)-S(4)	121.0(5)	C(64)-C(63)-C(62)	116.8(14)
C(2)-C(3)-S(6)	116.6(5)	C(64')-C(63')-C(62)	100.6(12)
S(4)-C(3)-S(6)	122.4(4)	N(2)-C(71)-C(72)	115.9(6)
C(2')-C(3')-S(4')	120.6(5)	C(71)-C(72)-C(73)	111.0(7)
C(2')-C(3')-S(6')	116.9(5)	C(74)-C(73)-C(72)	114.3(7)
S(4')-C(3')-S(6')	122.5(4)	C(82)-C(81)-N(2)	117.6(5)
S(7)-C(4)-S(6)	123.1(4)	C(81)-C(82)-C(83)	108.8(5)
S(7)-C(4)-S(5)	124.1(4)	C(84)-C(83)-C(82)	111.1(5)

Appendix Table D-4: Crystallographic data for $(Et_4N)_2\{tto[Ni(dmit)]_2\}$ (**132**).

Empirical formula	C16 H24 N2 Ni2 S14
Formula weight	810.63
Temperature	173(2) K
Wavelength	0.71073 Å
Crystal system	Monoclinic
Space group	C2/m
Unit cell dimensions	a = 13.8043(4) Å , α = 90° b = 10.1081(1) Å, β = 115.239(1)° c = 12.0483(3) Å, γ = 90°
Volume, Z	1520.67(6) $Å^3$, 2
Density (calculated)	1.770 Mg/m^3
Absorption coefficient	2.213 mm^{-1}
F(000)	828
Crystal size	0.32 x 0.21 x 0.07 mm^3
Theta range for data collection	1.87 to 26.99°
Limiting indices	-16<=h<=11, -12<=k<=12, -10<=l<=15
Reflections collected	7557
Independent reflections	1563 [R(int) = 0.0698]
Absorption correction	Semi-empirical from psi-scans
Max. and min. transmission	0.9345 and 0.7285
Refinement method	Full-matrix least-squares on F^2
Data / restraints / parameters	1550 / 0 / 88
Goodness-of-fit on F^2	1.111
Final R indices [I>2sigma(I)]	R1 = 0.0338, wR2 = 0.0813
R indices (all data)	R1 = 0.0380, wR2 = 0.0891

Extinction coefficient	0.0017(4)
Largest diff. peak and hole	0.386 and -0.555 e.A^{-3}

Appendix Table D-5: Fractional Coordinates and Equivalent Isotropic[a] Thermal Parameters ($Å^2$) for the Non-H Atoms of $(Et_4N)_2\{tto[Ni(dmit)]_2\}$ (**132**).

atom	x	y	z	U(eq)
Ni	8217(1)	-5000	17459(1)	19(1)
S(1)	9108(1)	-6528(1)	18745(1)	24(1)
S(2)	7361(1)	-6559(1)	16181(1)	23(1)
S(3)	5443(1)	-6432(1)	13683(1)	22(1)
S(4)	3793(1)	-5000	11553(1)	35(1)
C(1)	10000	-5707(3)	20000	18(1)
C(2)	6431(1)	-5673(2)	14972(2)	18(1)
C(3)	4835(2)	-5000	12906(3)	21(1)
N	1898(2)	-5000	7838(2)	25(1)
C(4)	3006(3)	-5000	7918(4)	43(1)
C(5)	1098(4)	-5000	6526(4)	58(1)
C(6)	1744(2)	-3780(2)	8450(2)	33(1)

Appendix Table D-6: Bond Lengths (Å) and Angles (°) for the non-H atoms of $(Et_4N)_2\{tto[Ni(dmit)]_2\}$ (**132**).

Ni-S(1)#1	2.1616(5)	C(1)-C(1)#2	1.430(6)
Ni-S(1)	2.1617(5)	C(1)-S(1)#3	1.704(2)
Ni-S(2)#1	2.1674(5)	C(2)-C(2)#1	1.361(4)
Ni-S(2)	2.1675(5)	C(3)-S(3)#1	1.733(2)
S(1)-C(1)	1.704(2)	N-C(4)	1.492(4)
S(2)-C(2)	1.726(2)	N-C(5)	1.493(4)
S(3)-C(3)	1.733(2)	N-C(6)#1	1.497(3)
S(3)-C(2)	1.748(2)	N-C(6)	1.497(3)
S(4)-C(3)	1.651(3)		
S(1)#1-Ni-S(1)	91.19(3)	C(2)#1-C(2)-S(2)	121.25(7)
S(1)#1-Ni-S(2)#1	87.75(2)	C(2)#1-C(2)-S(3)	116.01(7)
S(1)-Ni-S(2)#1	178.52(2)	S(2)-C(2)-S(3)	122.74(12)
S(1)#1-Ni-S(2)	178.52(2)	S(4)-C(3)-S(3)#1	123.39(8)
S(1)-Ni-S(2)	87.75(2)	S(4)-C(3)-S(3)	123.39(8)
S(2)#1-Ni-S(2)	93.28(3)	S(3)#1-C(3)-S(3)	113.2(2)
C(1)-S(1)-Ni	105.27(9)	C(4)-N-C(5)	110.0(3)
C(2)-S(2)-Ni	101.92(7)	C(4)-N-C(6)#1	109.0(2)
C(3)-S(3)-C(2)	97.37(11)	C(5)-N-C(6)#1	109.0(2)
C(1)#2-C(1)-S(1)	119.13(9)	C(4)-N-C(6)	109.0(2)
C(1)#2-C(1)-S(1)#3	119.13(9)	C(5)-N-C(6)	109.0(2)
S(1)-C(1)-S(1)#3	121.7(2)	C(6)#1-N-C(6)	110.9(2)

Appendix Table D-7: Crystallographic data for $(Me_4N)_2\{tto[Ni(dmit)]_2\}$ (**133**).

Empirical formula	C16 H24 N2 Ni2 S14
Formula weight	810.63
Temperature	173(2) K
Wavelength	0.71073 Å
Crystal system	Monoclinic
Space group	C2/m
Unit cell dimensions	a = 13.8043(4) Å, $\alpha = 90^\circ$ b = 10.1081(1) Å, $\beta = 115.239(1)^\circ$ c = 12.0483(3) Å, $\gamma = 90^\circ$
Volume, Z	1520.67(6) $Å^3$, 2
Density (calculated)	1.770 Mg/m^3
Absorption coefficient	2.213 mm^{-1}
F(000)	828
Crystal size	0.32 x 0.21 x 0.07 mm
Theta range for data collection	1.87 to 26.99°
Limiting indices	-16<=h<=11, -12<=k<=12, -10<=l<=15
Reflections collected	7557
Independent reflections	1563 [R(int) = 0.0698]
Absorption correction	Semi-empirical from psi-scans
Max. and min. transmission	0.9345 and 0.7285
Refinement method	Full-matrix least-squares on F^2
Data / restraints / parameters	1550 / 0 / 88
Goodness-of-fit on F^2	1.111
Final R indices [I>2sigma(I)]	R1 = 0.0338, wR2 = 0.0813
R indices (all data)	R1 = 0.0380, wR2 = 0.0891

Extinction coefficient	0.0017(4)
Largest diff. peak and hole	0.386 and -0.555 e.A^{-3}

Appendix Table D-8: Fractional Coordinates and Equivalent Isotropic[a] Thermal Parameters ($Å^2$) for the Non-H Atoms of $(Me_4N)_2\{tto[Ni(dmit)]_2\}$ (**133**).

atom	x	y	z	U(eq)
Ni	8217(1)	-5000	17459(1)	19(1)
S(1)	9108(1)	-6528(1)	18745(1)	24(1)
S(2)	7361(1)	-6559(1)	16181(1)	23(1)
S(3)	5443(1)	-6432(1)	13683(1)	22(1)
S(4)	3793(1)	-5000	11553(1)	35(1)
C(1)	10000	-5707(3)	20000	18(1)
C(2)	6431(1)	-5673(2)	14972(2)	18(1)
C(3)	4835(2)	-5000	12906(3)	21(1)
N	1898(2)	-5000	7838(2)	25(1)
C(4)	3006(3)	-5000	7918(4)	43(1)
C(5)	1098(4)	-5000	6526(4)	58(1)
C(6)	1744(2)	-3780(2)	8450(2)	33(1)

Appendix Table D-9: Bond Lengths (Å) and Angles (°) for the non-H atoms of $(Me_4N)_2\{tto[Ni(dmit)]_2\}$ (**133**).

Ni-S(1)#1	2.1616(5)	C(1)-C(1)#2	1.430(6)
Ni-S(1)	2.1617(5)	C(1)-S(1)#3	1.704(2)
Ni-S(2)#1	2.1674(5)	C(2)-C(2)#1	1.361(4)
Ni-S(2)	2.1675(5)	C(3)-S(3)#1	1.733(2)
S(1)-C(1)	1.704(2)	N-C(4)	1.492(4)
S(2)-C(2)	1.726(2)	N-C(5)	1.493(4)
S(3)-C(3)	1.733(2)	N-C(6)#1	1.497(3)
S(3)-C(2)	1.748(2)	N-C(6)	1.497(3)
S(4)-C(3)	1.651(3)		
S(1)#1-Ni-S(1)	91.19(3)	C(2)#1-C(2)-S(2)	121.25(7)
S(1)#1-Ni-S(2)#1	87.75(2)	C(2)#1-C(2)-S(3)	116.01(7)
S(1)-Ni-S(2)#1	178.52(2)	S(2)-C(2)-S(3)	122.74(12)
S(1)#1-Ni-S(2)	178.52(2)	S(4)-C(3)-S(3)#1	123.39(8)
S(1)-Ni-S(2)	87.75(2)	S(4)-C(3)-S(3)	123.39(8)
S(2)#1-Ni-S(2)	93.28(3)	S(3)#1-C(3)-S(3)	113.2(2)
C(1)-S(1)-Ni	105.27(9)	C(4)-N-C(5)	110.0(3)
C(2)-S(2)-Ni	101.92(7)	C(4)-N-C(6)#1	109.0(2)
C(3)-S(3)-C(2)	97.37(11)	C(5)-N-C(6)#1	109.0(2)
C(1)#2-C(1)-S(1)	119.13(9)	C(4)-N-C(6)	109.0(2)
C(1)#2-C(1)-S(1)#3	119.13(9)	C(5)-N-C(6)	109.0(2)
S(1)-C(1)-S(1)#3	121.7(2)	C(6)#1-N-C(6)	110.9(2)

Symmetry transformations used to generate equivalent atoms:
#1 x,-y-1,z #2 -x+2,-y-1,-z+4 #3 -x+2,y,-z+4

Appendix Table D-10: Crystallographic data for $(Bu_4N)_2\{tto[Ni(dsit)]_2\}$ (**134**).

Empirical formula	C40 H72 N2 Ni2 S10 Se4
Formula weight	1334.86
Temperature	173(2) K
Wavelength	0.71073 A
Crystal system	Monoclinic
Space group	P2(1)/c
Unit cell dimensions	a = 9.8893(1) Å, $\alpha = 90^\circ$ b = 15.3544(1) Å, $\beta = 90.561(1)^\circ$ c = 17.8825(2) Å, $\gamma = 90^\circ$
Volume, Z	2715.23(4) A^3, 2
Density (calculated)	1.633 Mg/m^3
Absorption coefficient	3.789 mm^{-1}
F(000)	1356
Crystal size	0.48 x 0.16 x 0.07 mm^3
Theta range for data collection	1.75 to 27.50°
Limiting indices	-13<=h<=13, 0<=k<=21, 0<=l<=24
Reflections collected	17641
Independent reflections	6015 [R(int) = 0.0299]
Absorption correction	Semi-empirical from psi-scans
Max. and min. transmission	0.9382 and 0.5325
Refinement method	Full-matrix least-squares on F^2
Data / restraints / parameters	5943 / 0 / 263
Goodness-of-fit on F^2	1.105
Final R indices [I>2sigma(I)]	R1 = 0.0319, wR2 = 0.0703
R indices (all data)	R1 = 0.0441, wR2 = 0.0809

Extinction coefficient	0.00128(12)
Largest diff. peak and hole	0.495 and -0.579 e. A^{-3}

Appendix Table D-11: Fractional Coordinates and Equivalent Isotropic[a] Thermal Parameters (Å^2) for the Non-H Atoms of $(Bu_4N)_2\{tto[Ni(dsit)]_2\}$ (**134**).

atom	x	y	z	U(eq)
Ni	3933(1)	10060(1)	1553(1)	20(1)
Se(3)	1797(1)	9865(1)	1994(1)	23(1)
Se(4)	4951(1)	9950(1)	2700(1)	26(1)
S(1)	3029(1)	10211(1)	452(1)	26(1)
S(2)	5939(1)	10086(1)	1084(1)	24(1)
S(5)	880(1)	9492(1)	3653(1)	28(1)
S(6)	3588(1)	9546(1)	4267(1)	29(1)
S(7)	1286(1)	9192(1)	5293(1)	36(1)
C(1)	4321(3)	10030(2)	-149(2)	21(1)
C(2)	2177(3)	9693(2)	3022(2)	23(1)
C(3)	3434(3)	9719(2)	3305(2)	23(1)
C(4)	1882(3)	9392(2)	4454(2)	26(1)
N(1)	1717(2)	12600(1)	3194(1)	21(1)
C(11)	2235(3)	13035(2)	2490(2)	24(1)
C(12)	2713(3)	12419(2)	1879(2)	31(1)
C(13)	3433(3)	12904(2)	1253(2)	32(1)
C(14)	2593(4)	13614(2)	889(2)	42(1)
C(21)	2834(3)	12081(2)	3581(2)	26(1)
C(22)	4036(3)	12620(2)	3840(2)	34(1)
C(23)	5128(3)	12073(2)	4214(2)	33(1)
C(24)	6260(4)	12644(2)	4527(2)	48(1)
C(31)	1224(3)	13327(2)	3702(2)	22(1)
C(32)	756(3)	13045(2)	4474(2)	28(1)
C(33)	-190(3)	13727(2)	4788(2)	31(1)
C(34)	-600(4)	13545(3)	5587(2)	42(1)
C(41)	565(3)	11974(2)	3012(2)	24(1)
C(42)	-660(3)	12385(2)	2634(2)	31(1)
C(43)	-1827(3)	11748(2)	2545(2)	33(1)
C(44)	-3052(3)	12188(2)	2178(2)	41(1)

Appendix Table D-12: Bond Lengths (Å) and Angles (°) for the non-H atoms of $(Bu_4N)_2\{tto[Ni(dsit)]_2\}$ (**134**).

Ni-S(2)	2.1617(7)	N(1)-C(11)	1.518(3)
Ni-S(1)	2.1663(7)	N(1)-C(31)	1.522(3)
Ni-Se(3)	2.2821(4)	N(1)-C(41)	1.524(3)
Ni-Se(4)	2.2840(4)	N(1)-C(21)	1.524(3)
Se(3)-C(2)	1.890(3)	C(11)-C(12)	1.524(4)
Se(4)-C(3)	1.891(3)	C(12)-C(13)	1.527(4)
S(1)-C(1)	1.700(3)	C(13)-C(14)	1.514(4)
S(2)-C(1)#1	1.699(3)	C(21)-C(22)	1.518(4)
S(5)-C(4)	1.741(3)	C(22)-C(23)	1.518(4)
S(5)-C(2)	1.744(3)	C(23)-C(24)	1.525(4)
S(6)-C(4)	1.739(3)	C(31)-C(32)	1.524(4)
S(6)-C(3)	1.746(3)	C(32)-C(33)	1.515(4)
S(7)-C(4)	1.646(3)	C(33)-C(34)	1.515(4)
C(1)-C(1)#1	1.444(5)	C(41)-C(42)	1.519(4)
C(1)-S(2)#1	1.699(3)	C(42)-C(43)	1.520(4)
C(2)-C(3)	1.338(4)	C(43)-C(44)	1.529(4)
S(2)-Ni-S(1)	91.05(3)	S(7)-C(4)-S(6)	123.9(2)
S(2)-Ni-Se(3)	173.07(3)	S(7)-C(4)-S(5)	124.1(2)
S(1)-Ni-Se(3)	87.34(2)	S(6)-C(4)-S(5)	112.0(2)
S(2)-Ni-Se(4)	87.19(2)	C(11)-N(1)-C(31)	106.5(2)
S(1)-Ni-Se(4)	177.48(3)	C(11)-N(1)-C(41)	111.0(2)
Se(3)-Ni-Se(4)	94.62(2)	C(31)-N(1)-C(41)	110.3(2)
C(2)-Se(3)-Ni	100.30(9)	C(11)-N(1)-C(21)	111.0(2)
C(3)-Se(4)-Ni	100.49(8)	C(31)-N(1)-C(21)	110.3(2)
C(1)-S(1)-Ni	104.54(9)	C(41)-N(1)-C(21)	107.6(2)
C(1)#1-S(2)-Ni	104.40(10)	N(1)-C(11)-C(12)	115.6(2)
C(4)-S(5)-C(2)	97.58(14)	C(11)-C(12)-C(13)	111.9(2)
C(4)-S(6)-C(3)	97.76(13)	C(14)-C(13)-C(12)	114.1(3)
C(1)#1-C(1)-S(2)#1	119.2(3)	C(22)-C(21)-N(1)	114.5(2)
C(1)#1-C(1)-S(1)	118.7(3)	C(21)-C(22)-C(23)	112.6(2)
S(2)#1-C(1)-S(1)	122.1(2)	C(22)-C(23)-C(24)	111.1(3)
C(3)-C(2)-S(5)	116.5(2)	N(1)-C(31)-C(32)	115.8(2)
C(3)-C(2)-Se(3)	122.6(2)	C(33)-C(32)-C(31)	109.5(2)
S(5)-C(2)-Se(3)	120.9(2)	C(34)-C(33)-C(32)	113.2(3)
C(2)-C(3)-S(6)	116.1(2)	C(42)-C(41)-N(1)	115.1(2)
C(2)-C(3)-Se(4)	121.9(2)	C(41)-C(42)-C(43)	112.4(2)
S(6)-C(3)-Se(4)	122.0(2)	C(42)-C(43)-C(44)	111.0(3)

Symmetry transformations used to generate equivalent atoms:
#1 -x+1,-y+2,-z

Appendix Table D-13: Crystallographic data for $(Bu_4N)_2\{tto[Ni(dmise)]_2\}$ (**135**).

Empirical formula	C40 H72 N2 Ni2 S12 Se2
Formula weight	1241.06
Temperature	173(2) K
Wavelength	0.71073 Å
Crystal system	Orthorhombic
Space group	P2(1)2(1)2(1)
Unit cell dimensions	a = 9.8286(2) Å, α = 90° b = 16.1741(3) Å, β = 90° c = 34.3022(1) Å, γ = 90°
Volume, Z	5452.98(2) $Å^3$, 4
Density (calculated)	1.512 Mg/m^3
Absorption coefficient	2.515 mm^{-1}
F(000)	2568
Crystal size	0.48 x 0.23 x 0.17 mm^3
Theta range for data collection	1.73 to 25.00°
Limiting indices	-13<=h<=13, 0<=k<=21, 0<=l<=47
Reflections collected	34872
Independent reflections	8982 [R(int) = 0.0524]
Absorption correction	Semi-empirical from psi-scans
Max. and min. transmission	0.981 and 0.480
Refinement method	Full-matrix least-squares on F^2
Data / restraints / parameters	8967 / 6 / 523
Goodness-of-fit on F^2	1.084
Final R indices [I>2sigma(I)]	R1 = 0.0414, wR2 = 0.0948
R indices (all data)	R1 = 0.0462, wR2 = 0.0997

Absolute structure parameter	0.030(10)
Extinction coefficient	0.00028(5)
Largest diff. peak and hole	0.514 and -0.682 e. $Å^{-3}$

Appendix Table D-14: Fractional Coordinates and Equivalent Isotropic[a] Thermal Parameters ($Å^2$) for the Non-H Atoms of $(Bu_4N)_2\{tto[Ni(dmise)]_2\}$ (**135**).

atom	x	y	z	U(eq)
Ni'	5238(1)	4974(1)	1034(1)	23(1)
Ni	4769(1)	5053(1)	-711(1)	27(1)
Se	4133(1)	5252(1)	-2821(1)	52(1)
Se'	5898(1)	4706(1)	3146(1)	46(1)
S(1')	3774(1)	4509(1)	619(1)	27(1)
S(1)	3592(1)	4506(1)	-248(1)	36(1)
C(1')	5621(5)	5246(3)	152(1)	24(1)
C(1)	4386(5)	4775(3)	174(1)	24(1)
S(2)	6212(1)	5553(1)	-295(1)	28(1)
S(2')	6472(1)	5482(1)	569(1)	26(1)
C(2')	4882(5)	4680(3)	1905(1)	25(1)
C(2)	3928(5)	4899(3)	-1559(2)	33(1)
S(3)	3288(2)	4553(1)	-1115(1)	42(1)
S(3')	3929(1)	4495(1)	1488(1)	25(1)
C(3)	5093(5)	5348(3)	-1580(1)	29(1)
C(3')	6128(5)	5058(3)	1881(1)	28(1)
S(4)	6017(1)	5582(1)	-1166(1)	26(1)
S(4')	6773(1)	5392(1)	1443(1)	31(1)
C(4')	5751(6)	4764(3)	2619(1)	30(1)
C(4)	4262(6)	5209(4)	-2295(2)	34(1)
S(5')	4350(1)	4401(1)	2372(1)	32(1)
S(5)	3105(2)	4708(1)	-2002(1)	44(1)
S(6)	5593(1)	5645(1)	-2047(1)	33(1)
S(6')	6974(1)	5183(1)	2324(1)	32(1)
N(1)	1224(4)	6747(2)	1193(1)	25(1)
C(11)	25(5)	7217(3)	1018(2)	29(1)
C(12)	-1155(5)	7414(3)	1295(2)	34(1)
C(13)	-2309(6)	7820(4)	1066(2)	42(1)
C(14)	-3439(6)	8098(5)	1330(2)	60(2)
C(21)	808(6)	5876(3)	1309(2)	29(1)
C(22)	261(5)	5322(3)	988(2)	29(1)
C(23)	70(6)	4449(3)	1142(2)	34(1)
C(24)	-505(7)	3871(4)	836(2)	51(2)
C(31)	2346(6)	6702(3)	884(2)	32(1)
C(32)	3043(6)	7511(3)	791(2)	38(1)
C(33)	4086(7)	7384(4)	463(2)	48(2)
C(34)	3490(9)	7237(5)	71(2)	69(2)
C(41)	1724(6)	7188(3)	1555(2)	32(1)
C(42)	3006(6)	6838(3)	1741(2)	37(1)
C(43)	3411(8)	7340(4)	2094(2)	60(2)
C(44)	4659(7)	6999(4)	2291(2)	57(2)
N(2)	3567(5)	1755(3)	1030(2)	37(1)
C(51)	2584(6)	1669(4)	1365(2)	42(2)
C(52)	2038(8)	2481(4)	1523(2)	61(2)
C(53)	922(10)	2335(6)	1820(3)	87(3)
C(54)	1368(14)	1957(7)	2165(3)	141(6)

C(61)	4827(7)	2247(4)	1142(2)	53(2)
C(62)	5528(7)	2053(6)	1511(2)	86(3)
C(63)	6751(10)	2684(7)	1491(3)	55(3)
C(64)	7344(13)	2848(8)	1912(3)	73(4)
C(63')	7039(13)	2166(12)	1658(8)	76(8)
C(64')	7078(31)	3140(12)	1638(9)	89(9)
C(71)	2962(7)	2206(3)	685(2)	46(2)
C(72)	1616(6)	1857(4)	531(2)	46(2)
C(73)	1245(9)	2278(5)	149(2)	66(2)
C(74)	2062(7)	2004(4)	-195(2)	59(2)
C(81)	3965(6)	870(3)	921(2)	34(1)
C(82)	4633(6)	733(3)	528(2)	36(1)
C(83)	4998(5)	-195(3)	492(2)	35(1)
C(84)	5244(7)	-427(4)	69(2)	51(2)

Appendix Table D-15: Bond Lengths (Å) and Angles (°) for the non-H atoms of $(Bu_4N)_2\{tto[Ni(dmise)]_2\}$ (**135**).

Ni'-S(1')	2.1595(14)	N(1)-C(11)	1.526(6)
Ni'-S(3')	2.1633(14)	N(1)-C(31)	1.530(7)
Ni'-S(2')	2.1643(14)	C(11)-C(12)	1.533(7)
Ni'-S(4')	2.168(2)	C(12)-C(13)	1.528(8)
Ni-S(1)	2.156(2)	C(13)-C(14)	1.501(9)
Ni-S(4)	2.1617(14)	C(21)-C(22)	1.519(7)
Ni-S(3)	2.167(2)	C(22)-C(23)	1.519(7)
Ni-S(2)	2.1677(14)	C(23)-C(24)	1.516(8)
Se-C(4)	1.812(5)	C(31)-C(32)	1.510(7)
Se'-C(4')	1.817(5)	C(32)-C(33)	1.538(8)
S(1')-C(1)	1.696(5)	C(33)-C(34)	1.487(10)
S(1)-C(1)	1.699(5)	C(41)-C(42)	1.522(8)
C(1')-C(1)	1.435(6)	C(42)-C(43)	1.513(8)
C(1')-S(2')	1.700(5)	C(43)-C(44)	1.505(9)
C(1')-S(2)	1.714(5)	N(2)-C(51)	1.507(8)
C(2')-C(3')	1.371(7)	N(2)-C(71)	1.511(8)
C(2')-S(3')	1.735(5)	N(2)-C(61)	1.521(8)
C(2')-S(5')	1.747(5)	N(2)-C(81)	1.531(6)
C(2)-C(3)	1.358(8)	C(51)-C(52)	1.518(8)
C(2)-S(3)	1.741(5)	C(52)-C(53)	1.515(11)
C(2)-S(5)	1.746(5)	C(53)-C(54)	1.403(13)
C(3)-S(4)	1.729(5)	C(61)-C(62)	1.477(11)
C(3)-S(6)	1.743(5)	C(61)-C(62)	1.477(11)
C(3')-S(4')	1.720(5)	C(62)-C(63')	1.579(8)
C(3')-S(6')	1.744(5)	C(62)-C(63)	1.579(8)
C(4')-S(6')	1.711(5)	C(63)-C(64)	1.578(8)
C(4')-S(5')	1.719(6)	C(63')-C(64')	1.578(8)
C(4)-S(6)	1.712(5)	C(71)-C(72)	1.532(9)
C(4)-S(5)	1.721(6)	C(72)-C(73)	1.520(9)
N(1)-C(41)	1.515(7)	C(73)-C(74)	1.494(10)
N(1)-C(21)	1.520(6)	C(81)-C(82)	1.516(8)
C(82)-C(83)	1.548(7)	C(83)-C(84)	1.518(8)

S(1')-Ni'-S(3')	87.35(5)	S(6)-C(4)-Se	122.2(3)
S(1')-Ni'-S(2')	91.17(5)	S(5)-C(4)-Se	123.7(3)
S(3')-Ni'-S(2')	177.49(6)	C(4')-S(5')-C(2')	97.1(2)
S(1')-Ni'-S(4')	177.25(6)	C(4)-S(5)-C(2)	96.8(3)
S(3')-Ni'-S(4')	93.43(5)	C(4)-S(6)-C(3)	97.3(3)
S(2')-Ni'-S(4')	88.15(5)	C(4')-S(6')-C(3')	97.7(2)
S(1)-Ni-S(4)	177.86(6)	C(41)-N(1)-C(21)	108.0(4)
S(1)-Ni-S(3)	87.62(6)	C(41)-N(1)-C(11)	109.7(4)
S(4)-Ni-S(3)	93.84(6)	C(21)-N(1)-C(11)	110.9(4)
S(1)-Ni-S(2)	91.10(5)	C(41)-N(1)-C(31)	110.9(4)
S(4)-Ni-S(2)	87.46(5)	C(21)-N(1)-C(31)	109.4(4)
S(3)-Ni-S(2)	178.58(6)	C(11)-N(1)-C(31)	108.0(4)
C(1)-S(1')-Ni'	105.6(2)	N(1)-C(11)-C(12)	116.4(4)
C(1)-S(1)-Ni	106.0(2)	C(13)-C(12)-C(11)	109.4(5)
C(1)-C(1')-S(2')	119.5(3)	C(14)-C(13)-C(12)	111.6(6)
C(1)-C(1')-S(2)	119.1(3)	N(1)-C(21)-C(22)	116.8(4)

S(2')-C(1')-S(2)	121.5(3)	C(23)-C(22)-C(21)	109.8(4)
C(1')-C(1)-S(1')	118.7(3)	C(24)-C(23)-C(22)	112.1(5)
C(1')-C(1)-S(1)	118.8(3)	C(32)-C(31)-N(1)	115.6(4)
S(1')-C(1)-S(1)	122.5(3)	C(31)-C(32)-C(33)	109.9(5)
C(1')-S(2)-Ni	105.1(2)	C(34)-C(33)-C(32)	115.0(6)
C(1')-S(2')-Ni'	105.0(2)	N(1)-C(41)-C(42)	115.9(4)
C(3')-C(2')-S(3')	120.7(4)	C(43)-C(42)-C(41)	110.8(5)
C(3')-C(2')-S(5')	115.9(4)	C(44)-C(43)-C(42)	112.2(6)
S(3')-C(2')-S(5')	123.4(3)	C(51)-N(2)-C(71)	112.8(5)
C(3)-C(2)-S(3)	121.5(4)	C(51)-N(2)-C(61)	112.2(5)
C(3)-C(2)-S(5)	116.1(4)	C(71)-N(2)-C(61)	105.4(5)
S(3)-C(2)-S(5)	122.4(3)	C(51)-N(2)-C(81)	105.4(4)
C(2)-S(3)-Ni	101.4(2)	C(71)-N(2)-C(81)	111.1(4)
C(2')-S(3')-Ni'	102.2(2)	C(61)-N(2)-C(81)	110.1(5)
C(2)-C(3)-S(4)	121.2(4)	N(2)-C(51)-C(52)	114.8(5)
C(2)-C(3)-S(6)	115.7(4)	C(53)-C(52)-C(51)	111.2(6)
S(4)-C(3)-S(6)	123.2(3)	C(54)-C(53)-C(52)	114.1(9)
C(2')-C(3')-S(4')	121.4(4)	C(62)-C(61)-N(2)	119.0(6)
C(2')-C(3')-S(6')	115.3(4)	C(61)-C(62)-C(63')	133.4(11)
S(4')-C(3')-S(6')	123.4(3)	C(61)-C(62)-C(63)	100.4(7)
C(3)-S(4)-Ni	102.0(2)	C(64)-C(63)-C(62)	110.5(9)
C(3')-S(4')-Ni'	102.2(2)	C(64')-C(63')-C(62)	97.1(14)
S(6')-C(4')-S(5')	114.1(3)	N(2)-C(71)-C(72)	115.7(5)
S(6')-C(4')-Se'	123.6(3)	C(73)-C(72)-C(71)	109.9(6)
S(5')-C(4')-Se'	122.3(3)	C(74)-C(73)-C(72)	114.7(6)
S(6)-C(4)-S(5)	114.1(3)	C(82)-C(81)-N(2)	117.7(4)
C(81)-C(82)-C(83)	108.2(4)	C(84)-C(83)-C(82)	110.7(5)

LIST OF REFERENCES

1. Onnes, H. K. *Akad. van Wetenschappen (Amsterdam)* **1911**, *14*, 113.

2. McCoy, H. N.; Moore, W. C. *J. Am. Chem. Soc.* **1911**, *33*, 273.

3. Williams, J. M.; Schultz, A. J.; Geiser, U.; Carlson, K. D.; Kini, A. M.; Wang, H. H.; Kwok, W. K.; Whangbo, M. H.; Schirber, J. E. *Science*, **1991**, *252*, 1501.

4. Little, W. A. *Phys. Rev.* **1964**, *134A*, 1416.

5. Little, W. A. *Sci. Am.* **1965**, *212*, 21.

6. Ferraris, J.; Cowan, D. O.; Walatka, V. J.; Perlstein, J. H. *J. Am. Chem. Soc.* **1973**, *95*, 948.

7. Bechgaard, K.; Cowan, D. O.; Bloch, A. N. *J. Chem. Soc., Chem. Commun.* **1974**, 937.

8. Jerome, D.; Mazaud, A.; Ribault, M.; Bechgaard, K. *J. Phys. (Paris) Lett.* **1980**, *41*, L95.

9. Bechgaard, K.; Jacobsen, C. S.; Mortensen, K.; Pedersen, M. J.; Thorup, N. *Solid State Commun.* **1980**, *33*, 1119.

10. Bechgaard, K.; Carneiro, K.; Rasmussen, F. G.; Olsen, K.; Rindorf, G.; Jacobsen, C. S.; Pederson, H. J.; Scott, J. E. *J. Am. Chem. Soc.* **1981**, *103*, 2440.

11. Mizuno, M.; Garito, A. F.; Cava, M. P. *J. Chem. Soc., Chem. Commun.* **1978**, 18.

12. Parkin, S. S. P.; Engler, E. M.; Schumaker, R. R.; Lagier, R.; Lee, V. Y.; Scott, J. C.; Greene, R. L. *Phys. Rev. Lett.* **1983**, *50*, 270.

13. Yagubskii, E. B.; Shchegolev, I. F.; Laukhin, V. N.; Kononovich, P. A.; Kartsovnik, M. V.; Zvarykina, A. V.; Buravov, L. I. *JETP Lett.* **1984**, *39*, 12.

14. Williams, J. M.; Kini, A. M.; Wang, H. H.; Carlson, K. D.; Geiser, U.; Montgomery, L. K.; Pyrka, G. J.; Watkins, D. M.; Kommers, J. M.; Boryschuk, S. J.; Strieby-Crouch, A. V.; Kwok, W. K.; Schirber, J. E.; Overmyer, D. L.; Jung, D.; Whangbo, M. H. *Inorg. Chem.* **1990**, *29*, 3262.

15. Kini, A. M.; Geiser, U.; Wang, H. H.; Carlson, K. D.; Williams, J. M.; Kwok, W. K.; Vandervoort, K. G.; Thompson, J. E.; Stupka, D. L.; Jung, D.; Whangbo, M. H. *Inorg. Chem.* **1990**, *29*, 2555.

16. Williams, J. M.; Ferraro, J. R.; Thorn, R. J.; Carlson, K. D.; Geiser, U.; Wang, H. H.; Kini, A. M.; Whangbo, M. H. *Organic Superconductors (Including Fullerenes)*; Prentice Hall: Englewood Cliffs, NJ, 1992.

17. Kurmoo, M.; Graham, A. W.; Day, P.; Coles, S. J.; Hursthouse, M. B.; Caulfield, J. L.; Singleton, J.; Pratt, F. L.; Hayes, W.; Ducasse, L.; Guionneau, P. *J. Am. Chem. Soc.* **1995**, *117*, 12209.

18. Tajima, H.; Inokuchi, M.; Kobayashi, A.; Ohta, T.; Kato, R.; Kobayashi, H.; Kuroda, H. *Chem. Lett.* **1993**, 1235.

19. Krätschmer, W.; Lamb, L. D.; Fostiropolis, K.; Huffman, D. R. *Nature* **1990**, *347*, 354.

20. Khemani, K. C.; Prato, M.; Wudl, F. *J. Org. Chem.* **1992**, *57*, 3254.

21. Hebard, A. F.; Rosseinsky, M. J.; Haddon, R. C.; Murphy, D. W.; GLarum, S. H.; Palstra, T. T. M.; Ramirez, A. P.; Kortan, A. R. *Nature* **1991**, *350*, 600.

22. Iqbal, Z.; Baughman, R. H.; Ramakrishna, B. L.; Khare, S.; Murthy, N. S.; Bornemann, H. J.; Morris, D. E. *Science* **1991**, *254*, 826.

23. Bednorz, J. G.; Muller, K. A. *Z. Phys.* **1986**, *B64*, 189.

24. Wu, M. K.; Ashburn, J. R.; Torng, C. J.; Hor, P. H.; Meng, R. L.; Gao, L.; Huang, Z. J.; Wang, Y. Q.; Chu, C. W. Phys. Rev. Lett. **1987**, *58*, 908.

25. Sheng, Z. Z.; Hermann, A. M. *Nature* **1988**, *332*, 55.

26. Schilling, A.; Cantoni, M.; Guo, J. D.; Ott, H. R. *Nature* **1993**, *363*, 56.

27. Laguës, M.; Xie, X. M.; Tebbji, H.; Xu, X. Z.; Mairet, V.; Hetterer, C.; Beuran, C. F.; Deville-Cavellin, C. *Science* **1993**, *262*, 1850.

28. McCleverty, J. A. *Progr. Inorg. Chem.* **1968**, *10*, 49.

29. Hoyer, E.; Dietzsch, W.; Schroth, W. *Z. Chem.* **1971**, *11*, 41.

30. Cassoux, P.; Interrante, L. V. *Comments Inorg. Chem.* **1991**, *12*, 47.

31. Interrante, L. V.; Browall, K. W.; Hart, Jr., H. R.; Jacobs, I. S.; Watkins, G. D.; Wee, S. H. *J. Am. Chem. Soc.* **1975**, *97*, 889.

32. Kasper, J. S.; Interrante, L. V.; Secauer, C. A. *J. Am. Chem. Soc.* **1975**, *97*, 890.

33. Interrante, L. V. *Adv. Chem.* **1976**, *150*, 1.

34. Kasper, J. S.; Interrante, L. V. *Acta Cryst.* **1976**, *B32*, 2914.

35. Jacobs, I. S.; Hart, Jr., H. R.; Interrante, L. V.; Bray, J. S.; Bonner, J. C. *Physica B* **1977**, *86-88*, 655.

36. Bonner, J. C.; Wei, T. S.; Hart, Jr., H. R.; Interrante, L. V.; Jacobs, I. S.; Kasper, J. S.; Watkins, G. S.; Bloete, H. W. J. *J. Appl. Phys.* **1978**, *49*, 1321.

37. Bray, J. W.; Hart, Jr., H. R.; Interrante, L. V.; Jacobs, I. S.; Kasper, J. S.; Watkins, G. D.; Wee, S. H.; Bonner, J. C. *Phys. Rev. Lett.* **1975**, *35*, 744.

38. Jacobs, I. S.; Bray, J. W.; Hart, Jr., H. R.; Interrante, L. V.; Kasper, J. S.; Watkins, G. D.; Prober, D. E.; Bonner, J. C. *Phys. Rev. B* **1976**, *14*, 3036.

39. Moncton, D. E.; Birgeneau, R. J.; Interrante, L. V.; Wudl, F. *Phys. Rev. Lett.* **1977**, *39*, 507.

40. Kasper, J. S.; Moncton, D. E. *Phys. Rev. B* **1979**, *20*, 2341.

41. Bray, J. W.; Interrante, L. V.; Jacobs, I. S.; Bonner, J. C. *Extended Linear Chain Compounds*; ed. Miller, J. S.; Prentice Hall: New York, 1983.

42. Bähr, G.; Schleitzer, G. *Chem. Ber.* **1957**, *90*, 438.

43. Underhill, A. E.; Ahmad, M. M. *J. Chem. Soc., Chem. Commun.* **1981**, 67.

44. Ahmad, M. M.; Underhill, A. E. *J. Chem. Soc. Dalton Trans.* **1982**, 1065.

45. Kobayashi, A.; Sasaki, Y.; Kobayashi, H.; Underhill, A. E.; Ahmad, M. M. *J. Chem. Soc., Chem. Commun.* **1982**, 390.

46. Williams, J. M.; Schultz, A. J.; Underhill, A. E.; Carneiro, K. *Extended Linear Chain Compounds*; ed. Miller, J. S.; Plenum Press: New York, 1982.

47. Underhill, A. E.; Watkins, D. M.; Williams, J. M.; Carneiro, K. *Extended Linear Chain Compounds*; ed. Miller, J. S.; Plenum Press: New York, 1982.

48. Underhill, A. E.; Wood, D. J.; Carneiro, K. *Synth. Met.* **1979**, *1*, 395.

49. Carneiro, K.; Petersen, A. S.; Underhill, A. E.; Wood, D. J.; Watkins, D. M.; MacKenzie, G. A. *Phys. Rev. B* **1979**, *19*, 6279.

50. Underhill, A. E.; Tonge, J. S.; Clemenson, P. I.; Wang, H. H.; Williams, J. M. *Mol. Cryst. Liq. Cryst.* **1985**, *125*, 439.

51. Reith, W.; Polborn, K.; Amberger, E. *Angew. Chem. Int. Ed. Engl.* **1988**, *27*, 699.

52. Shklover, V. E.; Nagapetyan, S. S.; Struchkov, Y. T. *Usp. Khim.* **1990**, *59*, 1179.

53. Cassoux, P.; Valade, L.; Kobayashi, H.; Kobayashi, A.; Clark, R. A.; Underhill, A. E. *Coord. Chem. Rev.* **1992**, *110*, 115.

54. Olk, R. M.; Olk, B.; Dietzsch, W.; Kirmse, R.; Hoyer, E. *Coord. Chem. Rev.* **1992**, *117*, 99.

55. Svenstrup, N.; Becher, J. *Synth.* **1995**, 215.

56. Steimecke, G.; Kirmse, R.; Hoyer, E. *Z. Chem.* **1975**, *15*, 28.

57. Fetkenheuer, B.; Fetkenheuer, H.; Lecus, H. *Chem. Ber.* **1927**, *60*, 2528.

58. Bottcher, B.; Luttringhaus, A. *Liebigs Ann. Chem.* **1947**, *557*, 89.

59. Luttringhaus, A.; Konig, H. B.; Bottcher, B. *Liebigs Ann. Chem.* **1948**, *560*, 201.

60. Steimecke, G.; Sieler, H. J.; Kirmse, R.; Hoyer, E. *Phosphorus and Sulfur* **1979**, *7*, 49.

61. Valade, L.; Bousseau, M.; Gleizes, A.; Cassoux, P. *J. Chem. Soc., Chem. Commun.* **1983**, 110.

62. Valade, L.; Legros, J. P.; Bousseau, M.; Cassoux, P.; Garbauskas, M.; Interrante, L. V. *J. Chem. Soc. Dalton Trans.* **1985**, 783.

63. Bousseau, M.; Valade, L.; Bruniquel, M. F.; Cassoux, P.; Garbauskus, M.; Interrante, L. V.; Kasper, *J. Nouv. J. Chim.* **1984**, *8*, 3.

64. Bousseau, M.; Valade, L.; Legros, J. P.; Cassoux, P.; Garbauskas, M.; Interrante, L. V. *J. Am. Chem. Soc.* **1986**, *108*, 1908.

65. Brossard, L.; Ribault, M.; Bousseau, M.; Valade, L.; Cassoux, P. *C. R. Acad. Sci. Ser. II* **1986**, *302*, 205.

66. Brossard, L.; Ribault, M.; Valade, L.; Cassoux, P. *Physica B & C (Amsterdam)* **1986**, *143*, 378.

67. Brossard, L.; Ribault, M.; Valade, L.; Cassoux, P. *Phys. Rev. B* **1990**, *42*, 3935.

68. Pauling, L. *Nature of the Chemical Bond*; Cornell University Press: Ithaca, New York, 1960.

69. Kim, H.; Kobayashi, A.; Sasaki, Y.; Kato, R.; Kobayashi, H. *Chem. Lett.* **1987**, 1799.

70. Kobayashi, A.; Kim, H.; Sasaki, Y.; Kato, R.; Kobayashi, H.; Moriyama, S.; Nishio, Y.; Kajita, K.; Sasaki, W. *Chem. Lett.* **1987**, 1819.

71. Kobayashi, A.; Kim, H.; Sasaki, Y.; Moriyama, S.; Nishio, Y.; Kajita, K.; Sasaki, W.; Kato, R.; Kobayashi, H. *Synth. Met.* **1988**, *27*, B339.

72. Clark, R. A.; Underhill, A. E. *J. Chem. Soc., Chem. Commun.* **1989**, 228.

73. Clark, R. A.; Underhill, A. E.; Friend, R.; Allen, M.; Marsden, I.; Kobayashi, A.; Kobayashi, H. *The Physics and Chemistry of Organic Superconductors*; Saito, G.; Kagoshima, S. eds.; Springer Verlag: Berlin, 1990.

74. Papavassiliou, G. C. *Mol. Cryst. Liq. Cryst.* **1982**, *86*, 159.

75. Cassoux, P.; Valade, L.; Legros, J. P.; Interrante, L. V.; Roucau, C. *Physica B & C (Amsterdam)* **1986**, *143*, 313.

76. Legros, J. P.; Valade, L. *Solid State Commun.* **1988**, *68*, 599.

77. Brossard, L.; Hurdequint, H.; Ribault, M.; Valade, L.; Legros, J. P.; Cassoux, P. *Synth. Met.* **1988**, *27*, B157.

78. Brossard, L.; Ribault, M.; Valade, L.; Cassoux, P. *J. Phys. (Paris)* **1989**, *50*, 1521.

79. Ravy, S.; Pouget, J. P.; Valade, L.; Legros, J. P. *Europhys. Lett.* **1989**, *9*, 391.

80. Legros, J. P.; Valade, L.; Cassoux, P. *Synth. Met.* **1988**, *27*, B347.

81. Canadell, E.; Rachidi, E. I.; Ravy, S.; Pouget, J. P.; Brossard, L.; Legros, J. P. *J. Phys. (Paris)* **1989**, *50*, 2967.

82. Canadell, E.; Ravy, S.; Pouget, J. P.; Brossard, L. *Solid State Commun.* **1990**, *75*, 633.

83. Kobayashi, H.; Bun, K.; Naito, T.; Kato, R.; Kobayashi, A. *Chem. Lett.* **1992**, 1909.

84. Kobayashi, A.; Kobayashi, H.; Miyamoto, A.; Kato, R.; Clark, R. A.; Underhill, A. E. *Chem. Lett.* **1991**, 2163.

85. Olk, R. M.; Dietzsch, W.; Köhler, K.; Kirmse, R.; Reinhold, J.; Hoyer, E. *Z. Anorg. Allg. Chem.* **1988**, *567*, 131.

86. Olk, R. M.; Olk, B.; Rohloff, J.; Reinhold, J.; Sieler, J.; Trübenbach, K.; Kirmse, R.; Hoyer, E. *Z. Anorg. Allg. Chem.* **1992**, *609*, 103.

87. Olk, R. M.; Röhr, A.; Sieler, J.; Köhler, K.; Kirmse, R.; Dietzsch, W.; Hoyer, E.; Olk, B. *Z. Anorg. Allg. Chem.* **1989**, *577*, 206.

88. Olk, R. M.; Kirmse, R.; Hoyer, E.; Faulmann, C.; Cassoux, P. *Z. Anorg. Allg. Chem.* **1994**, *620*, 90.

89. Olk, R. M.; Dietzscg, W.; Kirmse, R.; Stach, J.; Hoyer, E.; Golic, L. *Inorg. Chim. Acta* **1987**, *128*, 251.

90. Singh, J. D.; Singh, H. B. *Polyhedron* **1993**, *12*, 2849.

91. Dhindsa A. S.; Badyal, J. P.; Pearson, C.; Bryce, M. R.; Petty, M. C. *J. Chem. Soc., Chem. Commun.* **1991**, 322.

92. Gupta, S. K.; Taylor, D. M.; Dynarowicz, P.; Barlow, E.; Wainwright, C. E. A.; Underhill, A. E. *Langmuir* **1992**, *8*, 3057.

93. Pearson, C.; Dhindsa, A. S.; Goldenberg, L. M.; Singh. R. A.; Dieing, R.; Moore, A. J.; Bryce, M. R.; Petty, M. C. *J. Mater. Chem.* **1995**, *5*, 1601.

94. Fettouhi, M.; Ouahab, L.; Codjovi, E.; Kahn, O. *Mol. Cryst. Liq. Cryst.* **1995**, *273*, 29.

95. Doidge-Harrison, S. M. S. V.; Howie, R. A.; Irvine, J. T. S.; Spencer, G.; Wardell, J. L. *J. Organomet. Chem.* **1991**, *414*, C5.

96. Doidge-Harrison, S. M. S. V.; Irvine, J. T. S.; Spencer, G. M.; Wardell, J. L.; Ganis, P.; Valle, G.; Tagliavini, G. *Polyhedron* **1996**, *15*, 1807-1815.

97. Cerrada, E.; Jones, P. G.; Laguna, A.; Laguna, M. *Inorg. Chem.* **1996**, *35*, 2995.

98. Montgomery, L. K. in *Organic Conductors, Fundamentals and Applications,* ed. Farges, J. P.; Marcel Dekker: New York, 1994.

99. Ward, M. D. *J. Electroanal. Chem.* **1989**, *273*, 79.

100. Ward, M. D. in *Electroanalytical Chemistry*, ed. Bard, A. J.; Marcel Dekker: New York, 1989, p. 181.

101. Li, S. L.; White, H. S.; Ward, M. D. *Chem. Mater.* **1992**, *4*, 1082.

102. Tommasino, J. B.; Pomarede, B.; Medus, D.; de Montauzon, D.; Cassoux, P. *Mol. Cryst. Liq. Cryst.* **1993**, *237*, 445.

103. Bard, A. J.; Faulkner, L. R. in *Electrochemical Methods*, J. Wiley & Sons: New York, 1980.

104. Valade, L.; Legros, J. P.; Tejel, C.; Pomarede, B.; Garreau, B.; Bruniquel, M. F.; Cassoux, P.; Ulmet, J. P.; Audouard, A.; Brossard, L. *Synth. Met.* **1991**, *42*, 2268.

105. Tejel, C.; Pomarede, B.; Legros, J. P.; Valade, L.; Cassoux, P. Ulmet, J. P. *Chem. Mater.* **1989**, *1*, 578.

106. Ulmet, J. P.; Mazzaschi, M.; Tejel, C.; Cassoux, P.; Brossard, L. *Solid State Commun.* **1990**, *74*, 91.

107. Alvarez, S.; Vicente, R.; Hoffmann, R. *J. Am. Chem. Soc.* **1985**, *107*, 6253.

108. Götzfried, F.; Beck, W.; Lerf, A.; Sebald, A. *Angew. Chem. Int. Ed. Engl.* **1979**, *18*, 463.

109. Rivera, N. M.; Engler, E. M.; Schumaker, R. R. *J. Chem. Soc., Chem. Commun.* **1979**, 184.

110. Poleschner, H.; John, W.; Hoppe, F.; Fanghänel, E. *J. F. Prakt. Chem.* **1983**, *6*, 957.

111. Vicente, R.; Ribas, J.; Cassoux, P.; Valade, L. *Synth. Met.* **1986**, *13*, 265.

112. Reynolds, J. R.; Lillya, C. P.; Chien, J. C. W. *Macromolecules* **1987**, *20*, 1184.

113. Reynolds, J. R.; Jolly, C. A.; Krichene, S.; Cassoux, P.; Faulmann, C. *Synth. Met.* **1989**, *31*, 109.

114. Vicente, R.; Ribas, J.; Alvarez, S.; Segui, A.; Solans, X.; Verdaguer, M. *Inorg. Chem.* **1987**, *26*, 4004.

115. Yang, X.; Doxsee, D. D.; Rauchfuss, T. B.; Wilson, S. R. *J. Chem. Soc., Chem. Commun.* **1994**, 821.

116. McCullough, R. D.; Belot, J. A. *Chem. Mater.* **1994**, *6*, 1396.

117. McCullough, R. D.; Belot, J. A.; Rheingold, A. L.; Yap, G. P. A. *J. Am. Chem. Soc.* **1995**, *117*, 9913.

118. McCullough, R. D.; Belot, J. A.; Seth, J.; Rheingold, A. L.; Yap, G. P. A.; Cowan, D. O. *J. Mater. Chem.* **1995**, *5(10)*, 1581.

119. Cowie, J. M. G. *Alternating Copolymerization*, pp. 377-422 in *Comprehensive Polymer Science*, Vol. 4, Eastman, G. C.; Ledwith, A.; Russo, S.; Sigwalt, P., eds.; Pergamon Press: Oxford, 1984.

120. Fox, M. A.; Channon, M. *Photoinduced Electron Transfer*; Elsevier: Amsterdam, 1988, Part D.

121. "Photoinduced Electron Transfer" *Top. Curr. Chem.* **1990**, 159.

122. Atkins, P. W. *Physical Chemistry*, 4th ed., W. H. Freeman and Co.: New York, 1990.

123. Liu, H. L.; Tanner, D. B.; Pullen, A. E.; Abboud, K. A.; Reynolds, J. R. *Phys. Rev. B* **1996**, *53*, 10557.

124. Kato, R.; Kobayashi, H.; Kim, H.; Kobayashi, A.; Sasaki, Y.; Mori, T.; Inokuchi, H. *Synth. Met.* **1988**, *27*, B359.

125. Pullen, A. E.; Piotraschke, J.; Abboud, K. A.; Reynolds, J. R.; Liu, H. L.; Tanner, D. B. *Polym. Mater. Sci. Eng. Symp. Proc.* **1995**, *72*, 321.

126. Nakamura, T.; Underhill, A. E.; Coomber, T.; Friend, R. H.; Tajima, H.; Kobayashi, A.; Kobayashi, H. *Inorg. Chem.* **1995**, *34*, 870.

127. Nakamura, T.; Underhill, A. E.; Coomber, T.; Friend, R. H.; Tajima, H.; Kobayashi, A.; Kobayashi, H. *Synth. Met.* **1995**, *70*, 1061.

128. Pullen, A. E.; Abboud, K. A.; Reynolds, J. R.; Piotraschke, J.; Zeltner, S.; Olk, R. M.; Hoyer, E.; Liu, H. L.; Tanner, D. B. *Synth. Met.*, in press.

129. Pullen, A. E.; Liu, H. L.; Tanner, D. B.; Abboud, K. A.; Reynolds, J. R. *J. Mater. Chem.*, in press.

130. Papavassiliou, G. C.; Cotsilios, A. M.; Jacobsen, C. S. *J. Mol. Struct.* **1984**, *15*, 41.

131. Tajima, H.; Naito, T.; Tamura, M.; Kobayashi, A.; Kuroda, H.; Kato, R.; Kobayashi, H.; Clark, R. A.; Underhill, A. E. *Solid State Commun.* **1991**, *79*, 337.

132. Tajima, H.; Tamura, M.; Naito, T.; Kobayashi, A.; Kato, R.; Kobayashi, H.; Clark, R. A.; Underhill, A. E. *Mol. Cryst. Liq. Cryst.* **1990**, *181*, 233.

133. Tamura, M.; Masuda, R.; Naito, T.; Tajima, H.; Kuroda, H.; Kobayashi, A.; Yakushi, K.; Kato, R.; Kobayashi, H.; Tokumoto, M.; Kinoshita, N.; Anzai, H. *Synth. Met.* **1991**, *41*, 2499.

134. Jacobsen, C. S.; Yartsev, V. M.; Tanner, D. B.; Bechgaard, K. *Synth. Met.* **1993**, *55*, 1925.

135. Barreto, W. J.; Ribeiro, M. C. C.; Santos, P. S. *J. Mol. Struct.* 1992, *269*, 75.

136. Sheldrick, G. M. L.; SHELXTL plus; Nicolet XRD Corp.: Madison, WI, 1990.

137. *International Tables for X-ray Crystallography*; Kynoch Press: Birmingham, 1974, Vol. IV.

138. Cromer, D. T.; Mann, J. B. *Acta Cryst.* **1986**, *A24*, 321.

139. Cromer, D. T.; Liberman, D. *J. Phys. Chem.* **1970**, *53*, 1891.

140. Stewart, R. F.; Davidson, D. R.; Simpson, W. T. *J. Chem. Phys.* **1965**, *42*, 3175.

141. Wooten, F. *Optical Properties of Solids*, Academic Press: New York, 1972.

142. Doublet, M. L.; Canadell, E.; Pouget, J. P.; Yagubskii, E. B.; Ren. J.; Whangbo, M. H. *Solid State Commun.* **1993**, *88*, 699.

143. Faulmann, C.; Legros, J. P.; Cassoux, P.; Cornelissen, J.; Brossard, M.; Inokuchi, M.; Tajima, H.; Tokumoto, M. *J. Chem. Soc. Dalton Trans.* **1994**, 249.

144. Kato, R.; Liu, Y. L.; Sawa, H.; Aonuma, S.; Ichikawa, A.; Takahashi, H.; Mori, N. *Solid State Commun.* **1995**, *94*, 973.

145. Kobayashi, A.; Sato, A.; Kawano, K.; Naito, T.; Kobayashi, H.; Watanabe, T. *J. Mater. Chem.* **1995**, *5*, 1671.

146. Faulmann, C.; Errami, A.; Donnadieu, B.; Malfant, I.; Legros, J. P.; Cassoux, P.; Rovira, C.; Canadell, E. *Inorg. Chem.* **1996**, *35*, 3856.

147. Tanner, D. B. in *Extended Linear Chain Compounds*, ed. Miller, J. S.; Plenum Press: New York, 1982, Vol II.

148. Kobayashi, A.; Kim, H.; Sasaki, Y.; Kato, R.; Kobayashi, H. *Solid State Commun.* **1987**, *62*, 57.

149. Errami, A.; Bowlas, C. J.; Menou, F.; Faulmann, C.; Gangneron, F.; Valade, L.; Cassoux, P.; Lahlil, K.; Moradpour, A. *Synth. Met.* **1995**, *71*, 1895.

150. Piotraschke, J.; Pullen, A. E.; Abboud, K. A.; Reynolds, J. R. *Inorg. Chem.* **1995**, *34*, 4011.

151. Pullen, A. E.; Zeltner, S.; Olk, R. M.; Hoyer, E.; Abboud, K. A.; Reynolds, J. R. *Inorg. Chem.* **1996**, *35*, 4420.

152. Jeroschewski, P. *Z. Chem.* **1981**, *21*, 412.

153. Billig, E.; Williams, R.; Bernal, I.; Waters, J. H.; Gray, H. B. *Inorg. Chem.* **1964**, *3*, 663.

154. Matsubayashi, G.; Takahashi, K.; Tanaka, T. *J. Chem. Soc., Dalton Trans.* **1988**, 967.

155. Lever, A. B. P. *Inorganic Electronic Spectroscopy*, 2nd ed., Elsevier: Amsterdam, 1984.

156. Lund, H.; Hoyer, E.; Groenbaeck-Hazell, R. *Acta Chem. Scand., Ser. B* **1982**, *36*, 207.

157. Hansen, L. K.; Sieler, J.; Strauch, P.; Dietzsch, W.; Hoyer, E. *Acta Chem. Scand., Ser. A* **1985**, *39*, 571.

158. Pullen, A. E.; Piotraschke, J.; Abboud, K. A.; Reynolds, J. R. *Inorg. Chem.* **1996**, *35*, 793.

159. Olk, R. M. Ph.D. Dissertation, University of Leipzig, 1985.

160. Persaud, L.; Langford, C. H. *Inorg. Chem.* **1985**, *24*, 3562.

161. Pullen, A. E.; Olk, R. M.; Zeltner, S.; Hoyer, E.; Abboud, K. A.; Reynolds, J. R. *Inorg. Chem.*, submitted for publication.

162. Pullen, A. E.; Zeltner, S.; Olk, R. M.; Hoyer, E.; Abboud, K. A.; Reynolds, J. R. *Inorg. Chem.*, submitted for publication.

163. Maj, J. J.; Rae, A. D.; Dahl, L. F. *J. Am. Chem. Soc.* **1982**, *104*, 4278.

164. Gasiorowski, R.; Jorgensen, T.; Moller, J.; Hansen, T. K.; Pietraszkiewicz, M.; Becher, J. *Adv. Mater.* **1992**, *4*, 568.

165. Zeltner, S.; Olk, R. M.; Pink, M.; Jelonek, S.; Jörchel, P.; Gelbrich, T.; Sieler, J.; Kirmse, R. *Z. Anorg. Allg. Chem.*, in press.

166. Zeltner, S.; Dietzsch, W.; Olk, R. M.; Kirmse, R.; Richter, R.; Schröder, U.; Olk, B.; Hoyer, E. *Z. Anorg. Allg. Chem.* **1994**, *620*, 1768.

167. Wudl, F. *J. Am. Chem. Soc.* **1975**, *97*, 1962.

168. Bacher, A. D.; Sens, I.; Müller, U. *Z. Naturforsch.* **1992**, *47b*, 702.

169. Dietzsch, W.; Strauch, P.; Hoyer, E. *Coord. Chem. Rev.* **1992**, *121*, 43.

170. Cornelissen, J. P.; Haasnoot, J. G.; Reedijk, J.; Faulmann, C.; Legros, J. P.; Cassoux, P.; Nigrey, P. J. *Inorg. Chim. Acta* **1992**, *202*, 131.

171. Olk, R, M.; Röhr, A.; Olk, B.; Hoyer, E. *Z. Chem.* **1988**, *28*, 304.

BIOGRAPHICAL SKETCH

Anthony Edward Pullen was born in Muncie, Indiana on August 27, 1970. He spent his entire childhood in Yorktown, Indiana where he attended Daleville Elementary and Junior-High School and graduated from Yorktown High School in 1988. That same year he entered Rose-Hulman Institute of Technology in Terre Haute, Indiana where he attended one year as a chemical engineering major. In 1989, he transferred to Ball State University in Muncie, Indiana and graduated in 1992 with a Bachelors degree in chemistry. There he worked with Professor Bruce N. Storhoff on molecular modeling and 2-D NMR. In 1992, he came to the University of Florida in Gainesville to begin doctoral studies with Professor John R. Reynolds in polymer chemistry.

Anthony and his parents are extremely happy that he has completed his doctoral studies and eight long years of college. His first job as a Ph.D. will begin early 1997 in Toulouse, France as a post-doctoral chemist in the research group of Professor Patrick Cassoux. He is going to miss attending Florida Gator football games.

Anthony has many interests. These include basketball, tennis, boxing, travel, art, reading, eating good food, listening to music and spending time with his wife Sande. Anthony is very thankful for the stay he had at the University of Florida but is ready to move on to Europe to see the world and for more exciting things.

I certify that I have read this study and that in my opinion it conforms to acceptable standards of scholarly presentation and is fully adequate, in scope and quality, as a dissertation for the degree of Doctor of Philosophy.

John R. Reynolds, Chairman
Professor of Chemistry

I certify that I have read this study and that in my opinion it conforms to acceptable standards of scholarly presentation and is fully adequate, in scope and quality, as a dissertation for the degree of Doctor of Philosophy.

Kenneth B. Wagener
Professor of Chemistry

I certify that I have read this study and that in my opinion it conforms to acceptable standards of scholarly presentation and is fully adequate, in scope and quality, as a dissertation for the degree of Doctor of Philosophy.

James M. Boncella
Associate Professor of Chemistry

I certify that I have read this study and that in my opinion it conforms to acceptable standards of scholarly presentation and is fully adequate, in scope and quality, as a dissertation for the degree of Doctor of Philosophy.

Daniel R. Talham
Associate Professor of Chemistry

I certify that I have read this study and that in my opinion it conforms to acceptable standards of scholarly presentation and is fully adequate, in scope and quality, as a dissertation for the degree of Doctor of Philosophy.

David B. Tanner
Professor of Physics

This dissertation was submitted to the Graduate Faculty of the Department of Chemistry in the College of Liberal Arts and Sciences and to the Graduate School and was accepted as partial fulfillment of the requirements for the degree of Doctor of Philosophy.

December, 1996

Dean, Graduate School

LD
1780
1996
.P982

UNIVERSITY OF FLORIDA
3 1262 08554 9326